



Durham E-Theses

Mechanistic studies on the role of cationic palladium hydride initiators in addition polymerization of exo-and endo-functionalized norbornenes

Cooper, Alan Thomas

How to cite:

Cooper, Alan Thomas (2008) *Mechanistic studies on the role of cationic palladium hydride initiators in addition polymerization of exo-and endo-functionalized norbornenes*, Durham theses, Durham University. Available at Durham E-Theses Online: <http://etheses.dur.ac.uk/2219/>

Use policy

The full-text may be used and/or reproduced, and given to third parties in any format or medium, without prior permission or charge, for personal research or study, educational, or not-for-profit purposes provided that:

- a full bibliographic reference is made to the original source
- a [link](#) is made to the metadata record in Durham E-Theses
- the full-text is not changed in any way

The full-text must not be sold in any format or medium without the formal permission of the copyright holders.

Please consult the [full Durham E-Theses policy](#) for further details.

**Mechanistic Studies on the Role of Cationic Palladium
Hydride Initiators in Addition Polymerization of *Exo*-
and *Endo*-Functionalized Norbornenes**

Submitted by Alan Thomas Cooper

In partial fulfilment for the degree of PhD

Durham University

Feb 2008

The copyright of this thesis rests with the author or the university to which it was submitted. No quotation from it, or information derived from it may be published without the prior written consent of the author or university, and any information derived from it should be acknowledged.

01 SEP 2008



Acknowledgements

First and foremost I would like to thank Dr. Ezat Khosravi and Dr. Andrew Bell for their continued help and advice throughout this period of study. My deepest thanks are extended to Dr. Alan Kenwright, Ian McKeag and Catherine Heffernan for their considerable patience and assistance in obtaining NMR spectra. I would like to thank Dr. Andrew Teale for his generous donation of time and molecular modelling expertise. The contribution of Dr. Mike Jones and Lara Turner (MS), Lenny Lauchran (GC), Andrei Batsanov (X-ray Crystallography) and Dr. Ann G-Jensen (statistical analysis) during the course of this project is also gratefully acknowledged.

Finally I would like to thank Promerus LLC for their financial support, supply of catalysts, catalyst precursors and monomers.

Abstract

Simple routes to $[\text{Pd}(\text{P-}i\text{-Pr}_3)_2(\text{O}_2\text{CCH}_3)(\text{NCCH}_3)][\text{B}(\text{C}_6\text{F}_5)_4]$ (**Pd1206**) have been developed. Reactions of *trans*- $[(i\text{-Pr}_3\text{P})_2\text{Pd}(\text{O}_2\text{CCH}_3)_2]$ with $\text{Li}(\text{Et}_2\text{O})_{2.5}[\text{B}(\text{C}_6\text{F}_5)_4]$ or $[\text{HN}(\text{Ph})(\text{Me})_2][\text{B}(\text{C}_6\text{F}_5)_4]$ in acetonitrile led to carboxylate abstraction and formation of **Pd1206** in excellent yield. Reaction of *trans*- $[(i\text{-Pr}_3\text{P})_2\text{Pd}(\text{O}_2\text{CCH}_3)_2]$ with $\text{K}[\text{B}(\text{C}_6\text{F}_5)_4]$ in acetonitrile led to carboxylate abstraction and formation of **Pd1206** in only 40% yield but the addition of 1 equivalent of LiOTf pushed the reaction to completion.

The thermolysis behaviour of **Pd1206** and $[\text{Pd}(\text{P-}i\text{-Pr}_3)_2(\kappa^2\text{-OAc})][\text{B}(\text{C}_6\text{F}_5)_4]$ (**Pd1165**) in THF-*d*₈ and CDCl_3 , is shown to be complex by ¹H and ³¹P NMR spectroscopy. The reactions reveal a number of new thermodynamically unstable intermediates that lead to the thermodynamically stable $[\text{Pd}(\text{P-}i\text{-Pr}_3)_2(\text{NCCH}_3)(\text{H})][\text{B}(\text{C}_6\text{F}_5)_4]$ (**Pd1148**) in approximately 40-45% yield and a number of other closely related cationic palladium hydride complexes. The thermolysis behaviour of **Pd1206** and **Pd1165** depends heavily on the reaction solvent and temperature, with coordinating THF-*d*₈ giving a faster reaction rate than non-coordinating CDCl_3 . ¹H and ³¹P VT-NMR, ³¹P-¹H and ³¹P-³¹P 2D-NMR, between 25 and -60°C, using CDCl_3 as solvent, allowed the characterisation of key reaction intermediates and products including *cis/trans*- $[\text{Pd}(\text{P-}i\text{-Pr}_3)(\text{P}(i\text{-Pr}_2)(\kappa^2\text{-C}(\text{CH}_3)_2))(\text{NCCH}_3)][\text{B}(\text{C}_6\text{F}_5)_4]$ (**Pd1146M**), $[\text{Pd}(\text{P-}i\text{-Pr}_3)((i\text{-Pr}_2)\text{P-C}(\text{CH}_3)=\text{CH}_2)(\text{NCCH}_3)(\text{H})][\text{B}(\text{C}_6\text{F}_5)_4]$ (**Pd1146H**) and $[\text{Pd}(\text{P-}i\text{-Pr}_3)((i\text{-Pr}_2)\text{P-C}(\text{CH}_3)=\text{CH}_2)_2(\text{H})][\text{B}(\text{C}_6\text{F}_5)_4]$ (**Pd1273H**).

The cyclometallated *cis/trans*-**Pd1146M** is formed via the reversible carboxylate abstraction reaction from **Pd1165**. The **Pd1146H** is identified using ³¹P NMR spectroscopy at -60°C (202.3 MHz, CDCl_3): δ (ppm) = *cis*-**Pd1146M**, 92.6%; 50.4 (d, non-metalated P, $J = 31.56$), 41.7 (d, metalated P, $J = 31.56$); *trans*-**Pd1146M**, 7.4%; 38.2 (d, non-metalated P, $J = 236.30$), 14.8 (d, metalated P, $J = 236.30$). The cyclometallated phosphine ligand in **Pd1146M** undergoes a rapid hydride abstraction reaction, above 0°C, resulting in **Pd1146H** that now has two different *trans*-phosphine ligands. The **Pd1146H** is identified using ³¹P NMR spectroscopy (121.4 MHz, CDCl_3): δ (ppm) = 52.2 (AB-system, $J = 322.0$ Hz). **Pd1146H** is identified using ¹H NMR spectroscopy (200.0 MHz, CDCl_3): δ (ppm) = 5.86 (d, 1H, $^3J_{\text{PH}} = 34.8$, vinylic H *trans* to P), 5.67 (d, 1H, $^3J_{\text{PH}} = 16.1$, vinylic H *cis* to P), -15.25 (t, 1H, $J = 7.16$, Pd-H). The **Pd1146H** is highly thermodynamically unstable above 0°C, resulting in rapid phosphine ligand exchange to give **Pd1148** and a range of other mixed phosphine ligand cationic palladium hydride complexes. The tris-phosphine complex **Pd1273H** was identified using ³¹P NMR spectroscopy (121.4 MHz, CDCl_3): δ (ppm) = 69.8 (dd, $J = 110.4$ & 29.3, $((i\text{-Pr}_2)\text{P-C}(\text{CH}_3)=\text{CH}_2)$), 60.0 (dd, $J = 32.5$ & 29.3, $((i\text{-Pr}_2)\text{P-C}(\text{CH}_3)=\text{CH}_2)$), 56.9 (dd, $J = 110.4$ & 32.5, $\text{P-}i\text{-Pr}_3$).

The thermolytic transformation of **Pd1206** into cationic palladium hydrides is non-quantitative since a decarboxylation pathway leads to the formation of carbon dioxide and $[\text{Pd}(\text{P-}i\text{-Pr}_3)_2(\text{NCCH}_3)(\text{CH}_3)][\text{B}(\text{C}_6\text{F}_5)_4]$ (**Pd1162**). **Pd1162** readily undergoes decomposition to Pd metal under thermolysis conditions. The complicated thermolysis mechanism can be obviated and **Pd1148** generated in >90% yield from **Pd1206** via the addition of 1 equivalent of Et_3SiH in CDCl_3 . This methodology may be useful for the conversion of any general complex, $[\text{Pd}(\text{PR}_3)_2(\text{OAc})(\text{NCCH}_3)][\text{FABA}]$, into $[\text{Pd}(\text{PR}_3)_2(\text{H})(\text{NCCH}_3)][\text{FABA}]$, for any trialkylphosphine.

The **Pd1148** polymerizes *endo/exo*-5-decyl-2-norbornene ($k = 4.54 \times 10^{-3} \text{ s}^{-1}$) approximately four times faster than **Pd1206** ($k = 1.28 \times 10^{-3} \text{ s}^{-1}$) in toluene-*d*₈, at 70°C. The GPC data shows **Pd1148** generates a lower molecular weight polymer ($M_w = 33,000$ versus 60,000), sharper PDI ($M_w/M_n = 1.87$ versus 2.87), and higher yield than **Pd1206** under the same conditions.

^1H NMR spectroscopy is demonstrated as an analytical tool for probing the initiation and propagation steps of the stable cationic palladium hydride initiator, $[\text{Pd}(\text{PCy}_3)_2(\text{NCCH}_3)(\text{H})]\text{[B}(\text{C}_6\text{F}_5)_4]$ (**Pd1388**), with a range of technologically important functionalised norbornenes. The addition of CuCl causes instantaneous initiation and an increase in the polymerisation rate of norbornene monomers by a factor of $\times 3$. An increase in polymerisation solvent polarity causes an increase in polymerisation rate. *endo*-Substituted norbornenes are polymerised more slowly than their *exo*-analogues. The rate of polymerisation is independent of the steric size of the *exo*-functionality, however, for the *endo*-regioisomer, functional groups with larger steric size polymerise more slowly. The electronic nature of the functionality plays the major role in lowering polymerisation activity; with electron withdrawing functionalities causing reduced polymerisation activity. The introduction of methylene spacers between norbornene and its functionality reduces the electronic effect of the functionality and increases the monomers polymerisation activity. The polymerisation activities of *endo*- and *exo*-functionalised norbornene monomers are greatly affected by the penultimate group effect during co-polymerisation reactions.

The new single regioisomer monomers: *exo*-5-methoxy-2-norbornene (*exo*-NB-OMe), *exo*-5-acetate-2-norbornene (*exo*-NB-OAc), *exo*-5-benzyloxy-2-norbornene (*exo*-NB-OBz) and *endo*-5-acetate-2-norbornene (*endo*-NB-OAc) have been synthesised from *exo*- or *endo*-5-hydroxy-2-norbornene (NB-OH) and their polymerisation activity investigated. *exo*-NB-OMe showed very high polymerisation activity. Surprisingly, *exo*-NB-OAc showed lower polymerisation activity than *endo*-NB-OAc. The new single isomer acetate functionalised tetracyclododecenes: *exo*-TD-OAc or *endo*-TD-OAc, have been synthesised from the Diels-Alder cycloaddition reaction of cyclopentadiene with the corresponding *exo*- or *endo*-NB-OAc monomers. In both cases cycloaddition occurred selectively at the norbornene *exo* face. A single crystal of *exo*-TD-OAc was obtained from hexanes at -10°C over 4 weeks, and an X-ray structural diagram produced. Steric effects cause both TD-OAc isomers to show low polymerisation activity.

The single regioisomer monomers: *exo*-5-methyl methoxy-2-norbornene (*exo*-NB- CH_2OMe), *exo*-5-methyl acetate-2-norbornene (*exo*-NB- CH_2OAc), *endo*-5-methyl methoxy-2-norbornene (*endo*-NB- CH_2OMe) and *endo*-5-methyl acetate-2-norbornene (*endo*-NB- CH_2OAc) have been synthesised from *exo*- and *endo*-5-carboxylic acid-2-norbornene (NB- CO_2H) and their polymerisation activity investigated. Single crystals of *exo*-NB- CO_2H and *endo*-NB- CO_2H were obtained via slow sublimation at 20°C and X-ray structural diagrams produced.

The new single regioisomer monomers: *endo*-5-methyl-*exo*-5-trimethylsilyl carboxylate-2-norbornene (NB(*endo*-Me)(*exo*- CO_2TMS)), *endo*-5-methyl-*exo*-5-methyl methoxy-2-norbornene (NB(*endo*-Me)(*exo*- CH_2OMe)) and *endo*-5-methyl-*exo*-5-methyl trimethylsilyl carboxylate-2-norbornene (NB(*endo*-Me)(*exo*- $\text{CH}_2\text{CO}_2\text{TMS}$)) have been synthesised from *endo*-5-methyl-*exo*-5-carboxylic acid-2-norbornene (NB(*endo*-Me)(*exo*- CO_2H)) and their polymerisation activity investigated. A single crystal of NB(*endo*-Me)(*exo*- CO_2H) was obtained via slow recrystallisation from ethylacetate at 20°C and a X-ray structural diagram produced. NB(*endo*-Me)(*exo*- $\text{CH}_2\text{CO}_2\text{TMS}$) was produced using standard chain extension techniques.

The ^{13}C NMR spectroscopic shifts were employed in an attempt to rationalise the effects of introducing methylene spacers between norbornene and its functional group. The key bicyclic carbons within the monomer structures displayed no regular or consistent trends in ^{13}C NMR signal shifts, upon the methylene spacing of the $-\text{CO}_2\text{TMS}$, $-\text{OMe}$, $-\text{NHSO}_2\text{CF}_3$ and $-\text{OAc}$ functionalities.

Theoretical calculations are performed on isolated molecules of *endo*- and *exo*-NB- $(\text{CH}_2)_n\text{CO}_2\text{H}$, where $n = 0, 1$ and 2 , using the Gaussian 03 program, to rationalise the effects of introducing methylene spacers between norbornene and its functional group. The relationships between

polymerisation activity and bond lengths, bond angles and Mulliken atomic charges are examined. Although the relationships shown for the *exo*-regioisomers differ from those occurring in the analogous *endo*-regioisomers, the main structural changes for both regioisomers involve the C3, C4, C5 and perhaps C6, atoms, which is not surprising given that these carbon atoms are nearest the electron withdrawing substituent. The structural changes occurring could not be used to explain the monomers changes in polymerisation activity.

Chapter 1 - General Introduction and Background

1.1	Introduction	1
1.2	Addition Polymerisation Catalyst Development Using Late Transition Metals	3
1.3	Addition Polymerisation of Functionalised Norbornenes	9
1.3.1	Synthesis of Norbornene Monomers via Diels-Alder Route	10
1.3.2	Effect of Stereochemistry, Size and Chelate Formation	11
1.3.3	Effect of Functional group	12
1.4	Synthesis of <i>exo</i> -Functionalised Norbornene Monomers	14
1.4.1	Synthesis of <i>exo</i> -5-Amino-2-norbornene	15
1.4.2	Synthesis of <i>exo</i> -5-Aryl-2-norbornenes	16
1.4.3	Synthesis of <i>exo</i> -5-Thio-2-norbornene	16
1.4.4	Synthesis of <i>exo</i> -5-Hydroxy-2-norbornene	17
1.4.5	Synthesis of <i>endo</i> -5-Methyl-2-norbornene- <i>exo</i> -5-carboxylic acid	18
1.5	Optoelectronic Materials	19
1.5.1	Dielectric Polymers	19
1.5.2	Optical Polymers	20
1.5.3	Photoresist Polymers	21
1.6	References	25

Chapter 2 - Formation of Palladium Hydride Initiators from [Pd(P-*i*-Pr₃)₂(NCCH₃)(OAc)][B(C₆F₅)₄]: Mechanism and Characterization by NMR Spectroscopy

2.1	Introduction	29
2.2	Results and Discussion	31
2.2.1	New Synthesis Routes to [Pd(P- <i>i</i> -Pr ₃) ₂ (NCCH ₃)(OAc)][B(C ₆ F ₅) ₄] (Pd1206)	31
2.2.2	Thermolysis of [Pd(P- <i>i</i> -Pr ₃) ₂ (NCCH ₃)(OAc)][B(C ₆ F ₅) ₄] (Pd1206) in THF- <i>d</i> ₈ at Variable Temperatures	32
2.2.3	Thermolysis of [Pd(P- <i>i</i> -Pr ₃) ₂ (NCCH ₃)(OAc)][B(C ₆ F ₅) ₄] (Pd1206) in THF- <i>d</i> ₈ at 55°C	34
2.2.4	Thermolysis of [Pd(P- <i>i</i> -Pr ₃) ₂ (NCCH ₃)(CH ₃)][B(C ₆ F ₅) ₄] (Pd1162)	36

2.2.5	Thermolysis of $[\text{Pd}(\text{P-}i\text{-Pr}_3)_2(\text{NCCH}_3)(\text{CH}_3)][\text{B}(\text{C}_6\text{F}_5)_4]$ (Pd1162) + Acetic Acid in THF- d_8	38
2.2.6	Thermolysis of $[\text{Pd}(\text{P-}i\text{-Pr}_3)_2(\text{NCCH}_3)(\text{CH}_3)][\text{B}(\text{C}_6\text{F}_5)_4]$ (Pd1162) + Formic Acid	39
2.2.7	Thermolysis of $[\text{Pd}(\text{P-}i\text{-Pr}_3)_2(\kappa^2\text{-OAc})][\text{B}(\text{C}_6\text{F}_5)_4]$ (Pd1165) at 55°C in THF- d_8	40
2.2.8	Thermolysis of $[\text{Pd}(\text{P-}i\text{-Pr}_3)_2(\kappa^2\text{-OAc})][\text{B}(\text{C}_6\text{F}_5)_4]$ (Pd1165) + Acetonitrile	41
2.2.9	Synthesis and Characterisation of <i>cis</i> - & <i>trans</i> - $[\text{Pd}(\text{P-}i\text{-Pr}_3)(\text{P}(i\text{-Pr}_2)(\kappa^2\text{-C}(\text{CH}_3)_2))(\text{NCCH}_3)(\text{H})][\text{B}(\text{C}_6\text{F}_5)_4]$ (Pd1146M)	43
2.2.10	Synthesis and Characterisation of $[\text{Pd}(\text{P-}i\text{-Pr}_3)((i\text{-Pr})_2\text{P-C}(\text{CH}_3)=\text{CH}_2)(\text{NCCH}_3)(\text{H})][\text{B}(\text{C}_6\text{F}_5)_4]$ (Pd1146H)	47
2.2.11	Thermolysis of $[\text{Pd}(\text{P-}i\text{-Pr}_3)(\text{P}(i\text{-Pr}_2)(\kappa^2\text{-C}(\text{CH}_3)_2))(\text{NCCH}_3)(\text{H})][\text{B}(\text{C}_6\text{F}_5)_4]$ (Pd1146M) at 35°C	49
2.2.12	The Fate of the $(i\text{-Pr})_2\text{P-C}(\text{CH}_3)=\text{CH}_2$ Ligand	50
2.2.13	Effect of Additives on Generation of $[\text{Pd}(\text{P-}i\text{-Pr}_3)_2(\text{NCCH}_3)(\text{H})][\text{B}(\text{C}_6\text{F}_5)_4]$ from $[\text{Pd}(\text{P-}i\text{-Pr}_3)_2(\text{NCCH}_3)(\text{OAc})][\text{B}(\text{C}_6\text{F}_5)_4]$	52
2.2.14	Comparison of Polymerisation Activities	54
2.3	Conclusions	56
2.4	Experiment	56
2.4.1	Glossary of Cationic Palladium Species Experiment	56
2.4.2	Materials	57
2.4.3	Instrumentation and Measurements	57
2.4.3.1	Nuclear Magnetic Resonance	57
2.4.3.2	Gel Permeation Chromatography (GPC)	57
2.4.4	Synthesis and Characterisation	58
2.4.4.1	Synthesis of $[\text{Pd}(\text{P-}i\text{-Pr}_3)_2(\text{NCCH}_3)(\text{OAc})][\text{B}(\text{C}_6\text{F}_5)_4]$ (Pd1206) Using LiFABA	58
2.4.4.2	Synthesis of Pd1206 Using DANFABA	59
2.4.4.3	Attempted Synthesis of Pd1206 Using KFABA	59
2.4.4.4	Synthesis of Pd1206 Using KFABA and $\text{Li}[\text{O}_3\text{SCF}_3]$	59
2.4.4.5	Synthesis of Triisopropylphosphine Oxide	60
2.4.4.6	Triisopropylphosphonium FABA	60
2.4.4.7	Thermolysis of Pd1206 in THF- d_8	60
2.4.4.8	Thermolysis of Pd1206 + LiFABA in THF- d_8	61

3.4.4.9	Thermolysis of Pd1206 + DANFABA in THF- <i>d</i> ₈	62
3.4.4.10	Thermolysis of Pd1206 + 2,6-di-tert-butylpyridine in THF- <i>d</i> ₈	62
3.4.4.11	Thermolysis of Pd1206 + bis(dimethylamino)naphthalene in THF- <i>d</i> ₈	63
3.4.4.12	Thermolysis of Pd1206 + triisopropylphosphine in THF- <i>d</i> ₈	63
3.4.4.13	Thermolysis of Pd1206 + acetic acid in THF- <i>d</i> ₈	63
3.4.4.14	Thermolysis of Pd1206 + Triethylsilane	64
2.4.4.15	Stability of Pd1165 at Ambient Temperature in THF- <i>d</i> ₈	64
2.4.4.16	Thermolysis of Pd1165 at 55°C in THF- <i>d</i> ₈	65
2.4.4.17	Thermolysis of 1 Pd1165: 1 CH ₃ CN at Ambient Temperature in THF- <i>d</i> ₈	65
2.4.4.18	Thermolysis of 1 Pd1165: 1 CH ₃ CN at 55°C in THF- <i>d</i> ₈	66
2.4.4.19	Thermolysis of Pd1162 @ 55°C in THF- <i>d</i> ₈	66
2.4.4.20	Thermolysis of 1 Pd1162: 1 CH ₃ CO ₂ H @ 55°C in THF- <i>d</i> ₈	67
2.4.4.21	Thermolysis of Pd1162 + Formic Acid @ 50°C in CDCl ₃	67
2.4.4.22	Thermolysis of Pd1165 With Pyridine in THF- <i>d</i> ₈	67
2.4.4.23	Synthesis and Characterisation of Pd1146M	68
2.4.4.24	Thermolysis of Pd1146M at Ambient Temperature in THF- <i>d</i> ₈	70
2.4.4.25	Thermolysis of Pd1146M at Ambient Temperature in CDCl ₃	71
2.4.4.26	Thermolysis of Pd1146M at 35°C in CDCl ₃	71
2.4.4.27	Attempted Thermolysis of Pd1148	72
2.4.4.28	Attempted Synthesis of [Pd(P- <i>i</i> -Pr ₃)((<i>i</i> -Pr) ₂ P-C(CH ₃)=CH ₂) ₂ (H)]- [B(C ₆ F ₅) ₄] (Pd1273H)	72
2.4.4.29	Characterisation of [Pd(P- <i>i</i> -Pr ₃) ₂ (κ ² -OAc)][B(C ₆ F ₅) ₄] (Pd1165)	72
2.4.4.30	Characterisation of [Pd(P- <i>i</i> -Pr ₃) ₂ (Me)(MeCN)][B(C ₆ F ₅) ₄] (Pd1162)	73
2.4.4.31	Characterisation of [Pd(P- <i>i</i> -Pr ₃) ₂ (H)(MeCN)][B(C ₆ F ₅) ₄] (Pd1148)	73
2.4.4.32	NMR Scale Polymerisation of <i>endo/exo</i> -5-decyl-2-norbornene using Pd1206	74
2.4.4.33	NMR Scale Polymerisation of <i>endo/exo</i> -5-decyl-2-norbornene using Pd1148	74
2.5	References	75

Chapter 3 – Fundamental Studies on Cationic Palladium Hydride Initiators for the Addition Polymerisation of Functionalised Norbornene Monomers

3.1	Introduction	76
3.2	Results and Discussion	78
3.2.1	¹ H NMR Spectroscopy – Analytical Tool for Probing Addition Polymerisation	78
3.2.2	Effect of Initiator on the Rates of Initiation and Polymerisation	79
3.2.3	Effect of Copper Salts on the Rates of Initiation and Polymerisation	80
3.2.4	Effect of Temperature on the Rate of Polymerisation	82
3.2.5	Effect of Solvent on the Rate of Polymerisation	82
3.2.6	Effect of Functional Group on the Rate of Polymerisation	83
3.2.7	Steric Size of Functional Group in Norbornene Monomers	84
3.2.8	Penultimate Group Effect	86
3.2.9	Homologation (Methylene Spacing) of Functional Group	91
3.2.9.1	Trifluoromethanesulfonamide Functionalised Norbornenes	91
3.2.9.1	Trimethylsilyl Carboxylate Functionalised Norbornenes	93
3.2.9.1	Hexafluoroalcohol Functionalised Norbornenes	97
3.3	Conclusions	98
3.4	Experimental	99
3.4.1	Materials	99
3.4.2	Instrumentation and Measurements	99
3.4.2.1	Nuclear Magnetic Resonance	99
3.4.2.2	Gel Permeation Chromatography (GPC)	99
3.4.2.3	Mass Spectroscopy	100
3.4.2.4	Infra-Red Spectroscopy	100
3.4.3	NMR Scale Addition Polymerisation Reactions – Logistics and Error	100
3.4.3.1	Effect of Initiator, Phosphine Ligand (PR ₃) on Polymerisation of <i>endo/exo</i> -5-Decyl-2-norbornene	101
3.4.3.2	Polymerisation of <i>endo/exo</i> -5-alkyl-2-norbornene using Pd1388	102
3.4.3.3	Polymerisation of Trifluoromethanesulfonamide Functionalised Norbornenes (NB(CH ₂) _n TFS) using Pd1388	104

3.4.3.4	Polymerisation of Trimethylsilyl Carboxylate Functionalised Norbornenes (NB(CH ₂) _n CO ₂ TMS) using Pd1388	105
3.4.3.5	Polymerisation of Hexafluoroisopropanol Functionalised Norbornenes (NB(CH ₂) _n HFA) using Pd1388	105
3.4.3.6	Polymerisation of Trimethoxysilyl Functionalised Norbornenes (NB(CH ₂) _n Si(OMe) ₃) using Pd1388	106
3.4.4	Characterisation of Monomers	107
3.4.4.1	Characterisation of the <i>endo</i> -Regioisomer in <i>endo/exo</i> -5-Methyl-2-norbornene	107
3.4.4.2	Characterisation of the <i>exo</i> -Regioisomer in <i>endo/exo</i> -5-Methyl-2-norbornene	108
3.4.4.3	Characterisation of the <i>endo</i> -Regioisomer in <i>endo/exo</i> -5-Butyl-2-norbornene	108
3.4.4.4	Characterisation of the <i>exo</i> -Regioisomer in <i>endo/exo</i> -5-Butyl-2-norbornene	109
3.4.4.5	Characterisation of the <i>endo</i> -Regioisomer in <i>endo/exo</i> -5-Hexyl-2-norbornene	109
3.4.4.6	Characterisation of the <i>exo</i> -Regioisomer in <i>endo/exo</i> -5-Hexyl-2-norbornene	110
3.4.4.7	Characterisation of the <i>endo</i> -Regioisomer in <i>endo/exo</i> -5-Decyl-2-norbornene	111
3.4.4.8	Characterisation of the <i>exo</i> -Regioisomer in <i>endo/exo</i> -5-Decyl-2-norbornene	111
3.4.4.9	Characterisation of the <i>endo</i> -Regioisomer in <i>endo/exo</i> -5-Benzyl-2-norbornene	112
3.4.4.10	Characterisation of the <i>exo</i> -Regioisomer in <i>endo/exo</i> -5-Benzyl-2-norbornene	112
3.4.4.11	Characterisation of <i>exo</i> -Bis(trifluoromethyl)-2-norbornene-5-ethanol	113
3.4.4.12	Characterisation of the <i>endo</i> -Regioisomer in <i>endo/exo</i> -Bis(trifluoromethyl)-2-norbornene-5-ethanol	114
3.4.4.13	Characterisation of the <i>endo</i> -Regioisomer in <i>endo/exo</i> -Bis(trifluoromethyl)-2-norbornene-5-propanol	115

3.4.4.14	Characterisation of the <i>exo</i> -Regioisomer in <i>endo/exo</i> -Bis(trifluoromethyl)-2-norbornene-5-propanol	116
3.4.4.15	Characterisation of <i>exo</i> -5-Trimethylsilyl Carboxylate-2-norbornene	116
3.4.4.16	Characterisation of <i>endo</i> -5-Trimethylsilyl Carboxylate-2-norbornene	117
3.4.4.17	Characterisation of <i>endo/exo</i> -5-Methyl Trimethylsilyl Carboxylate-2-norbornene	118
3.4.4.18	Characterisation of <i>endo/exo</i> -5-Ethyl Trimethylsilyl Carboxylate-2-norbornene	119
3.4.4.19	Characterisation of <i>endo</i> -N-(2-norbornene-5-methyl)-1,1,1-trifluoromethanesulfonamide	120
3.4.4.20	Characterisation of <i>exo</i> -N-(2-norbornene-5-methyl)-1,1,1-trifluoromethanesulfonamide	121
3.4.4.21	Characterisation of <i>endo/exo</i> -N-(2-norbornene-5-ethyl)-1,1,1-trifluoromethanesulfonamide	121
3.4.4.22	Characterisation of <i>endo/exo</i> -N-(2-norbornene-5-propyl)-1,1,1-trifluoromethanesulfonamide	122
3.4.4.23	Characterisation of <i>endo/exo</i> -5-Trimethoxysilyl-2-norbornene	123
3.4.4.24	Characterisation of <i>endo/exo</i> -5-Ethyl Trimethoxysilyl-2-norbornene	124

Chapter 4 - Investigation of *exo*-Functionalised Norbornenes and Tetracyclododecenes

4.1	Introduction	126
4.2	Results and Discussion	127
4.2.1	Synthesis and Characterisation of <i>exo</i> -5-Hydroxy-2-norbornene	127
4.2.2	Synthesis and Characterisation of <i>endo</i> -5-Hydroxy-2-norbornene	129
4.2.3	Derivatisation of <i>endo</i> - or <i>exo</i> -5-Hydroxy-2-norbornene	129
4.2.4	Characterisation of <i>endo</i> - and <i>exo</i> -5-Carboxylic Acid-2-norbornene	130
4.2.5	Synthesis and Derivatisation of <i>endo</i> and <i>exo</i> -5-Methyl Hydroxy-2-norbornene	131
4.2.6	Derivatisation of <i>endo/exo</i> -5-Ethyl Hydroxy-2-norbornene	132

4.2.7	Synthesis and Characterisation of <i>exo</i> -Tetracyclododecene Acetate	133
4.2.8	Synthesis and Characterisation of <i>endo</i> -Tetracyclododecene Acetate	134
4.2.9	Polymerisation of <i>exo</i> - and <i>endo</i> -5-Acetate-2-norbornene	135
4.2.10	Polymerisation of Acetate Functionalised Norbornenes (NB(CH ₂) _n OAc)	137
4.2.11	Polymerisation of <i>exo</i> - and <i>endo</i> -Tetracyclododecene Acetate	137
4.2.12	Polymerisation of Methoxy Functionalised Norbornenes (NB(CH ₂) _n OMe)	139
4.3	Conclusions	140
4.4	Experimental	141
4.4.1	Materials	141
4.4.2	Instrumentation and Measurements	141
4.4.2.1	Nuclear Magnetic Resonance	141
4.4.2.2	Mass Spectroscopy	142
4.4.2.3	Infra-red Spectroscopy	142
4.4.3	General Synthesis	142
4.4.3.1	General Preparation of NB(CH ₂) _n OAc From NB(CH ₂) _n OH	142
4.4.3.2	General Preparation of NB(CH ₂) _n OH From NB(CH ₂) _n CO ₂ H	142
4.4.3.3	General Preparation of NB-(CH ₂) _n OMe From NB(CH ₂) _n OH	143
4.4.4	Monomer Synthesis and Characterisation	144
4.4.4.1	Synthesis and Characterisation of <i>exo</i> -5-Acetate-2-norbornene	144
4.4.4.2	Synthesis and Characterisation of <i>exo</i> -5-Hydroxy-2-norbornene	145
4.4.4.3	Synthesis and Characterisation of 2-Norbornene-5-one (method 1)	146
4.4.4.4	Alternative Synthesis and Characterisation of 2-Norbornene-5-one (method 2)	146
4.4.4.5	Synthesis and Characterisation of <i>endo</i> -5-Hydroxy-2-norbornene (method 1)	147
4.4.4.6	Alternative Synthesis and Characterisation of <i>endo</i> -5-Hydroxy-2-norbornene (Method 2)	148
4.4.4.7	Synthesis and Characterisation of <i>endo</i> -5-Acetate-2-norbornene	149
4.4.4.8	Synthesis and Characterisation of <i>exo</i> -Tetracyclododecene Acetate	150
4.4.4.9	Synthesis and Characterisation of <i>endo</i> -Tetracyclododecene Acetate	151
4.4.4.10	Characterisation of <i>endo</i> -5-Carboxylic Acid-2-norbornene	153

4.4.4.11	Characterisation of <i>exo</i> -5-Carboxylic Acid-2-norbornene	153
4.4.4.12	Synthesis and Characterisation of <i>exo</i> -5-Methyl Hydroxy-2-norbornene	154
4.4.4.13	Synthesis and Characterisation of <i>endo</i> -5-Methyl Hydroxy-2-norbornene	155
4.4.4.14	Synthesis and Characterisation of <i>exo</i> -5-Methyl Methoxy-2-norbornene	156
4.4.4.15	Characterisation of <i>endo</i> -5-Methyl Methoxy-2-norbornene	157
4.4.4.16	Synthesis and Characterisation of <i>exo</i> -5-Methoxy-2-norbornene	158
4.4.4.17	Synthesis and Characterisation of <i>endo</i> -5-Methyl Acetate-2-norbornene	159
4.4.4.18	Synthesis and Characterisation of <i>exo</i> -5-Methyl Acetate-2-norbornene	160
4.4.4.19	Synthesis and Characterisation of <i>endo/exo</i> -5-Ethyl Methoxy-2-norbornene	161
4.4.4.20	Synthesis and Characterisation of <i>endo/exo</i> -5-Ethyl Acetate-2-norbornene	162
4.4.4.21	Synthesis and Characterisation of <i>exo</i> -5-Benzoxy-2-norbornene	163
4.4.4.22	Synthesis and Characterisation of <i>exo</i> -5-(11-Phenyl Benzoxy)-2-norbornene	164
4.4.4.23	Synthesis and Characterisation of <i>exo</i> -5-(12-Bromo Benzoxy)-2-norbornene	165
4.4.5	NMR Scale addition Polymerisation Reactions	166
4.4.6	Polymerisation of Functionalised Norbornenes Using Pd1388	166
4.5	References	168

Chapter 5 - Investigation of Family of Monomers Based on *endo*-5-Methyl-*exo*-5-carboxylic Acid-2-norbornene

5.1	Introduction	169
5.2	Results and Discussion	170
5.2.1	Synthesis Tree	170

5.2.2	Synthesis and Characterisation of <i>endo</i> -5-Methyl- <i>exo</i> -5-carboxylic Acid-2-norbornene	170
5.2.3	Synthesis of the Trimethylsilyl Carboxylate Functionalised Norbornenes (NB(N-Me)(X-(CH ₂) _n CO ₂ TMS))	171
5.2.4	Synthesis of <i>endo</i> -5-Methyl- <i>exo</i> -5-methyl Hydroxy-2-norbornene	172
5.2.5	Synthesis of <i>endo</i> -5-Methyl- <i>exo</i> -5-methyl Methoxy-2-norbornene	172
5.2.6	Synthesis of <i>endo</i> -5-Methyl- <i>exo</i> -5-methyl Carboxylic Acid-2-norbornene	172
5.2.7	Attempted Synthesis of <i>endo</i> -5-methyl- <i>exo</i> -5-methylmagnesium Bromide-2-norbornene	174
5.2.8	Polymerisation of Monomers	174
5.3	Conclusions	177
5.4	Experimental	177
5.4.1	Materials	177
5.4.2	Instrumentation and Measurements	178
5.4.2.1	Nuclear Magnetic Resonance	178
5.4.2.2	Mass Spectroscopy	178
5.4.2.3	Infra-red Spectroscopy	178
5.4.3	Monomer Synthesis and Characterisation	179
5.4.3.1	Synthesis and Characterisation of <i>endo</i> -5-Methyl- <i>exo</i> -5-carboxylic Acid-2-norbornene	179
5.4.3.2	Synthesis and Characterisation of <i>endo</i> -5-Methyl- <i>exo</i> -5-trimethylsilyl Carboxylate-2-norbornene	180
5.4.3.3	Synthesis and Characterisation of <i>endo</i> -5-Methyl- <i>exo</i> -5-methyl Hydroxy-2-norbornene	181
5.4.3.4	Synthesis and Characterisation of <i>endo</i> -5-Methyl- <i>exo</i> -5-methyl Methoxy-2-norbornene	182
5.4.3.5	Synthesis and Characterisation of <i>endo</i> -5-Methyl- <i>exo</i> -5-methoxymesylate-2-norbornene	183
5.4.3.6	Synthesis and Characterisation of <i>endo</i> -5-Methyl- <i>exo</i> -5-bromomethyl-2-norbornene	184
5.4.3.7	Synthesis and Characterisation of <i>endo</i> -5-Methyl- <i>exo</i> -5-cyanomethyl-2-norbornene	185
5.4.3.8	Synthesis and Characterisation of <i>endo</i> -5-Methyl- <i>exo</i> -5-methyl Carboxylic Acid-2-norbornene	187

5.4.3.9	Synthesis and Characterisation of <i>endo</i> -5-Methyl- <i>exo</i> -5-methyl Trimethylsilyl Carboxylate-2-norbornene	188
5.4.4	NMR Scale Addition Polymerisation Reactions	189
5.4.5	Polymerisation of Functionalised Norbornenes using Pd1388	189
5.5	References	189

Chapter 6 - Origins of the Functional Group Homologation Effect: Molecular Modelling and NMR Spectroscopic Investigations

6.1	Introduction	191
6.2	Results and Discussion	192
6.2.1	Polymerisation Mechanism	192
6.2.2	Assessing Differences, Effects and Error	196
6.2.3	¹³ C NMR Spectroscopic Investigations	197
6.2.3.1	¹³ C NMR Spectroscopic Investigations of the <i>exo</i> -Regioisomers	198
6.2.3.2	¹³ C NMR Spectroscopic Investigations of the <i>endo</i> -Regioisomers	201
6.2.4	Molecular Modelling Studies of Carboxylic Acid Functionalised Norbornenes	202
6.2.4.1	Molecular Modelling of <i>exo</i> -Carboxylic Acid Functionalised Norbornenes	203
6.2.4.2	Molecular Modelling of <i>endo</i> -Carboxylic Acid Functionalised Norbornenes	208
6.3	Conclusions	213
6.4	References	214

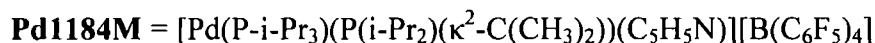
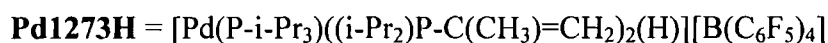
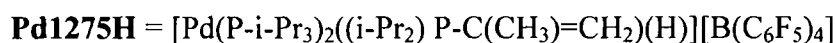
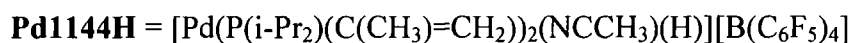
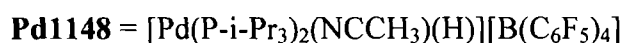
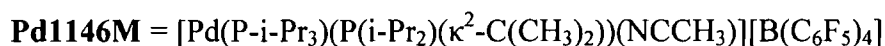
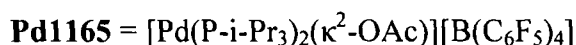
General List of Abbreviations

A	pre-exponential factor
br	broad
bs	broad singlet
Bu	butyl
Bz	benzyl
COSY	correlation spectroscopy
Cp	cyclopentyl
Cy	cyclohexyl
d	doublet
2D	2-dimensional
DANFABA	[HN(Ph)(Me) ₂][B(C ₆ F ₅) ₄]
DCM	dichloromethane
Dec	decyl
DMF	dimethylformamide
DMSO	dimethylsulphoxide
Ea	activation energy
ee	enantiomeric excess
ether	diethyl ether
FG	functional group
Et	ethyl group
EXSY	exchange spectroscopy
FABA	[B(C ₆ F ₅) ₄] ⁻
GCMS	gas chromatography mass spectroscopy
GPC	gel permeation chromatography
HFA	hexafluoroisopropanol (-C(CF ₃) ₂ OH)
HMBC	heteronuclear multiple bond correlation
H.O.M.O	highest occupied molecular orbital
h	hours
HSQC	heteronuclear single quantum correlation
Hx	hexyl
i-Pr	<i>iso</i> -propyl
IR	infrared

J	coupling constant
k	rate constant
L	ligand
L.U.M.O	lowest unoccupied molecular orbital
MAO	methyl aluminium oxide
MCM	multi chip module
Me	methyl group
MeCN	acetonitrile
mL	millilitre
M_n	number average molecular weight
M_w	number average molecular weight
n	nano
N	<i>endo</i>
NB	norbornene
NMR	nuclear magnetic resonance
NOESY	nuclear overhauser effect spectroscopy
^-OAc	acetate anion or carboxylate
^-OMs	mesylate anion (methane-sulphonic anion)
^-OTf	triflate anion (trifluoro-sulphonic anion)
^-OTs	tosylate anion (toluene-sulphonic anion)
Ph	phenyl group
PDI	polydispersity index
ppb	parts per billion
ppm	parts per million
py	pyridine
r.t	room temperature
RT	retention time
s	second
ROMP	ring opening metathesis polymerisation
t	triplet
tBu	tertiary butyl group
TCE	tetrachloroethane
TD	tetracyclododecene
T_g	glass transition temperature

TFS	trifluoromethane sulfonamide (-NHSO ₂ CF ₃)
TMS	trimethylsilyl
THF	tetrahydrofuran
μ	micro
WCA	weakly coordinating anion
X	<i>exo</i>

Catalyst Abbreviations



Monomer Abbreviations

NB = 2-norbornene = bicyclo[2.2.1]hept-2-ene

N/X-NB-Me = *endo/exo*-5-methyl-2-norbornene

N/X-NB-Bu = *endo/exo*-5-butyl-2-norbornene

N/X-NB-Hex = *endo/exo*-5-hexyl-2-norbornene

N/X-NB-Dec = *endo/exo*-5-decyl-2-norbornene

N/X-NB-Bz = *endo/exo*-5-benzyl-2-norbornene

X-NB-CH₂C(CF₃)₂OH = *exo*-bis(trifluoromethyl)-2-norbornene-5-ethanol

N-NB-CH₂C(CF₃)₂OH = *endo*-bis(trifluoromethyl)-2-norbornene-5-ethanol

N/X-NB-(CH₂)₂C(CF₃)₂OH = *endo/exo*-bis(trifluoromethyl)-2-norbornene-5-propanol
 X-NB-CO₂SiMe₃ = *exo*-5-trimethylsilyl carboxylate-2-norbornene
 N-NB-CO₂SiMe₃ = *endo*-5-trimethylsilyl carboxylate-2-norbornene
 N/X-NB-CH₂CO₂SiMe₃ = *endo/exo*-5-methyl trimethylsilyl carboxylate-2-norbornene
 N/X-NB-(CH₂)₂CO₂SiMe₃ = *endo/exo*-5-ethyl trimethylsilyl carboxylate-2-norbornene
 N-NB-CH₂NHSO₂CF₃ = *endo*-N-(2-norbornene-5-methyl)-1,1,1-trifluoromethanesulfonamide
 X-NB-CH₂NHSO₂CF₃ = *exo*-N-(2-norbornene-5-methyl)-1,1,1-trifluoromethanesulfonamide
 N/X-NB-(CH₂)₂NHSO₂CF₃ = *endo/exo*-N-(2-norbornene-5-ethyl)-1,1,1-trifluoromethanesulfonamide
 N/X-NB-(CH₂)₃NHSO₂CF₃ = *endo/exo*-N-(2-norbornene-5-propyl)-1,1,1-trifluoromethanesulfonamide
 N/X-NB-Si(OMe)₃ = *endo/exo*-5-trimethoxysilyl-2-norbornene
 N/X-NB-(CH₂)₂Si(OMe)₃ = *endo/exo*-5-ethyl trimethoxysilyl-2-norbornene
 X-NB-OH = *exo*-5-hydroxy-2-norbornene
 N-NB-OH = *endo*-5-hydroxy-2-norbornene
 X-NB-O₂CMe = *exo*-5-acetate-2-norbornene
 N-NB-O₂CMe = *endo*-5-acetate-2-norbornene
 NB=O = 2-norbornene-5-one
 X-NB-OMe = *exo*-5-methoxy-2-norbornene
 X-NB-CO₂H = *exo*-5-carboxylic acid-2-norbornene
 N-NB-CO₂H = *endo*-5-carboxylic acid-2-norbornene
 X-NB-CH₂OMe = *exo*-5-methyl hydroxy-2-norbornene
 N-NB-CH₂OH = *endo*-5-methyl hydroxy-2-norbornene
 N-NB-CH₂O₂CMe = *endo*-5-methyl acetate-2-norbornene
 X-NB-CH₂O₂CMe = *exo*-5-methyl acetate-2-norbornene
 X-NB-CH₂OMe = *exo*-5-methyl methoxy-2-norbornene
 N-NB-CH₂OMe = *endo*-5-methyl methoxy-2-norbornene
 N/X-NB-(CH₂)₂O₂CMe = *endo/exo*-5-ethyl acetate-2-norbornene
 N/X-NB-(CH₂)₂OH = *endo/exo*-5-ethyl hydroxy-2-norbornene
 N/X-NB-(CH₂)₂OMe = *endo/exo*-5-ethyl methoxy-2-norbornene
 X-TD-OAc = *exo*-tetracyclododecene acetate = tetracyclo[4,4,0.1^{2,5}.1^{7,10}]dodec-3-ene-8-acetate
 N-TD-OAc = *endo*-tetracyclododecene acetate = tetracyclo[4,4,0.1^{2,5}.1^{7,10}]dodec-3-ene-8-acetate
 X-NB-OCH₂Ph = *exo*-5 benzoxy-2-norbornene
 X-NB-OBzPh = *exo*-5-(11-phenyl benzoxy)-2-norbornene
 X-NB-OBzBr = *exo*-5-(12-bromo benzoxy)-2-norbornene
 (N-Me)NB(X-CO₂H) = *endo*-5-methyl-*exo*-5-carboxylic acid-2-norbornene

(N-Me)NB(X-CH₂OH) = *endo*-5-methyl-*exo*-5-methyl hydroxy-2-norbornene

(N-Me)NB(X-CH₂OMe) = *endo*-5-methyl-*exo*-5-methyl methoxy-2-norbornene

(N-Me)NB(X-CH₂CO₂H) = *endo*-5-methyl-*exo*-5-methyl carboxylic acid-2-norbornene

(N-Me)NB(X-CH₂OSO₂CH₃) = *endo*-5-methyl-*exo*-5-methoxy-mesylate-2-norbornene

(N-Me)NB(X-CH₂CN) = *endo*-5-methyl-*exo*-5-cyanomethyl-2-norbornene

(N-Me)NB(X-CH₂Br) = *endo*-5-methyl-*exo*-5-bromomethyl-2-norbornene

(N-Me)NB(X-CH₂MgBr) = *endo*-5-methyl-*exo*-5-methylmagnesium bromide-2-norbornene

(N-Me)NB(X-CO₂SiMe₃) = *endo*-5-methyl-*exo*-5-trimethylsilyl carboxylate-2-norbornene

(N-Me)NB(X-CH₂CO₂SiMe₃) = *endo*-5-methyl-*exo*-5-methyl trimethylsilyl carboxylate-2-norbornene

Chapter 1

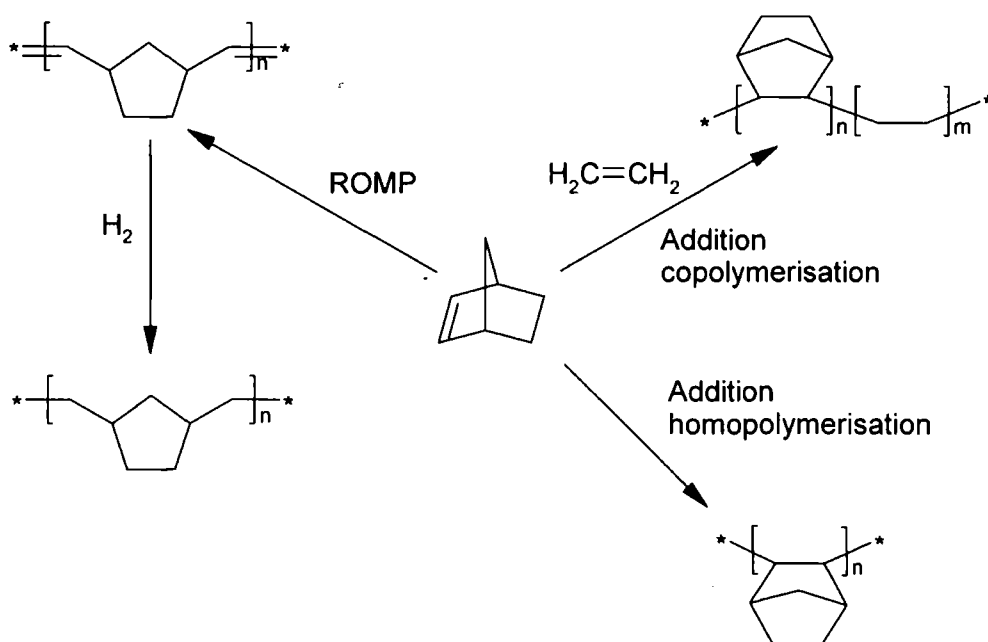
1 General Introduction and Background

1.1 Introduction

It is well recognised that polymers prepared by the polymerisation of cyclic olefins represent the next platform of high performance materials for a variety of demanding, emerging optical applications, due to two factors: the development of new single-site catalysts that will polymerise these types of monomers with good activity; the realisation that polymers containing sufficient quantities of these bicyclic monomers exhibit unique properties such as high glass transition temperature and transparency.

There are three different mechanisms shown in scheme 1.1, by which norbornene can be polymerised to reasonably high molecular weights: ring opening metathesis polymerisation (ROMP); vinyl addition co-polymerisation with acyclic olefins such as ethylene, and vinyl addition homo-polymerisation. Carbocationic and free-radical initiated polymerisations are ignored since they yield only low molecular weight oligomers.¹





Scheme 1.1. The different types of norbornene polymerisation.

ROMP and vinyl addition co-polymerisation of cyclic olefins (e.g. norbornene) and acyclic olefins (e.g. ethylene) produce amorphous polymers with good optical properties. ROMP polymers suffer from thermo-oxidative instability due to the presence of allylic hydrogens. However, the Japanese company, Nippon Zeon, commercialised hydrogenated versions of ROMP polymers in order to make them more stable to oxidation (e.g. Zeonex[®], Zeonor[®], and Arton[®]). While the co-polymerisation of norbornene with ethylene creates polymers without allylic hydrogens, these copolymers suffer from relatively low glass transition temperatures (T_g), around 140 - 180°C. However, for certain applications, this T_g is sufficient and this polymer has been commercialised as Topas^{®2} and Apel[®],³ by Ticona. Topas[®] is a co-polymer from norbornene and ethylene made through metallocene polymerisation.

This review is particularly concerned with developments of late transition metals, in particular palladium, for the addition polymerisation of norbornenes, with the emphasis on the synthesis of functionalised norbornene polymers for a variety of reasons:

- a) Functionalised norbornenes represent a wide variety of monomers and hence polymers and application areas.

b) This area has developed into a number of commercial applications, thanks largely to the pioneering work carried out by Promerus LLC, formerly B. F. Goodrich Company, using cationic palladium initiators.

1.2 Addition Polymerisation Catalyst Development Using Late Transition Metals

The vinyl addition homo-polymerisation of norbornene, resulting in poly(2,3-norbornene) was first mentioned in the early 1960's using classical TiCl_4 -based Ziegler systems.⁴ These catalysts afforded only very low molecular weight materials (molecular weights < 1000) at low yields. Metallocene catalysts, which consist of a metallocene of group IV (mostly zirconium) and methyl aluminium oxide (MAO) as co-catalyst are reported to afford high polymers, but these polymers decompose in air at high temperatures before they melt and are insoluble in organic solvents, figure 1.1.⁵

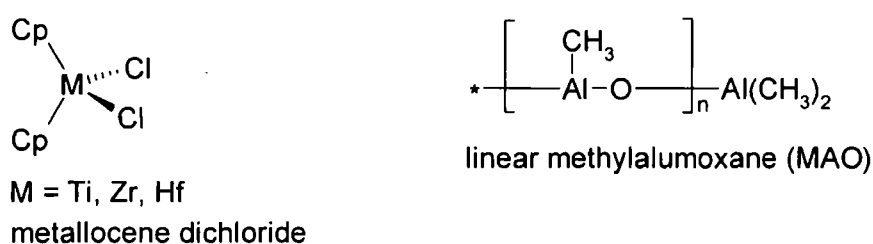


Figure 1.1

Additionally, for the homo-polymerisation of norbornene, zirconocene catalysts exhibit low activity and require the use of a large excess of expensive MAO.

The first vinyl polymerisation of norbornene and substituted norbornene derivatives with palladium catalysts was mentioned in 1966 using PdCl_2 ,⁶ and then again in the late 1970's using $\text{PdCl}_2(\text{C}_6\text{H}_5\text{CN})_2$ and also $\text{PdCl}_2(\text{Ph}_3\text{P})_2$.⁷

Eventually, the cationic palladium(II) catalyst system $[\text{Pd}(\text{CH}_3\text{CN})_4][\text{BF}_4]_2$ became the most frequently mentioned system for the polymerisation of norbornene, figure 1.2. Sen's team first introduced the system in 1981 with regard to the polymerisation of olefins.⁸

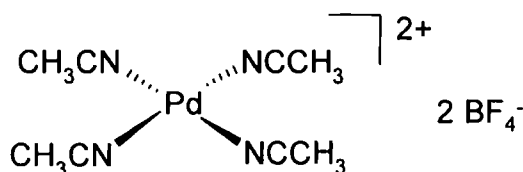


Figure 1.2

It was not until 1991 that the polymers being produced by the above catalyst were effectively characterised by Risse.⁹ When the vinyl polymerisation of norbornene was carried out in solvents such as nitromethane, the resulting polymers were reasonably soluble in solvents such as tetrachloroethylene and chlorinated aromatics. Characterisation showed these polymers to have molecular weights in excess of 100000 and high glass transition temperatures ($T_g > 300^\circ\text{C}$).

The most significant aspect of the research carried out by Risse was that he demonstrated the ability of palladium catalysts such as $(\eta^3\text{-allyl})\text{Pd}(\text{II})(\text{SbF}_6)$, to tolerate substituted norbornene monomers; importantly oxygen functionalised norbornene monomers such as esters.¹⁰ The addition polymerisation of *exo*- and *endo*-5-ester-2-norbornene monomers were investigated.¹¹ However, the rate of polymerisation was reduced in comparison with non-oxygen containing monomers. Unlike early transition metals, late transition metals are more tolerant of oxygen functionalities in the monomer and polymer. This behaviour stems from the preference of the late transition metals for soft ligands due to their higher electronegativity and lower oxidation states. This allows these palladium catalysts to have a high tolerance toward functional groups (such as carboxylic acids, esters and ethers) and therefore allows the homo- and co-polymerisation of a wide variety of norbornene monomers bearing functional groups. This discovery has driven the development of cationic palladium initiators, in the anticipation that they will permit the formation of novel functionalised polymers for optoelectronic applications.

A broad family of new single- and multi-component catalysts were discovered by the B. F. Goodrich Company, for the polymerisation of norbornene type monomers based on nickel and palladium. Unlike the ROMP route, a saturated (thermally and oxidatively stable) polymer is generated in a single step. Moreover, unlike the ethylene/norbornene co-polymerisation route, it is possible to achieve complete conversion of the norbornene monomer, eliminating the need for recycling of the monomer. The most successful of these

early catalysts was the “naked” nickel system, $[(\eta^3\text{-allyl})\text{Ni}(1,5\text{-cyclooctadiene})]^+$ (figure 1.3), so called because all of its ligands could be easily displaced by monomer.¹²

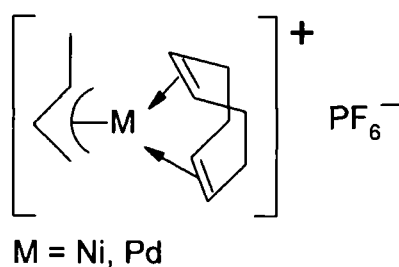
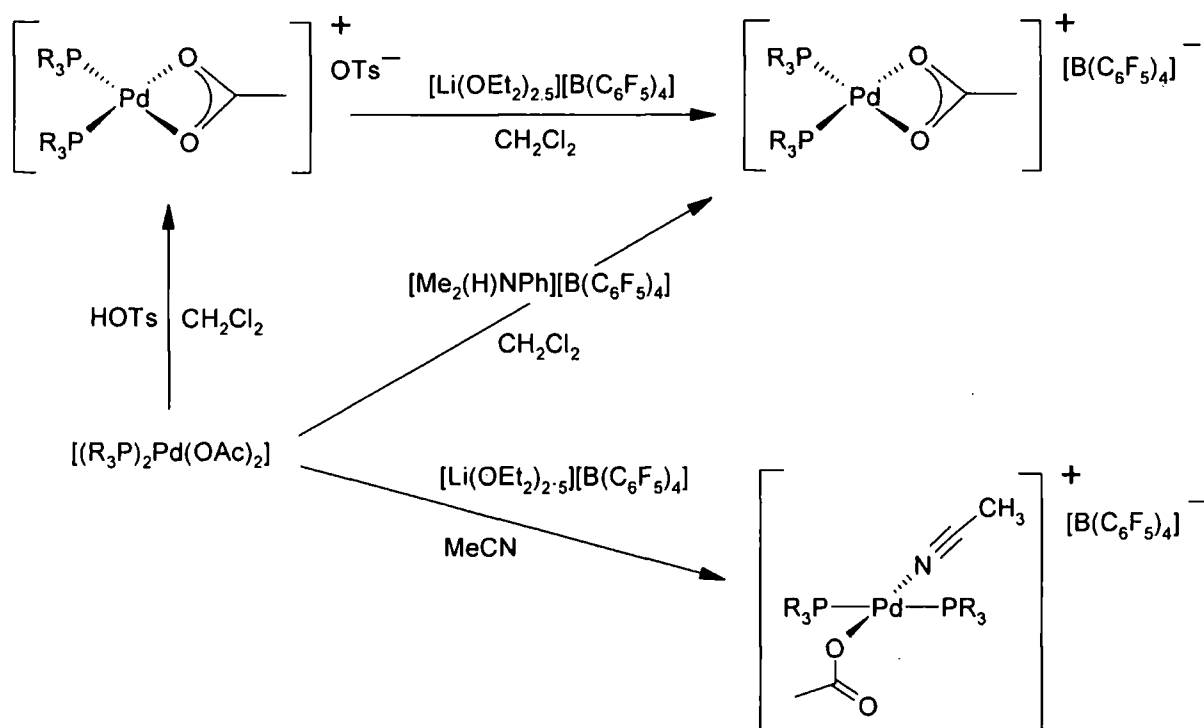


Figure 1.3

The palladium analogue was shown to be surprisingly less active and so further higher activity derivatives have been produced.^{13, 14} The systems described then rely on a cationic palladium complex containing an initiating ligand (metal-carbon σ -bond, which can be part of an allylic system), a neutral, two-electron-donor phosphine ligand, and a weakly coordinating anion. An example of such a complex is the highly active catalyst based on η^3 -allyl palladium complexes coordinated by phosphine ligands. The palladium complex $[(\eta^3\text{-allyl})\text{Pd}(\text{PCy}_3)(\text{ether})][\text{B}(3,5\text{-(CF}_3)_2\text{C}_6\text{H}_3)_4]$ was found to co-polymerise 5-butyl-2-norbornene and 5-triethoxysilyl-2-norbornene (95:5 molar ratio) with truly high activity and is capable of producing more than a metric tonne of co-polymer per mole of Pd per hour.¹³ Other more basic neutral nickel catalysts such as $(\eta^6\text{-toluene})\text{Ni}(\text{C}_6\text{F}_5)_2$, have found utility in the polymerisation of highly functionalised monomers for photoresist applications.¹⁵

During efforts to explain how mixtures of *trans*- $[(\text{R}_3\text{P})_2\text{Pd}(\text{OAc})_2]$ and either $[\text{Li}(\text{Et}_2\text{O})_{2.5}][\text{B}(\text{C}_6\text{F}_5)_4]$ or $[\text{Me}_2(\text{H})\text{NC}_6\text{H}_5][\text{B}(\text{C}_6\text{F}_5)_4]$ are able to promote the polymerisation of norbornene upon thermal activation,¹⁶ several novel cationic palladium acetate complexes were discovered and structurally characterised, scheme 1.2.^{17, 18, 19}



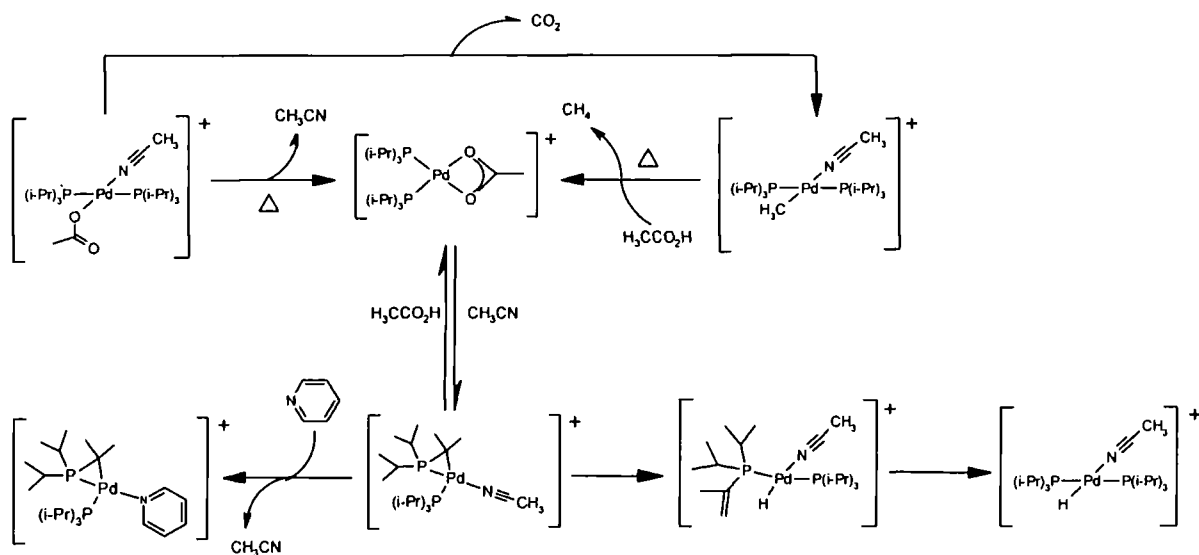
Scheme 1.2. Synthesis of novel cationic palladium acetate complexes.

Performing acetate abstraction reactions using $[Li(OEt)_{2.5}][B(C_6F_5)_4]$ or $[Me_2(H)NPh][B(C_6F_5)_4]$ in acetonitrile led to the selective formation of *trans*- $[(R_3P)_2Pd(OAc)(MeCN)][B(C_6F_5)_4]$ ($R = Cy, ^iPr$) bearing mono-dentate acetate ligands. The geometry of the palladium centre was shown by crystallographic analysis to be square planar. It was shown that a chelating acetate binding mode, $[(R_3P)_2Pd(\kappa^2-OAc)][B(C_6F_5)_4]$ ($R = Cy, ^iPr$) could be generated by altering the reaction solvent to CH_2Cl_2 . More effective carboxylate abstraction procedures allowed the synthesis of $[(R_3P)_2Pd(\kappa^2-OAc)][B(C_6F_5)_4]$ ($R = Cy, ^iPr$) in high yield and purity.

The acetonitrile is labile, and various Lewis base adducts are easily accessible in high yields, although the addition of acetonitrile to $[(R_3P)_2Pd(\kappa^2-OAc)][B(C_6F_5)_4]$ does not produce $[(R_3P)_2Pd(OAc)][B(C_6F_5)_4]$. The addition of acetonitrile to $[(R_3P)_2Pd(\kappa^2-OAc)][B(C_6F_5)_4]$ results in the reversible formation of a three-membered palladacycle via elimination of acetate as acetic acid and β -hydrogen elimination from one of the Me_2CH groups of iPr_3P ligands. The phosphines in this palladacycle were suggested to be in a *cis*-conformation around palladium via the 1H NMR spectroscopic investigation, showing small $^2J_{pp}$ coupling constants (29 and 30 Hz, respectively). The yield of the palladium metallacycles were

increased by the addition of sodium carbonate but a clean sample was not obtained. The addition of two equivalents of pyridine to $[(R_3P)_2Pd(\kappa^2-OAc)][B(C_6F_5)_4]$ resulted in the quantitative formation of the closely related palladacycle, allowing for crystallographic analysis. The X-ray structural diagram confirmed the *cis* arrangement of phosphines around palladium. These new cationic carboxylate complexes were shown to be competent thermally activated catalyst pro-initiators for the addition polymerization of norbornene derivatives.

Unlike conventional palladium catalysts bearing Pd-R or Pd-H bonds that are set for olefin insertion, these catalysts lack such groups, and thus have had their thermolytic behaviour examined, scheme 1.3.¹⁸ The solution thermolysis of $[(R_3P)_2Pd(OAc)(MeCN)][B(C_6F_5)_4]$ ($R = Cy, ^iPr$) at elevated temperatures, analysed via 1H and ^{31}P NMR spectroscopy revealed new cationic palladium complexes. The main product of the thermolysis is the cationic palladium hydride complex $[(R_3P)_2Pd(H)(MeCN)][B(C_6F_5)_4]$. Analysis of the gaseous products produced during thermolysis via GCMS revealed CO_2 and CH_4 .



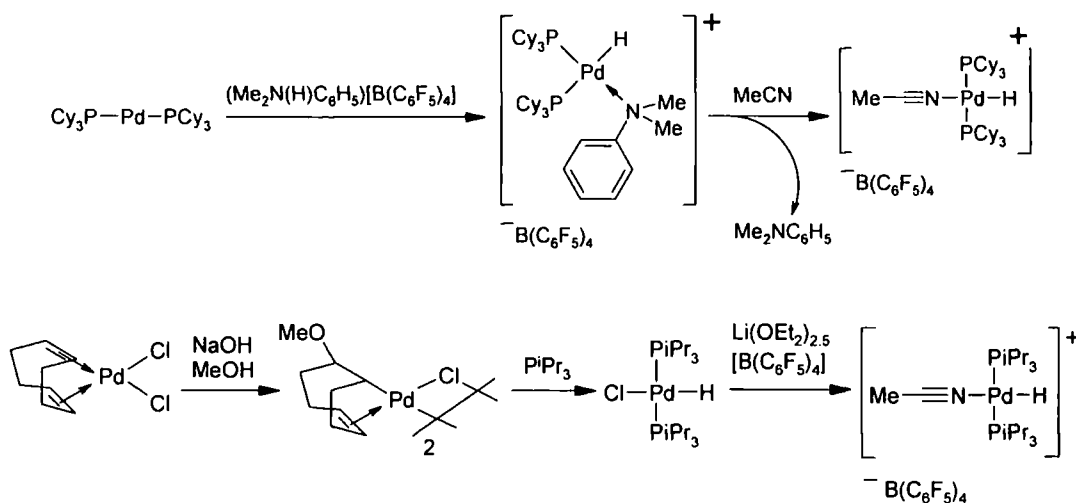
Scheme 1.3. Proposed mechanism for the thermolysis of $[(^iPr_3P)_2Pd(OAc)(MeCN)][B(C_6F_5)_4]$.^{16, 17, 18, 19}

Although the patent¹⁸ suggests the thermolysis mechanism and potential cationic palladium complexes involved in $[(R_3P)_2Pd(H)(MeCN)][B(C_6F_5)_4]$ formation, no evidence is given for many of the speculated intermediates.

Palladium hydride complexes have found diverse usage in numerous synthetic transformations. Palladium hydride complexes such as *trans*-MHX(PR₃)₂, where M = Ni or Pd, have been shown to act as catalysts for many organic transformations, especially when the products involve hydrogen transfers,²⁰ such as butadiene oligomerisation.²¹ The multiple insertion of bulky aromatic isocyanide into the palladium-hydride bond of *trans*-[Pd(H)Cl(PPh₃)₂], leading to formation of heterobicyclic and pyrrole compounds has been demonstrated.²²

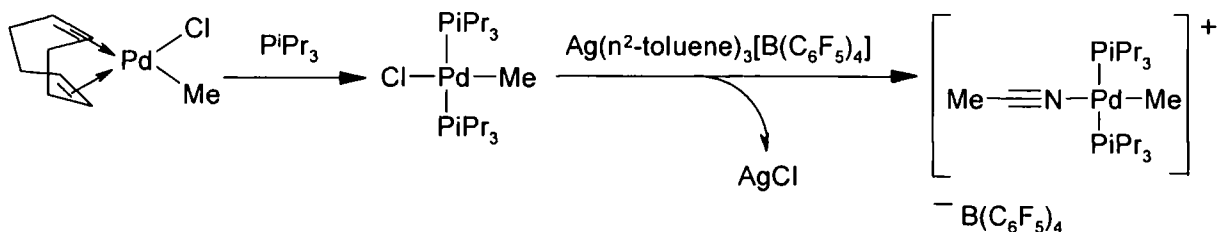
In contrast to the neutral palladium hydride complexes described, the preparation and usage of cationic palladium hydride complexes has received far less attention. A few publications claim the active species during their respective reactions are *in situ* formed cationic palladium hydride species.²³ The suggestion that cationic palladium hydride complexes may be the active component for the polymerisation of norbornene monomers has led Promerus LLC to create new and adapt previous methodology for their formation.

The syntheses of [(R₃P)₂Pd(H)(L)][X] (where R = ^tBu or Cy, L = H₂O or CH₃CN, X = BF₃OH, BF₄ or BPh₄) have been described in early literature from the corresponding palladium(II) bis(trialkylphosphine) via oxidative addition of acids such as [H₃O⁺][X⁻] (X = BF₃OH or BF₄).²⁴ The cationic palladium hydrides [PdH(PR₃)(dppe)]⁺[PF₆]⁻, where R = cyclohexyl or ^tPr, have also been prepared and their reactions with butadiene explored.²¹ Protasiewicz *et al.* showed the treatment of Pd(PCy₃)₂ with [Me₂(H)NPh][B(C₆F₅)₄] in acetonitrile, can be used to produce [(Cy₃P)₂Pd(H)(Me₂NPh)][B(C₆F₅)₄], which can be readily converted to [(Cy₃P)₂Pd(H)(MeCN)][B(C₆F₅)₄] via sonication to eliminate dimethylaniline, scheme 1.4. The synthesis of the thermally stable hydrides of palladium of the type (^tPr₃P)₂Pd(Cl)H is described in the literature,²⁵ so only the extraction of the chloride is needed to generate the desired [(^tPr₃P)₂Pd(H)(MeCN)][B(C₆F₅)₄], scheme 1.4.



Scheme 1.4. Syntheses of $[(R_3P)_2Pd(H)(MeCN)][B(C_6F_5)_4]$.

The generation of $[(^iPr_3P)_2Pd(Me)(MeCN)][B(C_6F_5)_4]$ occurs in an analogous way to palladium hydride formation, scheme 1.5.



Scheme 1.5. Synthesis of $[(^iPr_3P)_2Pd(Me)(MeCN)][B(C_6F_5)_4]$.

The synthesis new, well defined, high activity addition polymerisation catalysts, from a perspective of improved activity and functional group tolerance is vital if continued improvements are to be made in polymeric optoelectronic materials. Whilst the role of the catalyst is undoubtedly critical in achieving improved polymeric materials, it is also important to acknowledge and address the important roles that the monomers structure and functional group play in defining the vital characteristics of the final polymeric material.

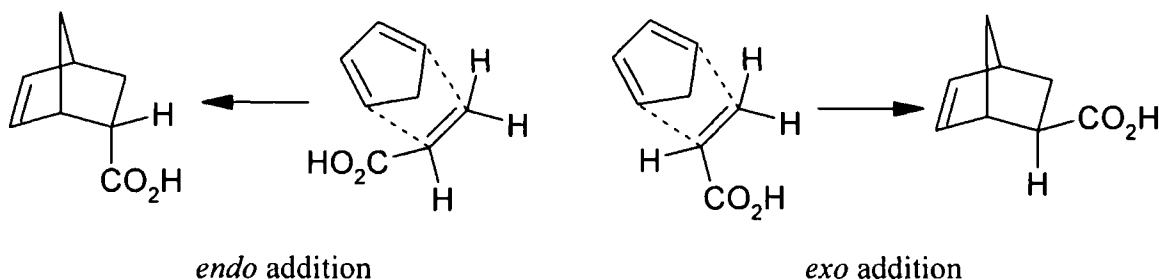
1.3 Addition Polymerisation of Functionalised Norbornenes

Metal-catalysed addition polymerisation of functionalised norbornene derivatives is an area of great current interest in polymeric materials chemistry because the addition of functionalities to a polymer that is otherwise non-polar can greatly enhance the range of

attainable properties.²⁶ The norbornene functional groups that are commonly utilised to give the optoelectronic polymeric materials their key characteristic properties (discussed later in this chapter) are esters, protected carboxylic acids, hexafluoroisopropanol, trifluoromethanesulfonamide, ethers, acetates, trimethoxysilyl and alkyl. The diversity of norbornene functional groups utilised in the making these polymeric materials can create problems since they all affect the norbornene monomers polymerisation activity differently. This section will review the key challenges that are being faced within the addition polymerisation of functionalised norbornene monomers.

1.3.1 Synthesis of Norbornene Monomers via Diels-Alder Route

Current norbornene functionalisation strategies are based primarily upon elaboration of esters synthesised as an 80:20 *endo/exo* isomeric mixture via the Diels-Alder reaction of cyclopentadiene and asymmetric dienophiles. When the diene is cyclic, there are two possible ways in which addition can occur if the dienophile is not symmetrical. The larger side of the dienophile may be under the ring (*endo* addition), or it may be the smaller side (*exo* addition), scheme 1.6.



Scheme 1.6

In this work, *exo*- or *endo*-addition can occur depending upon the conditions. Under moderate temperature conditions the addition is predominately *endo*, the kinetically favoured product. This is usually attributed to the fact that the dienophile is added so as to give a maximum of 'secondary overlap' of π -molecular orbitals in the transition state. In order to obtain the more thermodynamically stable *exo*-adduct, severe temperature conditions, longer reaction times and repeated recrystallisations are usually necessary.²⁷ The pure 100% *exo*- or *endo*-isomers are not formed initially in the diene synthesis.

Earlier work in other labs^{28, 10} as well as our own has shown that the *endo*-functionalised norbornenes are polymerised more slowly. The drop in polymerisation rates for *endo/exo* norbornene mixtures has been attributed to many different factors, discussed in the following sections.

1.3.2 Effect of Stereochemistry, Size and Chelate Formation

The formation of a chelate can occur by coordination of the metal to the functionality and the C=C bond along the *endo* face, figure 1.4.



Figure 1.4. Modes of bonding for functionalised norbornene derivatives (X = coordinating functionality).

This has two detrimental effects on polymerisation. First, chelation strengthens metal-olefin interaction, thereby raising the barrier for the insertion step. Second, it forces insertion through the *endo* face, in contrast to the known preference for norbornene to insert into metal-carbon bonds through the less hindered *exo* face.²⁹

The *endo, endo* insertion of the *endo* isomer of an ester-functionalised norbornene into the Pt-H bond of $(Et_3P)_2PtH^+$ results in the formation of a chelate platinum complex, figure 1.5.³⁰ The chelate system was determined conclusively using NMR and crystallographic analysis and owes its stability to the stable six member chelate ring.

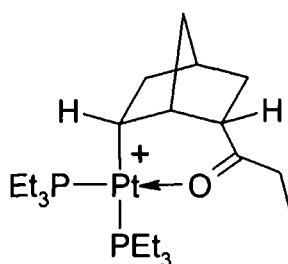
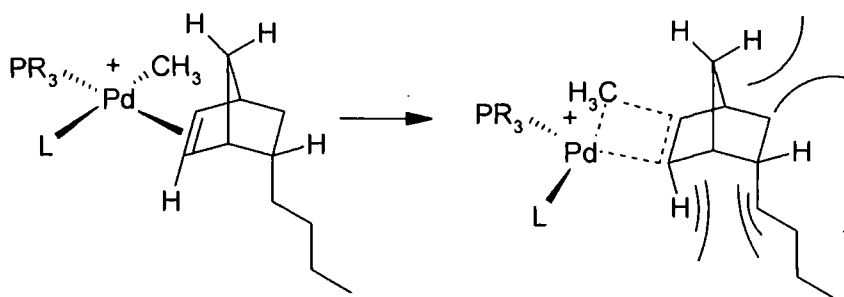


Figure 1.5. Model chelate platinum complex.

The coordination of the *endo* functionality is not the sole explanation for the preferential uptake of the *exo*-isomers. 5-Butyl-2-norbornene exhibits a huge preference for *exo* uptake. The rate of polymerisation has been shown to decrease in the order 5-butyl-2-norbornene > 5-hexyl-2-norbornene > 5-decyl-2-norbornene.³¹



Scheme 1.7. Steric compression in the insertion of the *endo*-5-butyl-2-norbornene.

Even for coordination and insertion through the *exo* face, in the *endo* isomer there is an unfavourable interaction between the substituent and the vinylic hydrogen, which is being rehybridised from sp^2 to sp^3 , upon coordination and insertion into the palladium-alkyl bond, scheme 1.7. This raises the energy barrier for the insertion of the *endo* isomer, resulting in a decreased polymerisation rate.

1.3.3 Effect of Functional Group

In addition to coordination-chelation and steric effects, a further, and even greater, reason for the diminution of activity of both the *endo*- and the *exo*-functionalised isomers is simply the coordination of the functionality to the metal centre, figure 1.6.

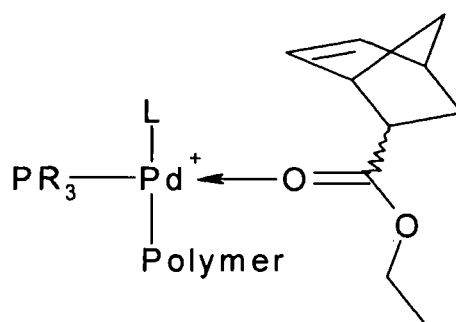


Figure 1.6. Chelation by *exo*- or *endo*-5-ethyl ester-2-norbornene.

This was supported by the observation that coordinating solvents, such as acetonitrile sharply attenuate the polymerisation activity of the catalyst.

The electronic effect of the functional group opposite the C=C bond has been largely dismissed for both addition polymerisation and ROMP. The Sen group recently quoted “On the basis of ^{13}C shifts, one can surmise that the electronic effect of the substituents on the C=C bond is minimal (not surprising given the distance between the two). Thus, the vinyl carbons of norbornene resonate at 135.5 ppm, while those of 5-ethyl ester-2-norbornene appear at 137.7 and 132.5 ppm (*endo*) and 138.1 and 135.9 ppm (*exo*)”.³¹

In contrast, William Tam’s group have carried out extensive research into the long-range electronic effects that substituents in various places on norbornene and norbornadiene have on the C=C bond.³² They have demonstrated that the rates of various cycloaddition, oxymercuration and palladium catalysed hydroarylation reactions with the C=C bond of 5 or 7-substituted norbornenes is greatly controlled by the electron donating or withdrawing ability of the substituents, the conclusion being that electron withdrawing substituents give lower rates of cycloaddition in all cases, figure 1.7.

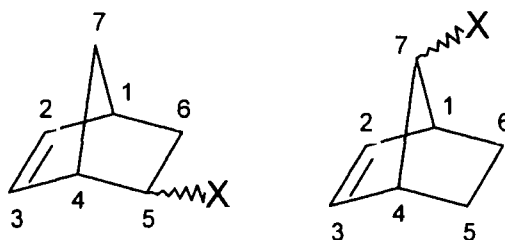


Figure 1.7. 5- and 7-substituted norbornenes

They have also used theoretical computational investigations to rationalise the effects of the substituents on the regio-selectivity in terms of extra negative charge at the carbon atoms C₂ and C₃. The charge distribution between C₂ and C₃ upon substitution at the 5-position of norbornene depends on the position of the substituents (*exo* or *endo*) and on its conformation. For the *exo* forms the extra negative charge is always at C₃ where as it is variable for *endo* isomers.

1.4 Synthesis of *exo*-Functionalised Norbornene Monomers

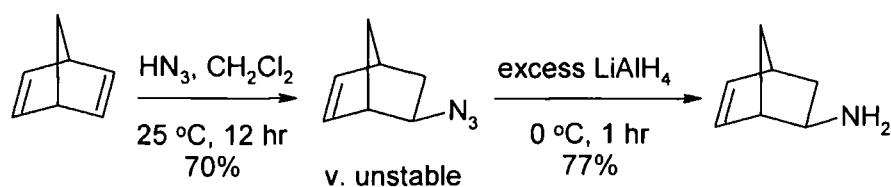
The much scrutinised and detrimental effect that *endo* functionalised norbornene monomers have on the rate of addition polymerisation and ROMP has led many research groups³³ to employ the use of isomerically pure *exo*-norbornene monomers. The monomers currently utilised by our own and other research groups for ROMP are commonly *exo*-norbornene esters³⁴ and N-alkyl-*exo*-dicarboxyimides (nadimides).³⁵ The development and utilisation of these two types of monomers for addition polymerisation has received far less attention due to the low molecular weights obtained in the case of nadimides³⁶ and time consuming preparations needed in the case of *exo*-norbornene esters.

Bell *et al.* have developed convenient and efficient routes to *exo*-5-carboxylic acid-2-norbornene and *exo*-5-allyl-2-norbornene. From these *exo*-functionalised norbornene monomers a whole new range of previously inaccessible *exo*-functionalised norbornene monomers have been obtained, many of which are used during the course of this thesis. These new monomers are particularly useful since they can be modified into a large range of functionalities and also allow standard chain extension techniques to be employed, resulting in methylene spaced functional groups. This methylene spacing of the norbornene functional group is thought to be particularly useful in reducing the electronic effect of the functionality on the C=C of the norbornene monomer, described by Tam *et al.*³² My own literature search for other accessible routes to *exo*-norbornene monomers will be discussed in this section.

1.4.1 Synthesis of *exo*-5-Amino-2-norbornene

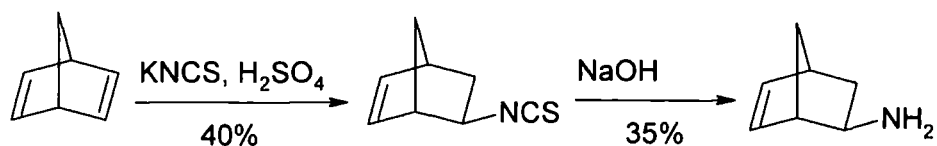
exo-5-Amino-2-norbornene (*exo*-NB-NH₂) has potential as a new *exo* monomer due to the ease with which it can be elaborated upon to provide functionality in the resulting polymer. Primary amines can be alkylated by reaction with a primary alkyl halide, although these are difficult to control and often give mixtures of products. Primary and secondary amines can also be acylated by reaction with acid chlorides or acid anhydrides to yield amides.

The polar addition of hydrazoic acid to norbornadiene gives *exo*-5-azido-2-norbornene³⁷ (*exo*-NB-N₃) in good yield (70%) but this compound slowly polymerises when neat, if allowed to stand overnight at room temperature. Thus, the azide has to be used in the next step immediately, which rules out the possibility of purification by distillation due to the high temperatures involved and therefore column chromatography is used instead, which can only be used on a relatively small scale. The azide can be readily converted to the corresponding amine via reduction with lithium aluminium hydride, with subsequent purification via column chromatography on silica gel, scheme 1.8.



Scheme 1.8. Synthesis of *exo*-5-amino-2-norbornene.

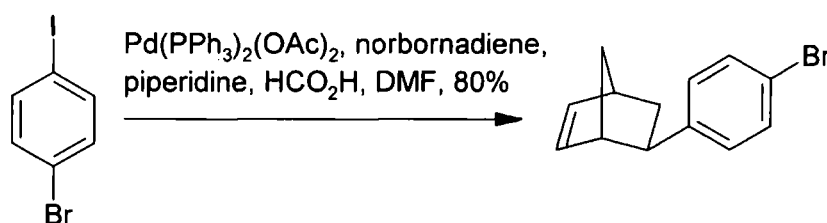
exo-5-amino-2-norbornene can also be readily obtained in two steps from the reaction of norbornadiene with potassium isothiocyanate to afford the *exo*-5-isothiocyanate-2-norbornene, which can be readily reduced with lithium aluminium hydride to give *exo*-5-amino-2-norbornene, scheme 1.9.³⁸ Although this synthetic pathway suffers from low yields, it has the advantage that it can be scaled-up relatively easily due to both steps relying on distillation under reduced pressure, for purification.



Scheme 1.9. Alternative synthesis of *exo*-5-amino-2-norbornene

1.4.2 Synthesis of *exo*-5-Aryl-2-norbornenes

The formation of C-C bonds is increasingly investigated by enantioselective catalysis with the palladium-catalysed hydroarylation of norbornadiene, being a new reaction of this type. The palladium(II) acetate catalysed hydroarylation of norbornadiene with aryl iodides, triethylamine and formic acid was rendered enantioselective by using optically active phosphine ligands as co-catalysts.³⁹ This method has produced *exo*-5-aryl-2-norbornenes with enantioselectivities of up to 40.6 % ee. The most promising reaction of this kind is where 4-bromiodobenzene was coupled to norbornadiene via a palladium catalysed *exo*-hydroarylation reaction, scheme 1.10.⁴⁰



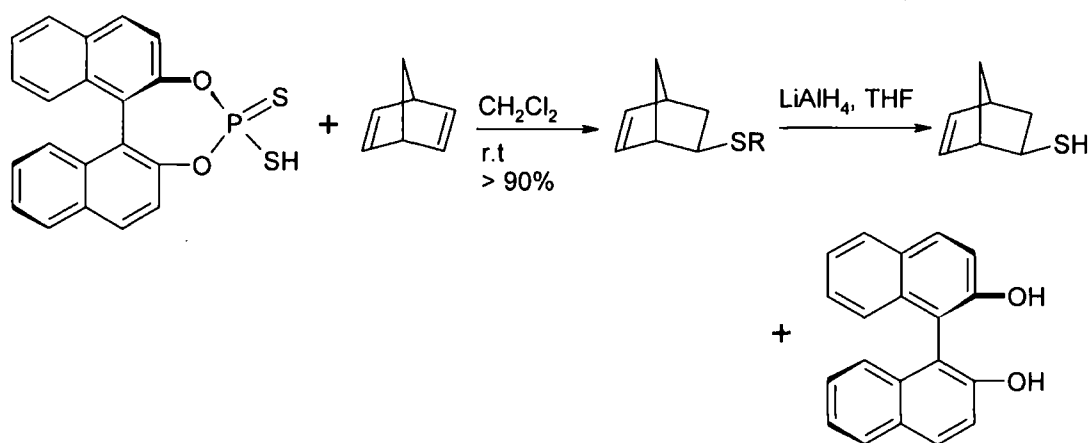
Scheme 1.10. Hydroarylation of norbornadiene.

The resulting norbornene monomer can be further elaborated upon to high yield, by coupling functional groups to the aryl group, via substitution of the bromide group.

1.4.3 Synthesis of Enantiomerically Pure *exo*-5-Thio-2-norbornene

The idea of using enantiomerically pure monomers for the syntheses of novel polymers is very interesting due to the lack of research in this area. The molecular architectures of such polymers could have an immense effect on the physical and optical properties of the

materials formed. The thiol group of such monomers should be relatively easy to functionalise, although thiols have been known to discolour the polymeric materials formed. Isomerically pure *exo*-5-mercapto-2-norbornene can be prepared in high yield,⁴¹ by the radical addition of the binaphthol-derived thiophosphonate to norbornadiene followed by recrystallisation from dichloromethane and ethanol. The intermediate is readily transformed into the free thiol by reduction with lithium aluminium hydride in THF in virtually quantitative yield, scheme 1.11.



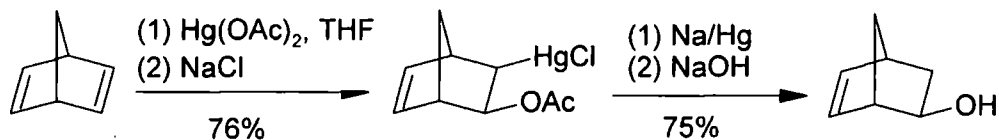
Scheme 1.11. Synthesis of *exo*-5-thio-2-norbornene.

The reaction mixture can be distilled to afford the thiol as the volatile component and the diol as the residue of distillation. With this method, concomitant recovery of binaphthol is also achieved and thus could be recycled in subsequent experiments. The binaphthol-derived thiophosphonate is a crystalline solid, which is readily available with simple procedures.⁴² They are soluble in most solvents, air stable and virtually non-odorous.

1.4.4 Synthesis of *exo*-5-Hydroxy-2-norbornene

exo-5-Hydroxy-2-norbornene has great potential as a new *exo*-monomer due to the ease with which it can be elaborated upon to provide functionality in the resulting polymer. The alcohol group can be converted to ethers and esters, which are known to yield colourless, transparent polymers. Two different synthesis routes are described in the literature.

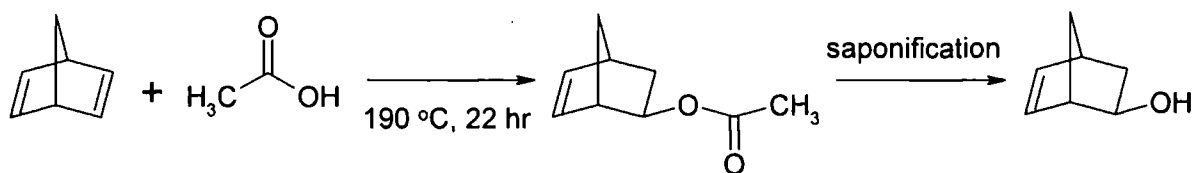
The oxymercuration of norbornadiene gives the anti addition product. Demercuration and hydrolytic cleavage of the acetate group can be achieved in a single step using sodium amalgam in NaOH, to yield the *exo*-5-hydroxy-2-norbornene, scheme 1.12.⁴³



Scheme 1.12. Synthesis of *exo*-5-hydroxy-2-norbornene.

The disadvantage of this procedure is that it requires two separate purification steps using column chromatography.

The second synthesis (> 98:2 *exo/endo* selectivity) involves the reaction of acetic acid with excess norbornadiene at high temperature, to give the *exo* monoacetate, followed by the usual saponification under alkali conditions, scheme 1.13.⁴⁴



Scheme 1.13. Synthesis of *exo*-5-hydroxy-2-norbornene.

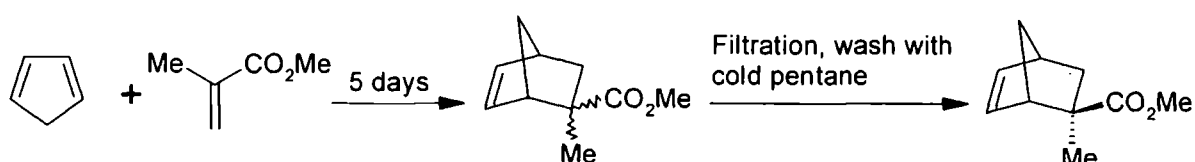
The selectivity of this reaction is quite amazing considering the absence of a catalyst. The monomer can be synthesised in high yield and purity, relying on distillation under reduced pressure of the *exo*-5-acetate-2-norbornene and subsequent recrystallisation of the *exo*-5-hydroxy-2-norbornene for purification.

1.4.5 Synthesis of *endo*-5-Methyl-2-norbornene-*exo*-5-carboxylic acid

The Diels-Alder cycloaddition of cyclopentadiene and methacrylic acid is well known to produce a mixture of *endo* and *exo* isomers, with the ratio dependent on the reaction conditions. A pure sample of *endo*-5-methyl-2-norbornene-*exo*-5-carboxylic acid was

thought to be possible only via numerous recrystallisations or via a multi-step lactonisation method.

It was reported that a pure sample of *endo*-5-methyl-2-norbornene-*exo*-5-carboxylic acid could be obtained in a large-scale preparation. It is noted that when equimolar amounts of methacrylic acid and freshly cracked cyclopentadiene were stirred for 5 days the product would be an *exo/endo* ratio of 65 to 35, respectively. Importantly, the desired *exo* isomer precipitates directly from the reaction mixture, needing filtration and washing with cold pentane to give pure *exo* product in 33% yield, scheme 1.14.⁴⁵



Scheme 1.14. Synthesis of *endo*-5-methyl-2-norbornene-*exo*-5-carboxylic acid.

1.5 Optoelectronic Materials

1.5.1 Dielectric Polymers

The electronic industry's requirement for speed, miniaturisation and lower costs is driving the need for advancements in silicon wafer technology, including higher performance dielectric materials for packaging. Materials for packaging range from metals, to ceramics, to organic polymers. Industry trends have headed toward polymer packaging materials for a variety of applications ranging from interlayer dielectrics to chip encapsulants (both moulding and adhesive) and underfill materials.

Although most chips are packaged as single chips today, applications requiring advanced high-density chips are more in demand. Multichip packages (or modules, MCM) are becoming preferred since they decrease the wiring distance between chips by packaging the chips as close together as possible. This reduces the propagation delay and increases the packaging interconnect wiring. For most MCM, polymers have become the dielectric

packaging materials of choice because the low dielectric constants of polymers allow higher packaging densities, faster transmission speeds, and lower power consumption. Keeping the dielectric constant as low as possible relies on the very low moisture absorption of these polymeric systems, since water is a poor insulator and would degrade the dielectric properties. Additional benefits over ceramic systems are the ease of processing and tailor ability of polymeric systems.⁴⁶

A new family of dielectric polymers based on functionalised polynorbornenes are continually under development and commercialised by Promerus LLC under the trade name Avatrel™.⁴⁷ Avatrel dielectric polymers exhibit many of the key performance criteria required for this demanding application. The bicyclic hydrocarbon backbone gives a material with a high glass transition temperature and low moisture absorption. A co-polymer containing an 80:20 molar ratio of norbornene and 5-triethoxysilyl-2-norbornene (adhesion) had a tensile modulus of 1.4 GPa, an elongation to break of 15% and a T_g of 355°C. This material exhibited excellent transparency with greater than 90% average transmission between 400 and 700 nm and a low dielectric constant (2.67) suggesting that this material could find utility in optical and optoelectronic applications.⁴⁶

1.5.2 Optical Polymers

The optical polymers have a similar composition, primarily an alkylnorbornene to impart toughness and a small amount (< 10%) of a norbornene bearing an oxygen-containing functional group (to increase chain-chain interactions, improving overall polymer properties). The potential applications for optical polymers such as Appear® include flat panel display substrates, optical film, optical wave-guides and optical data storage. The properties that appear to make it suitable for these applications are: low transmission loss; wide spectral range; low birefringence; consistent difference in refractive index over a wide range of temperatures; long term thermal stability; high glass transition temperature and low moisture absorption. The combination of these characteristics offers advantages over existing plastic materials for visible and near IR applications such as those used in the datacom market.⁴⁸

1.5.3 Photoresist Polymers

The ability to pack more components on a chip is related to the feature size of the components themselves. Photolithography enables the chip designer to transfer the electronic circuitry that is written on a photo-mask onto the silicon wafer. There are two types of photoresist. The negative resist reacts upon exposure to light to form an insoluble form of the photoresist. Addition of a developer then dissolves the unexposed regions of the resist. A positive resist reacts when irradiated to produce a soluble form of the resist that is then washed away by the developer to give a three-dimensional relief image of the mask in the photoresist film. Next, the image is transferred to the underlying substrate via plasma etching to which the remaining photoresist is resistant.⁴⁹ The review will concentrate on positive resists.

Great advances have been made in the last decade with respect to photoresist materials. Feature sizes have shrunk as the wavelength of the light used to image the photoresist has successfully moved from 436 to 365 to 248 to 193 nm. The key to these advances is the design of polymers for use with each new imaging technology that are sufficiently transparent at their respective wavelengths. Without sufficient transparency, light cannot penetrate to the bottom of the resist film, resulting in only a partially developed resist. The industry is preparing for 157 nm imaging which will require totally new polymers from those used in 248 nm resists because water, oxygen gas, and simple hydrocarbons such as ethylene absorb very strongly in this spectral region. The polymer design also has to accommodate all the other characteristics of a good resist such as resistance to the plasma etching process, tuneable adhesion characteristics and exceptional mechanical properties.

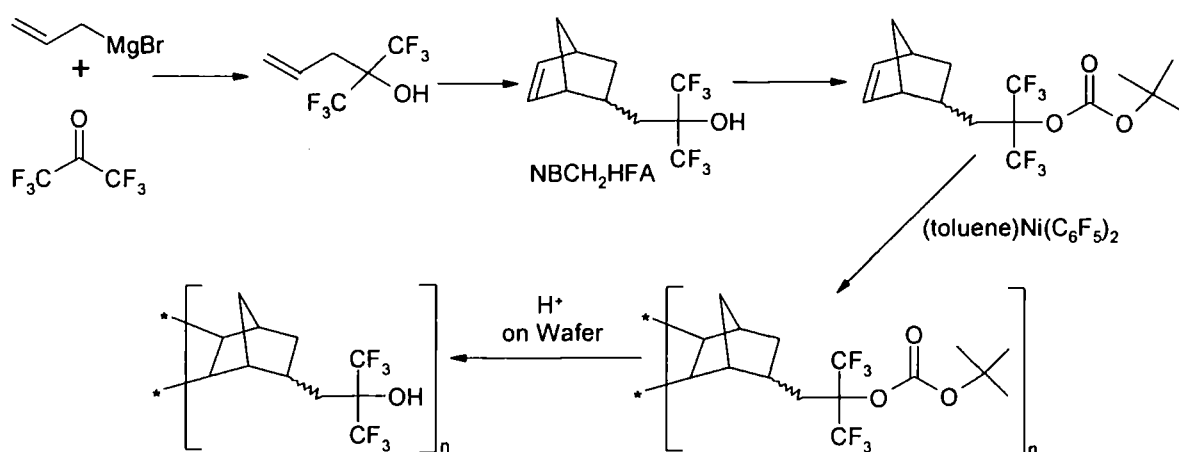
Many publications often refer to a “modular” approach to the design of the resist polymer.⁵⁰ This involves the copolymerisation of a number of functionalised monomers, where each type of functional group is used to impart one or more necessary properties upon the resulting resist polymer. The key modules are:

- Backbone that tethers the functional substituents and provides mechanical properties such as etch resistance and transparency.
- Photosensitive acid generator.

- Solubility switch. Acid sensitive moiety that undergoes an acid catalysed deprotection, forming a functionality that renders the formally solvent soluble polymer aqueous base soluble.

It is clear that an abundance of C-H bonds in a resist polymer will render it opaque. This has led to other candidate materials such as fluorinated hydrocarbons and organosiloxanes being highly scrutinised as early studies showed these materials to be relatively transparent at 157 nm region.⁵¹ It is not hard to understand why the main area of current research is looking towards functionalised norbornene polymers to create the new generation of 157 nm resists. Given the new generation of late transition metal initiators that will polymerise a huge diversity of functionalised norbornenes containing vital acid labile groups, esters, aldehydes, ketones, ethers, alcohols and amines and the superior etch resistance shown by the resulting polymers.

Hexafluoro-2-propanol and α -trifluoromethylcarboxylic acid groups have been shown to be relatively transparent acid group modules and have been incorporated into a norbornene monomer and polymerised using the addition polymerisation catalyst $(\eta^6\text{-toluene})\text{Ni}(\text{C}_6\text{F}_5)_2$, scheme 1.15.¹⁵ The absorbance spectra of the resulting polymer and its deprotected analogue showed a significant reduction in absorbance at 157 nm wavelength.⁵⁰

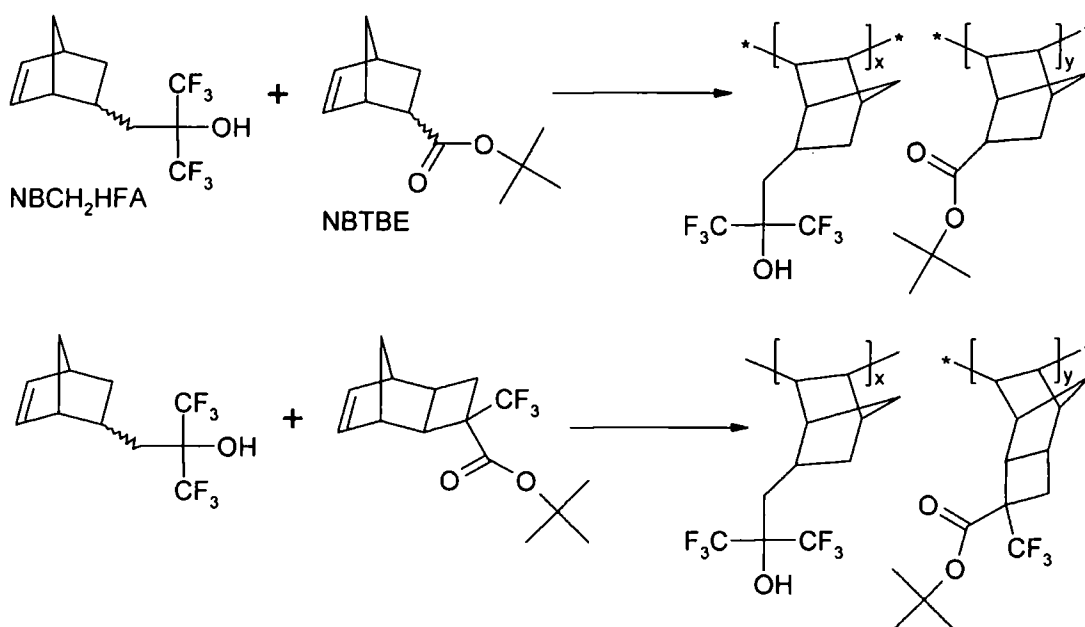


Scheme 1.15

Following from earlier successes the same research group have synthesised a range of co-polymers that incorporate a norbornene monomer functionalised with hexafluoro-2-propanol (NBCH₂HFA) and evaluated them in formulating photoresists for 157 nm lithography

imaging.⁵² The co-polymer of NBCH₂HFA with NBCO₂^tBu (NBTBE) was first polymerised using (η^6 -toluene)Ni(C₆F₅)₂ and gave an absorption that was much lower than poly(NBTBE) but slightly higher than poly(NBCH₂HFA) at 157 nm wavelength, scheme 1.16. Lithographic evaluation showed the molecular weight of this polymer to be too high, causing excess swelling and attempts to lower the molecular weight using excess catalyst and chain transfer agents were unsuccessful. The molecular weight and molecular weight distribution of the polymer is important because it is strongly related to the dissolution behaviour, higher molecular weight polymer tending to dissolve more slowly in aqueous base than lower molecular weight analogues.

Partially successful attempts were made to prepare the same co-polymer, scheme 1.16, using Risse's allyl palladium catalyst (η^3 -allyl)Pd(SbF₆),¹⁰ but molecular weight could only be controlled via very high catalyst loadings.⁵² Molecular weights less than 9000 could only be obtained by using >5 mol % catalyst. The catalyst is not only expensive but also requires removal down to 15 parts per billion (ppb) of palladium for photoresist applications. 1-Hexene was shown to be very poor at reducing molecular weight via chain transfer in these systems. An additional problem was the cleavage of acid protecting groups via HSbF₆ but this was resolved using the easily separable Proton Sponge, bis(dimethylamino)naphthalene.



Scheme 1.16. Synthesis of 157 nm resist materials.

In the same publication⁵² the related co-polymer, scheme 1.16, was demonstrated as a potentially good system due to its very low absorbance at 157 nm. The resists formulated from this co-polymer performed well in preliminary lithographic evaluations allowing images as small as 70 nm to be printed.

Promerus LLC replicated the homo- and co-polymerisation of NBCH₂HFA and NBTBE using the more highly active cationic palladium catalyst systems discussed earlier in this chapter and olefinic chain transfer agents such as 1-hexene and ethylene to control molecular weight.⁵³ A homo-polymer of NBCH₂HFA was successfully produced using a much improved monomer:catalyst ratio using chain transfer agents: 25000:1 (chain transfer agent = ethylene) or 50000:1 (chain transfer agent = 1-hexene). The co-polymerisation of NBCH₂HFA and NBTBE required a higher catalyst loading (5000 monomer: 1 catalyst), thought to be because of coordination of the carbonyl functionality to the cationic palladium centre. The chain transfer agents 1-hexene and ethylene were shown to be relatively successful in controlling molecular weight when very large amounts of transfer agents were employed. The polymers formed using these chain transfer agents were shown to have olefinic end groups, which would render the polymers opaque at 157 nm wavelength. Therefore, better chain transfer agents for reduction of the olefinic groups would be necessary before reliable resist materials can be formed with these systems.

It has already been mentioned that the dissolution behaviour of the resist polymer is of great importance in the reliability and quality of the lithographic material formed and so many attempts have been made to find ways of gaining control over this characteristic. The molecular weight and the ratio of *endo* and *exo* isomers of NBCH₂HFA in the resist polymer have been shown to affect the dissolution behaviour of homo and co-polymers.⁵⁴ The use of the high *exo*-NBCH₂HFA monomer for resist applications has also appeared in a few patents, which suggest that this property could be quite important.⁵⁵

1.6 References

- ¹ Gaylord, N. G.; Deshpande, A. B.; Mandal, B. M.; Martan, M. *J. Macromol. Sci. Chem.* **1977**, *A11(5)*, 1053.
- ² *Modern Plastics* **1995**, *72 (9)*, 137.
- ³ Parshall, G. W.; Ittel, S. D. *Homogenous Catalysis, Wiley-Interscience, New York*, 2nd edn. **1992**, 63 and 224.
- ⁴ Eleuterio, H. S. *J. Mol. Catal. A: Chem.* **1991**, *65*, 55 - 61.
- ⁵ Kaminski, W.; Bark, A.; Dake, I. *Stud. Surf. Sci. Catal.* **1990**, *56*, 425.
- ⁶ Schultz, R. G. *Polym. Lett.* **4**, **1966**, 541 - 546.
- ⁷ Tanialian, C.; Kiennemann, A.; Osparpuca, T. *Can. J. Chem.* **1979**, *57*, 2022 - 2027.
- ⁸ Sen, A.; Lai, T. W. *J. Am. Chem. Soc.* **1981**, *103*, 4627 - 4629.
- ⁹ Seehof, N.; Mehler, S.; Breunig, W.; Risse, W. *J. Mol. Catal.* **1992**, *76*, 219 - 228.
- ¹⁰ Breunig, W.; Risse, W. *Macromol. Chem.* **1992**, *193*, 2915 - 2927.
- ¹¹ Mehler, C.; Risse, W. *Macromol. Chem., Rapid Commun.* **1992**, *13*, 455 - 459.
- ¹² Goodall, B. L.; Benedikt, G. M.; Jayaraman, S.; Mcintosh, L. H. III.; Barnes, D. A.; Rhodes, L. F.; Shick, R. A. *Polym. Prep., Am. Chem. Soc. Div. Polym. Chem.* **1998**, *39 (1)*, 216.
- ¹³ Lipian, J.; Minma, R. A.; Fondran, J. C.; Yandulov, D.; Shick, R. A.; Goodall, B. R.; Rhodes, L. F.; Huffman, J. C. *Macromolecules* **2002**, *35*, 8969 - 8977.
- ¹⁴ Hennis, A. D.; Polley, J. D.; Long, G. S.; Sen, A.; Yandulov, D.; Lipian, J.; Benedikt, G.; Rhodes, L. F. *Organometallics*, **2001**, *20*, 2802 - 2812.
- ¹⁵ Rhodes, L.F.; Bell, A.; Jayaraman, J. L.; Goodall, B. L.; Shick, R. A. *International Patent* WO9914256 **1999**.
- ¹⁶ (a) Lipian, J. -H.; Rhodes, L. F.; Goodall, B. L.; Bell, A.; Minma, R. A.; Fondran, J. C.; Hennis, A. D.; Elia, C. N.; Polley, J. D.; Sen, A.; Saikumar, J. *PCT Int. Appl.* WO 0020472 **2000**. (b) Zhao, X. -M.; Shick, R. A.; Ravikiran, R.; Neal, P. S.; Rhodes, L. F.; Bell, A. *PCT Int. Appl.* WO 0210231 **2002**.
- ¹⁷ Thirupathi, N.; Amoroso, D.; Bell, A.; Protasiewicz, J. D. *Organometallics* **2005**, *24*, 4099 - 4102.
- ¹⁸ Bell, A.; Amoroso, D.; Protasiewicz, J. D.; Thirupathi, N. US 2005/0187398 A1.
- ¹⁹ Thirupathi, N.; Amoroso, D.; Bell, A.; Protasiewicz, J. D. *Organometallics* **2007**, *26*, 3157 - 3166.

- ²⁰ (a) Wilke, G.; Bogdanovic, B.; Heimbach, P.; Kroner, M.; Muller, E. W. *Adv. Chem. Ser.* **1962**, *34*, 137. (b) Brenner, W.; Heimbach, P.; Wilke, G. *Annalen*, **1960**, *727*, 194.
- ²¹ Green, M. L. H.; Munakata, H. *J. Chem. Soc., Inorg. Chem.* **1974**, 269.
- ²² Tanase, T.; Ohizumi, T.; Kobayashi, K.; Yamamoto, Y. *Organometallics*, **1996**, *15* (15), 3404 -3411.
- ²³ (a) Tezuka K.; Ishizaki Y.; Inoue Y. *Journal of Molecular Catalysis A: Chemical* **1998**, *129* (2), 199-206. (b) Chernyshev M. L.; Tkach V. S.; Dmitrieva T. V.; Ratovskii G. V.; Zinchenko S. V.; Shmidt F. K. *Kinetics and Catalysis* **1997**, *38* (4), 527 - 531.
- ²⁴ Sommovigo, M.; Pasquali, M. *Journal of Organometallic Chemistry* **1991**, *418*, 119 - 126.
- ²⁵ Leoni, P.; Sommovigo, M.; Pasquali, M.; Midollini, S.; Braga, D.; Sabatino, P. *Organometallics* **1991**, *10*, 1038.
- ²⁶ Gibson, L. S.; Spitzmesser, S. K. *Chem. Rev.* **2003**, *103*, 283 - 315.
- ²⁷ Sauer, J. *Angew. Chem. Internat. Edit.* **1967**, *6* (1), 16.
- ²⁸ (a) Mathew, J. P.; Reinmuth, A.; Risse, W.; Melia, J.; Swords, N. *Macromolecules* **1996**, *29*, 2755 - 2763. (b) Heinz, B. S.; Alt, F. P.; Heitz, W. *Macromol. rapid. Commun.* **1998**, *19*, 251 - 256.
- ²⁹ Sen, A. *Acc. Chem. Res.* **1993**, *26*, 303 - 310.
- ³⁰ Hennis, A. D.; Polley, J. D.; Long, G. S.; Sen, A.; Yandulov, D.; Lipian, J.; Benedikt, G. M.; Rhodes, L. F.; Huffman, J. *Organometallics* **2001**, *20*, 2802 - 2812.
- ³¹ Funk, J. K.; Andes, C. E.; Sen, A. *Organometallics* **2004**, *23*, 1680 - 1683.
- ³² (a) Jordan, R. W.; Tam, W. *Organic Letters* **2000**, *2* (19), 3031 - 3034. (b) Jordan, R. W.; Tam, W. *Organic letters* **2001**, *3* (15), 2367 - 2370. (c) Mayo, P.; Orlova, G.; Goddard, J. D.; Tam, W. *J. Org. Chem.* **2001**, *66*, 5182 - 5191. (d) Jordan, R. W.; Tam, W. *Tetrahedron Letters* **2002**, *43*, 6051 - 6054. (e) Mayo, P.; Tam, W. *Tetrahedron* **2002**, *58*, 9527 - 9540. (f) Jordan, R. W.; Khoury, P. R.; Goddard, J. D.; Tam, W. *J. Org. Chem.* **2004**, *69*, 8467 - 8474.
- ³³ (a) Bell *et al.* (b) Pollino, J. M.; Stubbs, L. P.; Weck, M. *Macromolecules* **2003**, *36* (7), 2230 -2234.
- ³⁴ Pollino, J. M.; Stubbs, L. P.; Weck, M. *Polymer Reprints* **2003**, *44* (1), 730.
- ³⁵ Khosravi, E.; Al-Hajaji, A. A. *Eur. Polym. J.* **1998**, *34*, 153 - 157.
- ³⁶ Madan, R.; Anand, R. C.; Varma, I. K. *Journal of Thermal Analysis and Calorimetry* **2000**, *59*, 531 - 539.

- ³⁷ Marchard, A. P.; Sorokin, V. D.; Rajagopal, D.; Bott, S. G. *Synthetic Communications* **1994**, *24* (21), 3141 - 3147.
- ³⁸ Scammells, P. J.; Baker, S. P.; Bellardinelli, L.; Olsson, R. A.; Russell, R. A.; Wright, D. M. J. *Tetrahedron* **1996**, *52*, 4735 - 4744.
- ³⁹ Brunner, H.; Kramler, K. *Synthesis* **1991**, *Stuttgart* (12), 1121.
- ⁴⁰ Arstad, E.; Barrett, A. G. M.; Hopkins, B. T.; Kobberling, J. *Organic Letters* **2002**, *4* (11), 1975 - 1977.
- ⁴¹ Fabbi, D.; Delogu, G.; Lucchi, O. D. *Tetrahedron: Assymetry* **1993**, *4*, 1591 - 1596.
- ⁴² Gong, B. Q.; Chen, W. Y.; Hu, B. F. *Phosphorus, Sulphur, and Silicone* **1991**, *57*, 87.
- ⁴³ Mayo, P.; Orlova, G.; Goddard, J. D.; Tam, W. *J. Org. Chem.* **2001**, *66*, 5182 - 5191.
- ⁴⁴ Feiring, A. E.; Crawford, M. K.; Farnham, W. B.; French, R. H.; Leffew, K. W.; Petrov, V. A.; Schadt, F. L.; Wheland, R. C.; Zumsteg, F. C. *J. Fluorine Chem.* **2003**, *122*, 11 - 16.
- ⁴⁵ Katritzky, A. R.; Hong, Q.; Yang, Z.; Cundy, D. J.; Brown-Wensley, K. *Organic Preparations and procedures international* **1995**, *27* (5), 574 - 575.
- ⁴⁶ Feger, C. In *Multichip Module Technologies and Alternatives. The Basics*; Doane, D. A.; Franzon, P. D., Eds., Van Nostrand Reinhold: New York, **1993**, 311.
- ⁴⁷ Shick, R. A.; Jayaraman, S. K.; Goodall, B. L.; Rhodes, L. F.; McDougall, W. C.; Kohl, P.; Bidstrup-Allen, P.; Chiniwalla, P. *Advancing Microelectronics* **1998**, *25* (5), 13 - 14.
- ⁴⁸ Glukh, K.; Lipian, J. H.; mimna, R.; Neal, P. S.; Ravikiran, R.; Rhodes, L. F.; Shick, R. A.; Zhao, X-M. *High-performance polymeric materials for waveguide applications*, The BFGoodrich Company, Electronic Materials Division.
- ⁴⁹ Hinsberg, W. D.; Wallrath, G. M.; Allen, R. D. "Kirk-Othmer Encyclopedia of Chemical Technology", 4th edition, Supplement Volume, John Wiley & Sons, New York **1998**, 233 - 236.
- ⁵⁰ Chiba, T.; Hung, R. J.; Yamada, S.; Trinque, B.; Yamachika, M.; Brodsky, C.; Patterson, K.; Heyden, A. V.; Jamison, A.; Lin, S-H.; Somerwell, M.; Byers, J.; Conley, Will.; Willson, C. G. *Journal of Photopolymer Science and Technology* **2000**, *13* (4), 657 - 664.
- ⁵¹ Kunz, R. R.; Bloomstein, T. M.; Hardy, D. E.; Goodman, R. B.; Downs, D. K.; Curtin, J. E. *Proc. SPIE*, 3678 **1999**, 13 - 23.
- ⁵² Tran, H. V.; Hung, R. J.; Chiba, T.; Yamada, S.; Mrozek, T.; Hsieh, Y-T.; Chambers, C. R.; Osborn, B. P.; Trinque, B. C.; Matthew, J. P.; MacDonald, S. A.; Willson, C. G. *Macromolecules* **2002**, *35*, 6539 - 6549.

⁵³ Chang, C.; Lipian, J.; Barnes, D. A.; Seger, L.; Burns, C.; Bennett, B.; Bonney, L.; Rhodes, L. F.; Benedikt, G. M.; Lattimer, R.; Huang, S. S.; Day, V. W. *Makromol. Chem. Phys.* **2005**, *206*, 1988 - 2000.

⁵⁴ Ito, H.; Truong, H. D.; Rhodes, L.; Chang, C.; Langsdorf, L. J.; Sidaway, H. A.; Maeda, K.; Sumida, S. *Journal of Photopolymer Science and Technology* **2004**, *17*, 609 - 620.

⁵⁵ (a) Feiring, A. E.; Petrov, V. A.; Schadt III, F. L. *Preparation and use of exo-2-fluoroalkyl(bicyclo[2.2.1]hept-5-enes)* US 2005/00588932 A1. (b) Feiring, A. E.; Petrov, V. A.; Schadt III, F. L. *Preparation and use of exo-2-fluoroalkyl(bicyclo[2.2.1]hept-5-enes)*US 6,875,555 B1.

Chapter 2

2 Formation of Palladium Hydride Initiators From $[\text{Pd}(\text{P-}i\text{-Pr}_3)_2(\text{NCCH}_3)(\text{OAc})]\text{-}[\text{B}(\text{C}_6\text{F}_5)_4]$ (Pd1206): Mechanism and Characterisation by NMR Spectroscopy

2.1 Introduction

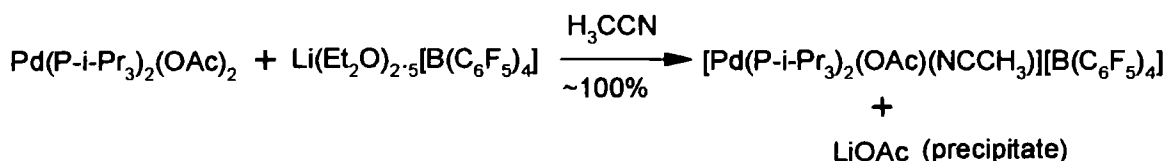
In the last few years a Case Western Reserve University/Promerus LLC partnership has isolated and identified an important group of proinitiators based on $\text{Pd}(\text{PR}_3)_2(\text{O}_2\text{CCH}_3)_2$, which are activated by weakly coordinating anion (WCA) salts to yield highly active catalyst systems. These single component proinitiators readily generate palladium hydride initiating species in solution, under mild conditions.^{1, 2, 3}

Our main research focuses on the kinetics of initiation and polymerisation of addition polymerisable norbornene monomers using cationic palladium hydride systems. Our interest in these proinitiators stems from the apparent high thermal stability and polymerisation activity observed. Over the last 3 years in collaboration with Promerus LLC we have been investigating one particular family based on $\text{P}(i\text{-Pr})_3$, which include $[\text{Pd}(\text{P-}i\text{-Pr}_3)_2(\text{O}_2\text{CCH}_3)(\text{NCCH}_3)][\text{B}(\text{C}_6\text{F}_5)_4]$ (Pd1206), $[\text{Pd}(\text{P-}i\text{-Pr}_3)_2(\kappa^2\text{-O}_2\text{CCH}_3)]\text{-}[\text{B}(\text{C}_6\text{F}_5)_4]$ (Pd1165) and $[\text{Pd}(\text{P-}i\text{-Pr}_3)(\text{P}(i\text{-Pr})_2(\kappa^2\text{-C}(\text{CH}_3)_2))(\text{NCCH}_3)][\text{B}(\text{C}_6\text{F}_5)_4]$ (Pd1146M). During our further detailed reactivity and mechanistic studies we have found numerous reaction pathways, which generate previously unknown compounds.

2.2 Results and Discussion

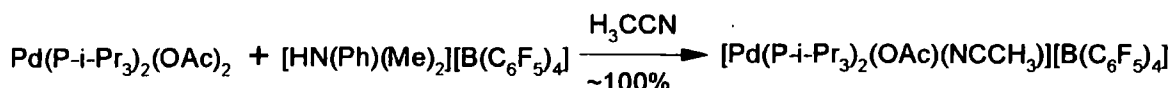
2.2.1 New Synthesis Routes to [Pd(P-*i*-Pr₃)₂(NCCH₃)(OAc)][B(C₆F₅)₄] (Pd1206)

Protasiewicz *et al.*,^{2, 3} have shown previously that carboxylate abstraction from *trans*-[(R₃P)₂Pd(OAc)₂] using lithium salts of weakly coordinating anions (WCA) results in the quantitative formation of Pd1206, scheme 2.2. The driving force for this reaction appears to be the precipitation of the LiOAc side product, with Pd1206 remaining soluble in organic solvent. This synthesis was used to prepare clean samples of Pd1206.



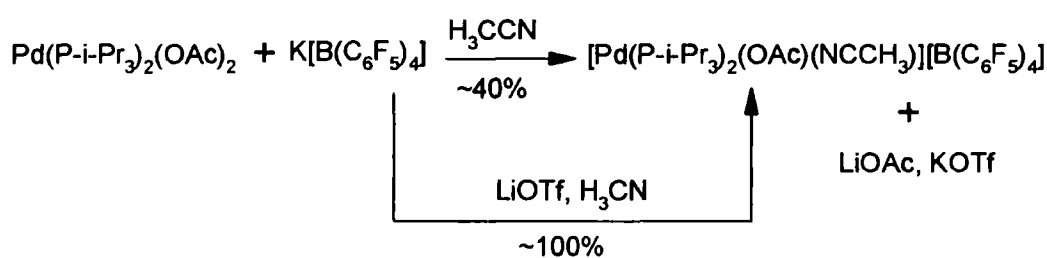
Scheme 2.2. Synthesis of Pd1206 using LiFABA.

Protasiewicz *et al.*,^{2, 3} have also shown previously that an alternative synthesis using 1 equivalent of [HN(Ph)(Me)₂][B(C₆F₅)₄] (DANFABA) also results in the quantitative formation of Pd1206, scheme 2.3, which can be easily precipitated into hexanes to remove any by-products. This synthesis was used to prepare clean samples of Pd1206. The ³¹P NMR spectrum revealed only one resonance signal at 45.6 ppm which is shifted ~ 11 ppm downfield from that of the neutral starting material. The ¹H NMR spectrum showed no sign of residual free acetic acid and showed only those signals expected from Pd1206's structure. The ¹⁹F NMR spectrum showed the 3 signals in a ratio of 2:1:2 as expected for the WCA structure.



Scheme 2.3. Synthesis of Pd1206 using DANFABA.

Due to the commercial availability and much lower cost of KFABA, we have investigated it as a replacement for LiFABA for the formation of **Pd1206**, owing to the fact that LiFABA is produced from KFABA. The addition of 1-5 equivalents of KFABA to $\text{Pd}(\text{P}(\text{i-Pr})_2(\text{O}_2\text{CCH}_3))_2$ in acetonitrile results in only the partial formation of **Pd1206** in ~ 40 % yield so a variety of additives were investigated to drive through the reaction. Lithium salts were added to the system in order to aid the formation of carboxylate salt. The addition of 1 equivalent of LiBr resulted in the scrambling of signals in the ^{31}P NMR spectrum. However, the addition of 1 equivalent of LiOTf resulted in the clean, quantitative formation of **Pd1206**, scheme 2.4, which gave NMR spectra as expected.



Scheme 2.4. Synthesis of **Pd1206** using KFABA.

2.2.2 Thermolysis of $[\text{Pd}(\text{P}(\text{i-Pr})_2(\text{NCCH}_3)(\text{OAc}))][\text{B}(\text{C}_6\text{F}_5)_4]$ (**Pd1206**) in $\text{THF-}d_8$ at Variable Temperatures

Protasiewicz *et al.*,^{2, 3} have shown previously in a collection of publications and patents that **Pd1206** goes through a complicated thermolysis pathway, eventually resulting in cationic palladium hydride species. Protasiewicz *et al.*,^{2, 3} suggested the route to the cationic palladium hydride species using a series of synthesis and substitution reactions and basic thermolysis experiments. The aim of this work is to focus on what is actually happening during thermolysis with a view to using this new mechanistic information to improve the yields of the cationic palladium hydride species, thought responsible for catalytic activity.

The thermolysis of **Pd1206** at varying temperatures in $\text{THF-}d_8$ was monitored via ^{31}P and ^1H VT-NMR spectroscopy to find the optimum temperature that would make it possible to view any thermolysis intermediates, aiding the elucidation of the thermolysis pathway, scheme 2.1. In all cases the solution develops a red colour and eventually produces palladium metal, as a

black precipitate. Analysis of the reaction mixture by combined ^1H and ^{31}P NMR spectroscopy at regular time intervals during the thermolysis reaction reveals the telltale signatures for cationic palladium complexes, although a greater variety of transient species could be observed at lower temperatures, with 55°C proving the most revealing.

The thermolysis data obtained using ^{31}P NMR at four different temperatures was used to determine the first order rate constants for the decomposition of **Pd1206**, by taking the gradient of a plot of $\ln([\text{Pd1206}]/[\text{Pd1206}]_0)$ versus time, figure 2.1.

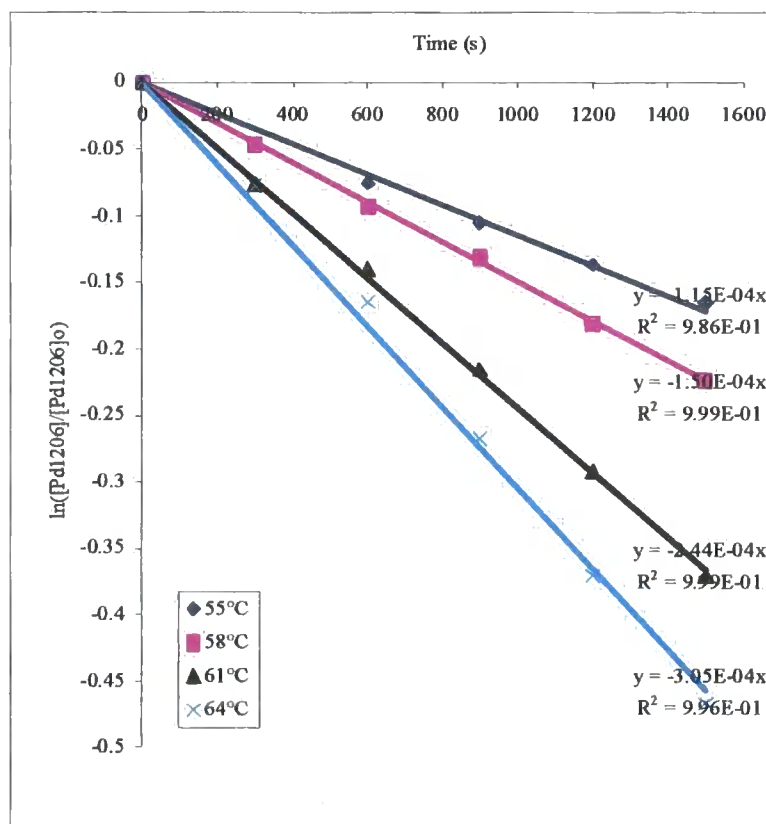


Figure 2.1. First order fitting for **Pd1206** thermolysis.

The first order rate constants obtained in figure 2.1, can be used to calculate the activation energy for the **Pd1206** thermolysis utilising the Arrhenius equation, $\ln(k) = \ln(A) - E_a/RT$. The activation energy (E_a) is calculated using the gradient of the plot of $\ln(k)$ versus $1/T$, figure 2.2, $E_a = R \times \text{gradient} = 8.314 \times 400.22 = 3.33 \text{ kJmol}^{-1}$. The pre-exponential factor (A) = $e^{-1.8243} = 0.161 \text{ s}^{-1}$.

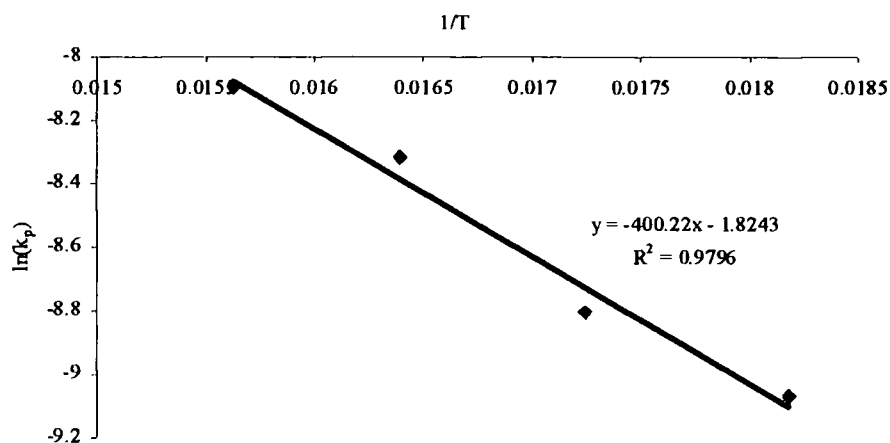


Figure 2.2. Calculation of activation energy for thermolysis **Pd1206** in THF-*d*₈.

2.2.3 Thermolysis of [Pd(P-*i*-Pr₃)₂(NCCH₃)(OAc)][B(C₆F₅)₄] (**Pd1206**) in THF-*d*₈ at 55°C

The main product of the thermolysis is the cationic palladium hydride complex [Pd(P-*i*-Pr₃)₂(NCCH₃)(H)][B(C₆F₅)₄] (**Pd1148**), scheme 2.1. The palladium hydride species (¹Pd-H) gives a distinctive triplet in the ¹H NMR spectrum at -15.2 ppm and also a signal in the ³¹P NMR spectrum at 56.9 ppm. **Pd1148** is found to be surprisingly stable under the conditions of thermolysis and be formed in less than 50 % yield. This yield is in agreement with the findings of Bell *et al.*,² 2005.

Monitoring the thermolysis of **Pd1206** by ³¹P VT-NMR spectroscopy, figure 2.3, shows that [Pd(P-*i*-Pr₃)₂(κ²-OAc)][B(C₆F₅)₄] (**Pd1165**) at 71.4ppm, appears as a transient species, suggesting it to be a necessary precursor to palladium hydride formation, scheme 2.1. Monitoring the thermolysis by ¹H NMR spectroscopy shows that the signal for free acetic acid increases over time, which suggests that the reaction pathway to the palladium hydride species involves an acetate abstraction process. These findings are in accordance with the substitution reactions carried out by Protasiewicz *et al.*,³ 2005. ¹H NMR spectroscopy also reveals that signals in the region of 7.5 – 4.5 ppm also increase during the thermolysis suggesting unsaturation is developing in the (P-*i*-Pr₃) ligand. This agrees with the notion that the trialkylphosphine ligands are providing the hydride ligand, and hence leaving a double bond on one of the trialkylphosphine ligands. This idea was first mentioned in a patent by

Bell *et al.*,² but the exact nature of the cationic palladium species resulting was not defined until after consultation with this new work.

A small and unusual AB-type resonance in the ³¹P NMR spectra appears as a transient species during the thermolysis of **Pd1206**. Further studies shown later in this chapter prove this species to be [Pd(P-*i*-Pr₃)((*i*-Pr₂)P-C(CH₃)=CH₂)(NCCH₃)(H)][B(C₆F₅)₄] (**Pd1146H**), containing the two different *trans*-phosphine ligands, P-*i*-Pr₃ and (*i*-Pr₂)P-C(CH₃)=CH₂, figure 2.14. The huge excess of competing THF ligand probably encourages the rapid conversion of **Pd1146H** into **Pd1148** during this thermolysis. This helps to displace and interconvert phosphine ligands, but leaves the question of what happens to the (*i*-Pr₂)-C(CH₃)=CH₂ ligand after it has been displaced. The answer to this question is investigated later in this chapter, section 2.2.12. Notably, the **Pd1146M** intermediate, first identified by Protasiewicz *et al.*,^{2, 3} is not visible in the ³¹P NMR during the thermolysis of **Pd1206**, probably due to its high instability and rapid conversion to **Pd1146H**, scheme 2.1.

The signal for [Pd(P-*i*-Pr₃)₂(NCCH₃)(CH₃)][B(C₆F₅)₄] (**Pd1162**) is evident in the ¹H NMR spectra (triplet at 0.43 ppm) and the ³¹P NMR spectra (41.3 ppm) both during and after the thermolysis of **Pd1206**. This evidence may seem contradictory to the proposed acetate abstraction route to **Pd1148** (Pd-H) already discussed, unless there are multiple reaction pathways, scheme 2.1.

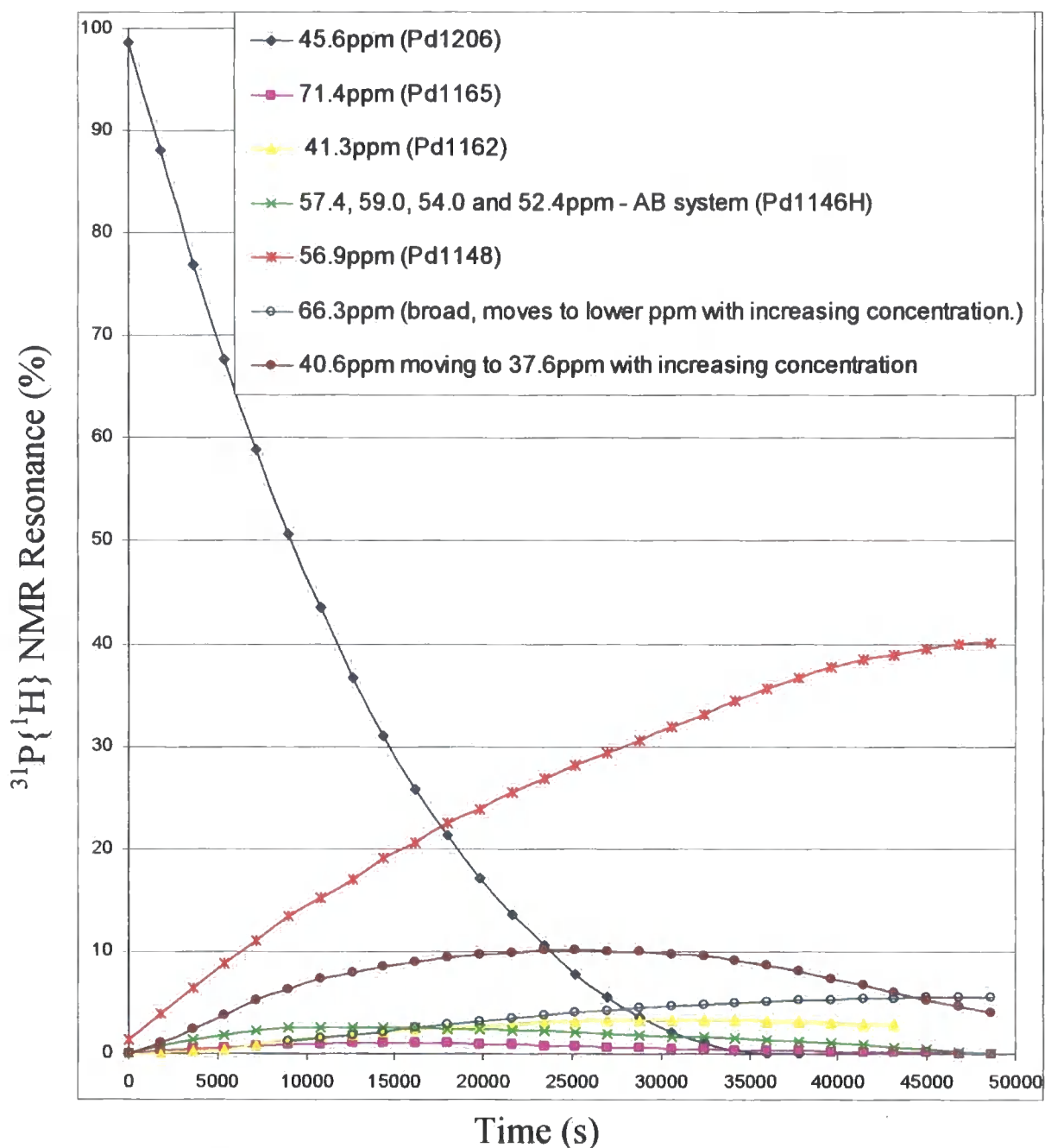


Figure 2.3. Thermolysis of Pd1206 at 55°C in THF- d_8 .

2.2.4 Thermolysis of $[\text{Pd}(\text{P-}i\text{-Pr}_3)_2(\text{NCCH}_3)(\text{CH}_3)][\text{B}(\text{C}_6\text{F}_5)_4]$ (Pd1162)

Monitoring the thermolysis of Pd1162 (Pd-Me) by ^{31}P and ^1H NMR spectroscopy at 55°C in THF- d_8 shows no evidence for the formation of palladium hydride species (Pd1148/Pd1146H), figure 2.4. The Pd1162 concentration decreases with the formation of two new species, but the identities of the species formed are unknown.

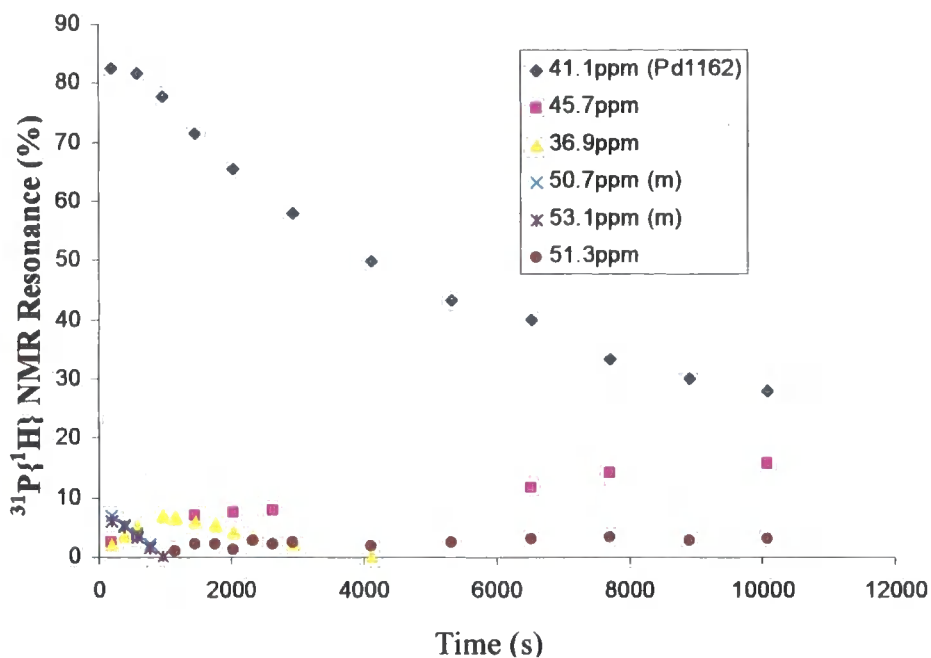


Figure 2.4. Thermolysis of **Pd1162** at 55°C in THF- d_8 .

The GCMS analysis of the gaseous products produced during the thermolysis of **Pd1206** was carried out by Promerus LLC and revealed that CO_2 and CH_4 were not produced as volatile products. The rate of decomposition of **Pd1162** at 55°C is coincidentally the same as the rate of decomposition of **Pd1206** under identical conditions but this has no obvious meaning, compare figures 2.1 and 2.5.

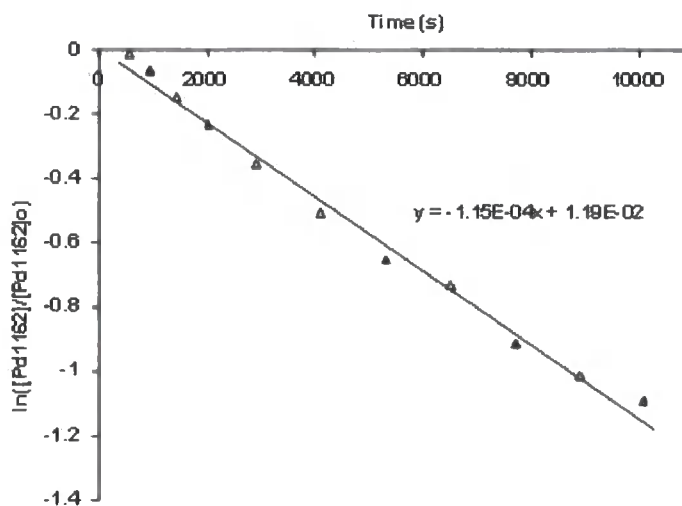


Figure 2.5. First order fitting for thermolysis of **Pd1162** at 55°C in THF- d_8 .

The **Pd1162** (Pd-Me) was a transient species in the thermolysis of **Pd1206**, figure 2.3, and yet it does not produce the palladium hydride species when heated on its own, figure 2.4. This suggests that other labile ligands in the reaction mixture are allowing this Pd-Me species to re-enter the thermolysis pathway or it is simply decomposing, scheme 2.1.

2.2.5 Thermolysis of $[\text{Pd}(\text{P-}i\text{-Pr}_3)_2(\text{NCCH}_3)(\text{CH}_3)][\text{B}(\text{C}_6\text{F}_5)_4]$ (**Pd1162**) + Acetic Acid in THF- d_8

The thermolysis of **Pd1162** with 1 equivalent of acetic acid was monitored by ^{31}P and ^1H NMR spectroscopy at 55°C in THF- d_8 . The solution went from a very pale yellow colour to a dark green/yellow colour, with a palladium precipitate evident. Telltale signals in the ^{31}P NMR spectra were evident for **Pd1165** (71.0 ppm) and two different palladium hydride species (56.4 and 55.8 ppm), figure 2.6.

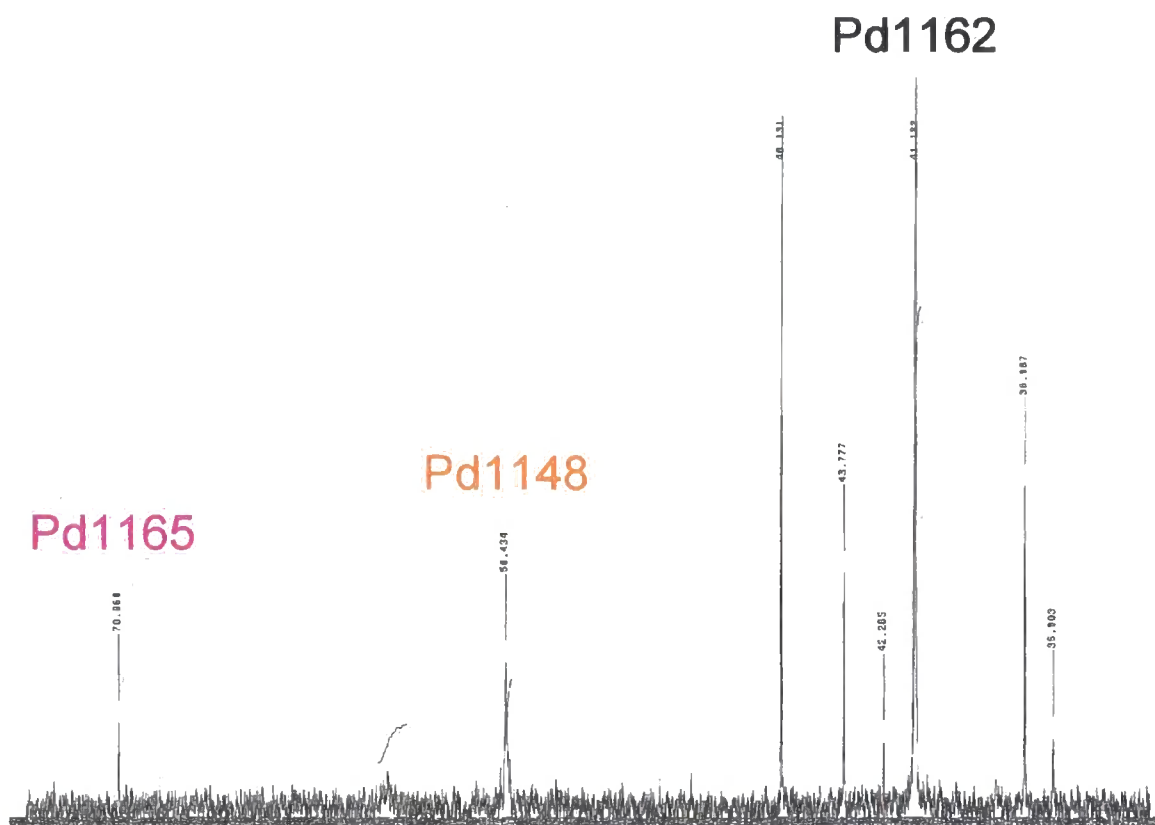


Figure 2.6. ^{31}P NMR spectrum of **Pd1162** + acetic acid in $\text{THF-}d_8$, after 160 minutes at 55°C .

The ^1H NMR spectra also gave evidence for two different palladium hydride species, giving broad signals at -14.5 and -15.1 ppm, respectively. These results suggest that the acetic acid is capable of protonating-off the methyl group from the **Pd1162** (Pd-Me) to re-enter the cycle as **Pd1165** and/or **Pd1206**, scheme 2.1.

2.2.6 Thermolysis of $[\text{Pd}(\text{P-}i\text{-Pr}_3)_2(\text{NCCH}_3)(\text{CH}_3)][\text{B}(\text{C}_6\text{F}_5)_4]$ (**Pd1162**) + Formic Acid

The results from the previous acetic acid experiment lead to the investigation of the chain transfer type-effect of formic acid in the absence of norbornene monomer on the thermolysis of **Pd1162**. The addition of an excess of formic acid to a solution (CDCl_3) of **Pd1162** resulted in the slow, unclean conversion to **Pd1148**, with many side products and palladium metal being produced. The reaction was driven to completion by heating at 40°C for 24

hours, although this also increased the undesirable side products, shown by ^{31}P NMR spectroscopy.

2.2.7 Thermolysis of $[\text{Pd}(\text{P-}i\text{-Pr}_3)_2(\kappa^2\text{-OAc})][\text{B}(\text{C}_6\text{F}_5)_4]$ (Pd1165) at 55°C in $\text{THF-}d_8$

Monitoring the thermolysis of Pd1165 by ^{31}P and ^1H NMR spectroscopy, at 55°C in $\text{THF-}d_8$, figure 2.7, shows evidence for the formation of a cationic palladium hydride species. The ^1H NMR spectra have a telltale signal at -19.1 ppm. There is no acetonitrile present in the solution so this palladium hydride species is likely to be a THF adduct of Pd1148. The species at 45.6 ppm is unknown.

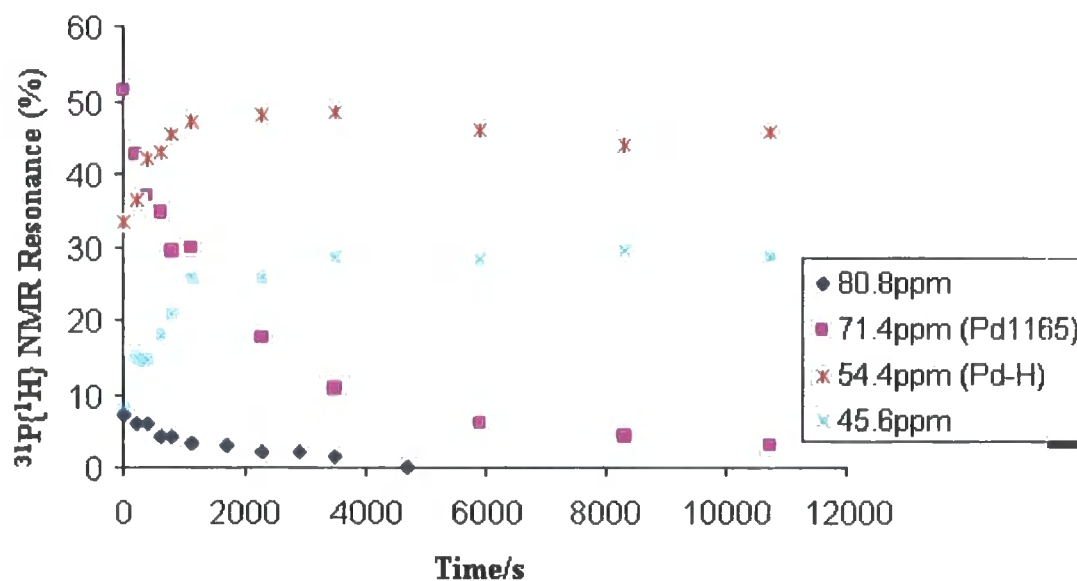


Figure 2.7. Thermolysis of Pd1165 at 55°C in $\text{THF-}d_8$.

The first order rate constant for the decomposition of Pd1165 at 55°C (figure 2.8) is 6 times greater than that of Pd1206 and Pd1162 (figures 2.1 and 2.5) under identical conditions, suggesting this species to be relatively unstable. This explains the small concentration of Pd1165 detected by ^{31}P NMR, during the thermolysis of Pd1206, figure 2.3.

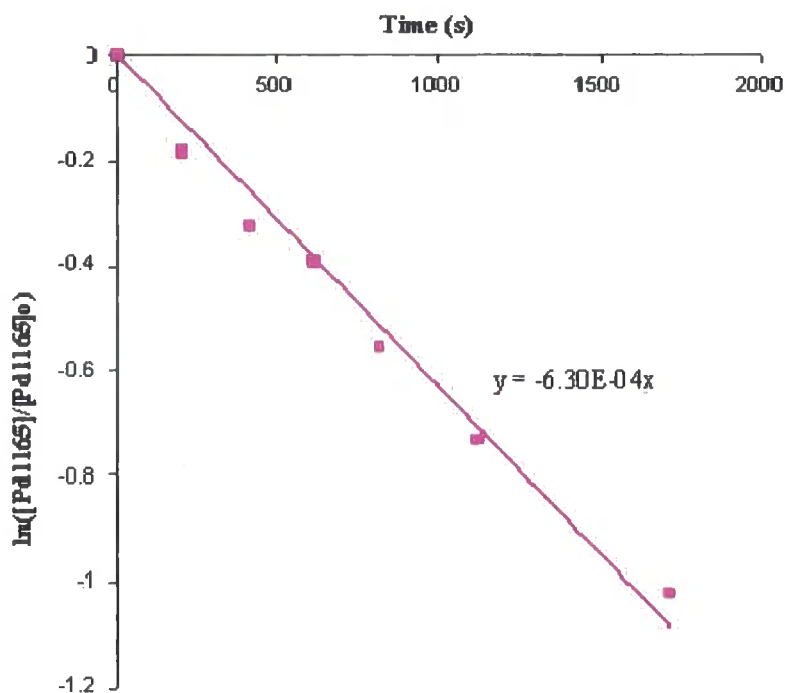


Figure 2.8. First order plot for thermolysis of **Pd1165** at 55°C in THF-*d*₈.

2.2.8 Thermolysis of [Pd(P-*i*-Pr₃)₂(κ²-OAc)][B(C₆F₅)₄] (**Pd1165**) + Acetonitrile

Monitoring the thermolysis of **Pd1165** with 1 equivalent of acetonitrile by ³¹P and ¹H NMR spectroscopy, at 55°C in THF-*d*₈, reveals that the formation of the metallated intermediate, **Pd1146M**, is the key to understanding the formation of palladium hydride species, scheme 2.1. The thermolysis is already well underway before the first spectra could be run due to the rapid conversion of **Pd1165** into **Pd1146M**, figure 2.9. The **Pd1146H** can be seen as a transient species, in relatively large concentrations (> 10%) during the thermolysis, due to the large concentration of **Pd1146M**, from which it is formed.

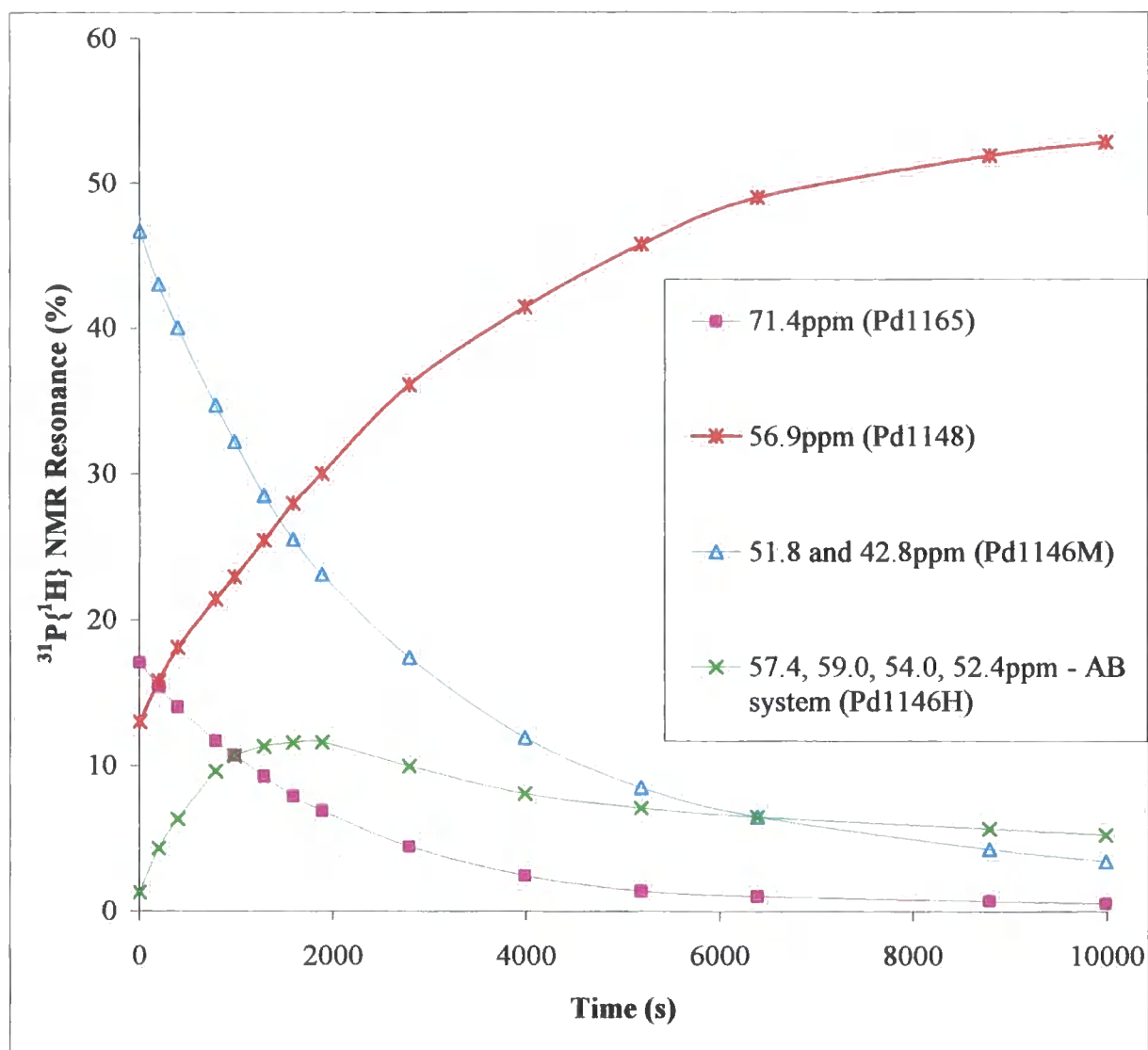


Figure 2.9. Thermolysis of **Pd1165** + acetonitrile at 55°C in THF-*d*₈.

It is notable that no appreciable amount of **Pd1162** is generated during this thermolysis, confirming that the Pd-CH₃ is formed from **Pd1206**. This also has the effect of making the thermolysis much cleaner with respect to palladium metal formation and less unknown signals in the ³¹P NMR spectra.

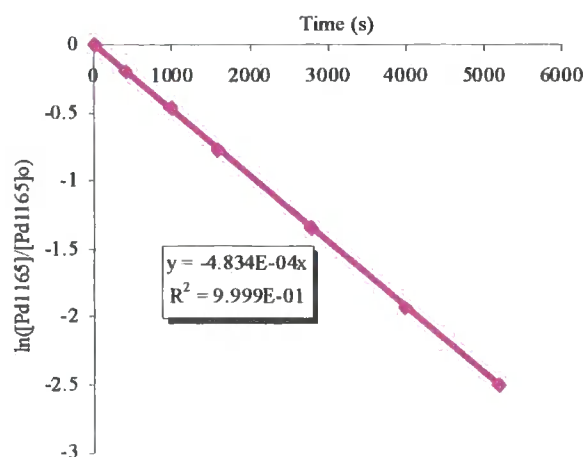


Figure 2.10. First order plot for thermolysis of **Pd1165** + acetonitrile at 55°C in THF-*d*₈.

The first order rate constant for the decomposition of **Pd1165** at 55°C is slower with acetonitrile, figure 2.10, confirming that the acetonitrile plays a significant role in the thermolysis pathway, scheme 2.1.

2.2.9 Synthesis and Characterisation of

cis- & *trans*-[Pd(P-*i*-Pr₃)(P(*i*-Pr)₂)(κ²-C(CH₃)₂)(NCCH₃)] [B(C₆F₅)₄] (**Pd1146M**)

When **Pd1165** is dissolved in acetonitrile for just a short period of time, a new species is reversibly formed which gives two distinctively broad signals in the ³¹P NMR spectra at 51.9 and 43.3 ppm. This suggests that the two phosphine ligands are non-identical and in rapid exchange, figure 2.11. This new species is thought to be **Pd1146M** which has the tertiary carbon of an isopropyl group bonded directly to the palladium centre. It is formed via a reversible carboxylate abstraction process, scheme 2.1. It has been found by Protasiewicz *et al.*,^{2,3} that **Pd1146M** can be synthesised in a relatively pure form at low temperatures by adding a base such as sodium bicarbonate to the **Pd1165**/acetonitrile mixture. This is believed to drive the carboxylate abstraction process through to completion by neutralising the free acetic acid produced. The addition of carboxylic acids to **Pd1146M** has been shown by Protasiewicz *et al.*,^{2,3} to be a good route to any of the κ² species (i.e. **Pd1165**) and relies on the reversible carboxylate abstraction process already described, scheme 2.1.

The characterisation of the **Pd1146M** in solution has proved problematic since it is susceptible to rapid thermolysis at temperatures above approximately 0°C. Protasiewicz *et al.*,^{2,3} has shown that this problem can be partially resolved via the addition of an excess of pyridine (5 equivalents) to **Pd1165** or **Pd1146M**, this readily converts both species to the metallated pyridine adduct $[\text{Pd}(\text{P-}i\text{-Pr}_3)(\text{P}(i\text{-Pr}_2)(\kappa^2\text{-C}(\text{CH}_3)_2))(\text{C}_6\text{H}_5\text{N})][\text{B}(\text{C}_6\text{F}_5)_4]$ (**Pd1184**) due to pyridine being a good base, and less labile than acetonitrile, as shown in the reaction scheme 2.1. This is useful because the **Pd1184** species shows a slower phosphine exchange and gives two fairly distinct doublets in the ^{31}P NMR spectrum at 49.8 and 37.9ppm, with a coupling constant of 30.8 Hz, which authenticates the proposed *cis*-structure.^{2,3} The **Pd1184** has been found to be stable to thermolysis up to a minimum of 65°C in THF.

The structure and exchange mechanism observed for **Pd1146M** and its thermolysis products were investigated via low temperature NMR spectroscopy studies, which should slow the thermolysis and rapid phosphine exchange, hence aiding characterisation, figure 2.11. The experiment was carried out using CDCl_3 as a solvent because a non-coordinating solvent would also help to slow the thermolysis process. Whilst observing the ^{31}P NMR, the phosphine ligand exchange decreased and the signals sharpened for all species as the temperature was decreased.

It can be seen in the ^{31}P VT-NMR spectra that the signals for the *cis*-**Pd1146M** species sharpen into two clean doublets ($J = 31.6$ Hz) whilst the temperature and hence phosphine ligand exchange is decreased allowing it to be characterised. It is also notable that the two doublets for *cis*-**Pd1146M** shift up-field as the temperature is decreased. Simultaneously two new and unexpected doublet signals at approximately 38.2 and 15.8 ppm begin to sharpen and shift down-field with a coupling constant ($J = 236.3$ Hz) indicative of a *trans*-deposition of phosphines around the palladium centre.

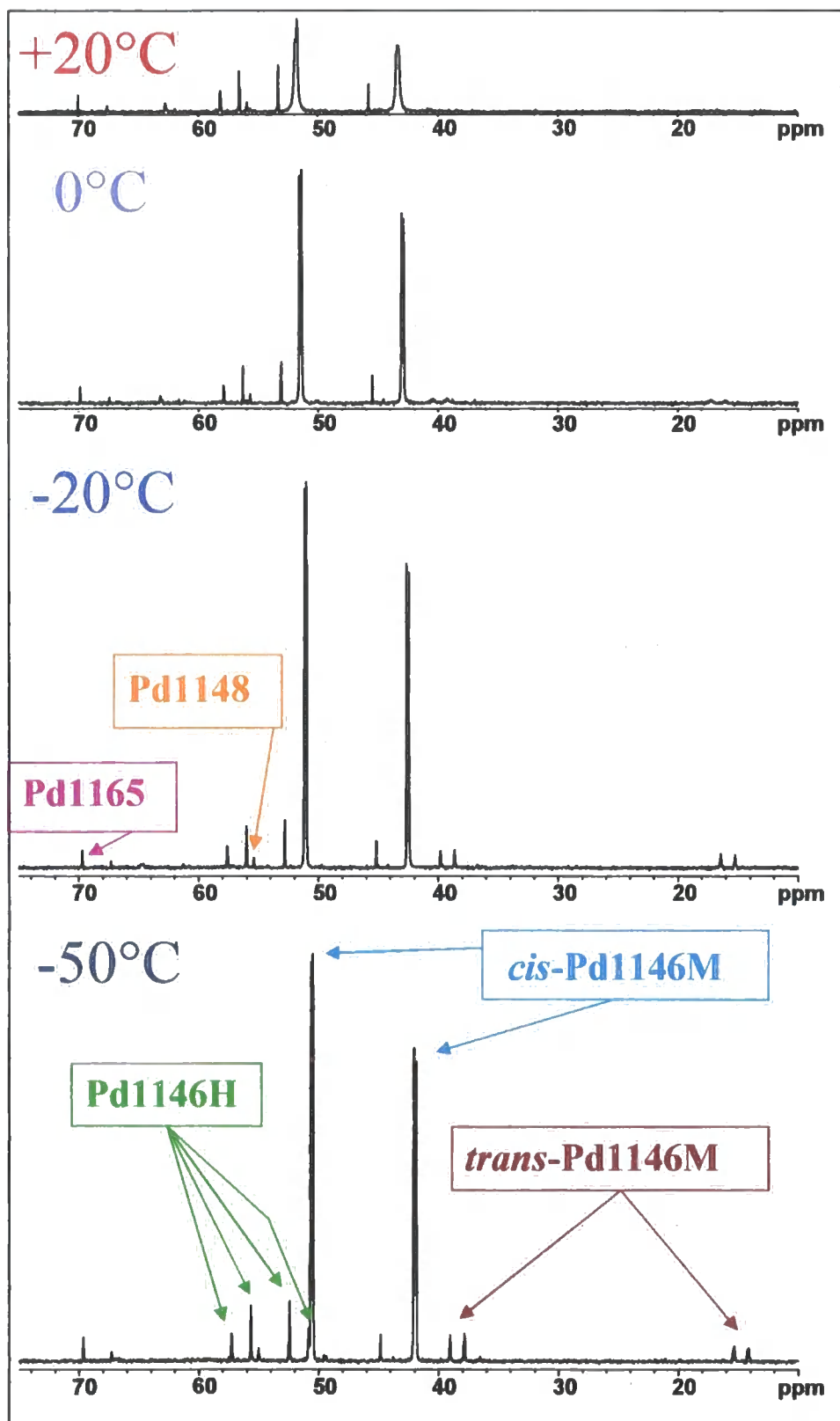


Figure 2.11. ^{31}P VT-NMR spectroscopic characterisation of Pd1146M.

The shifting of the two different sets of doublet signals in the ^{31}P VT-NMR is indicative of two species in exchange. The obvious explanation of these new doublets with a *trans*

disposition of phosphines that are seemingly in exchange with *cis*-Pd1146M is *trans*-Pd1146M. Low temperature VT-NMR suggests a *cis/trans* mixture of isomers in a ratio of 93/7, respectively, figure 2.12. The broad ^{31}P NMR resonance of Pd1146M at ambient temperatures is actually an average for the respective *cis*- and *trans*-isomers, in both position and integral value.

Resonances for the unavoidable thermolysis products; Pd1146H, Pd1148, Pd1165, and Pd1144H are also visible in figure 2.12 and will be discussed later in section 2.2.10.

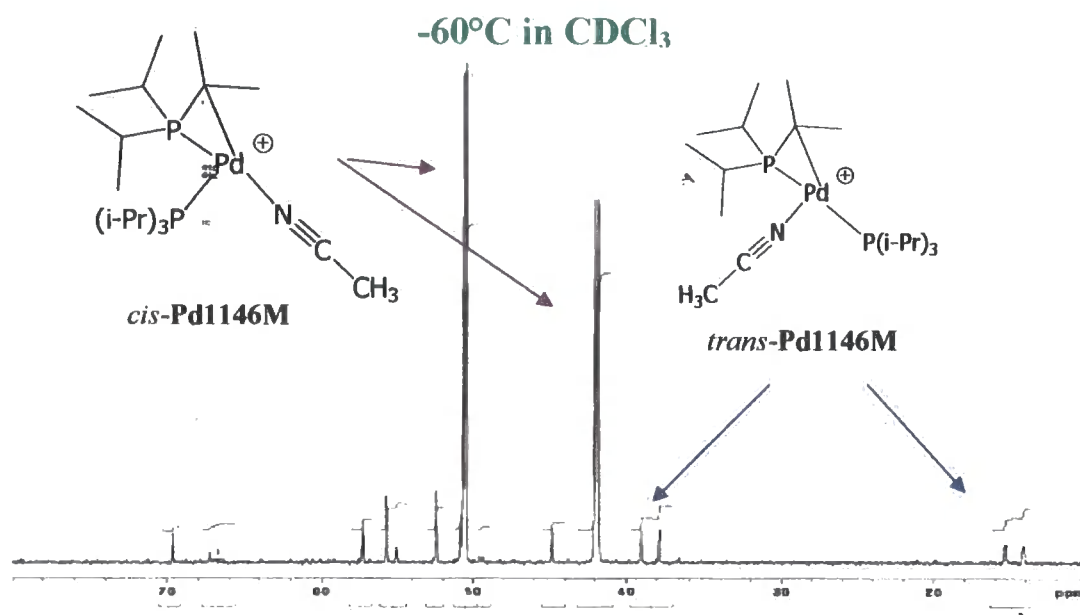


Figure 2.12. Low temperature (-60°C) $^{31}\text{P}\{^1\text{H}\}$ NMR spectrum of Pd1146M.

Exchange spectroscopy (EXSY), which is a form of ^{31}P - ^{31}P 2D NMR, was attempted at temperatures ranging from 25 to -60°C to find the temperature at which the *cis*- and *trans*-Pd1146M would be visible but still displaying a high enough level of exchange necessary to run the NMR experiment.

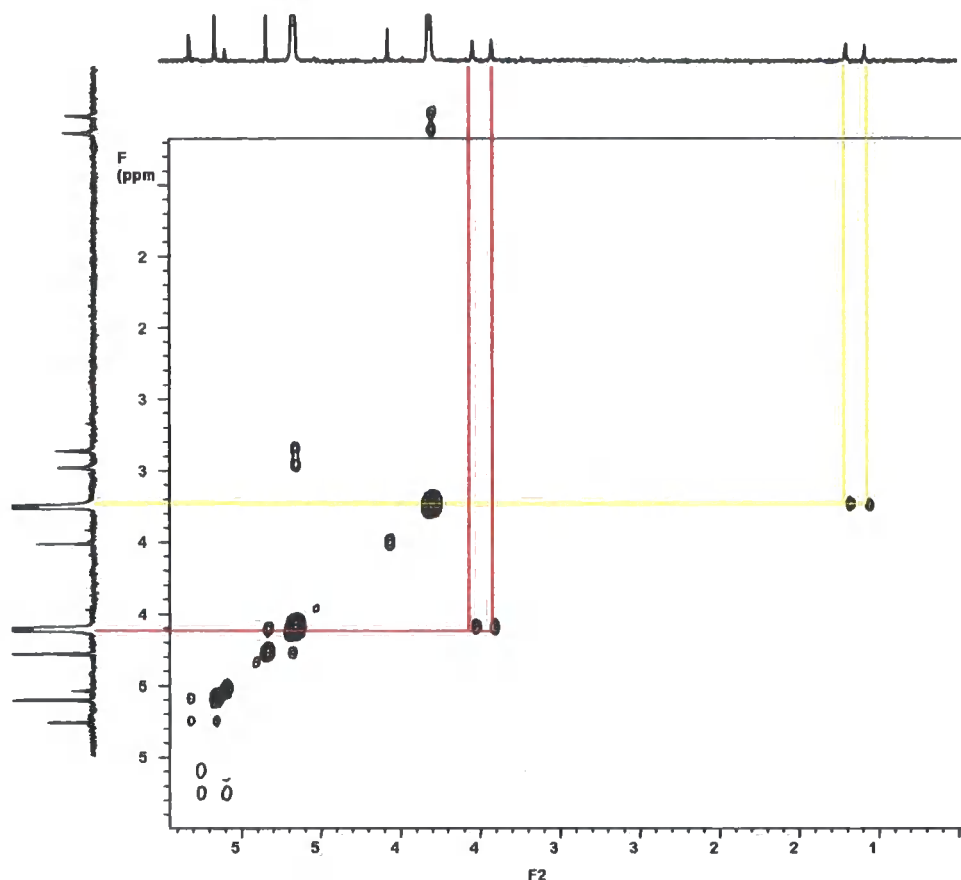


Figure 2.13. ^{31}P - ^{31}P 2D-NMR spectrum (EXSY) of **Pd1146M** at -20°C .

A positive correlation in the 2D-NMR between the two different sets of doublets belonging to *cis*- and *trans*-**Pd1146M** would prove that the two species are in exchange and hence confirm the *cis*- and *trans*-structure. A positive correlation and hence conclusive structural identification for *cis/trans*-**Pd1146M** was observed at -20°C , figure 2.13.

2.2.10 Synthesis and Characterisation of

[Pd(P-*i*-Pr₃)((*i*-Pr₂)P-C(CH₃)=CH₂)(NCCH₃)(H))[B(C₆F₅)₄] (Pd1146H**)**

The **Pd1146M** generated as described in section 2.2.9, undergoes a clean thermolysis to **Pd1146H**, which rapidly converts to **Pd1148** in THF-*d*₈ at ambient temperature. This inherent instability in coordinating solvents such as THF explains why both complexes are only ever present in small concentrations during the thermolysis of **Pd1206**, figure 2.3.

The thermolysis of **Pd1146M** was investigated at ambient temperature in the non-coordinating solvent, CDCl_3 , in an attempt to produce a stable form of **Pd1146H**, which would allow structural determination, figure 2.14. This attempt was only partially successful because it enabled the formation of **Pd1146H** in relatively large concentrations, but it did not push the thermolysis of **Pd1146M** to completion without causing the **Pd1146H** to undergo partial thermolysis, to produce **Pd1148**. The **Pd1146H** can be seen in the ^{31}P NMR spectra as an AB-system of signals ($J = 322.0$ Hz), which is consistent with two slightly different *trans*-phosphine ligands positioned around the palladium centre.

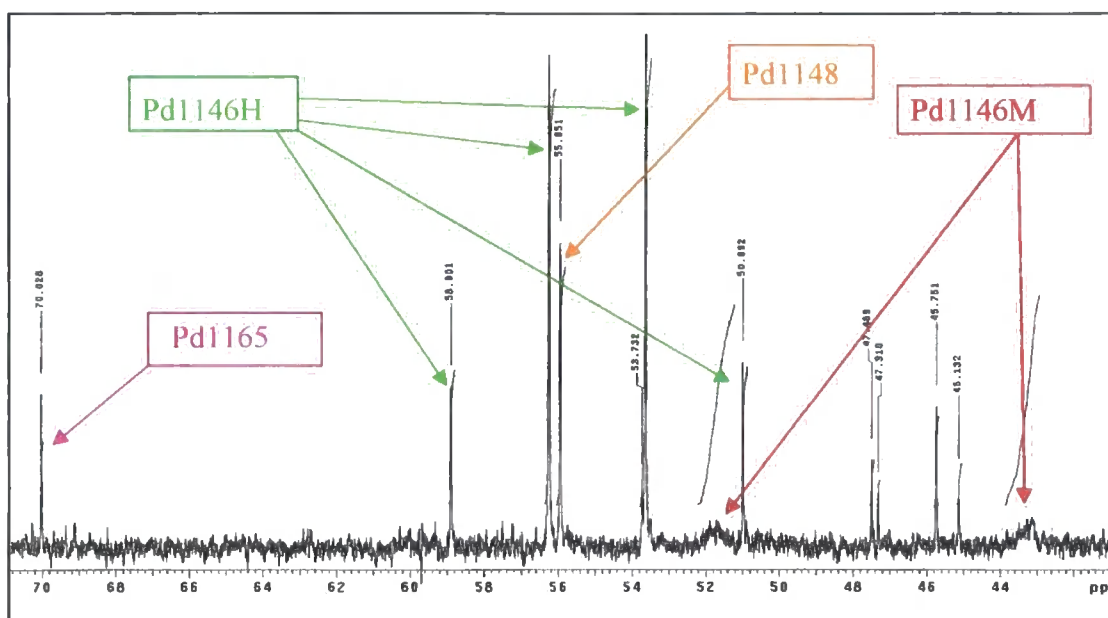


Figure 2.14. ^{31}P NMR spectrum of **Pd1146H** in CDCl_3 .

Pd1146H can also be identified in the ^1H NMR spectra by the characteristic resonances for the vinylic protons in the phosphine ligand and the Pd-H^+ generated via the rearrangement of **Pd1146M**, figure 2.15. The integral value for the vinyl resonance is exactly twice the intensity of the hydride resonance. The ^1H NMR coupling constants of $^3J_{\text{PH}} = 34.8$ (*trans* to P) and $^3J_{\text{PH}} = 16.1$ (*cis* to P) Hz, observed for the vinylic protons are consistent with 3-bond coupling to a *cis*- and *trans*-phosphine across the double bond. Although you would expect the Pd-H resonance coupling to be in the form of a doublet of doublets, you actually see a relatively clean triplet suggesting that the phosphines behave as near identical with respect to the hydride.

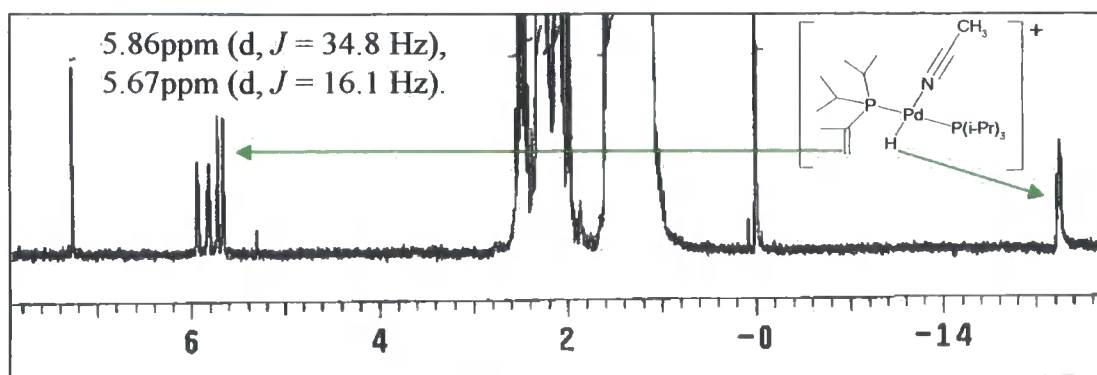


Figure 2.15. ^1H NMR spectrum of **Pd1146H** in CDCl_3 .

2.2.11 Thermolysis of $[\text{Pd}(\text{P-}i\text{-Pr}_3)(\text{P}(i\text{-Pr}_2)(\kappa^2\text{-C}(\text{CH}_3)_2))(\text{NCCH}_3)][\text{B}(\text{C}_6\text{F}_5)_4]$ (**Pd1146M**) at 35°C

The thermolysis of **Pd1146M** (in CDCl_3) at 35°C , over a period of 12 hours generates numerous cationic palladium hydride complexes, which are attributed to new tris-phosphine species. The ^{31}P NMR coupling constants characterise a cationic palladium species with an ABB disposition of phosphines around palladium, with A and B *trans*, figure 2.16. This allows **Pd1273H** or **Pd1275H** species to be postulated based on these ^{31}P NMR spectroscopic assignments. The new species accounts for approximately 60% of the ^{31}P NMR resonances. The **Pd1148** can also be seen in the ^{31}P NMR.

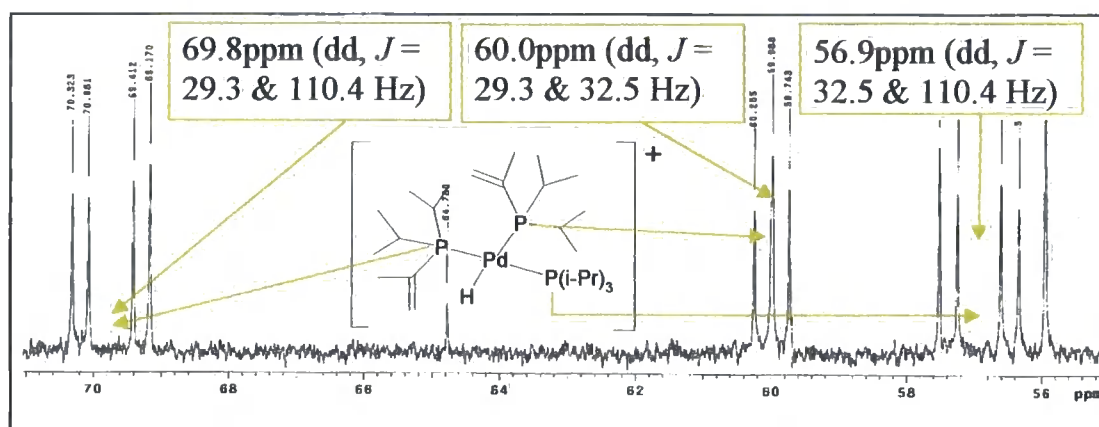


Figure 2.16. ^{31}P NMR spectrum of **Pd1273H** or **Pd1275H**

There are also a number of new unknown species generated during this thermolysis. Two doublets represent the most interesting species, at 44.6 and -48.1 ppm, with a coupling constant of 362.0 Hz. This coupling constant is indicative of two non-identical phosphines

in a *trans* deposition around palladium. The position of these doublets is quite perplexing, considering the 92.7 ppm gap between the resonances.

2.2.12 The Fate of the (i-Pr₂)P-C(CH₃)=CH₂ Ligand

During the thermolysis of **Pd1206**, **Pd1165** and **Pd1146M** in coordinating solvents such as THF, the only fully characterized and thermally stable product is **Pd1148**. According to the thermolysis mechanism there should be a 1:1 ratio of P(i-Pr)₃ to (i-Pr₂)P-C(CH₃)=CH₂, after complete thermolysis, giving a 50% maximum theoretical yield of **Pd1148**. The yield of **Pd1148** in all the above cases is always < 50%, which is consistent with the mechanism of thermolysis already suggested, considering loss of phosphine ligand due to side reactions.

The rapid thermolysis of **Pd1146H** in coordinating solvents suggests that the (i-Pr₂)P-C(CH₃)=CH₂ ligand is much more labile than the P(i-Pr)₃. An important issue arising from the proposed mechanism is, where the (i-Pr₂)P-C(CH₃)=CH₂ ligand goes after it is replaced by an P(i-Pr)₃ during the rearrangement of **Pd1146H** to give **Pd1148**.

A close examination of the ³¹P and ¹H NMR spectra, both during and after the thermolysis of **Pd1206**, reveals many clues, figure 2.17. There are three broad resonances in the ³¹P NMR spectra; 67.0 (light blue), 50.5 (dark blue) and 36.6 (red) ppm, which shift as their concentrations change, indicating that their phosphines are in exchange. This would be likely for any species containing the highly labile (i-Pr₂)P-C(CH₃)=CH₂ ligand. The corresponding ¹H NMR spectra reveal a scrambling of the vinylic signals displayed by the (i-Pr₂)P-C(CH₃)=CH₂ ligand in **Pd1146H**, suggesting that it is coordinated to numerous cationic palladium species.

³¹P-¹H 2D-NMR spectroscopy was used to investigate if the new vinylic signals in the ¹H NMR spectra correlate to any of the broad resonances in the ³¹P NMR spectra, at the end of **Pd1206**'s thermolysis. The vinylic signals in the ¹H NMR spectra correlated with the broad ³¹P NMR signals as shown in the correlation diagram.

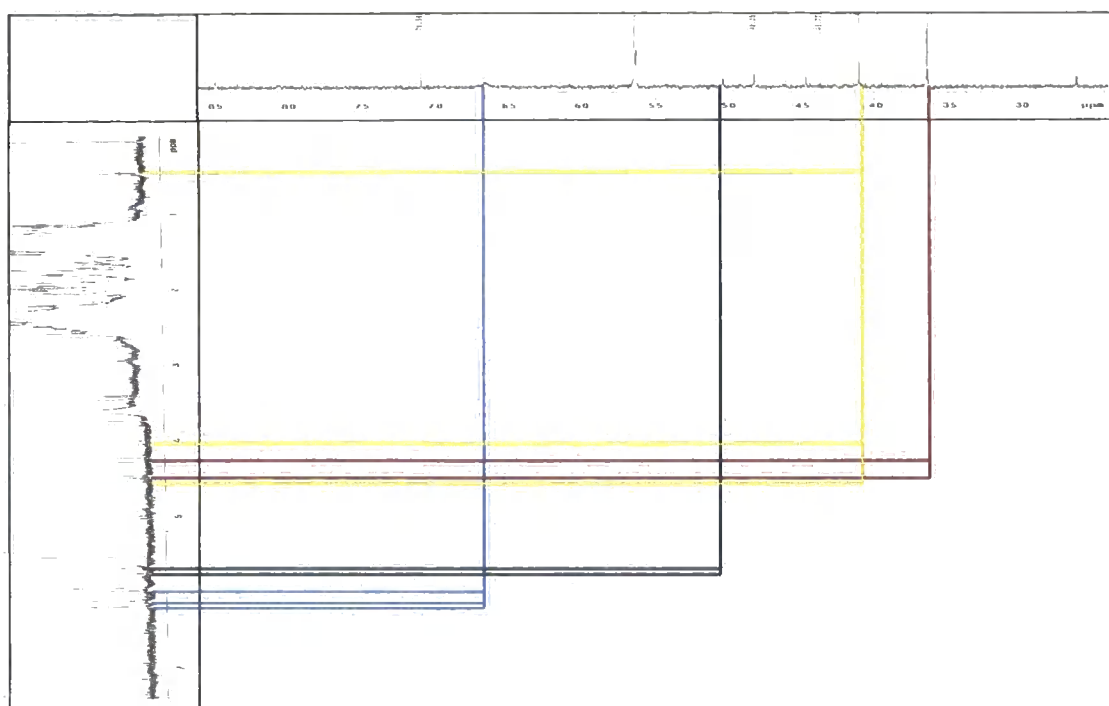


Figure 2.17. ^{31}P - ^1H 2D-NMR spectra near the end of the **Pd1206** thermolysis.

The vinylic signals in the ^1H NMR spectra at 6.16 and 5.91 ppm, with coupling constants of 37.0 and 18.0 Hz, respectively, are the most significant in size and were shown to correlate (light blue line) to the large, broad, shifting ^{31}P NMR resonance at approximately 67 ppm. These resonances closely resemble the ^1H NMR vinylic signals displayed by **Pd1146H** and the ^{31}P NMR resonance for **Pd1148**, which suggests this species, could be a close analogue, such as **Pd1144H**.

The ^1H NMR vinylic signals at 4.48 and 4.23 ppm, with coupling constants of 14.1 and 28.7 Hz, respectively, were shown to correlate (red line) to the large, sharp, shifting, ^{31}P NMR resonance at approximately 36 ppm. The nature of this species is unknown.

As expected a correlation occurs (yellow line) between the ^{31}P NMR resonance for **Pd1162** at 41.1 ppm and the triplet in the ^1H NMR at 0.42 ppm (Pd-Me^+) but surprisingly a correlation also occurs to a relatively small area of vinylic signals at 4.03 and 4.51 ppm, with coupling constants of 27.8 and 15.5 Hz, respectively. This suggests that the $(i\text{-Pr}_2)\text{P-C}(\text{CH}_3)=\text{CH}_2$ ligand is in exchange with $\text{P}(i\text{-Pr})_3$ for most species during the thermolysis of **Pd1206**.

2.2.13 Effect of Additives on Generation of $[\text{Pd}(\text{P-i-Pr}_3)_2(\text{NCCH}_3)(\text{H})][\text{B}(\text{C}_6\text{F}_5)_4]$ from $[\text{Pd}(\text{P-i-Pr}_3)_2(\text{NCCH}_3)(\text{OAc})][\text{B}(\text{C}_6\text{F}_5)_4]$

During the thermolysis of **Pd1206** numerous new, unidentifiable species were generated, which could be viewed by ^{31}P NMR spectroscopy. Attempts were made to identify these by matching the ^{31}P NMR signals to some likely model species such as triisopropylphosphine (20.9 ppm), triisopropylphosphine oxide (61.8 ppm), triisopropylphosphonium FABA (44.8 ppm) and $\text{Pd}(\text{i-Pr}_3)_2(\text{OAc})_2$ (33.6 ppm). These tests showed that the above compounds were not present during any of the thermolysis experiments.

Promerus LLC have been using additives during polymerisations using the initiators discussed, to increase the yield of polymer product. It was speculated that these additives were increasing the **Pd1206**'s activity by increasing the yield of palladium hydride generated upon thermolysis. The yield of palladium hydride species produced during the thermolysis of **Pd1206** is of importance because it is thought to be the most active species and will therefore have a direct effect on this complexes ability to polymerise norbornene monomers.

LiFABA and DANFABA have both been used as additives and can both be used to convert neutral species such as $\text{Pd}(\text{i-Pr}_3)_2(\text{OAc})_2$ into active cationic species such as **Pd1206**.^{1, 2, 3} The effects of these as additives were investigated during **Pd1206**'s thermolysis. Both of these additives had a negative effect on the thermolysis, creating more palladium metal and less palladium hydride. This result confirms that $\text{Pd}(\text{i-Pr}_3)_2(\text{OAc})_2$ is not observed during the thermolysis.

During the thermolysis of **Pd1206** an unwanted decarboxylation side reaction occurs to give **Pd1162**, which readily decomposes to give palladium metal and other unknown complexes. The use of acetic acid as an additive to the thermolysis of **Pd1206** was investigated, hoping that it would mop-up any of the **Pd1162** produced, bringing it back into the thermolysis loop as **Pd1206**, therefore reducing the level of unwanted palladium metal produced. In practice this acetic acid additive was shown to have a negative effect, increasing the production of **Pd1162** and palladium metal and decreasing the level of palladium hydride production.

Triisopropylphosphine was used as an additive in the thermolysis of **Pd1206**, hoping that it would deter unwanted side reactions and give a cleaner product. It was found to make the

thermolysis much slower and also cleaner, with less **Pd1162** and palladium metal produced. The yield of **Pd1148** was lower but this was due to the difficulty in pushing the thermolysis to completion.

The conversion of **Pd1165** through to **Pd1146M** is driven by the addition of bases to the reaction mixtures. Therefore, the use of organic bases were investigated as additives in the thermolysis of **Pd1206** and **Pd1165**, to evaluate whether it pushed the thermolysis through more quickly. This would mean that the complex would not have to be heated for as long, decreasing side reactions and palladium metal production. Experimentally this was not shown to be the case, with 2,6-di-tert-butylpyridine and bis(dimethylamino)naphthalene causing the decomposition of **Pd1206** and **Pd1165** into palladium metal.

Promerus LLC have been using chain transfer reagents, such as formic acid and triethylsilane (Et_3SiH), as additives during polymerisations because they believed that their additions increase the yield and give a lower polydispersity for the resulting polymer.

The effect of Et_3SiH upon the polymerization catalyst, **Pd1206**, was investigated under various conditions. The addition of 1 equivalent of Et_3SiH to a solution of **Pd1206** resulted in the near quantitative generation of **Pd1148** even at ambient temperature. The reaction was relatively rapid, with 50% conversion after 15 minutes and complete conversion within 60 minutes. A small quantity of palladium metal and unwanted side products could be viewed via ^{31}P NMR spectroscopy. A close study of the ^1H NMR spectra reveals that no unsaturation is generated during this reaction, suggesting that the complicated thermolysis sequence already discussed for **Pd1206** is obviated by the addition of Et_3SiH . These conclusions suggested that Et_3SiH may be employed for the conversion of any general complex, $[\text{Pd}(\text{PR}_3)_2(\text{OAc})(\text{NCCH}_3)][\text{FABA}]$, into $[\text{Pd}(\text{PR}_3)_2(\text{H})(\text{NCCH}_3)][\text{FABA}]$, for any trialkylphosphine. This methodology was used to attempt the 1g-scale synthesis of **Pd1148** from **Pd1206**. The synthesis was successful in generating **Pd1148** in high yield, but the small, undesirable side products could not be removed from the final product using precipitation of the complex from dichloromethane into hexanes.

2.2.14 Comparison of Polymerisation Activities

The work described above suggests that the likely active species during polymerisations involving **Pd1206** is its stable palladium hydride thermolysis product **Pd1148**. The palladium hydride is only produced in approximately 50% yield during thermolysis so it would be of interest to directly compare the activity of **Pd1206** versus **Pd1148** in a model system.

The polymerisation of *endo/exo*-5-decyl-2-norbornene was carried out in toluene-*d*₈, at 70°C in an NMR tube, in a ratio of 50 monomer:1 catalyst, figure 2.18 and 2.19. The rate of polymerization would be calculated via the reduction in the monomer vinyl resonances in the ¹H NMR spectra, over the first 5-6% conversion.

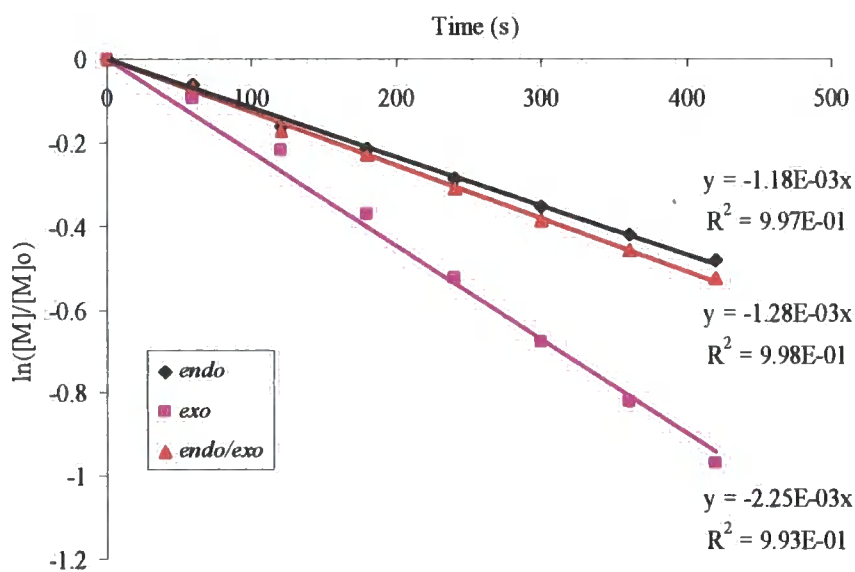


Figure 2.18. First order kinetic plot for the polymerisation of *endo/exo*-NBdecyl by **Pd1206** (50 monomer:1 catalyst) at 70°C in toluene-*d*₈.

The **Pd1148** ($k = 4.54 \times 10^{-3} \text{ s}^{-1}$) polymerizes *endo/exo*-5-decyl-2-norbornene approximately four times faster than **Pd1206** ($k = 1.28 \times 10^{-3} \text{ s}^{-1}$).

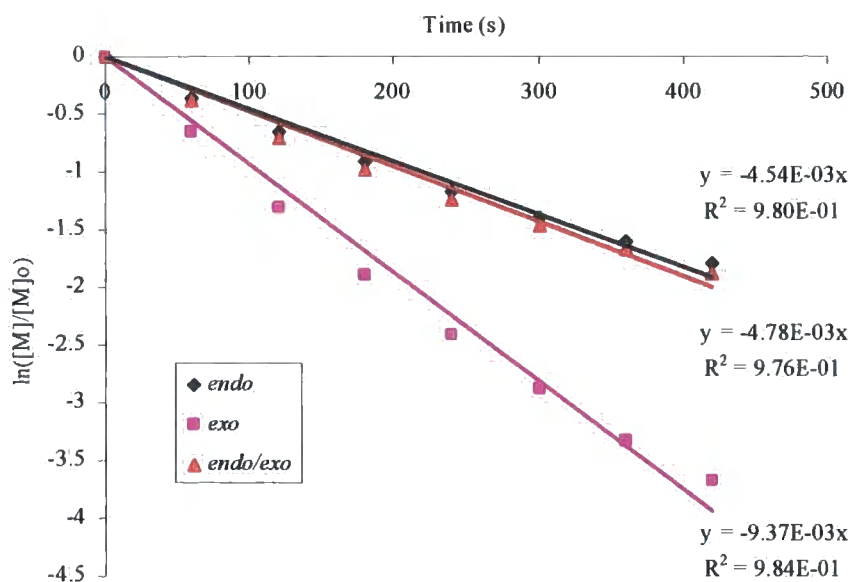


Figure 2.19. First order kinetic plot for the polymerisation of *endo/exo*-5-decyl-2-norbornene by **Pd1148** (50 monomer : 1 catalyst) at 70°C in toluene-*d*₈.

The GPC data for the same polymerisations on a 1g scale showed that **Pd1148** generates a lower molecular weight polymer ($M_w = 33000$ versus 60000), sharper PDI ($M_w/M_n = 1.87$ versus 2.87), and higher yield than **Pd1206** under the same conditions.

These results compare favorably with the results of Protasiewicz *et al.*,² where polymerisations were carried out in toluene (17 mL) for 3 hr at 63°C at 10.7 mM of 5-decyl-2-norbornene and 0.4 μ M of catalyst concentrations (5-decyl-2-norbornene/Initiator ratio: 26700). The GPC data for these polymerisations showed that **Pd1148** generates a lower molecular weight polymer ($M_w = 1369000$ versus 1924000), sharper PDI ($M_w/M_n = 1.8$ versus 3.1), and higher yield (92% versus 66%) than **Pd1206** under the same conditions.

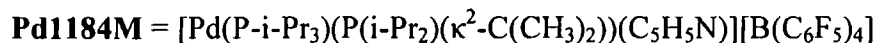
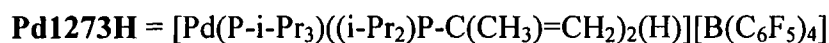
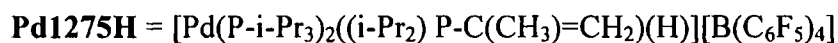
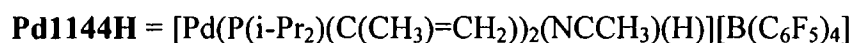
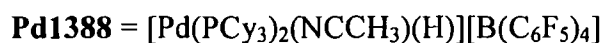
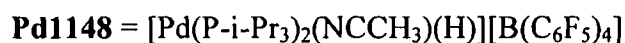
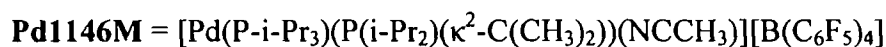
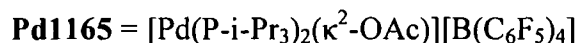
Protasiewicz *et al.*,² also demonstrated that the related cationic palladium hydride, $[\text{Pd}(\text{PCy}_3)_2(\text{NCCH}_3)(\text{H})][\text{B}(\text{C}_6\text{F}_5)_4]$ (**Pd1388**), displayed slightly improved polymerisation activity than **Pd1148**. The GPC data for these polymerisations showed that **Pd1388** generates a lower molecular weight polymer ($M_w = 1311000$ versus 1369000), similar PDI ($M_w/M_n = 1.8$ versus 1.8), but a higher yield (98% versus 92%) than **Pd1148** under the same conditions. This is thought to be due to the higher purity of the **Pd1388** catalyst versus **Pd1148**.

2.3 Conclusions

The results suggest that the cationic palladium hydride complexes are the active initiators during the polymerisation of norbornene type monomers, when this family of thermally activated complexes are utilised. The **Pd1148** is shown to be thermally stable under the conditions of thermolysis. It is expected that a better quality of polymer would be produced via the use of pure cationic palladium hydride initiators since a lower concentration of initiator could be used without the unnecessary production of palladium metal, observed during the thermolysis of **Pd1206**. The use of a thermally stable discrete cationic palladium hydride polymerisation catalyst should also allow more accurate mechanistic studies of polymerisation mechanism, enabling further advances in the polymeric materials to be made.

2.4 Experiment

2.4.1 Glossary of Cationic Palladium Species



2.4.2 Materials

The palladium catalysts, $\text{Li}(\text{Et}_2\text{O})_{2.5}[\text{B}(\text{C}_6\text{F}_5)_4]$ (LiFABA), $\text{K}[\text{B}(\text{C}_6\text{F}_5)_4]$ (KFABA), $[\text{HN}(\text{Ph})(\text{Me})_2][\text{B}(\text{C}_6\text{F}_5)_4]$ (DANFABA) and triisopropylphosphine were supplied by Promerus LLC and used without further purification. The following materials and solvents were purchased from Sigma Aldrich and used without further purification: sodium mesylate, sodium tosylate, lithium bromide, lithium triflate, magnesium sulphate, hydrogen peroxide, bis(dimethylamino)naphthalene, 2,6-di-tert-butylpyridine, formic acid, acetic acid, triethylsilane, acetonitrile, pyridine, dichloromethane, acetonitrile, diethylether.

All liquid monomers were degassed by freeze-thaw-pump cycles before being taken into the glove box.

Tetrahydrofuran- d_8 , chloroform- d , dichloromethane- d_2 , benzene- d_6 and toluene- d_8 were used as supplied in pre-sealed ampules and kept refrigerated in a glove box.

2.4.3 Instrumentation and Measurements

2.4.3.1 Nuclear Magnetic Resonance

^1H NMR spectra were recorded on a Varian Mercury 400 or a Varian Inova 500 using deuteriated solvent lock. Chemical shifts are quoted in ppm, relative to tetramethylsilane (TMS), as the internal reference. ^{31}P NMR spectra were recorded on a Varian/Mercury 400 or a Varian Inova 500 at 121.4 MHz and 202.4 MHz, respectively. The following abbreviations are used in listing NMR spectra: s = singlet, d = doublet, t = triplet, q = quartet, b = broad, m = multiplet.

2.4.3.2 Gel Permeation Chromatography (GPC)

Gel permeation chromatography (GPC) data was obtained using a Viscotek TDA 302 equipped with 2 x 300 mm PLgel $5\mu\text{m}$ mixed C columns. Tetrahydrofuran was used as the

eluent, at a flow rate of 1.0 mL/min at 30°C. The detectors were calibrated using polystyrene standards. This type of conventional GPC analysis, based on polystyrene standards, is unsuitable to determine actual molecular weights of poly(norbornene) derivatives, but can be used to compare relative molecular weights.

2.4.4 Synthesis and Characterisation

2.4.4.1 Synthesis of $[\text{Pd}(\text{P-}i\text{-Pr}_3)_2(\text{NCCH}_3)(\text{OAc})][\text{B}(\text{C}_6\text{F}_5)_4]$ (Pd1206) Using LiFABA

$\text{Li}(\text{Et}_2\text{O})_{2.5}[\text{B}(\text{C}_6\text{F}_5)_4]$ (960 mg, 1.102 mmol) was added to a stirred solution of $\text{Pd}(\text{P-}i\text{-Pr}_3)_2(\text{OAc})_2$ (600 mg, 1.102 mmol) in acetonitrile (30 mL). The mixture was stirred for 4 hours although ^{31}P NMR spectroscopy showed the reaction to be almost instantaneous. The mixture was filtered to remove LiOAc salt and the solvent removed under reduced pressure, taking care not to heat the solution. The product was dissolved into dichloromethane (25 mL), dried over MgSO_4 , filtered, and solvent removed under reduced pressure to yield a bright yellow solid in > 95% yield. The ^1H and ^{31}P NMR spectra showed the sample to be clean, figure 2.20.

^1H NMR (300 MHz, $\text{THF-}d_8$): δ (ppm) = 2.43 (s, 3H, $-\text{O}_2\text{CCH}_3$), 2.26 (m, 6H, $-\text{P}(\text{CHMe}_2)_3$), 1.90 (s, 3H, $-\text{NCCH}_3$), 1.39 (m, 36H, $-\text{P}(\text{CHMe}_2)_3$).

^{31}P NMR (121.4 MHz, $\text{THF-}d_8$): δ (ppm) = 45.6.

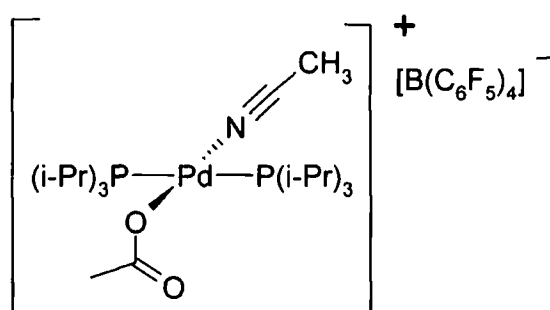


Figure 2.20

2.4.4.2 Synthesis of Pd1206 Using DANFABA

[HN(Ph)(Me)₂][B(C₆F₅)₄] (880 mg, 1.102 mmol) was added to a stirred solution of Pd(P-*i*-Pr₃)₂(OAc)₂ (600 mg, 1.102 mmol) in acetonitrile (30 mL). The mixture was stirred for 4 hours although ³¹P NMR spectroscopy showed the reaction to be complete almost instantaneously. The mixture was filtered and the solvent was removed under reduced pressure taking care not to heat the solution. The product was dissolved into DCM (25 mL), dried over MgSO₄, filtered, and the solvent reduced under reduced pressure. The remaining solution (~ 3 mL) was precipitated into hexanes to yield a bright yellow solid in > 95% yield. The ¹H and ³¹P NMR spectra showed the sample to be clean.

2.4.4.3 Attempted Synthesis of Pd1206 Using KFABA

K[B(C₆F₅)₄] (600 mg, 0.884 mmol) and Pd(P-*i*-Pr₃)₂(OAc)₂ (456 mg, 0.884 mmol) were added to stirred acetonitrile (42 mL). The conversion was followed via ³¹P NMR spectroscopy, after 24 hours the conversion had stopped at 40%. The following additives were used to push the reaction to completion without success: water, diethyl ether, NaOMs, NaOTs, LiBr.

2.4.4.4 Synthesis of Pd1206 Using KFABA and Li[O₃SCF₃]

The following solids were added to stirred acetonitrile (42 mL), K[B(C₆F₅)₄] (600 mg, 0.884 mmol), Pd(P-*i*-Pr₃)₂(OAc)₂ (456 mg, 0.884 mmol), LiOTf (132 mg, 0.884 mmol). The mixture was stirred for 1 hour although ³¹P NMR spectroscopy showed the reaction to be complete almost instantaneously. The mixture was filtered and the solvent removed under reduced pressure taking care not to heat the solution. The product was dissolved into DCM (25 mL), dried over MgSO₄, filtered, and solvent removed under reduced pressure to yield a bright yellow solid in > 95% yield. The ¹H and ³¹P NMR spectra showed the sample to be clean.

2.4.4.5 Synthesis of Triisopropylphosphine Oxide

Triisopropylphosphine (10 mg) was dissolved in THF- d_8 (0.6 mL) and hydrogen peroxide was added dropwise (10 drops). The sample was subjected to ^{31}P NMR spectroscopy.

^{31}P NMR (121.4 MHz, THF- d_8), δ (ppm): 59.2.

2.4.4.6 Triisopropylphosphonium FABA

The compound was provided by Promerus LLC as a reference material.

^{31}P NMR (121.4 MHz, THF- d_8), δ (ppm): 44.8.

2.4.4.7 Thermolysis of Pd1206 in THF- d_8

Pd1206 (50 mg, 4.15×10^{-5} mol) was dissolved in THF- d_8 (0.6 mL) and transferred to an NMR tube fitted with a Young's tap. The solution was then subjected to thermolysis at various temperatures inside the NMR probe. ^1H NMR spectra or ^{31}P NMR spectra were taken at regular time intervals during the thermolysis. The integral values of peaks, of known identity, were plotted in tables and graphs. The solution developed a red colour and produced a black palladium precipitate in all cases.

The table shows selected peaks and integral values during the thermolysis of **Pd1206** by ^1H NMR spectroscopy at 50°C. The numbers in the table have no real meaning, only to show how functionalities increase or decrease during thermolysis.

Table 2.1

Time/Minutes	10.34 ppm (CH ₃ CO ₂ H)	7.5 - 4.5 ppm (vinyl)	2.61 ppm (CH ₃ CO ₂ -Pd)	-15.26 ppm (Pd-H)
2.19	0.12		30	
10.93	0.65			
22.49	0.93		28.99	
27.49		2.29		
32.49	0.98		28.15	
42.5	1.26		26.73	
47.5		2.42		
57.5	1.57		24.84	0.92
117.52	3.06	3.54	18.07	1.88
177.52	3.32	4.63	13.6	2.4
237.52	3.77	5.11	10.25	2.85
297.53	3.75	5.9	8.24	3.12

The following are selected ³¹P NMR spectroscopy data for the thermolysis of **Pd1206** at 55°C.

³¹P NMR (121.4 MHz, THF-*d*₈), δ (ppm): Time = 0; 45.6 (100%, **Pd1206**). Time = 1000 mins; 71.4 (1.5%, **Pd1165**), 66.3 (8.2%, broad), 56.9 (41.9%, **Pd1148**), 50.5 (4.0%, broad), 43.8 (3.7%), 41.3 (4.7%, **Pd1162**), 36.6 (9.6%).

2.4.4.8 Thermolysis of Pd1206 + LiFABA in THF-*d*₈

Pd1206 (60.3 mg, 5.0 × 10⁻⁵ mol) and LiFABA (43.5 mg, 5.0 × 10⁻⁵ mol) were dissolved in THF-*d*₈ (0.6 mL) and transferred to an NMR tube fitted with a Young's tap. The solution was then subjected to thermolysis at 55°C for 450 minutes in an oil bath. ¹H and ³¹P NMR spectra were recorded at the end of the thermolysis. The solution developed a red colour and produced a black palladium precipitate.

³¹P NMR (121.4 MHz, THF-*d*₈), δ (ppm): 71.4 (3.0%, **Pd1165**), 57.1 (9.3%), 56.9 (34.0%, **Pd1148**), 36.1 (13.7%). Lots of small signals between 52 and 39 ppm.

¹H NMR (299.9 MHz, THF-*d*₈), δ (ppm): 10.6 (0.6H, broad, CH₃CO₂H), 7-5 (0.49H, m, vinyl), 0.40 (0.04H, m, Pd-CH₃), -15.1 (0.27H, m, Pd-H).

2.4.4.9 Thermolysis of Pd1206 + DANFABA in THF-*d*₈

Pd1206 (60.3 mg, 5.0×10^{-5} mol) and DANFABA (40.1 mg, 5.0×10^{-5} mol) were dissolved in THF-*d*₈ (0.6 mL) and transferred to an NMR tube fitted with a Young's tap. The solution was then subjected to thermolysis at 55°C for 450 minutes in an oil bath. ¹H and ³¹P NMR spectra were recorded at the end of the thermolysis. The solution developed a red colour and produced a black palladium precipitate.

³¹P NMR (121.4 MHz, THF-*d*₈), δ (ppm): 71.4 (3.0%, **Pd1165**), 60.0 (9.0%, broad), 56.9 (32.5%, **Pd1148**), 50.7 (4.6%, broad), 44.7 (6.8%), 43.8 (4.5%), 41.3 (2.6%, **Pd1162**), 36.1 (7.2%).

¹H NMR (299.9 MHz, THF-*d*₈), δ (ppm): 7-5 (1.02H, m, vinyl), 0.40 (0.01H, m, Pd-CH₃) - 15.1 (0.34H, m, Pd-H).

2.4.4.10 Thermolysis of Pd1206 + 2,6-di-tert-butylpyridine in THF-*d*₈

Pd1206 (60.3 mg, 5.0×10^{-5} mol) and 2,6-di-tert-butylpyridine (9.6 mg, 5.0×10^{-5} mol) were dissolved in THF-*d*₈ (0.6 mL) and transferred to an NMR tube fitted with a Young's tap. The solution was then subjected to thermolysis at 55°C for 450 minutes in an oil bath. ¹H and ³¹P NMR spectra were recorded at the end of the thermolysis. The solution initially developed a yellow colour but eventually produced an orange solution.

³¹P NMR (121.4 MHz, THF-*d*₈), δ (ppm): Huge amount of small unidentified signals, 56.4 (**Pd1148**, 2%).

¹H NMR (299.9 MHz, THF-*d*₈), δ (ppm): 7-5 (0.81H, m, vinyl), 0.40 (0.11H, m, Pd-CH₃) - 15.1 (0.06H, m, Pd-H).

2.4.4.11 Thermolysis of Pd1206 + Bis(dimethylamino)naphthalene in THF-*d*₈

Pd1206 (60.3 mg, 5.0×10^{-5} mol) and bis(dimethylamino)naphthalene (10.7 mg, 5.0×10^{-5} mol) were dissolved in THF-*d*₈ (0.6 mL) and transferred to an NMR tube fitted with a Young's tap. The solution was then subjected to thermolysis at 55°C for 450 minutes in an oil bath. ¹H and ³¹P NMR spectra were recorded at the end of the thermolysis. The solution produced a very dark red solution.

³¹P NMR (121.4 MHz, THF-*d*₈), δ (ppm): Huge amount of small unidentified signals, 56.4 (**Pd1148**, 8%).

¹H NMR (299.9 MHz, THF-*d*₈), δ (ppm): 7-5 (0.37H, m, vinyl), -15.1 (0.12H, m, Pd-H).

2.4.4.12 Thermolysis of Pd1206 + Triisopropylphosphine in THF-*d*₈

Pd1206 (60.3 mg, 5.0×10^{-5} mol) and triisopropylphosphine (8.0 mg, 5.0×10^{-5} mol) were dissolved in THF-*d*₈ (0.6 mL) and transferred to an NMR tube fitted with a Young's tap. The solution was then subjected to thermolysis at 55°C for 450 minutes in an oil bath. ¹H and ³¹P NMR spectra were recorded at the end of the thermolysis. The solution developed a bright yellow colour.

³¹P NMR (121.4 MHz, THF-*d*₈), δ (ppm): 71.4 (2.0%, **Pd1165**), 61.8 (3.5%), 59.2 (10%), 56.9 (35%, **Pd1148**), 51.4 (8%), 21.0 (3%). Lots of small, broad signals between 50 and 35 ppm.

¹H NMR (299.9 MHz, THF-*d*₈), δ (ppm): 11.4 (0.58H, broad, CH₃CO₂H), 7-5 (0.84H, m, vinyl), -15.1 (0.77H, m, Pd-H).

2.4.4.13 Thermolysis of Pd1206 + Acetic Acid in THF-*d*₈

Pd1206 (60.3 mg, 5.0×10^{-5} mol) and acetic acid (3.0 mg, 5.0×10^{-5} mol) were dissolved in THF-*d*₈ (0.6 mL) and transferred to an NMR tube fitted with a Young's tap. The solution

was then subjected to thermolysis at 55°C for 450 minutes in an oil bath. ^1H and ^{31}P NMR spectra were recorded at the end of the thermolysis. The solution developed a dark brown colour and a lot of palladium metal.

^{31}P NMR (121.4 MHz, THF- d_8), δ (ppm): 75.0 (4.0%, broad), 71.4 (3.0%, **Pd1165**), 62.0 (9.0%, broad), 56.9 (14.2%, **Pd1148**), 55.2 (6.1%), 52.0 (2.0%), 46.1 (1.7%), 44.7 (4.0%), 42.0 (2.8%), 41.1 (**Pd1162**, 11.1%), 38.9 (3%). Lots of small signals between 60 and 35 ppm.

^1H NMR (299.9 MHz, THF- d_8), δ (ppm): 9.0 (1.85H, broad, $\text{CH}_3\text{CO}_2\text{H}$), 7-5 (0.60H, m, vinyl), -15.1 (0.15H, m, Pd-H).

2.4.4.14 Thermolysis of Pd1206 + Triethylsilane

Pd1206 (1.00g, 8.3×10^{-4} mol) and triethylsilane (96.3 mg, 8.3×10^{-4} mol) were dissolved in DCM (20 mL). The solution was stirred for 4 hours (colour change from yellow to red), dried over MgSO_4 , filtered and reduced to ~ 1.5 mL under reduced pressure. The filtrate was slightly grey coloured because of palladium metal mixed with MgSO_4 . The DCM solution was precipitated into hexanes (5 mL), filtered and dried under reduced pressure to yield a red powder (0.85g, 90%). The red coloured powder was analysed by ^1H and ^{31}P NMR spectroscopy.

^{31}P NMR (121.4 MHz, THF- d_8), δ (ppm): 71.0 (**Pd1165**, 8.7%), 56.9 (**Pd1148**, 72.4%), 55.3 (1.9%), 48.7 (1.1%), 46.7 (4.2%), 45.9 (10.3%), 38.6 (1.4%).

^1H NMR (200.0 MHz, THF- d_8), δ (ppm): -15.20 (t, $^2J_{\text{PH}} = 7.35$, Pd-H).

2.4.4.15 Stability of Pd1165 at 20°C in THF- d_8

Pd1165 (25 mg, 2.15×10^{-5} mol) was dissolved in THF- d_8 (0.6 mL) and transferred to an NMR tube fitted with a Young's tap. The tube was left at room temperature for 24 hours to check the stability of the **Pd1165** species in solution. ^{31}P NMR spectra were run.

^{31}P NMR (121.4 MHz, THF- d_8), δ (ppm): Time = 0; 80.5 (7.8%), 71.0 (80.3%), 54.1 (11.9%). Time = 24 hours; 80.5 (6.6%), 71.0 (36.5%), 54.0 (25.1%), 48 – 41 (many small peaks, 31.8%).

2.4.4.16 Thermolysis of Pd1165 at 55°C in THF- d_8

Pd1165 (25 mg, 2.15×10^{-5} mol) was dissolved in THF- d_8 (0.6 mL) and transferred to an NMR tube fitted with a Young's tap. The solution was then subjected to thermolysis at 55°C inside the NMR probe. ^{31}P NMR (202 MHz, THF- d_8) spectra were recorded at regular time intervals. During the thermolysis of **Pd1165**, 4 main peaks in the ^{31}P NMR spectra were detected and their normalised integral values plotted as a function of time.

Interesting peaks in the ^1H NMR spectra were noted at the end of the thermolysis.

^1H NMR (300 MHz, THF- d_8): δ (ppm) = 11 – 10 (br, 0.68H, $\text{CH}_3\text{CO}_2\text{H}$), 7.68 (d, 0.39H, $J = 8.4$), 7.25 (d, 0.38H, $J = 8.4$), 6.42 (d, 0.18H, $J = 4.2$), 4.85 (d, 0.19H, $J = 4.2$), -15.1 (m, 0.13H, Pd- $\underline{\text{H}}$), -19.1 (m, 0.36H, Pd- $\underline{\text{H}}$).

2.4.4.17 Thermolysis of 1 Pd1165: 1 CH₃CN at 20°C in THF- d_8

Pd1165 (25 mg, 2.15×10^{-5} mol) and acetonitrile (1.2 μL , 1.52 mg, 2.15×10^{-5} mol) were dissolved in THF- d_8 (0.6 mL) and transferred to an NMR tube fitted with a Young's tap. The solution was then subjected to thermolysis at ambient temperature for 120 minutes. The solution developed a red colour and produced no palladium precipitate.

^{31}P NMR (121.4 MHz, THF- d_8): δ (ppm) = 71.0 (**Pd1165**, 31.0%), 56.4 (**Pd1148**, 5.0%), 52.0 (**Pd1146M**, 25%), 43.2 (**Pd1146M**, 25%).

2.4.4.18 Thermolysis of 1 Pd1165: 1 CH₃CN at 55°C in THF-*d*₈

Pd1165 (25 mg, 2.15×10^{-5} mol) and acetonitrile (1.2 μ L, 1.52 mg, 2.15×10^{-5} mol) were dissolved in THF-*d*₈ (0.6 mL) and transferred to an NMR tube fitted with a Young's tap. The solution was then subjected to thermolysis at 55°C inside the NMR probe. ³¹P NMR (202 MHz, THF-*d*₈) spectra were recorded at regular time intervals. The solution developed a red colour and produced a small amount of black precipitate. During the thermolysis of **Pd1165**, the main peaks in the ³¹P NMR spectra were detected and their integral values plotted as a function of time.

Interesting peaks in ³¹P and ¹H NMR spectra were noted at the end of the thermolysis.

³¹P NMR (121.4 MHz, THF-*d*₈): δ (ppm) = 71.0 (1.2%, **Pd1165**), 65.00 (5.1%), 56.4 (49%, **Pd1148**), 46.84 (3.3%), 43.80 (7.2%), 36.0 (3.3%). Lots of small signals which are difficult to integrate.

¹H NMR (300 MHz, THF-*d*₈): δ (ppm) = 7.68 (d, 0.39H, $J = 7.8$), 7.25 (d, 0.36H, $J = 7.8$), 6.2 – 5.6 (m, 1.24H), -15.1 (m, 0.79H, Pd-H).

2.4.4.19 Thermolysis of Pd1162 at 55°C in THF-*d*₈

Pd1162 (25 mg, 2.15×10^{-5} mol) was dissolved in THF-*d*₈ (0.6 mL) and transferred to an NMR tube fitted with a Young's tap. The solution was then subjected to thermolysis at 55°C inside the NMR probe. ³¹P NMR (202 MHz, THF-*d*₈) spectra were recorded at regular time intervals. During the thermolysis of **Pd1162**, the main peaks in the ³¹P NMR spectra were detected and their integral values plotted as a function of time.

No hydride peaks were detected in the ¹H NMR spectra at the end of the decomposition.

2.4.4.20 Thermolysis of 1 Pd1162: 1 CH₃CO₂H at 55°C in THF-*d*₈

Pd1162 (25 mg, 2.15×10^{-5} mol) and acetic acid (1.23 μ L, 1.29 mg, 2.15×10^{-5} mol) were dissolved in THF-*d*₈ (0.6 mL) and transferred to an NMR tube fitted with a Young's tap. The solution was then subjected to thermolysis at 55°C in an oil bath. The solution went from a very pale yellow to a dark green/yellow colour, with palladium precipitate evident. ³¹P NMR (121.4 MHz, THF-*d*₈) spectra were recorded at regular time intervals.

New peaks in the ³¹P NMR spectrum appeared over time. Time = 160 minutes, 71.0 (**Pd1165**, 1.4%), 61.0 (5.3%), 56.4 (**Pd1148**, 10.9%), 46.1 (9.6%), 43.8 (3.3%), 41.1 (**Pd1162**, 60.6%), 36.4 (6.6%).

The ¹H NMR spectrum showed two separate hydride peaks, at -14.5 and -15.1 ppm.

2.4.4.21 Thermolysis of Pd1162 + Formic Acid at 50°C in CDCl₃

Pd1162 (25 mg, 2.15×10^{-5} mol) and 10 equivalents of formic acid (8.4 mg, 2.15×10^{-4} mol) were dissolved in CDCl₃ (0.6 mL) and transferred to an NMR tube fitted with a Young's tap. The solution was then subjected to thermolysis at 50°C in an oil bath for 2 hours. The solution went from a very pale yellow to a dark red colour, with palladium precipitate evident. The sample was subjected to ³¹P and ¹H NMR spectroscopy.

³¹P NMR (121.4 MHz, CDCl₃): δ (ppm) = 69.2 (m, 3.8%), 64.0 (m, 5.3%), 55.9 (s, **Pd1148**, 42.6%), 45.7 (s, 12.3%), 45.3 (s, 13.5%), 40.6 (s, **Pd1162**, 17.2%), 37.3 (m, 5.3%).

¹H NMR (499.8 MHz, CDCl₃): δ (ppm) = 0.40 (t, 0.30H, Pd-CH₃ – **Pd1162**), -15.20 (t, 0.20H, Pd-H – **Pd1148**).

2.4.4.22 Thermolysis of Pd1165 with Pyridine in THF- d_8

Pd1165 (25 mg, 2.15×10^{-5} mol) and pyridine (8.5 mg, 10.7×10^{-5} mol) were dissolved in THF- d_8 (0.6 mL) and transferred to an NMR tube fitted with a Young's tap. ^1H and ^{31}P NMR spectroscopy was run on the sample. **Cis-Pd1184M** was observed, figure 2.21. This sample was heated to 65°C for 1 hour without showing any signs of change.

^{31}P NMR (121.4 MHz, CDCl_3): δ (ppm) = 49.8 (d, 1P, non-metallated P, $J = 30.8$), 38.0 (d, 1P, metallated P, $J = 30.8$).

^1H NMR (499.8 MHz, CDCl_3): δ (ppm) = 8.51 (d, 2H, $J = 4.20$, $\text{C}_5\text{H}_5\text{N}$), 7.87 (t, 1H, $J = 7.20$, $\text{C}_5\text{H}_5\text{N}$), 7.50 (t, 2H, $J = 6.30$, $\text{C}_5\text{H}_5\text{N}$), 2.50 (m, 2H, $-\text{CH}(\text{CH}_3)_2$), 2.00 (m, 3H, $-\text{CH}(\text{CH}_3)_2$), 1.50-1.40 (m, 12H, $-\text{CH}(\text{CH}_3)_2$), 1.20-1.15 (m, 24H, $-\text{CH}(\text{CH}_3)_2$, ring- $\text{C}(\text{CH}_3)_2$).

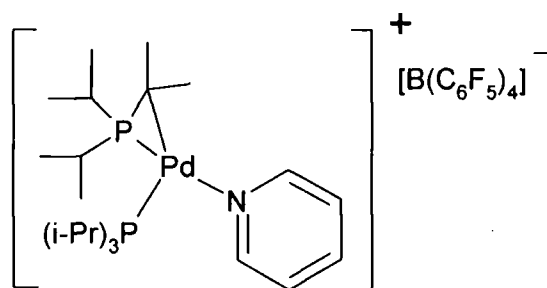


Figure 2.21

2.4.4.23 Synthesis and Characterisation of Pd1146M

Pd1165 (200 mg, 1.32×10^{-4} mol) was dissolved in acetonitrile (dry, 4 mL) and left for 24 hours at room temperature. The acetonitrile was then removed under reduced pressure. Some of the resulting **Pd1146M** solid (25 mg), figure 2.22, was dissolved in THF- d_8 (0.6 mL) and transferred to an NMR tube fitted with a Young's tap.

^{31}P NMR (121.4 MHz, THF- d_8): δ (ppm) = 51.9 (broad, non-metallated P), 43.3 (broad, metallated P).

^1H NMR (499.8 MHz, CDCl_3): δ (ppm) = 2.48 (m, 2H, $-\underline{\text{C}}\text{H}(\text{CH}_3)_2$), 2.40 (s, 3H, NCCH_3), 2.85 (m, 3H, $-\underline{\text{C}}\text{H}(\text{CH}_3)_2$), 1.54 (m, 6H, ring- $\text{C}(\text{CH}_3)_2$), 1.40 (m, 12H, $-\text{C}\text{H}(\underline{\text{C}}\text{H}_3)_2$), 1.32-1.12 (m, 18H, $-\text{C}\text{H}(\underline{\text{C}}\text{H}_3)_2$).

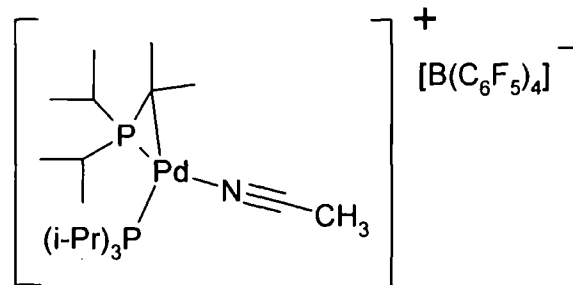


Figure 2.22

Some of the resulting solid (50 mg) was dissolved in CDCl_3 (0.6 mL) and transferred to an NMR tube fitted with a Young's tap. The sample was submitted for ^{31}P and ^1H VT-NMR spectroscopy.

^{31}P NMR at 20°C (202.3 MHz, CDCl_3): δ (ppm) = *cis*-**Pd1146M**, 100%; 51.8 (b, non-metalated P), 43.3 (b, metalated P).

^{31}P NMR at 10°C (202.3 MHz, CDCl_3): δ (ppm) = *cis*-**Pd1146M**, 100%; 51.7 (d, non-metalated P, $J = 31.56$), 43.0 (d, metalated P, $J = 31.56$).

^{31}P NMR at 0°C (202.3 MHz, CDCl_3): δ (ppm) = *cis*-**Pd1146M**, 91%; 51.5 (d, non-metalated P, $J = 31.56$), 42.8 (d, metalated P, $J = 31.56$). *trans*-**Pd1146M**, 9%; 39.9 (bd, non-metalated P, $J = 236.30$), 16.8 (bd, metalated P, $J = 236.30$).

^{31}P NMR at -10°C (202.3 MHz, CDCl_3): δ (ppm) = *cis*-**Pd1146M**, 93.5%; 51.2 (d, non-metalated P, $J = 31.56$), 42.6 (d, metalated P, $J = 31.56$). *trans*-**Pd1146M**, 6.5%; 39.5 (d, non-metalated P, $J = 236.30$), 16.2 (d, metalated P, $J = 236.30$).

^{31}P NMR at -20°C (202.3 MHz, CDCl_3): δ (ppm) = *cis*-**Pd1146M**, 91.7%; 51.0 (d, non-metalated P, $J = 31.56$), 42.4 (d, metalated P, $J = 31.56$). *trans*-**Pd1146M**, 8.3%; 39.3 (d, non-metalated P, $J = 236.30$), 15.9 (d, metalated P, $J = 236.30$).

^{31}P NMR at -40°C (202.3 MHz, CDCl_3): δ (ppm) = *cis*-**Pd1146M**, 92.6%; 50.8 (d, non-metalated P, $J = 31.56$), 42.2 (d, metalated P, $J = 31.56$). *trans*-**Pd1146M**, 7.4%; 38.8 (d, non-metalated P, $J = 236.30$), 15.2 (d, metalated P, $J = 236.30$).

^{31}P NMR at -50°C (202.3 MHz, CDCl_3): δ (ppm) = *cis*-**Pd1146M**, 92.6%; 50.6 (d, non-metalated P, $J = 31.56$), 42.0 (d, metalated P, $J = 31.56$). *trans*-**Pd1146M**, 7.4%; 38.4 (d, non-metalated P, $J = 236.30$), 14.8 (d, metalated P, $J = 236.30$).

^{31}P NMR at -60°C (202.3 MHz, CDCl_3): δ (ppm) = *cis*-**Pd1146M**, 92.6%; 50.4 (d, non-metalated P, $J = 31.56$), 41.7 (d, metalated P, $J = 31.56$). *trans*-**Pd1146M**, 7.4%; 38.2 (d, non-metalated P, $J = 236.30$), 14.8 (d, metalated P, $J = 236.30$).

^1H NMR at -60°C (499.8 MHz, CDCl_3): δ (ppm) = 2.48 (m, 2H, $-\underline{\text{C}}\text{H}(\text{CH}_3)_2$), 2.40 (s, 3H, NCCH_3), 2.85 (m, 3H, $-\underline{\text{C}}\text{H}(\text{CH}_3)_2$), 1.54 (m, 6H, ring- $\text{C}(\underline{\text{C}}\text{H}_3)_2$), 1.40 (m, 12H, $-\text{C}\text{H}(\underline{\text{C}}\text{H}_3)_2$), 1.32-1.12 (m, 18H, $-\text{C}\text{H}(\underline{\text{C}}\text{H}_3)_2$).

From the VT-NMR spectroscopic data it is clear that the *cis* and *trans*-**Pd1146M** isomers are in exchange. ^{31}P - ^{31}P 2D-NMR spectroscopy (EXSY-noesy) was run on the sample at -20°C to confirm this observation.

2.4.4.24 Thermolysis of **Pd1146M** at Ambient Temperature in $\text{THF-}d_8$

Pd1146M (50 mg, 4.36×10^{-5} mol) was dissolved into $\text{THF-}d_8$ (0.6 mL) and subjected to ^{31}P and ^1H spectroscopic analysis after 7 hours.

^1H NMR (200.0 MHz, $\text{THF-}d_8$): δ (ppm) = 6.1 – 5.4 (m, 1.18H, vinylic), -15.2 (m, 0.59H, Pd-H).

^{31}P NMR (81.0 MHz, $\text{THF-}d_8$): δ (ppm) = 54.6 (41.3%, **Pd1148**), 52.5 (5.6%), 49.5 (b, 28.6%, **Pd1146M**), 41.5 (b, 24.5%, **Pd1146M**).

2.4.4.25 Thermolysis of Pd1146M at 20°C in CDCl₃

Pd1146M (50 mg, 4.36×10^{-5} mol) was dissolved into CDCl₃ (0.6 mL) and subjected to ³¹P and ¹H NMR spectroscopic analysis at different time intervals.

³¹P NMR at 40 minutes (121.4 MHz, CDCl₃): δ (ppm) = 57.2 (d, $J = 322.0$, **Pd1146H**, 10%), 52.7 (d, $J = 322.0$, **Pd1146H**, 10%), 51.7 (b, **Pd1146M**, 40%), 43.3 (m, **Pd1146M**, 40%).

¹H NMR at 40 minutes (200.0 MHz, CDCl₃): δ (ppm) = 5.86 (d, 1H, $^3J_{\text{PH}} = 34.8$, vinylic H *trans* to P), 5.67 (d, 1H, $^3J_{\text{PH}} = 16.1$, vinylic H *cis* to P), -15.25 (t, 1H, $J = 7.16$, Pd-H).

³¹P NMR at 7 hours (121.4 MHz, CDCl₃): δ (ppm) = 70.0 (3%, **Pd1165**), 57.2 (d, $J = 322.0$, **Pd1146H**, 27%), 56.0 (s, **Pd1148**, 12%), 52.2 (d, $J = 322.0$, **Pd1146H**, 27%), 51.7 (b, **Pd1146M**, 10%), 47.5 (2%), 47.3 (2%), 45.8 (4%), 45.1 (2%), 43.3 (m, **Pd1146M**, 10%).

¹H NMR at 7 hours (200.0 MHz, CDCl₃): δ (ppm) = 5.86 (d, 1H, $^3J_{\text{PH}} = 34.8$, vinylic H *trans* to P), 5.67 (d, 1H, $^3J_{\text{PH}} = 16.1$, vinylic H *cis* to P), -15.25 (t, 1H, $J = 7.16$, Pd-H).

2.4.4.26 Thermolysis of Pd1146M at 35°C in CDCl₃

Pd1146M (50 mg, 4.36×10^{-5} mol) was dissolved into CDCl₃ (0.6 mL) and subjected to thermolysis at 35°C for 12 hours in an oil bath. ³¹P and ¹H NMR spectroscopy were run.

³¹P NMR (121.4 MHz, CDCl₃): δ (ppm) = 69.8 (dd, $J = 110.4$ & 29.3 , P^A, 20%), 60.0 (dd, $J = 32.5$ & 29.3 , P^A, 20%), 56.9 (dd, $J = 110.4$ & 32.5 , P^B, 20%), 56.0 (**Pd1148**, 6%), 47.5 (12%), 45.8 (8%), 44.6 (d, $J = 362.0$, P^a, 7%), -48.1 (d, $J = 362.0$, P^b, 7%).

¹H NMR (200.0 MHz, CDCl₃): δ (ppm) = 7-4 (m, 2H, vinyl), -15.1 (m, 1H, Pd-H).

2.4.4.27 Attempted Thermolysis of Pd1148

Pd1148 (50 mg, 4.36×10^{-5} mol) was dissolved into THF- d_8 (0.6 mL) and heated at 55°C for 90 minutes. ^{31}P and ^1H NMR spectroscopy showed no change.

2.3.4.28 Attempted Synthesis of $[\text{Pd}(\text{P-}i\text{-Pr}_3)((i\text{-Pr}_2)\text{P-C}(\text{CH}_3)=\text{CH}_2)_2(\text{H})]\text{-}[\text{B}(\text{C}_6\text{F}_5)_4]$ (Pd1273H)

Pd1148 (57.4 mg, 5.0×10^{-5} mol) and triisopropylphosphine (8.0 mg, 5.0×10^{-5} mol) were dissolved into THF- d_8 (0.6 mL) and stirred for 60 minutes. ^{31}P and ^1H NMR spectroscopy were run.

^1H NMR (300 MHz, THF- d_8): δ (ppm) = -14.51 (b, 0.04H, Pd-H), -15.11 (b, 0.72H, Pd-H).

^{31}P NMR (121.4 MHz, THF- d_8): δ (ppm) = 56.9 (50%, **Pd1148**), 56.0 (3%), 37.0 (4%), 21.1 (43%).

2.4.4.29 Characterisation of $[\text{Pd}(\text{P-}i\text{-Pr}_3)_2(\kappa^2\text{-OAc})][\text{B}(\text{C}_6\text{F}_5)_4]$ (Pd1165)

The catalyst was used as supplied by Promerus LLC and characterised using NMR spectroscopy, figure 2.23.

^1H NMR (300 MHz, THF- d_8): δ (ppm) = 2.50 (m, 6H, $-\text{P}(\text{CHMe}_2)_3$), 1.98 (s, 3H, $-\text{O}_2\text{CCH}_3$), 1.51 (m, 36H, $-\text{P}(\text{CHMe}_2)_3$).

^{31}P NMR (121.4 MHz, THF- d_8): δ (ppm) = 71.4.

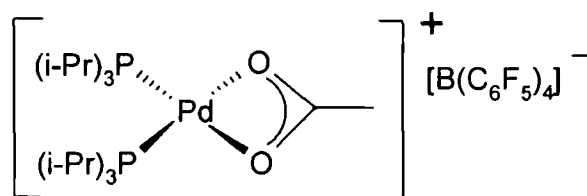


Figure 2.23

2.4.4.30 Characterisation of [Pd(P-*i*-Pr₃)₂(Me)(MeCN)][B(C₆F₅)₄] (Pd1162)

The catalyst was used as supplied by Promerus LLC and characterised using NMR spectroscopy, figure 2.24.

¹H NMR (300 MHz, THF-*d*₈): δ (ppm) = 2.60 – 2.20 (m, 6H, -P(CHMe₂)₃), 1.75 (s, 3H, -NCCH₃), 1.37 (m, 36H, -P(CHMe₂)₃), 0.45 (t, 3H, *J* = 5.70, Pd-CH₃).

³¹P NMR (121.4 MHz, THF-*d*₈): δ (ppm) = 41.3.

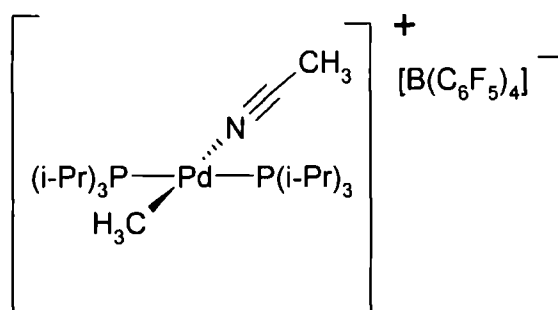


Figure 2.24

2.4.4.31 Characterisation of [Pd (P-*i*-Pr₃)₂(H)(MeCN)][B(C₆F₅)₄] (Pd1148)

The catalyst was used as supplied by Promerus LLC and characterised using NMR spectroscopy, figure 2.25.

¹H NMR (300 MHz, THF-*d*₈): δ (ppm) = 2.33 (s, 3H, -NCCH₃), 2.24 (m, 6H, -P(CHMe₂)₃), 1.18 (m, 36H, -P(CHMe₂)₃), -15.4 (t, 1H, ²*J*_{PH} = 7.35, Pd-H).

^{31}P NMR (121.4 MHz, THF- d_8): δ (ppm) = 56.9.

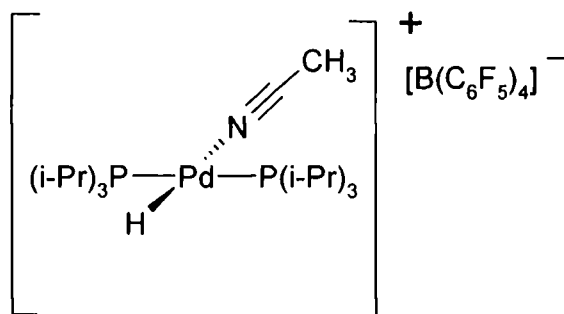


Figure 2.25

2.4.4.32 NMR Scale Polymerisation of *endo/exo*-5-decyl-2-norbornene using Pd1206

Pd1206 (4.3 mg, 3.60×10^{-6} mol) was dissolved in toluene- d_8 and the solution then added to *endo/exo*-5-decyl-2-norbornene (42.1 mg, 1.80×10^{-4}). The solution was syringed into an NMR tube and analysed by ^1H NMR spectroscopy at 70°C within the NMR probe. The changes in intensity of the monomer vinyl resonances were measured against the internal standard over time. First order plots were used to measure the rate of polymerisation of the *endo/exo*-NBdecyl.

$$k(\textit{endo}\text{-}5\text{-decyl}\text{-}2\text{-norbornene}) = 1.18 \times 10^{-3} \text{ s}^{-1}$$

$$k(\textit{exo}\text{-}5\text{-decyl}\text{-}2\text{-norbornene}) = 2.25 \times 10^{-3} \text{ s}^{-1}$$

$$k(\textit{endo/exo}\text{-}5\text{-decyl}\text{-}2\text{-norbornene}) = 1.28 \times 10^{-3} \text{ s}^{-1}$$

2.4.4.33 NMR Scale Polymerisation of *endo/exo*-5-decyl-2-norbornene using Pd1148

Pd1148 (4.1 mg, 3.60×10^{-6} mol) was dissolved in toluene- d_8 and the solution then added to *endo/exo*-5-decyl-2-norbornene (42.1 mg, 1.80×10^{-4}). The solution was syringed into an NMR tube and analysed by ^1H NMR spectroscopy at 70°C within the NMR probe. The change in intensity of the monomer vinyl resonances was measured against the internal standard over time. First order plots were used to measure the rate of polymerisation of the *endo/exo*-5-decyl-2-norbornene.

$$k (\text{endo-5-decyl-2-norbornene}) = 4.54 \times 10^{-3} \text{ s}^{-1}$$

$$k (\text{exo-5-decyl-2-norbornene}) = 9.37 \times 10^{-3} \text{ s}^{-1}$$

$$k (\text{endo/exo-5-decyl-2-norbornene}) = 4.78 \times 10^{-3} \text{ s}^{-1}$$

2.5 References

¹ (a) Lipian, J. -H.; Rhodes, L. F.; Goodall, B. L.; Bell, A.; Mimna, R. A.; Fondran, J. C.; Hennis, A. D.; Elia, C. N.; Polley, J. D.; Sen, A.; Saikumar, J. *PCT Int. Appl.* WO 0020472 **2000**. (b) Zhao, X. -M.; Shick, R. A.; Ravikiran, R.; Neal, P. S.; Rhodes, L. F.; Bell, A. *PCT Int. Appl.* WO 0210231 **2002**.

² Bell, A.; Amoroso, D.; Protasiewicz, J. D.; Thirupathi, N. US 2005/0187398 A1.

³ (a) Thirupathi, N.; Amoroso, D.; Bell, A.; Protasiewicz, J. D. *Organometallics* **2005**, *24*, 4099 - 4102. (b) Thirupathi, N.; Amoroso, D.; Bell, A.; Protasiewicz, J. D. *Organometallics* **2007**, *26*, 3157 - 3166.

Chapter 3

Fundamental Studies on Cationic Palladium Hydride Initiators for the Addition Polymerisation of Functionalised Norbornene Monomers

3.1 Introduction

The cationic palladium catalysed addition polymerisation of functionalised norbornenes is of immense current interest due to its perceived ability to generate polymers, which can fulfil the electronics industries needs for highly transparent, lithographic materials. These advanced lithographic materials require very specific physical properties. However, even low levels of residual metal and phosphines and anything but excellent polymer homogeneity, can cause an unfavourable distortion of these properties. Reliably producing these physical properties in the lithographic material is reliant on being able to gain full control of the polymerisation system. This can only be fully realised by gaining an appreciation for how the key factors such as initiator character and monomer functional group affect the polymerisation system.

The use of NMR spectroscopy as a tool for probing the key features of polymerisation reactions is not a new one and owes much of its development to the pioneering work of the early ROMP specialists. This technique has enabled important mechanistic information regarding initiation and propagation to be assessed, using discrete catalysts, with a view to improving catalytic activity.

All previous work undertaken in the field of addition polymerisation has tended to focus on the use of *in-situ* generated catalysts, with GCMS as the analytical tool, with limited success.¹ This technique can give useful information regarding polymerisation rates but nothing with respect to the intricacies of initiation and polymerisation.

This chapter will demonstrate the use of ¹H NMR spectroscopy as an analytical tool for the investigation of cationic palladium hydride in the addition polymerisation of functionalised norbornene monomers. The investigations will focus on the rates of initiation and

propagation of stable cationic palladium hydride initiators during the polymerisation of functionalised norbornene monomers. The influence of the catalyst character, nature of the substituents on norbornene, and polymerisation conditions, on the polymerisation reaction will be assessed.

The investigations will particularly focus on the initiation and propagation steps of the stable cationic palladium hydride species, $[\text{Pd}(\text{PCy}_3)_2(\text{NCCH}_3)(\text{H})][\text{B}(\text{C}_6\text{F}_5)_4]$ (**Pd1388**), with a range of technologically important functionalised norbornenes. The main aim of these investigations is to gain an appreciation of how the following affect the polymerisation system:

- Initiator Character
- Temperature
- Solvent
- Additives
- Functional group on norbornene:
 - Steric size
 - Regiochemistry
 - Methylene spacing (homologation)
 - Coordination

3.2 Results and Discussion

3.2.1 ^1H NMR Spectroscopy - Analytical Tool for Probing Addition Polymerisation

The synthesis and isolation of initiators of general structure $[\text{Pd}(\text{PR}_3)_2(\text{NCCH}_3)(\text{H})][\text{B}(\text{C}_6\text{F}_5)_4]$, by Promerus LLC, has provided the opportunity to investigate the initiation and polymerisation of functionalised norbornene monomers by ^1H NMR spectroscopy for the first time. Using the model initiator, **Pd1388**, it was envisaged that it would be possible to measure the rate of initiation via the reduction in the very distinct palladium hydride resonance, which shows as a triplet at ≈ -15.1 ppm. The rate of polymerisation could be measured via the decrease in the vinyl signals of norbornene, which appear at ≈ 6 ppm, after initiation is complete.

It was found that the ideal monomer:initiator ratio was 50:1, to ensure that signals due to the vinyl monomer, figure 3.2, and the hydride of the initiator, figure 3.1, would both be suitably visible by ^1H NMR spectroscopy. The polymerisation of *endo* (N)- and *exo* (X)-functionalised norbornene (NB-FG) isomers can be monitored independently via careful integration of the vinyl signals of the monomer.

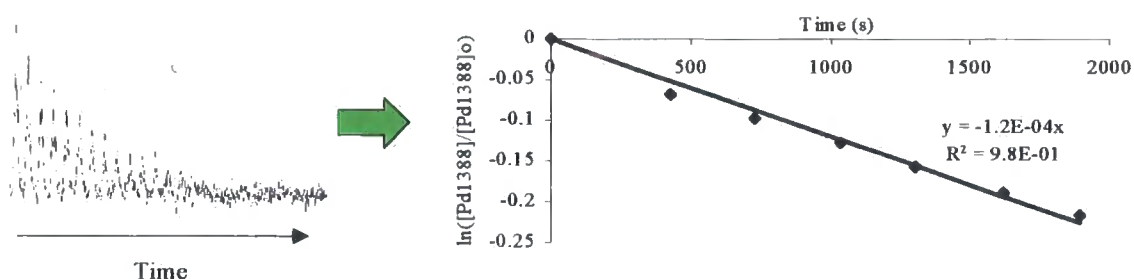


Figure 3.1. Palladium hydride ^1H NMR signal (**Pd1388**) versus time, 50 *endo/exo*-5-hexyl-2-norbornene: 1 **Pd1388**, at 20°C in CDCl_3 . First order kinetic plot to show rate of initiation.

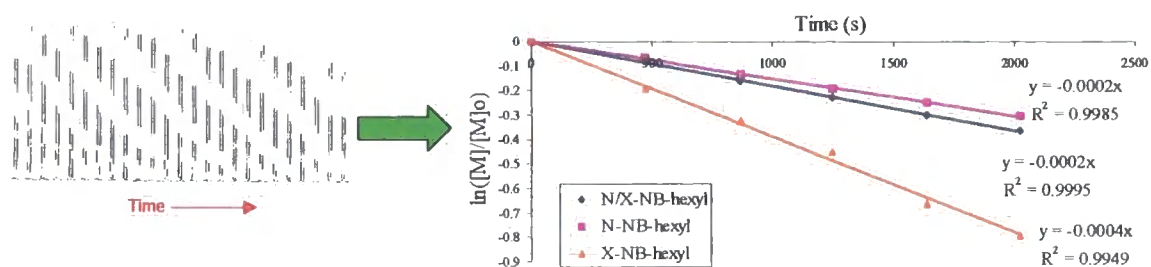


Figure 3.2. Monomer vinyl ^1H NMR signal versus time, 50 *endo/exo*-5-hexyl-2-norbornene: 1 Pd1388, at ambient temperature in CDCl_3 . First order kinetic plot to show rate of polymerisation.

3.2.2 Effect of Initiator on the Rates of Initiation and Polymerisation

The effect of the steric size of the trialkylphosphine ligand of the initiator, $[\text{Pd}(\text{PR}_3)_2(\text{NCCH}_3)(\text{H})][\text{B}(\text{C}_6\text{F}_5)_4]$, was investigated by monitoring the polymerisation of *endo/exo*-5-decyl-2-norbornene (N/X-NBdecyl) by the initiators described in table 3.1. The polymerisations were carried out at a monomer:initiator ratio of 50:1, using CDCl_3 as solvent, at ambient temperature. GPC data was obtained on the recovered polymer at the end of the polymerisations.

Table 3.1. Polymerisation data for different initiator, PR_3 ligands. 50 N/X-NBdecyl: 1 initiator, in CDCl_3 , at ambient temperature.

Initiator	PR_3	k_i (s^{-1})	k_p (s^{-1})	k_p/k_i	M_n	M_w	M_w/M_n
Pd1388	$\text{P}(\text{Cy})_3$	18×10^{-5}	16×10^{-5}	0.89	17500	29800	1.70
Pd1336	$\text{P}(\text{Cy})_2(\text{tBu})$	17×10^{-5}	32×10^{-5}	1.88	13700	29100	1.80
Pd1148	$\text{P}(\text{iPr})_3$	18×10^{-5}	56×10^{-5}	3.11	14200	17900	1.87
Pd1304	$\text{P}(\text{Cp})_3$	12×10^{-5}	49×10^{-5}	4.08	19100	39400	2.06
Pd1388 + CuCl	$\text{P}(\text{Cy})_3$	-	52×10^{-5}	-	11100	14900	1.57

The Palladium hydride species appear to initiate the polymerisation of the norbornene monomer at approximately the same rate, with $\text{PCy}_2\text{tBu} \approx \text{PCy}_3 \approx \text{P}^i\text{Pr}_3 > \text{PCp}_3$. The initiators with the smaller trialkylphosphines appear to give higher rates of polymerisation, with $\text{PCp}_3 > \text{P}^i\text{Pr}_3 > \text{PCy}_2\text{tBu} > \text{PCy}_3$. The ratio of k_p/k_i is the best indicator of polymerisation rate because the initiation was not complete before the rate of polymerisation was measured.

The polydispersity index (PDI) of the resulting polymers is in agreement with the initiation and polymerisation data, with k_p/k_i increasing in the same order as M_w/M_n .

3.2.3 Effect of Copper Salts on the Rates of Initiation and Polymerisation

Whilst monitoring the polymerisation of alkyl norbornenes by ^1H NMR spectroscopy, it was noticeable that not all of the palladium hydride initiator is consumed even at 50% monomer conversion. Some of the early work carried out in the field of ROMP of norbornene monomers showed that the addition of copper salts to the polymerisation mixture increased the rates of initiation and polymerisation by forming complexes with “free” phosphine ligands.³ The formation of these $\text{Cu}(\text{PR}_3)_x$ complexes is thought to increase the concentration of free active sites on the active metal centre, enabling more norbornene monomer to coordinate, insert and polymerise.

The polymerisation of *endo/exo*-5-decyl-2-norbornene (N/X-NBdecyl), without and with 1 equivalent of added CuCl per **Pd1388**, was used to investigate this theory, figure 3.3. It is notable that the CuCl only becomes soluble when both initiator and norbornene monomer are added to the CDCl_3 solution. This confirms that “free” trialkylphosphine is needed to improve the solubility of the copper salt. The NMR sample, which contained CuCl displayed no palladium hydride signal in the ^1H NMR spectra.

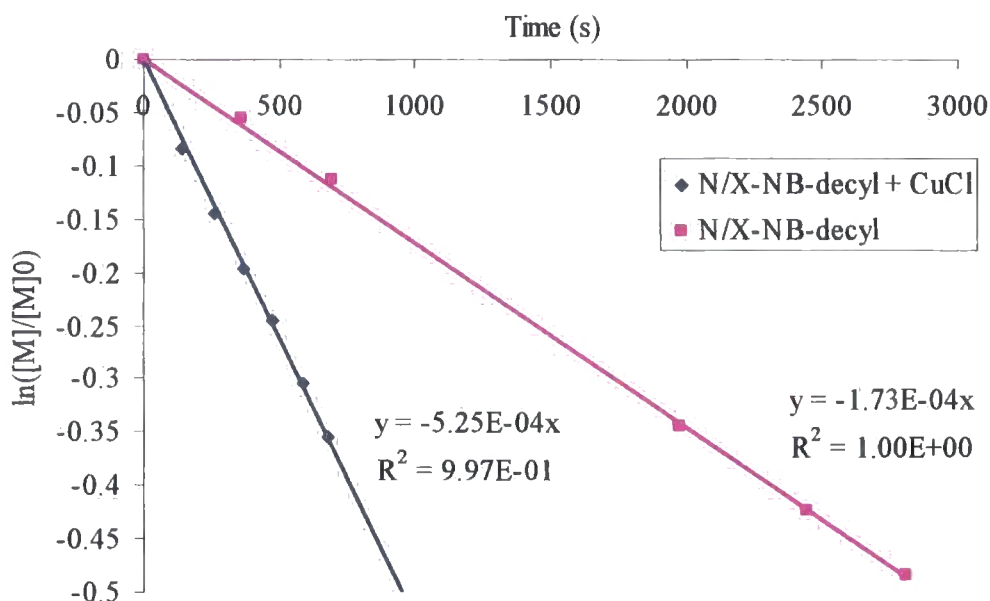


Figure 3.3. First order plot to show the rate of polymerisation of 50 (N/X-NBdecyl): 1 **Pd1388**, with and without added CuCl, in CDCl_3 at ambient temperature.

The rate of polymerisation for the system containing CuCl was shown by ^1H NMR spectroscopy to be $\approx \times 3$ greater than the same system without CuCl. The GPC data showed the polymer resulting from the addition of CuCl to have an $M_w/M_n = 1.6$, which is only marginally lower than for the polymer obtained without CuCl ($M_w/M_n = 1.7$). This is an unexpected result because the polymerisation system containing CuCl appeared to initiate very quickly. It is likely that the CuCl is deactivating the catalyst in some way during the polymerisation, resulting in the high polydispersity index.

These results compare favorably with the results of Protasiewicz *et al.*,² where polymerisations were carried out in toluene (17 mL) for 3 hr at 63°C at 10.7 mM of 5-decyl-2-norbornene and 0.4 μM of **Pd1388** catalyst concentrations (5-decyl-2-norbornene/Initiator ratio: 26700). The GPC data for these polymerisations showed that the **Pd1388** generates a polymer with similar PDI ($M_w/M_n = 1.8$).

3.2.4 Effect of Temperature on the Rates of Polymerisation

The effect of temperature on the rate of polymerisation of 5-decyl-2-norbornene (N/X-NBdecyl) by **Pd1388**, in benzene- d_6 , was investigated by measuring the rate of polymerisation at 40, 50 and 70°C. The Arrhenius plot showed that the rate of polymerisation increases as the temperature increases, in line with the Arrhenius equation, figure 3.4.

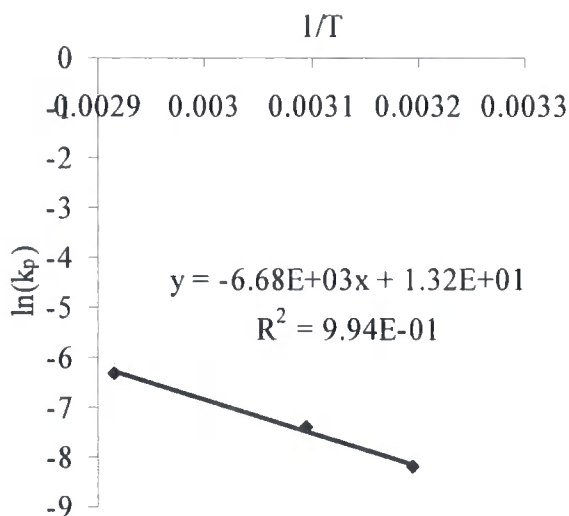


Figure 3.4. Arrhenius plot for polymerisation of (50 N/X-NBdecyl: 1 **Pd1388**), in benzene- d_6 at 40, 50 and 70°C. The Activation Energy (E_a) for N/X-NBdecyl in benzene- $d_6 = 55.6$ kJmol^{-1} .

3.2.5 Effect of Solvent on the Rate of Polymerisation

The effect of polymerisation solvent was investigated by determining the rate of polymerisation of 50 N/X-NBdecyl: 1 **Pd1388**, by ^1H NMR spectroscopy at 40°C, figure 3.5. The deuterated solvents used in the study were selected to cover a range of solvent polarities: toluene ($P' = 2.4$); benzene ($P' = 2.7$); chlorobenzene ($P' = 2.7$); dichlorobenzene ($P' = 3.1$) and tetrachloroethane ($P' = 3.1$). The general trend shows an increase in polymerisation rate, with an increase in polymerisation solvent polarity, which is as expected. The solvent effect is quite large with the polymerisation range being of a $\times 12$ magnitudes.

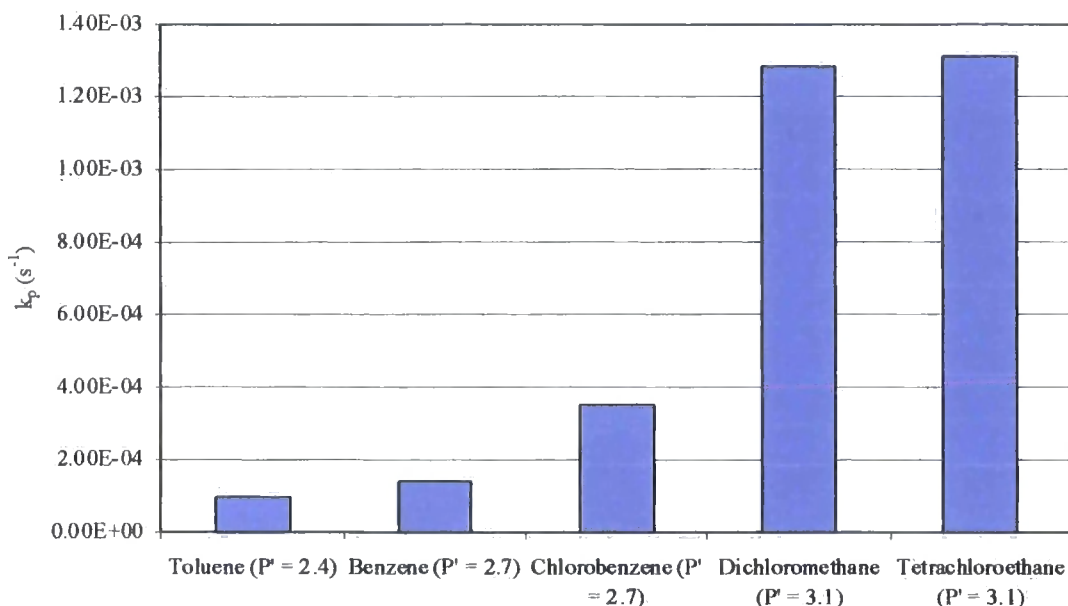


Figure 3.5. Graph shows rate of polymerisation of 50 N/X-NBdecyl: 1 **Pd1388**, in different solvents at 40°C, where P' = Rohrschneiders polarity parameter.

The 5-decyl-2-norbornene polymerisation rates, figure 3.5, were difficult to measure using ^1H NMR when the rate exceeds $2.0 \times 10^{-4} \text{ s}^{-1}$. This suggests that the most appropriate solvent system in which to run further polymerisation experiments should be selected from either toluene or benzene.

3.2.6 Effect of Functional Group on the Rate of Polymerisation

The role of the functional group (FG) in the monomer during the polymerisation of functionalised norbornenes (NB-FG) has been widely studied and yet the complexities of its influences have often led to misunderstanding and incorrect interpretations. Herein, we will attempt to unfold the different ways in which the substituent can influence the activity of palladium(II) catalysed addition polymerisation, with a view to developing monomers which are more likely to create polymers with greater homogeneity.

The graph shown in figure 3.6, displays a remarkable range of polymerisation rates for a range of functionalised norbornenes, under identical polymerisation conditions. For instance, *exo*-5-trimethoxysilyl-2-norbornene (X-NB-Si(OMe)₃) polymerises $\approx \times 700$ faster than *endo*-5-trimethylsilyl carboxylate-2-norbornene (N-NB-CO₂TMS). Through studying and comparing

the polymerisation kinetics of particular families of functionalised norbornenes it is now possible to explain these seemingly improbable differences in rates.

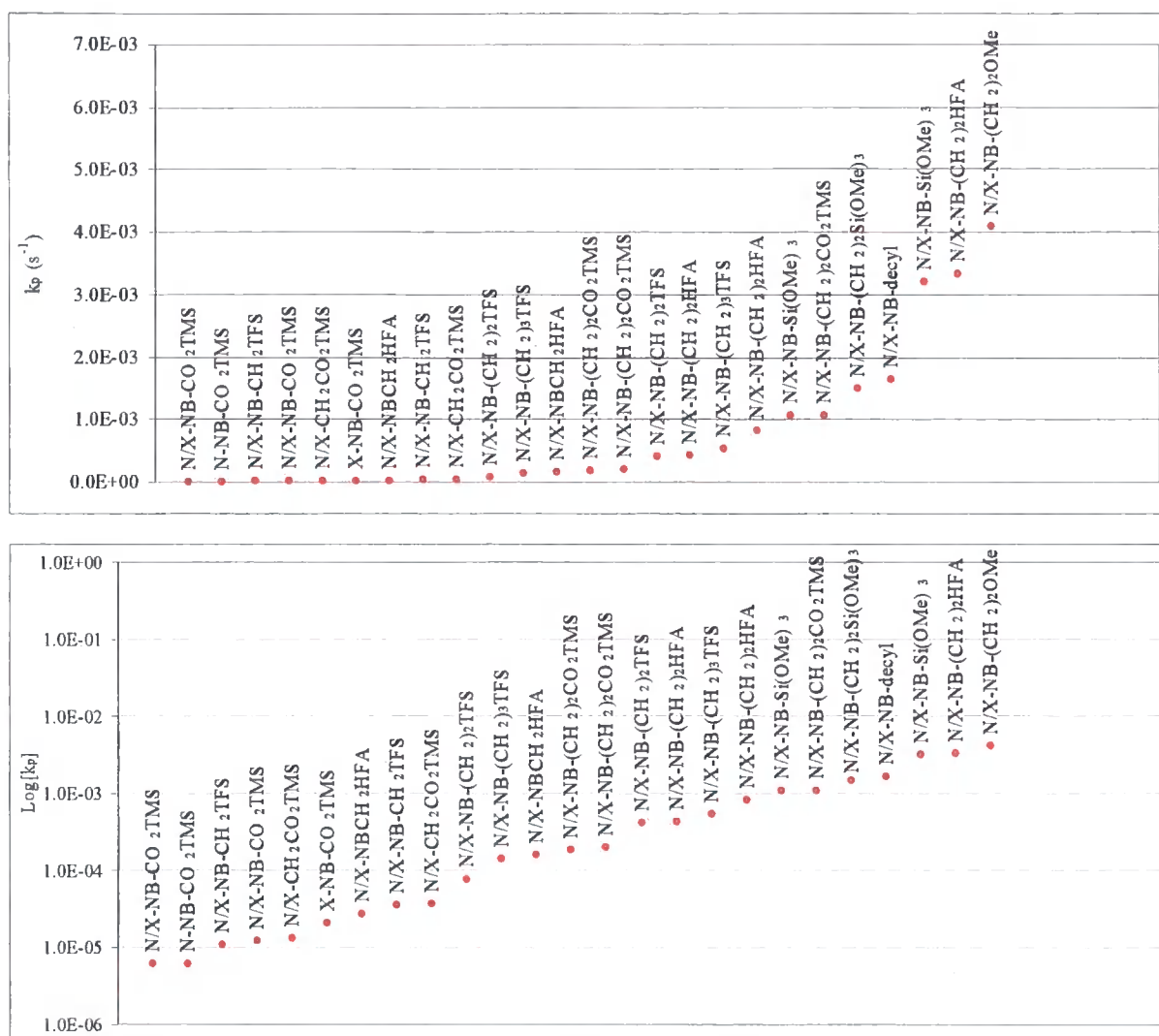


Figure 3.6. Scale and Log scale graphs showing differences in polymerisation rate for functionalised norbornenes at 70°C in benzene-*d*₆, 50 monomer: 1 **Pd1388**.

3.2.7 Steric Size of the Functional Group in Norbornene Monomers

There is a preferential uptake of the X-isomer (cream bars) over the N-isomer (blue bars) in the polymerisation of N/X-alkylnorbornenes by **Pd1388**, in CD₂Cl₂, at 20°C, figure 3.7.

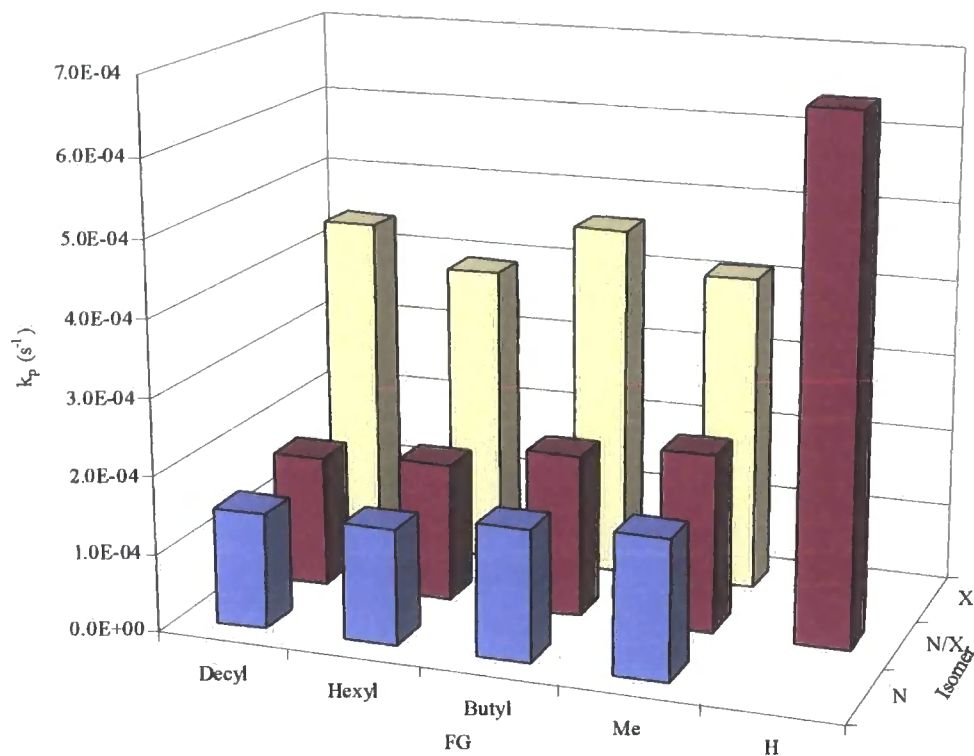
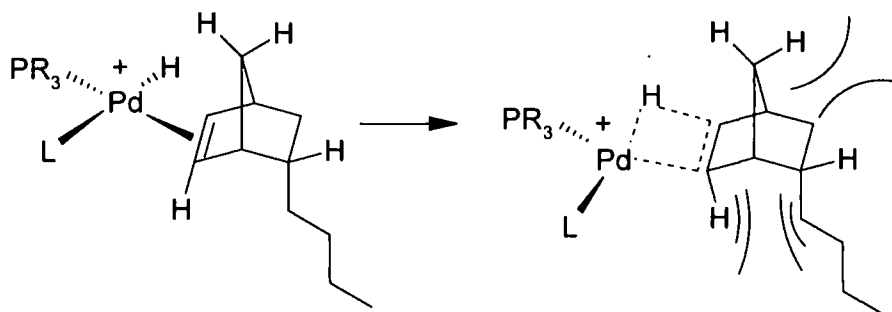


Figure 3.7. Polymerisation data of 50 N/X-NB-FG: 1 **Pd1388**, at 20°C in CD_2Cl_2 .

More importantly, it was possible to show that the rate of polymerisation is independent of the steric size of an *exo*-functionality for X-NB-FG (cream bars), with the rate of polymerisation displaying no apparent trend, Bu ($4.6 \times 10^{-4} s^{-1}$) > Dec ($4.4 \times 10^{-4} s^{-1}$) > Me ($4.1 \times 10^{-4} s^{-1}$) > Hex ($3.9 \times 10^{-4} s^{-1}$), figure 3.7. However, the rate of polymerisation for the *endo*-functionalised regioisomer, N-NB-FG (blue bars), was shown to decrease in the order Me ($1.5 \times 10^{-4} s^{-1}$) = Bu ($1.5 \times 10^{-4} s^{-1}$) > Hx ($1.7 \times 10^{-4} s^{-1}$) > Dec ($1.8 \times 10^{-4} s^{-1}$), figure 3.7. The steric effect of the functional group in the *endo*-regioisomer is caused by an unfavourable steric interaction between the functional group and the vinylic hydrogen that is being rehybridised from sp^2 to sp^3 upon coordination and insertion into the palladium-hydride bond, scheme 3.1.



Scheme 3.1

The ratio of N/X-regioisomers in the alkyl norbornenes is approximately 80:20, respectively. This causes the *endo*-regioisomer to dominate the overall combined rate of polymerisation of both regioisomers, meaning the N/X- mixture follows a similar trend to the *endo*-regioisomers, compare blue and purple bars, figure 3.7.

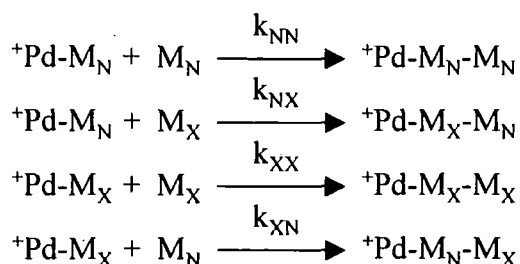
An interesting observation from figure 3.7 is that even though X-NB-FG shows no obvious signs of steric effects, it's rate of polymerisation is still not as fast as norbornene, with norbornene having a rate approximately $\times 1.5$ faster. This suggests that the alkyl group is having some deactivating effect upon the polymerisation of functionalised norbornenes, compared with the hydrogen substituent in norbornene.

3.2.8 Penultimate Group Effect

The polymerisation reaction of two or more monomers leads to co-polymers and the extent of incorporation of each monomer unit into the co-polymer chain is rarely equal. The factors that affect this are: concentration of each monomer; reactivity of each monomer; conversion (influences monomer concentrations), and reactivity of the cationic Pd-alkyl produced via the insertion of the last monomer into the polymer chain (penultimate group effect). The so-called "penultimate group effect" is where the rate of the last monomer inserted into the polymer chain has an effect on the next monomers insertion rate.

In essence the N- and X-regioisomers can be classified as different monomers and in theory, the polymerisation reaction of an N/X-NB-FG monomer is a co-polymerisation reaction. The

co-polymerisation reaction of the N-NB-FG (M_N) and X-NB-FG (M_X) monomers, can effectively be described by four reactions:



k_{NN} and k_{XX} are the rate constants for self-propagation and k_{NX} and k_{XN} are the rate constants for cross-propagation.

The reactivity ratio is a useful parameter, which is described as the rate of self-propagation compared to the rate of cross-propagation: $r_N = k_{NN}/k_{NX}$ and $r_X = k_{XX}/k_{XN}$. Thus, if: $r_N > 1$, ${}^+Pd-M_N$ prefers to react with M_N ($k_{NN} > k_{NX}$), tendency to homo-polymerise; $r_N < 1$, ${}^+Pd-M_N$ prefers to react with M_X ($k_{NN} < k_{NX}$), tendency to co-polymerise.³

The reactivity ratios can be used to describe five general types of co-polymerisation: random, $r_N = r_X = 1$; ideal, $r_N \times r_X = 1$; alternating, $r_N = r_X < 0.1$; statistical, $0 < r_N \times r_X > 1$; blocky, $r_N > 1$, $r_X > 1$. See figure 3.8. Only a purely random co-polymerisation reaction shows no penultimate group effect.³

The type of co-polymerisation reaction occurring between two different monomers can be ascertained by observing the characteristics of a plot of F_1 versus f_1 , where:

$$F_1 = 1 - F_2 = d[M_1]/d([M_1] + [M_2])$$

$$f_1 = 1 - f_2 = [M_1]/([M_1] + [M_2])$$

F_1 is defined as the mole fraction of M_1 in the co-polymer and f_1 is defined as the mole fraction of M_1 in initial monomer mixture (so-called feed-ratio).³

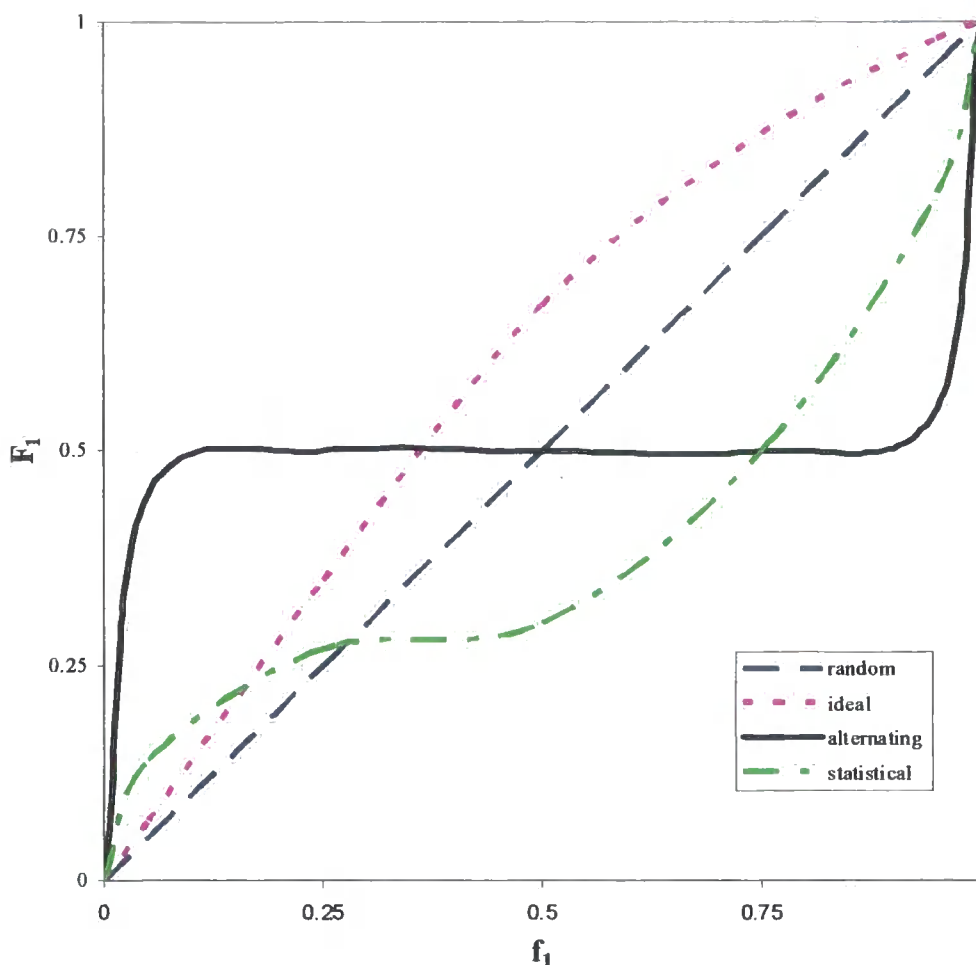


Figure 3.8. Types of co-polymerisation reaction.³

The prediction of co-polymerisation rates is complicated by the penultimate group effect, since it would change in severity for different types of functionality and could only be measured for a particular monomer by varying the N- and X-regioisomer ratio and then measuring their rates independently. The polymerisation rate would have to only be measured under < 5% conversion, otherwise the ratio of N:X regioisomers would change drastically and hence so would their polymerisation rates.

The *endo/exo*-N-(2-norbornene-5-methyl)-1,1,1-trifluoromethanesulfonamide (N/X-NB-CH₂NHSO₂CF₃ = NB-CH₂TFS) monomer was chosen to investigate whether the N- and X-regioisomers of the same monomer have a penultimate group effect upon each other during their co-polymerisation reactions. This investigation was made possible by new regioisomer specific synthesis routes developed by Promerus LLC. Co-polymerisation reactions of the N- and X-regioisomers were carried out at different isomeric ratios, using **Pd1388**, in benzene-*d*₆,

at 70°C, figure 3.9. The polymerisation rates were only measured over the first 5% monomer conversion because it was noted that the first order kinetic plots became increasingly non-linear (curved) above these conversion levels. These curved plots are a result of the penultimate group effect, since the isomeric ratios of the reaction mixture change during the polymerisation reaction.

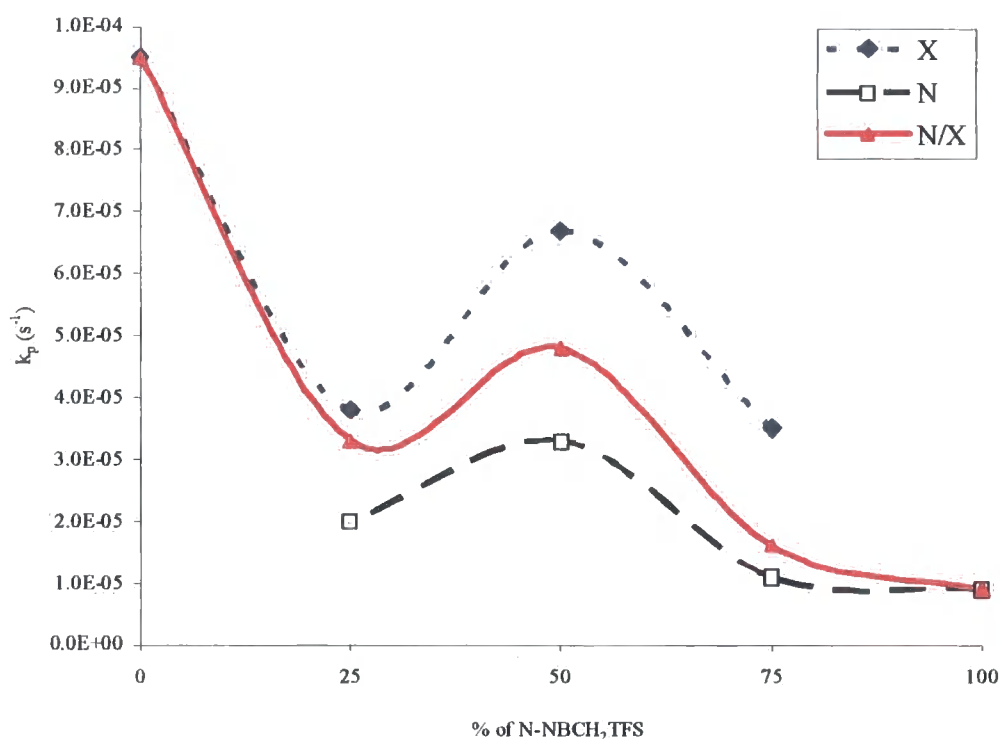


Figure 3.9. Rates of co-polymerisation of the N- and X-NB-CH₂TFS, at 50 NB-CH₂TFS: 1 Pd1388, in benzene-*d*₆ at 70°C, monitored via ¹H NMR spectroscopy.

It is very clear from figure 3.9 that a penultimate group effect is occurring during the co-polymerisations, with the rate of polymerisation for the N- and X-regioisomers and consequently for N/X-NB-CH₂TFS being heavily dependent on the N:X regioisomer ratio. If there were no penultimate group effect during the co-polymerisation reaction, we would expect to see a linear shaped line, in the graph in figure 3.9.

A clearer explanation for the rates of co-polymerisation of N- and X-NBCH₂TFS can be seen from a similar plot to figure 3.8, see figure 3.10. This new graph can easily be generated using the data from figure 3.9, since for a range of feed ratios (*f*_i) we can calculate the instantaneous co-polymer composition (*F*₁), from the known rates of polymerisation for N- and X-NBCH₂TFS.

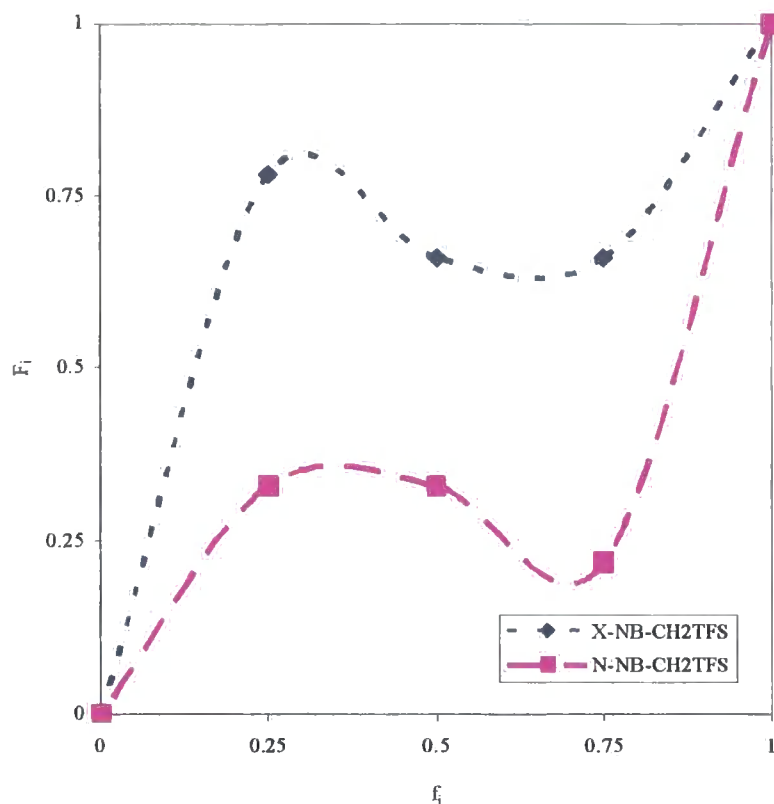


Figure 3.10. Instantaneous co-polymer composition (F_i) variation with monomer feed ratio (f_i) for N- and X-NB-CH₂TFS, at 50 NB-CH₂TFS: 1 Pd1388, in benzene-*d*₆ at 70°C.

The co-polymerisation plot in figure 3.10 is a very close fit to the statistical co-polymerisation plot ($0 < r_N \times r_X > 1$) in figure 3.8. This means that both N- and X-NBCH₂TFS have a preference for co-polymerisation: $r_N < 1$, ⁺Pd-M_N prefers to react with M_X ($k_{NN} < k_{NX}$); $r_X < 1$, ⁺Pd-M_X prefers to react with M_N ($k_{XX} < k_{XN}$).

This evidence has serious implications for the production of homogeneous polymers from monomers containing mixtures of regioisomers, since the feed ratio (f_i) changes as monomers are consumed at different rates, hence the instantaneous co-polymer composition (F_i) will also change, figure 3.10. This is often termed as composition drift and results in polymers with poor polymer homogeneity.

The implication of this behaviour is that pure norbornene isomers should yield polymers with greater homogeneity.

3.2.9 Homologation (Methylene Spacing) of Functional Group

During efforts by Promerus LLC to ascertain the rates of co-polymerisation reactions of monomers which are technologically significant in the synthesis of new lithographic materials, they noticed that monomers which had an increased “methylene spacing” between norbornene backbone and functional group, tended to show increased polymerisation activity. These observations were intriguing since it opposed the generally accepted idea that the electronic effect of the substituent upon the C=C bond in the norbornene backbone was minimal.⁴

In this work, the effect of functional group methylene spacing was investigated by measuring the rates of polymerisation in different families of functionalised norbornene monomers.

3.2.9.1 Trifluoromethanesulfonamide Functionalised Norbornenes

The investigation of the N/X-NB-(CH₂)_nTFS (trifluoromethanesulfonamide = TFS = NHSO₂CF₃) family of monomers revealed that the methylene group spacing of the functional group from the norbornene structure increased the polymerisation rate for both the N- (blue bars) and X-isomers (cream bars), figure 3.11. More importantly the magnitude of this increase in rate appears to be independent of functionalised norbornene regioisomer, table 3.2.

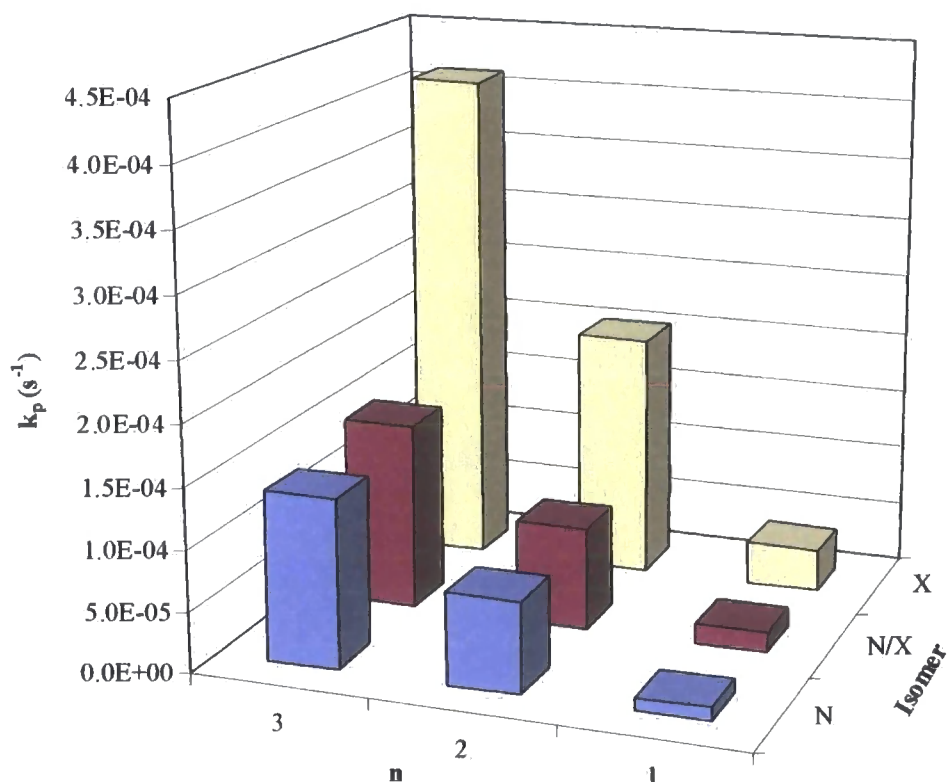


Figure 3.11. Polymerisation data for 50 N/X-NB-(CH₂)_nTFS : 1 Pd1388, at 70°C in benzene-*d*₆

The effect of the methylene group spacing on the rate of polymerisation is decreasing as the functional group moves further away from the norbornene structure. The rate of polymerisation increases by a factor of $\times 5.3$, when n goes from 1 to 2 and a factor of $\times 1.8$ when n goes from 2 to 3, table 3.2. This information suggests that the magnitude of the spacing effect will continue to decrease, as more methylene spacers are added. The polymerisation rate for N/X-NBdecyl ($k = 1.79 \times 10^{-3} \text{ s}^{-1}$) is approximately $\times 12$ faster than N/X-NB-(CH₂)₃TFS under identical conditions. It is unlikely that the rate of polymerisation of NB-(CH₂)₃TFS will increase by a factor of $\times 12$ upon further methylene spacing, suggesting that the simple coordination of the TFS functional group to the Pd centre is also in part responsible for this monomer's slower rates.

Table 3.2. Polymerisation data for 50 N/X-NB-(CH₂)_nTFS : 1 Pd1388, at 70°C in benzene-*d*₆

n	k _p (N) (s ⁻¹)	k _p (X) (s ⁻¹)	k _p (N/X) (s ⁻¹)	[k _p (X)] / [k _p (N)]
1	1.1 × 10 ⁻⁵	3.5 × 10 ⁻⁵	1.6 × 10 ⁻⁵	3.2
2	7.5 × 10 ⁻⁵	20.2 × 10 ⁻⁵	8.4 × 10 ⁻⁵	2.7
3	13.9 × 10 ⁻⁵	41.2 × 10 ⁻⁵	15.4 × 10 ⁻⁵	3.0

It appears, from the polymerisation data, that the chelation of the functional group in the N-isomer does not have a major influence on the polymerisation rate, since [k_p (X)] / [k_p (N)] changes very little, between n = 1, 2 and 3, table 3.2. If chelation was taking place in the N-isomers, the potential chelate ring sizes would change between n = 1, 2 and 3, and the [k_p (X)] / [k_p (N)] value would be expected to change with a change in n. The [k_p (X)] / [k_p (N)] data in table 3.2 is comparable to a [k_p (X)] / [k_p (N)] ≈ 2, for N/X-NBdecyl under identical polymerisation conditions.

3.2.9.2 Trimethylsilyl Carboxylate Functionalised Norbornenes

The N/X-NB-(CH₂)_nCO₂TMS (trimethylsilyl carboxylate = TMS = CO₂SiMe₃) family of monomers also reveals that the methylene group spacing of the functional group from the norbornene structure increases the polymerisation rate for both the N- and X-isomers, approximately equally, figure 3.12. The rate of polymerisation increases by a factor of × 2.3, when n goes from 0 to 1 and a factor of × 13.0 when n goes from 1 to 2, table 3.3. This data suggests that the nature of the “methylene group spacing” effect is dependant on the nature of the functionality, since the increase in magnitude of polymerisation rate upon methylene spacing is not the same for the -CO₂TMS (× 13.0 for n: 1→2) and -TFS (× 5.3 for n: 1→2) families of monomers.

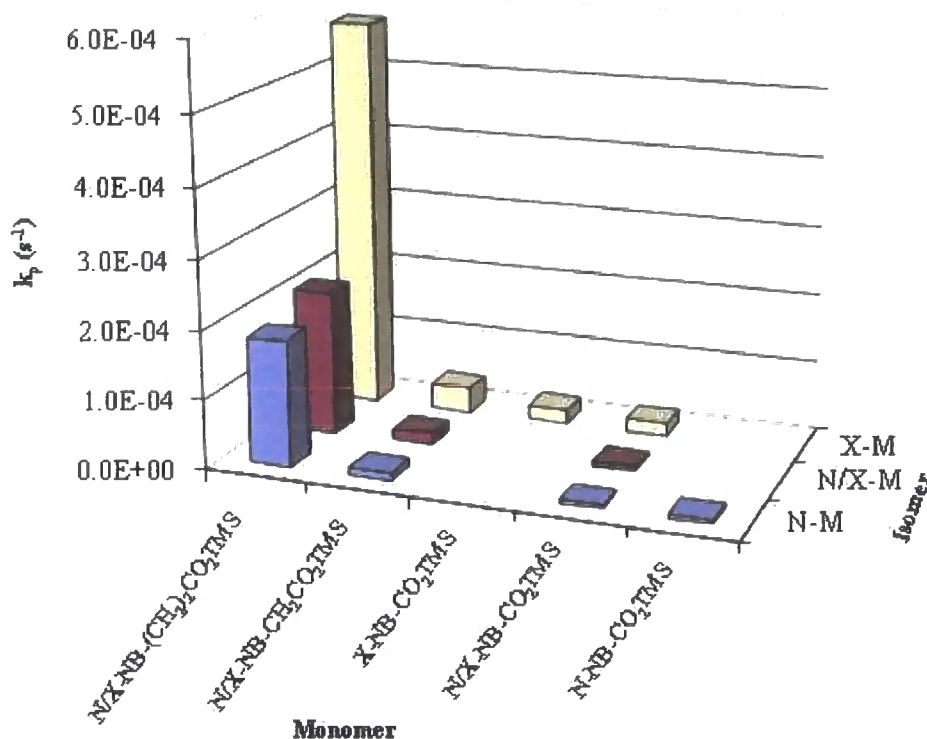


Figure 3.12. Polymerisation data of 50 N/X-NB-(CH₂)_nCO₂TMS : 1 Pd1388, at 70°C in benzene-*d*₆

The polymerisation data suggest that the chelation of the functional group in the N-isomer does not have a major influence on the polymerisation rate, since $[k_p(X)] / [k_p(N)] \approx 3$, when $n = 0, 1$ and 2 , table 3.3. This is very surprising since a favourable six-membered chelate ring could potentially form if chelation occurred in N-NB-CO₂TMS. This would be expected to slow the polymerisation of N-NB-CO₂TMS compared with X-NB-CO₂TMS, giving a $[k_p(X)] / [k_p(N)] > 3$.

Table 3.3. Polymerisation data of 50 N/X-NB-(CH₂)_nCO₂TMS : 1 Pd1388, at 70°C in benzene-*d*₆

n	$k_p(N)$ (s^{-1})	$k_p(X)$ (s^{-1})	$k_p(N/X)$ (s^{-1})	$[k_p(X)] / [k_p(N)]$
0	6×10^{-6}	18×10^{-6}	7×10^{-6}	3.0
1	13×10^{-6}	37×10^{-6}	16×10^{-6}	2.8
2	183×10^{-6}	573×10^{-6}	208×10^{-6}	3.1

The polymerisation rate for the pure N-NB-CO₂TMS monomer ($k = 6 \times 10^{-6} \text{ s}^{-1}$) is identical to that in the N/X-mixture (75N:25X) but the pure X-NB-CO₂TMS ($k = 21 \times 10^{-6} \text{ s}^{-1}$) polymerises slightly faster than in the N/X-mixture ($k = 18 \times 10^{-6} \text{ s}^{-1}$) due to a small penultimate group effect, table 3.3. The penultimate group effect does not appear to have a major influence over the N/X-NB-CO₂TMS polymerisation, which is in contrast to the major effect witnessed for the polymerisation of the N/X-NBCH₂TFS monomer, shown in figure 3.9.

The variation of penultimate group effect highlights just how difficult it would be to gain control over the composition of monomers in a co-polymerisation reaction involving two or more components. This is owing to the effects discussed here, which influence each monomer within the co-polymerisation differently.

3.2.9.3 Hexafluoroalcohol Functionalised Norbornenes

The N/X-NB-(CH₂)_nHFA (hexafluoroisopropanol = HFA = -C(CF₃)₂OH) family of monomers display many unexpected polymerisation rates.

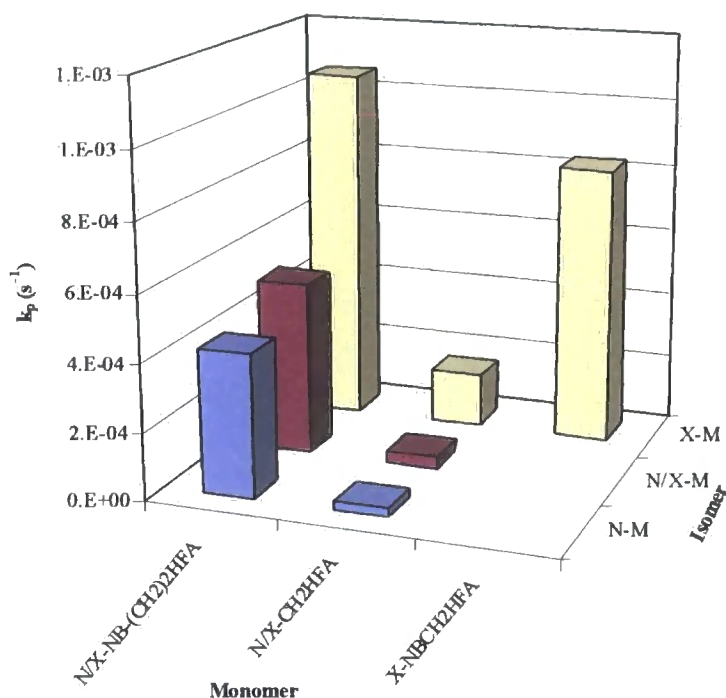


Figure 3.13. Polymerisation data for 50 N/X-NB-(CH₂)_nHFA : 1 Pd1388, at 70°C in benzene-*d*₆

The rate of polymerisation increases by a factor of $\times 14.7$, when *n* increases from 1 to 2, for the N/X-NB-(CH₂)_nHFA monomers, table 3.4, which is similar to the increase for the -CO₂TMS family of monomers. The homo-polymerisation rate of X-NB-CH₂HFA ($k = 83.0 \times 10^{-5} s^{-1}$) is $\times 5$ faster than the X-regioisomer ($k = 16.1 \times 10^{-5} s^{-1}$) within the N/X-copolymerisation (75N:25X) reaction, figure 3.13. This suggests a very strong penultimate group effect.

Table 3.4. Polymerisation data for 50 N/X-NB-(CH₂)_nHFA : 1 Pd1388, at 70°C in benzene-*d*₆

n	k _p (N) (s ⁻¹)	k _p (X) (s ⁻¹)	k _p (N/X) (s ⁻¹)	[k _p (X)] / [k _p (N)]
1	2.7 × 10 ⁻⁵	16.1 × 10 ⁻⁵	3.5 × 10 ⁻⁵	6.0
2	42.6 × 10 ⁻⁵	106.3 × 10 ⁻⁵	51.6 × 10 ⁻⁵	2.5

The -TFS, -HFA and -CO₂TMS families of norbornene monomers discussed here have all displayed a large increase in polymerisation rate, as the functional group has been spaced away from the norbornene moiety by methylene groups. The -TFS, -HFA and -CO₂TMS functional groups are all highly electron withdrawing, which suggests that the withdrawal of negative charge from the norbornene bicyclic structure has a deactivating effect upon the norbornene structure, with respect to polymerisation. This idea would explain why the alkyl norbornenes show very good polymerisation activity, since an alkyl group is not likely to withdraw charge from the norbornene structure.

3.2.9.4 Trimethoxysilyl Functionalised Norbornenes

The N/X-NB-(CH₂)_nSi(OMe)₃ (trimethoxysilyl = TMS = -Si(OMe)₃) family of norbornene monomers is very interesting since the TMS functional group is slightly electron donating in nature, so one might expect to see a reversal of the methylene group spacing trend, with the polymerisation rate decreasing as the methylene spacing (n) increases.

Table 3.5. Polymerisation data for 50 N/X-NB-(CH₂)_nSi(OMe)₃ : 1 Pd1388, at 70°C in benzene-*d*₆

n	k _p (N) (s ⁻¹)	k _p (X) (s ⁻¹)	k _p (N/X) (s ⁻¹)	N:X Monomer Ratio
0	106 × 10 ⁻⁵	409 × 10 ⁻⁵	178 × 10 ⁻⁵	64:36
2	149 × 10 ⁻⁵	332 × 10 ⁻⁵	167 × 10 ⁻⁵	79:21

There is no significant difference in the rate of polymerisation between $n = 0$ or 2 , table 3.5. Any differences which may have been visible are complicated by the penultimate group effect, since the regio isomeric ratios are different when $n = 0$ and 2 .

It is notable that these monomers polymerise at a slightly faster rate than alkylnorbornenes under identical conditions, which adds weight to the theory that the norbornene substituent has an electronic influence upon the norbornene structure, which ultimately controls polymerisation activity.

3.3 Conclusions

This chapter has successfully demonstrated the use of ^1H NMR spectroscopy as an analytical tool for the investigation of cationic palladium hydride initiators in the addition polymerisation of functionalised norbornene monomers. The initiator identity and the reaction conditions predictably affect the polymerisation reaction. *Endo*-substituted norbornenes are polymerised more slowly than their corresponding *exo*-isomers, with the steric size of the substituent playing a role. However, the electronic nature of the functionality plays the major role in lowering polymerisation activity; with electron withdrawing functionalities causing reduced polymerisation activity. The introduction of methylene spacers between norbornene and its functionality reduces the electronic effect of the functionality and increases the monomers polymerisation activity. The co-polymerisation reaction of functionalised norbornene monomers is also shown to be greatly effected by the nature of the functional group, with the $-\text{TFS}$ functionalised monomers displaying a large penultimate group effect during co-polymerisation reactions. The exact cause and generality of this penultimate group effect for other types of functionalised norbornene monomers is not known and further reactivity studies are needed for general conclusions to be made.

It is clear that in order to simplify co-polymerisation reactions and reduce polymerisation attenuating functional group electronic and steric effects; single regioisomer, methylene or multi-methylene spaced, functionalised norbornene monomers must be employed.

3.4 Experiment

3.4.1 Materials

The palladium catalysts were supplied by Promerus LLC and used without further purification. All liquid monomers were degassed by freeze-thaw-pump cycles before being taken into the glove box. THF- d_8 , chloroform- d , dichloromethane- d_2 , tetrachloroethane- d_2 , benzene- d_6 , chlorobenzene- d_5 and toluene- d_8 were used as supplied in pre-sealed ampoules and subsequently kept refrigerated in a glove box. All other solvents were used without prior purification. Copper chloride was used as supplied by Sigma Aldrich.

3.4.2 Instrumentation and Measurements

3.4.2.1 Nuclear Magnetic Resonance

^1H NMR spectra were recorded on a Varian Mercury 400 or a Varian Inova 500 using deuteriated solvent lock. Chemical shifts are quoted in ppm, relative to tetramethylsilane (TMS), as the internal reference. ^{31}P NMR spectra were recorded on a Varian/Mercury 400 or a Varian Inova 500 at 121.4 MHz and 202.4 MHz, respectively. ^{13}C NMR spectra were recorded at 125 MHz (2000 scans) using continuous broad band proton decoupling and a 3 S recycle delay, and are therefore not quantitative; chemical shifts are quoted in ppm, relative to CDCl_3 (77.550 ppm). The following abbreviations are used in listing NMR spectra: s = singlet, d = doublet, t = triplet, q = quartet, b = broad, m = multiplet.

3.4.2.2 Gel Permeation Chromatography (GPC)

Gel permeation chromatography (GPC) data was obtained using a Viscotek TDA 302 equipped with 2 x 300 mm PLgel 5 μm mixed C columns. Tetrahydrofuran was used as the eluent, at a flow rate of 1.0 mL/min at 30°C. The detectors were calibrated using polystyrene standards. This type of conventional GPC analysis, based on polystyrene standards, is

unsuitable to determine actual molecular weights of poly(norbornene) derivatives, but can be used to compare relative molecular weights.

3.4.2.3 Mass Spectroscopy

Electron Impact (EI) and Electrospray (ES⁺) mass spectra were recorded on a Micromass Autospec spectrometer operating at 70 eV with the ionisation mode as indicated.

3.4.2.4 Infra-red Spectroscopy

Infra-red spectra were recorded on a Perkin Elmer 1600 series FTIR. The spectra obtained were of the pure compound between sodium chloride discs.

3.4.3 NMR Scale Addition Polymerisation Reactions - Logistics and Error

All addition polymerisation reactions were prepared in a Braun glove box under an inert atmosphere. Typically, the relevant palladium complex (3.60×10^{-6} mole, 1 equivalent) was dissolved in deuterated solvent. The relevant monomer (1.80×10^{-4} mole, 50 equivalents) was then added to the initiator solution. The solutions were transferred to an NMR tube fitted with a Young's tap, allowing the vessel to be closed under a nitrogen atmosphere. The reactions were monitored using arrayed ¹H spectroscopy. In all cases, the integrated intensities of the vinyl signals of the monomer (polymerisation) and initiator Pd-H signal (initiation) were measured against the previous NMR integrations. Selected experiments were also subjected to GPC analysis.

A preliminary estimate of uncertainty in the polymerisation rate results is obtained from 2 polymerisation reactions for the X/N-NB-CO₂TMS monomer. Replicated runs provide information about the expected variation in polymerisation rate results produced under identical conditions. This information may be used as a baseline for comparing polymerisation rate results produced under different conditions (different monomers). The results from the replicated runs are in table 3.6.

Table 3.6. Propagation rate results from replicated runs.

Run	k_p N (s^{-1})	k_p X (s^{-1})
1	1.265×10^{-5}	3.657×10^{-5}
2	1.283×10^{-5}	3.652×10^{-5}
Average	1.274×10^{-5}	3.6545×10^{-5}
Std. Dev.	1.27279×10^{-7}	3.53553×10^{-8}
Range	1.8000×10^{-7}	5.0000×10^{-8}

To conclude that different monomers yield significantly different k_p results, the observed difference between monomers should be at least 6.4×10^{-7} for the N-regioisomer and 1.8×10^{-7} for the X-regioisomer. These values are 5 times the standard deviation in replicated run results for the N and X-regioisomers, respectively.

3.4.3.1 Effect of Initiator, Phosphine Ligand (PR_3) on Polymerisation of *endo/exo*-5-Decyl-2-norbornene

Table 3.7 shows the experimental details and results for the polymerisation of *endo/exo*-5-decyl-2-norbornene (N/X-NBdecyl) using different initiators, under identical conditions. The polymerisations were set up as described in section 3.3.3.



Table 3.7. Polymerisation of 50 N/X-NBdecyl (42.1 mg, 1.80×10^{-4} mol): 1 initiator.

Initiator	Temp (°C)	Solvent	k_i (s ⁻¹)	k_p (s ⁻¹)	M_n	M_w	M_w/M_n
Pd1388 (5.0 mg, 3.60×10^{-6} mol)	20°C	DCM- <i>d</i> ₂	18×10^{-5}	16×10^{-5}	17500	29800	1.70
Pd1336 (4.8 mg, 3.60×10^{-6} mol)	20°C	DCM- <i>d</i> ₂	17×10^{-5}	32×10^{-5}	13700	29100	1.80
Pd1148 (4.1 mg, 3.60×10^{-6} mol)	20°C	DCM- <i>d</i> ₂	18×10^{-5}	56×10^{-5}	14200	17900	1.87
Pd1304 (4.7 mg, 3.60×10^{-6} mol)	20°C	DCM- <i>d</i> ₂	12×10^{-5}	49×10^{-5}	19100	39400	2.06
Pd1388 (5.0 mg, 3.60×10^{-6} mol), CuCl (0.36 mg, 3.60×10^{-6} mol)	20°C	DCM- <i>d</i> ₂	-	52×10^{-5}	11100	14900	1.57

3.4.3.2 Polymerisation of *endo/exo*-5-alkyl-2-norbornene using Pd1388

Table 3.8 shows the experimental details and results for the polymerisation of *endo/exo*-5-alkyl-2-norbornene (N/X-NBalkyl) using the initiator **Pd1388**, under differing conditions. The polymerisations were set up as described in section 3.3.3.

Table 3.8. Polymerisation of 50 N/X-NBalkyl: 1 Pd1388 (5.0 mg, 3.60×10^{-6} mol).

Monomer	Temp (°C)	Solvent	k_p (N/X) (s ⁻¹)	k_p (N) (s ⁻¹)	k_p (X) (s ⁻¹)	k_i (N/X) (s ⁻¹)
N/X-NBdecyl (42.1 mg, 1.80×10^{-4} mol)	40	Benzene- <i>d</i> ₆	14×10^{-5}	11×10^{-5}	27×10^{-5}	52×10^{-5}
N/X-NBdecyl (42.1 mg, 1.80×10^{-4} mol)	50	Benzene- <i>d</i> ₆	60×10^{-5}	50×10^{-5}	114×10^{-5}	70×10^{-5}
N/X-NBdecyl (42.1 mg, 1.80×10^{-4} mol)	70	Benzene- <i>d</i> ₆	179×10^{-5}	164×10^{-5}	321×10^{-5}	179×10^{-5}
N/X-NBdecyl (42.1 mg, 1.80×10^{-4} mol)	40	Toluene- <i>d</i> ₈	10×10^{-5}	8×10^{-5}	20×10^{-5}	-

Monomer	Temp (°C)	Solvent	k_p (N/X) (s ⁻¹)	k_p (N) (s ⁻¹)	k_p (X) (s ⁻¹)	k_i (N/X) (s ⁻¹)
N/X-NBdecyl (42.1 mg, 1.80×10^{-4} mol)	40	Benzene- <i>d</i> ₆	14×10^{-5}	11×10^{-5}	27×10^{-5}	52×10^{-5}
N/X-NBdecyl (42.1 mg, 1.80×10^{-4} mol)	40	Chlorobenzene- <i>d</i> ₅	35×10^{-5}	30×10^{-5}	59×10^{-5}	23×10^{-5}
N/X-NBdecyl (42.1 mg, 1.80×10^{-4} mol)	40	DCM- <i>d</i> ₂	128×10^{-5}	109×10^{-5}	241×10^{-5}	-
N/X-NBdecyl (42.1 mg, 1.80×10^{-4} mol)	40	TCE- <i>d</i> ₂	131×10^{-5}	111×10^{-5}	247×10^{-5}	129×10^{-5}
N/X-NBdecyl (42.1 mg, 1.80×10^{-4} mol)	20	DCM- <i>d</i> ₂	17×10^{-5}	15×10^{-5}	44×10^{-5}	14×10^{-5}
N/X-NBhexyl (32.1 mg, 1.80×10^{-4} mol)	20	DCM- <i>d</i> ₂	18×10^{-5}	15×10^{-5}	39×10^{-5}	11×10^{-5}
N/X-NBbutyl (27.0 mg, 1.80×10^{-4} mol)	20	DCM- <i>d</i> ₂	21×10^{-5}	17×10^{-5}	46×10^{-5}	12×10^{-5}
N/X-NBmethyl (19.5 mg, 1.80×10^{-4} mol)	20	DCM- <i>d</i> ₂	23×10^{-5}	18×10^{-5}	41×10^{-5}	15×10^{-5}
NB (42.1 mg, 1.80×10^{-4} mol)	20	DCM- <i>d</i> ₂	67×10^{-5}	-	-	12×10^{-5}
N/X-NB(CH ₂) ₂ Ph (35.7 mg, 1.80×10^{-4} mol)	20	DCM- <i>d</i> ₂	7.4×10^{-5}			17×10^{-5}
N/X-NBdecyl (42.1 mg, 1.80×10^{-4} mol)	50	Benzene- <i>d</i> ₆	60×10^{-5}	50×10^{-5}	114×10^{-5}	-
N/X-NBhexyl (32.1 mg, 1.80×10^{-4} mol)	50	Benzene- <i>d</i> ₆	44×10^{-5}	39×10^{-5}	89×10^{-5}	-
N/X-NBbutyl (27.0 mg, 1.80×10^{-4} mol)	50	Benzene- <i>d</i> ₆	52×10^{-5}	45×10^{-5}	97×10^{-5}	-
N/X-NBmethyl (19.5 mg, 1.80×10^{-4} mol)	50	Benzene- <i>d</i> ₆	40×10^{-5}	32×10^{-5}	81×10^{-5}	-
N/X-NB(CH ₂) ₂ Ph (35.7 mg, 1.80×10^{-4} mol)	50	Benzene- <i>d</i> ₆	21×10^{-5}	17×10^{-5}	44×10^{-5}	-

3.4.3.3 Polymerisation of Trifluoromethanesulfonamide Functionalised Norbornenes (NB(CH₂)_nTFS) using Pd1388

Table 3.9 shows the experimental details and results for the polymerisation of -TFS functionalised norbornenes using the initiator **Pd1388**, under identical conditions. The polymerisations were set up as described in section 3.3.3.

Table 3.9. Polymerisation of 50 NB(CH₂)_nTFS : 1 Pd1388 (5.0 mg, 3.60 × 10⁻⁶ mol).

Monomer	Temp (°C)	Solvent	k _p (N/X) (s ⁻¹)	k _p (N) (s ⁻¹)	k _p (X) (s ⁻¹)
N-NBCH ₂ TFS (45.9 mg, 1.80 × 10 ⁻⁴ mol)	70	Benzene- <i>d</i> ₆	-	9 × 10 ⁻⁶	-
N-NBCH ₂ TFS (11.5 mg, 0.45 × 10 ⁻⁴ mol) + X-NBCH ₂ TFS (34.4 mg, 1.35 × 10 ⁻⁴ mol)	70	Benzene- <i>d</i> ₆	33 × 10 ⁻⁶	20 × 10 ⁻⁶	33 × 10 ⁻⁶
N-NBCH ₂ TFS (22.9 mg, 0.9 × 10 ⁻⁴ mol) + X-NBCH ₂ TFS (22.9 mg, 0.9 × 10 ⁻⁴ mol)	70	Benzene- <i>d</i> ₆	48 × 10 ⁻⁶	33 × 10 ⁻⁶	67 × 10 ⁻⁶
N-NBCH ₂ TFS (34.4 mg, 1.35 × 10 ⁻⁴ mol) + X-NBCH ₂ TFS (11.5 mg, 0.45 × 10 ⁻⁴ mol)	70	Benzene- <i>d</i> ₆	16 × 10 ⁻⁶	11 × 10 ⁻⁶	35 × 10 ⁻⁶
X-NBCH ₂ TFS (45.9 mg, 1.80 × 10 ⁻⁴ mol)	70	Benzene- <i>d</i> ₆	-	-	95 × 10 ⁻⁶
N/X-NBCH ₂ TFS (45.9 mg, 1.80 × 10 ⁻⁴ mol)	70	Benzene- <i>d</i> ₆	16 × 10 ⁻⁶	11 × 10 ⁻⁶	35 × 10 ⁻⁶
N/X-NB(CH ₂) ₂ TFS (48.4 mg, 1.80 × 10 ⁻⁴ mol)	70	Benzene- <i>d</i> ₆	84 × 10 ⁻⁶	75 × 10 ⁻⁶	202 × 10 ⁻⁶
N/X-NB(CH ₂) ₃ TFS (50.9 mg, 1.80 × 10 ⁻⁴ mol)	70	Benzene- <i>d</i> ₆	154 × 10 ⁻⁶	139 × 10 ⁻⁶	412 × 10 ⁻⁶

3.4.3.4 Polymerisation of Trimethylsilyl Carboxylate Functionalised Norbornenes (NB(CH₂)_nCO₂TMS) using Pd1388

Table 3.10 shows the experimental details and results for the polymerisation of –CO₂TMS functionalised norbornenes using the initiator Pd1388, under identical conditions. The polymerisations were set up as described in section 3.3.3.

Table 3.10. Polymerisation of 50 NB(CH₂)_nCO₂TMS : 1 Pd1388 (5.0 mg, 3.60 × 10⁻⁶ mol)

Monomer	Temp (°C)	Solvent	k _p (N/X) (s ⁻¹)	k _p (N) (s ⁻¹)	k _p (X) (s ⁻¹)
N-NB-CO ₂ TMS (37.8 mg, 1.80 × 10 ⁻⁴ mol)	70	Benzene- <i>d</i> ₆	-	6 × 10 ⁻⁶	-
X-NB-CO ₂ TMS (37.8 mg, 1.80 × 10 ⁻⁴ mol)	70	Benzene- <i>d</i> ₆	-	-	21 × 10 ⁻⁶
N/X-NB-CO ₂ TMS (37.8 mg, 1.80 × 10 ⁻⁴ mol)	70	Benzene- <i>d</i> ₆	7 × 10 ⁻⁶	6 × 10 ⁻⁶	18 × 10 ⁻⁶
N/X-NB-CH ₂ CO ₂ TMS (40.3 mg, 1.80 × 10 ⁻⁴ mol)	70	Benzene- <i>d</i> ₆	16 × 10 ⁻⁶	13 × 10 ⁻⁶	37 × 10 ⁻⁶
N/X-NB(CH ₂) ₂ TMS (42.8 mg, 1.80 × 10 ⁻⁴ mol)	70	Benzene- <i>d</i> ₆	208 × 10 ⁻⁶	183 × 10 ⁻⁶	573 × 10 ⁻⁶

3.4.3.5 Polymerisation of Hexafluoroisopropanol Functionalised Norbornenes (NB(CH₂)_nHFA) using Pd1388

Table 3.11 shows the experimental details and results for the polymerisation of –HFA functionalised norbornenes using the initiator Pd1388, under varying conditions. The polymerisations were set up as described in section 3.3.3.

Table 3.11. Polymerisation of 50 NB(CH₂)_nHFA : 1 Pd1388 (5.0 mg, 3.60 × 10⁻⁶ mol)

Monomer	Temp (°C)	Solvent	k _p (N/X) (s ⁻¹)	k _p (N) (s ⁻¹)	k _p (X) (s ⁻¹)
X-NB-CH ₂ HFA (50.0 mg, 1.80 × 10 ⁻⁴ mol)	70	Benzene- <i>d</i> ₆	-	-	83 × 10 ⁻⁵
N/X-NB-CH ₂ HFA (50.0 mg, 1.80 × 10 ⁻⁴ mol)	70	Benzene- <i>d</i> ₆	3.5 × 10 ⁻⁵	2.7 × 10 ⁻⁵	16.1 × 10 ⁻⁵
N/X-NB-(CH ₂) ₂ HFA (52.5 mg, 1.80 × 10 ⁻⁴ mol)	70	Benzene- <i>d</i> ₆	51.6 × 10 ⁻⁵	42.6 × 10 ⁻⁵	106.3 × 10 ⁻⁵
X-NB-CH ₂ HFA (50.0 mg, 1.80 × 10 ⁻⁴ mol)	50	Benzene- <i>d</i> ₆	-	-	30 × 10 ⁻⁵
N/X-NB-CH ₂ HFA (50.0 mg, 1.80 × 10 ⁻⁴ mol)	50	Benzene- <i>d</i> ₆	1.4 × 10 ⁻⁵	1.0 × 10 ⁻⁵	4.8 × 10 ⁻⁵

3.4.3.6 Polymerisation of Trimethoxysilyl Functionalised Norbornenes (NB(CH₂)_nSi(OMe)₃) using Pd1388

Table 3.12 shows the experimental details and results for the polymerisation of -Si(OMe)₃ functionalised norbornenes using the initiator **Pd1388**, under varying conditions. The polymerisations were set up as described in section 3.3.3.

Table 3.12. Polymerisation of 50 NB(CH₂)_nSi(OMe)₃ : 1 Pd1388 (5.0 mg, 3.60 × 10⁻⁶ mol)

Monomer	Temp (°C)	Solvent	k _p (N/X) (s ⁻¹)	k _p (N) (s ⁻¹)	k _p (X) (s ⁻¹)
N/X-NB-Si(OMe) ₃ (38.5 mg, 1.80 × 10 ⁻⁴ mol)	70	Benzene- <i>d</i> ₆	17.8 × 10 ⁻⁴	10.6 × 10 ⁻⁴	40.9 × 10 ⁻⁴
N/X-NB-(CH ₂) ₂ Si(OMe) ₃ (43.6 mg, 1.80 × 10 ⁻⁴ mol)	70	Benzene- <i>d</i> ₆	16.7 × 10 ⁻⁴	14.9 × 10 ⁻⁴	33.2 × 10 ⁻⁴
N/X-NB-Si(OMe) ₃ (38.5 mg, 1.80 × 10 ⁻⁴ mol)	50	Benzene- <i>d</i> ₆	7.0 × 10 ⁻⁴	4.3 × 10 ⁻⁴	9.9 × 10 ⁻⁴
N/X-NB-(CH ₂) ₂ Si(OMe) ₃ (43.6 mg, 1.80 × 10 ⁻⁴ mol)	50	Benzene- <i>d</i> ₆	3.9 × 10 ⁻⁴	2.6 × 10 ⁻⁴	7.5 × 10 ⁻⁴

Monomer	Temp (°C)	Solvent	k_p (N/X) (s ⁻¹)	k_p (N) (s ⁻¹)	k_p (X) (s ⁻¹)
N/X-NBSi(OMe) ₃ (38.5 mg, 1.80 × 10 ⁻⁴ mol)	ambient	DCM- <i>d</i> ₂	2.7 × 10 ⁻⁴	2.4 × 10 ⁻⁴	2.9 × 10 ⁻⁴
N/X-NB(CH ₂) ₂ Si(OMe) ₃ (43.6 mg, 1.80 × 10 ⁻⁴ mol)	ambient	DCM- <i>d</i> ₂	1.7 × 10 ⁻⁴	1.2 × 10 ⁻⁴	3.8 × 10 ⁻⁴

3.4.4 Characterisation of Monomers

The following monomers were supplied by Promerus LLC and characterised without further purification. In all cases the monomers were of greater than 99% purity by GCMS.

3.4.4.1 Characterisation of the *endo*-Regioisomer in *endo/exo*-5-Methyl-2-norbornene

The monomer was characterised by ¹H NMR, ¹³C NMR, GCMS and IR. The numbering system shown in figure 3.14 was used for the assignment of the peaks in the NMR spectra.

¹H NMR (500 MHz, CDCl₃): δ (ppm) = 6.14 (dd, 1H, *J* = 5.62 & 3.04, H₂), 5.96 (dd, 1H, *J* = 5.62 & 2.98, H₃), 2.76 (bs, 1H, H₁), 2.67 (bs, 1H, H₄), 2.11 (m, 1H, H₅), 1.88 (ddd, 1H, *J* = 11.28 & 9.11 & 3.86, H₇), 1.40 (m, 1H, H₆), 1.26 (m, 1H, H₆), 0.80 (d, 3H, *J* = 6.92, H₈), 0.45 (ddd, 1H, *J* = 11.28 & 4.29 & 2.61, H₇).

¹³C NMR (125.7 MHz, CDCl₃): δ (ppm) = 137.21 (C₂), 132.67 (C₃), 50.41 (C₆), 47.55 (C₄), 43.42 (C₁), 34.05 (C₇), 32.76 (C₅), 19.65 (C₈).

GCMS (EI⁺): RT = 5.01, N-NB-CH₃ (80%), 108.0 (C₈H₁₂, M⁺).

IR (KBr disc, cm⁻¹): 3080 (olefinic C-H stretching), 2980-2867 (saturated C-H stretching).

3.4.4.2 Characterisation of the *exo*-Regioisomer in *endo/exo*-5-Methyl-2-norbornene

The monomer was characterised by ^1H NMR, ^{13}C NMR, GCMS and IR. The numbering system shown in figure 3.14 was used for the assignment of the peaks in the NMR spectra.

^1H NMR (500 MHz, CDCl_3): δ (ppm) = 6.12 (dd, 1H, $J = 5.62$ & 3.04 , H_2), 6.02 (dd, 1H, $J = 5.62$ & 2.98 , H_3), 2.80 (bs, 1H, H_1), 2.41 (bs, 1H, H_4), 1.47 (m, 1H, H_5), 1.40 (m, 1H, H_6), 1.31 (m, 1H, H_6), 1.30 (m, 1H, H_7), 1.09 (d, 3H, $J = 7.01$, H_8), 1.07 (m, 1H, H_7).

^{13}C NMR (125.7 MHz, CDCl_3): δ (ppm) = 137.31 (C_2), 136.26 (C_3), 48.50 (C_4), 45.03 (C_6), 42.52 (C_1), 34.76 (C_7), 32.76 (C_5), 21.84 (C_8).

GCMS (EI^+): RT = 5.01, X-NB- CH_3 (20%), 108.0 (C_8H_{12} , M^+).

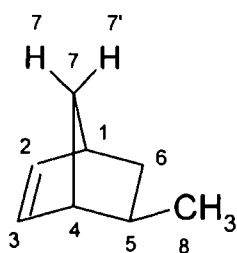


Figure 3.14. Assignment of C and H atoms in N/X-NB- CH_3 .

3.4.4.3 Characterisation of the *endo*-Regioisomer in *endo/exo*-5-Butyl-2-norbornene

The monomer was characterised by ^1H NMR, ^{13}C NMR, GCMS and IR. The numbering system shown in figure 3.15 was used for the assignment of the peaks in the NMR spectra.

^1H NMR (500 MHz, CDCl_3): δ (ppm) = 6.12 (dd, 1H, $J = 5.75$ & 3.12 , H_2), 5.93 (dd, 1H, $J = 5.75$ & 2.83 , H_3), 2.78 (bs, 1H, $\text{H}_{1\&4}$), 2.78 (bs, 1H, $\text{H}_{1\&4}$), 1.98 (m, 1H, H_5), 1.87 (ddd, 1H, $J = 11.23$ & 8.99 & 3.91 , H_7), 1.40 (m, 1H, H_6), 1.38 – 1.24 (m, 4H, $\text{H}_{8\&9\&10}$), 1.23 (m, 1H, H_6), 1.09 (m, 2H, $\text{H}_{8\&9\&10}$), 0.89 (m, 3H, H_{11}), 0.51 (ddd, 1H, $J = 11.23$ & 4.05 & 2.70 , H_7).

^{13}C NMR (125.7 MHz, CDCl_3): δ (ppm) = 137.10 ($\text{C}_{2\&3}$), 132.73 ($\text{C}_{2\&3}$), 49.84, 45.69, 42.81, 39.03, 34.81, 32.73, 31.23, 23.25, 14.44.

GCMS (EI^+): RT = 9.91 (75%), N-NB- $(\text{CH}_2)_3\text{CH}_3$, 150.1 ($\text{C}_{11}\text{H}_{18}$, M^+).

IR (KBr disc, cm^{-1}): 3080 (olefinic C-H stretching), 2980-2867 (saturated C-H stretching).

3.4.4.4 Characterisation of the *exo*-Regioisomer in *endo/exo*-5-Butyl-2-norbornene

The monomer was characterised by ^1H NMR, ^{13}C NMR, GCMS and IR. The numbering system shown in figure 3.15 was used for the assignment of the peaks in the NMR spectra.

^1H NMR (500 MHz, CDCl_3): δ (ppm) = 6.10 (dd, 1H, $J = 5.69$ & 3.00 , H_2), 6.02 (dd, 1H, $J = 5.69$ & 2.86 , H_3), 2.79 (bs, 1H, $\text{H}_{1\&4}$), 2.52 (bs, 1H, $\text{H}_{4\&1}$), other peaks obscured from view.

^{13}C NMR (125.7 MHz, CDCl_3): δ (ppm) = 137.23 ($\text{C}_{2\&3}$), 136.42 ($\text{C}_{2\&3}$), 46.64, 45.50, 42.15, 36.61, 33.39, 31.44, 23.26, 14.46.

GCMS (EI^+): RT = 9.91 (25%), X-NB- $(\text{CH}_2)_3\text{CH}_3$, 150.1 ($\text{C}_{11}\text{H}_{18}$, M^+).

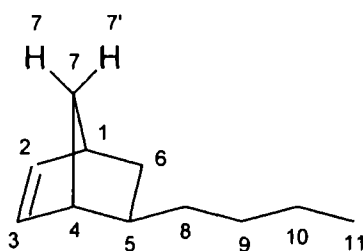


Figure 3.15. Assignment of C and H atoms in N/X-NB- $(\text{CH}_2)_3\text{CH}_3$.

3.4.4.5 Characterisation of the *endo*-Regioisomer in *endo/exo*-5-Hexyl-2-norbornene

The monomer was characterised by ^1H NMR, ^{13}C NMR, GCMS and IR. The numbering system shown in figure 3.16 was used for the assignment of the peaks in the NMR spectra.

^1H NMR (500 MHz, CDCl_3): δ (ppm) = 6.12 (dd, 1H, $J = 5.66$ & 3.08 , H_2), 5.93 (dd, 1H, $J = 5.66$ & 2.87 , H_3), 2.77 (bs, 1H, $\text{H}_{1\&4}$), 2.75 (bs, 1H, $\text{H}_{1\&4}$), 1.98 (m, 1H, H_5), 1.85 (ddd, 1H, $J = 11.34$ & 8.96 & 3.94 , H_7), 1.40 (m, 1H, H_6), 1.38 – 1.24 (m, 8H, H_{8-12}), 1.23 (m, 1H, H_6), 1.09 (m, 2H, H_{8-12}), 0.90 (m, 3H, H_{13}), 0.51 (ddd, 1H, $J = 11.34$ & 4.30 & 2.63 , $\text{H}_{7'}$).

^{13}C NMR (125.7 MHz, CDCl_3): δ (ppm) = 137.10 ($\text{C}_{2\&3}$), 132.73 ($\text{C}_{2\&3}$), 49.84, 45.69, 42.81, 39.06, 35.13, 32.73, 32.25, 32.23, 29.91, 28.94, 23.00, 14.41.

GCMS (EI^+): RT = 13.00 (79%), N-NB-(CH_2) $_5$ CH $_3$, 178.1 ($\text{C}_{13}\text{H}_{22}$, M^+).

IR (KBr disc, cm^{-1}): 3080 (olefinic C-H stretching), 2980-2867 (saturated C-H stretching).

3.4.4.6 Characterisation of the *exo*-Regioisomer in *endo/exo*-5-Hexyl-2-norbornene

The monomer was characterised by ^1H NMR, ^{13}C NMR, GCMS and IR. The numbering system shown in figure 3.16 was used for the assignment of the peaks in the NMR spectra.

^1H NMR (500 MHz, CDCl_3): δ (ppm) = 6.10 (dd, 1H, $J = 5.71$ & 3.08 , H_2), 6.03 (dd, 1H, $J = 5.71$ & 2.91 , H_3), 2.79 (bs, 1H, $\text{H}_{1\&4}$), 2.52 (bs, 1H, $\text{H}_{4\&1}$), other peaks obscured from view.

^{13}C NMR (125.7 MHz, CDCl_3): δ (ppm) = 137.23 ($\text{C}_{2\&3}$), 136.42 ($\text{C}_{2\&3}$), 46.64, 45.50, 42.15, 36.94, 33.38, 29.16, other peaks obscured from view.

GCMS (EI^+): RT = 13.05 (21%), X-NB-(CH_2) $_5$ CH $_3$, 178.1 ($\text{C}_{13}\text{H}_{22}$, M^+).

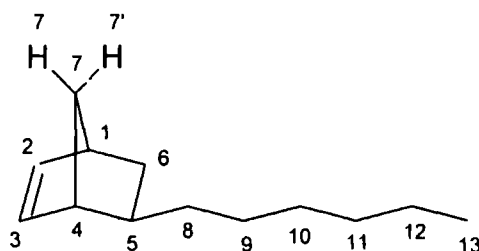


Figure 3.16. Assignment of C and H atoms in N/X-NB-(CH_2) $_5$ CH $_3$.

3.4.4.7 Characterisation of the *endo*-Regioisomer in *endo/exo*-5-Decyl-2-norbornene

The monomer was characterised by ^1H NMR, ^{13}C NMR, GCMS and IR. The numbering system shown in figure 3.17 was used for the assignment of the peaks in the NMR spectra.

^1H NMR (500 MHz, CDCl_3): δ (ppm) = 6.12 (dd, 1H, $J = 5.76$ & 3.06 , H_2), 5.93 (dd, 1H, $J = 5.64$ & 2.82 , H_3), 2.78 (bs, 1H, $\text{H}_{1\&4}$), 2.76 (bs, 1H, $\text{H}_{1\&4}$), 1.98 (m, 1H, H_5), 1.86 (ddd, 1H, $J = 11.15$ & 9.00 & 3.96 , H_7), 1.40 (m, 1H, H_6), 1.38 – 1.24 (m, 16H, H_{8-16}), 1.23 (m, 1H, H_6), 1.08 (m, 2 H_{8-16}), 0.91 (m, 3H, H_{17}), 0.51 (ddd, 1H, $J = 11.23$ & 4.05 & 2.70 , H_7).

^{13}C NMR (125.7 MHz, CDCl_3): δ (ppm) = 137.10 ($\text{C}_{2\&3}$), 132.73 ($\text{C}_{2\&3}$), 49.85, 45.70, 42.82, 39.06, 35.13, 32.74, 32.25, 30.26, 30.03, 30.02, 29.98, 29.69, 29.00, 23.01, 14.42.

GCMS (EI^+): RT = 18.18 (79%), N-NB-(CH_2) $_9$ CH $_3$, 234.2 ($\text{C}_{17}\text{H}_{30}$, M^+).

IR (KBr disc, cm^{-1}): 3080 (olefinic C-H stretching), 2980-2867 (saturated C-H stretching).

3.4.4.8 Characterisation of the *exo*-Regioisomer in *endo/exo*-5-Decyl-2-norbornene

The monomer was characterised by ^1H NMR, ^{13}C NMR, GCMS and IR. The numbering system shown in figure 3.17 was used for the assignment of the peaks in the NMR spectra.

^1H NMR (500 MHz, CDCl_3): δ (ppm) = 6.10 (dd, 1H, $J = 5.73$ & 3.06 , H_2), 6.03 (dd, 1H, $J = 5.73$ & 2.89 , H_3), 2.79 (bs, 1H, $\text{H}_{1\&4}$), 2.52 (bs, 1H, $\text{H}_{1\&4}$), other peaks obscured from view.

^{13}C NMR (125.7 MHz, CDCl_3): δ (ppm) = 137.22 ($\text{C}_{2\&3}$), 136.42 ($\text{C}_{2\&3}$), 46.65, 45.51, 42.16, 36.95, 33.40, 30.27, 30.05, 29.22, 23.01, 14.01. Other peaks obscured from view.

GCMS (EI^+): RT = 18.21 (21%), X-NB-(CH_2) $_9$ CH $_3$, 234.2 ($\text{C}_{17}\text{H}_{30}$, M^+).

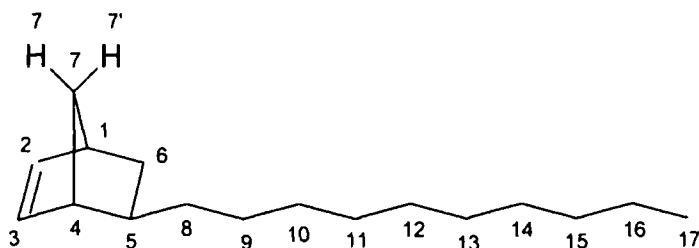


Figure 3.17. Assignment of C and H atoms in N/X-NB-(CH₂)₉CH₃.

3.4.4.9 Characterisation of the *endo*-Regioisomer in *endo/exo*-5-Benzyl-2-norbornene

The monomer was characterised by ¹H NMR, ¹³C NMR, GCMS and IR. The numbering system shown in figure 3.18 was used for the assignment of the peaks in the NMR spectra.

¹H NMR (500 MHz, CDCl₃): δ (ppm) = 7.34 (m, 2H, H₁₁), 7.25 (m, 3H, H_{12&13}), 6.21 (dd, 1H, *J* = 5.53 & 3.00, H₂), 6.03 (dd, 1H, *J* = 5.53 & 2.73, H₃), 2.88 (bs, 1H, H_{1&4}), 2.84 (bs, 1H, H_{1&4}), 2.68 (m, 2H, H₉), 2.10 (m, 1H, H₅), 1.94 (ddd, 1H, *J* = 11.12 & 9.04 & 3.97, H₇), 1.60 – 1.35 (m, 3H, H_{6&8}) 1.30 (m, 1H, *J* = 7.95, H₆), 0.63 (ddd, 1H, *J* = 11.12 & 3.93 & 2.59, H₇).

¹³C NMR (125.7 MHz, CDCl₃): δ (ppm) = 143.22 (-Ph), 137.36 (C_{2&3}), 132.57 (C_{2&3}), 128.61 (-Ph), 128.49 (-Ph), 125.80 (-Ph), 49.85, 45.67, 42.83, 38.63, 37.00, 35.25, 32.65.

GCMS (EI⁺): RT = 16.88, N-NB-(CH₂)₂Ph (80%), 198.1 (C₁₅H₁₈, M⁺).

IR (KBr disc, cm⁻¹): 3080 (olefinic C-H stretching), 2990-2850 (saturated C-H stretching).

3.4.4.10 Characterisation of the *exo*-Regioisomer in *endo/exo*-5-Benzyl-2-norbornene

The monomer was characterised by ¹H NMR, ¹³C NMR, GCMS and IR. The numbering system shown in figure 3.18 was used for the assignment of the peaks in the NMR spectra.

^1H NMR (500 MHz, CDCl_3): δ (ppm) = 7.34 (m, 2H, H_{11}), 7.25 (m, 3H, $\text{H}_{12\&13}$), 6.16 (dd, 1H, $J = 5.58$ & 3.02 , H_2), 6.10 (dd, 1H, $J = 5.58$ & 2.87 , H_3), 2.88 (bs, 1H, $\text{H}_{1\&4}$), 2.64 (bs, 1H, $\text{H}_{1\&4}$), 2.74 (m, 2H), 1.78 (m, 2H, H_6), 1.24 (m, 1H, H_7), other peaks obscured from view.

^{13}C NMR (125.7 MHz, CDCl_3): δ (ppm) = 143.09 (-Ph), 137.07 ($\text{C}_{2\&3}$), 136.50 ($\text{C}_{2\&3}$), 128.65 (-Ph), 128.53 (-Ph), 125.86 (-Ph), 46.63, 45.59, 42.19, 38.82, 38.68, 35.48, 33.34.

GCMS (EI^+): RT = 16.88, X-NB- $(\text{CH}_2)_2\text{Ph}$ (20%), 198.1 ($\text{C}_{15}\text{H}_{18}$, M^+).

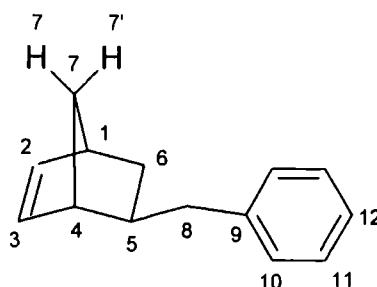


Figure 3.18. Assignment of C and H atoms in N/X-NB- CH_2Ph .

3.4.4.11 Characterisation of *exo*-Bis(trifluoromethyl)-2-norbornene-5-ethanol

The monomer was characterised by ^1H NMR, ^{13}C NMR, GCMS and IR. The numbering system shown in figure 3.19 was used for the assignment of the peaks in the NMR spectra.

^1H NMR (500 MHz, CDCl_3): δ (ppm) = 6.13 (dd, 1H, $J = 5.57$ & 3.00 , H_3), 6.08 (dd, 1H, $J = 5.57$ & 3.00 , H_2), 2.96 (bs, 1H, -OH), 2.88 (bs, 1H, H_1), 2.65 (bs, 1H, H_4), 2.12 (dd, 1H, $J = 15.14$ & 5.30 , H_8), 2.05 (dd, 1H, $J = 15.14$ & 8.08 , H_8), 1.74 (m, 1H, H_5), 1.46 (ddd, 1H, $J = 11.71$ & 8.19 & 2.36 , H_7), 1.40 (m, 1H, $J = 8.80$, H_6), 1.35 (m, 1H, H_6), 1.30 (m, 1H, $J = 11.71$, H_7).

^{13}C NMR (125.7 MHz, CDCl_3): δ (ppm) = 137.09 (C_2), 136.65 (C_3), 123.51 (q, $J = 286.29$, C_{10}), 76.94 (septet, $J = 28.65$, C_9), 48.56 (C_4), 45.49 (C_6), 42.48 (C_1), 36.60 (C_8), 34.78 (C_7), 32.48 (C_5).

GCMS (EI⁺): RT = 9.70, X-NBCH₂C(CF₃)₂OH, 274.0 (C₁₁H₁₂OF₆, M⁺).

IR (KBr disc, cm⁻¹): 3100-3650 (O-H), 3080 (olefinic C-H stretching), 2980-2867 (saturated C-H stretching).

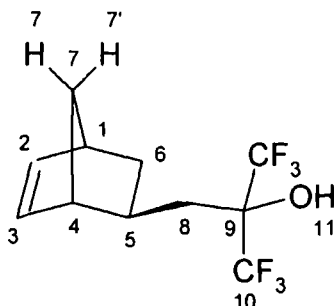


Figure 3.19. Assignment of C and H atoms in X- NB-CH₂C(CF₃)₂OH.

3.4.4.12 Characterisation of the *endo*-Regioisomer in *endo/exo*-Bis(trifluoromethyl)-2-norbornene-5-ethanol

The monomer was characterised by ¹H NMR, ¹³C NMR, GCMS and IR. The numbering system shown in figure 3.20 was used for the assignment of the peaks in the NMR spectra.

¹H NMR (500 MHz, CDCl₃): δ (ppm) = 6.23 (dd, 1H, *J* = 5.72 & 3.04, H), 5.99 (dd, 1H, *J* = 5.72 & 2.86, H), 2.93 (bs, 1H, -OH), 2.82 (bs, 1H, H₄), 2.80 (bs, 1H, H₁), 2.38 (bs, 1H, H₅), 2.03 (ddd, 1H, *J* = 11.66 & 8.99 & 3.92, H₇), 1.87 (dd, 1H, *J* = 15.30 & 6.48, H₈), 1.70 (dd, 1H, *J* = 15.30 & 7.29, H₈), 1.46 (m, 1H, *J* = 8.35, H₆), 1.29 (m, 1H, *J* = 8.35, H₆), 0.67 (ddd, 1H, *J* = 11.66 & 4.19 & 2.80, H₇).

¹³C NMR (125.7 MHz, CDCl₃): δ (ppm) = 138.50 (C₂), 132.28 (C₃), 123.51 (q, *J* = 286.29, C₁₀), 77.06 (septet, *J* = 28.78, C₉), 49.82 (C₆), 47.32 (C₄), 42.83 (C₁), 34.89 (C₈), 34.16 (C₇), 32.60 (C₅).

GCMS (EI⁺): RT = 9.67, N-NBCH₂C(CF₃)₂OH (80%), 274.0 (C₁₁H₁₂OF₆, M⁺).

IR (KBr disc, cm⁻¹): 3100-3650 (O-H), 3080 (olefinic C-H stretching), 2980-2867 (saturated C-H stretching).

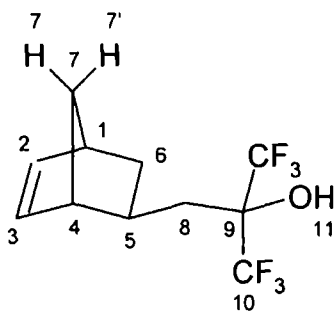


Figure 3.20. Assignment of C and H atoms in N/X- NB-CH₂C(CF₃)₂OH.

3.4.4.13 Characterisation of the *endo*-Regioisomer in *endo/exo*-Bis(trifluoromethyl)-2-norbornene-5-propanol

The monomer was characterised by ¹H NMR, ¹³C NMR, GCMS and IR. The numbering system shown in figure 3.21 was used for the assignment of the peaks in the NMR spectra.

¹H NMR (500 MHz, CDCl₃): δ (ppm) = 6.17 (dd, 1H, *J* = 5.68 & 3.03, H₂), 5.94 (dd, 1H, *J* = 5.68 & 2.89, H₃), 3.18 (bs, 1H, -OH), 2.81 (m, 2H, H_{1&4}), 2.03-1.87 (m, 2H, H₉), 1.95 (m, 1H, H₅), 1.90 (m, 1H, H₇), 1.45 (m, 1H, *J* = 8.29, H₆), 1.32 (m, 2H, H₈), 1.25 (m, 1H, H₆), 0.54 (ddd, 1H, *J* = 11.12 & 3.88 & 2.71, H₇).

¹³C NMR (125.7 MHz, CDCl₃): δ (ppm) = 137.95 (C₂), 132.05 (C₃), 123.48 (q, *J* = 286.29, C₁₁), 76.49 (septet, *J* = 28.78, C₁₀), 49.83 (C₆), 45.39 (C₄), 42.78 (C₁), 39.27 (C₅), 32.53 (C₇), 29.75 (C₉), 26.91 (C₈).

GCMS (EI⁺): RT = 11.33, N-NB(CH₂)₂C(CF₃)₂OH (80%), 288.0 (C₁₂H₁₄OF₆, M⁺).

IR (KBr disc, cm⁻¹): 3100-3650 (O-H), 3080 (olefinic C-H stretching), 2980-2867 (saturated C-H stretching).

3.4.4.14 Characterisation of the *exo*-Regioisomer in *endo/exo*-Bis(trifluoromethyl)-2-norbornene-5-propanol

The monomer was characterised by ^1H NMR, ^{13}C NMR, GCMS and IR. The numbering system shown in figure 3.21 was used for the assignment of the peaks in the NMR spectra.

^1H NMR (500 MHz, CDCl_3): δ (ppm) = 6.10 (dd, 1H, $J = 5.60$ & 2.99 , H_2), 6.06 (dd, 1H, $J = 5.60$ & 2.88 , H_3), 3.28 (bs, 1H, -OH), 2.84 (m, 1H, H_1), 2.56 (bs, 1H, H_4), 1.98 (m, 2H, H_9), 1.62 (m, 2H, H_8), 1.37 (m, 2H, H_6), 1.33 (m, 1H, H_7), 1.30 (m, 1H, H_5), 1.12 (m, 1H, $J = 10.65$, H_7).

^{13}C NMR (125.7 MHz, CDCl_3): δ (ppm) = 136.87 (C_2), 136.82 (C_3), 123.48 (q, $J = 286.29$, C_{11}), 76.53 (septet, $J = 28.78$, C_{10}), 46.52 (C_4), 45.51 (C_6), 42.15 (C_1), 39.44 (C_5), 33.21 (C_7), 30.02 (C_9), 28.60 (C_8).

GCMS (EI^+): RT = 11.36, X-NB(CH_2) $_2$ C(CF_3) $_2$ OH (20%), 288.0 ($\text{C}_{12}\text{H}_{14}\text{OF}_6$, M^+).

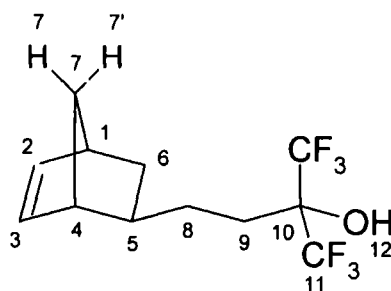


Figure 3.21. Assignment of C and H atoms in N/X- NB-(CH_2) $_2$ C(CF_3) $_2$ OH.

3.4.4.15 Characterisation of *exo*-5-Trimethylsilyl Carboxylate-2-norbornene

The monomer was characterised by ^1H NMR, ^{13}C NMR, GCMS and IR. The numbering system shown in figure 3.22 was used for the assignment of the peaks in the NMR spectra.

^1H NMR (500 MHz, CDCl_3): δ (ppm) = 6.11 (m, 2H, $\text{H}_{2\&3}$), 3.03 (m, 1H, $\text{H}_{1\&4}$), 2.89 (m, 1H, $\text{H}_{1\&4}$), 2.20 (m, 1H, H_5), 1.88 (m, 1H, $J = 11.78$, H_7), 1.47 (m, 1H, $J = 8.22$, H_6), 1.38-1.30 (m, 2H, $\text{H}_{6\&7'}$), 0.28 (s, 9H, H_9).

^{13}C NMR (125.7 MHz, CDCl_3): δ (ppm) = 177.09 (C_8), 138.21 (C_2), 136.05 (C_3), 46.83 (C_4), 46.56 (C_6), 44.99 (C_5), 41.90 (C_1), 30.62 (C_7), 0.04 (C_9).

GCMS (EI^+): RT = 12.39, X-NB- CO_2TMS , 210.0 ($\text{C}_{11}\text{H}_{18}\text{O}_2\text{Si}$, M^+).

IR (KBr disc, cm^{-1}): 3080 (olefinic C-H stretching), 2980-2867 (saturated C-H stretching), 1736 (asymmetric and symmetric C=O stretching).

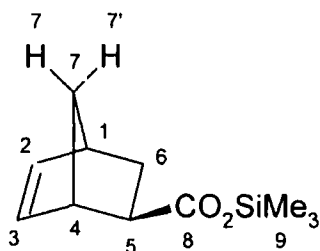


Figure 3.22. Assignment of C and H atoms in X-NB- CO_2TMS .

3.4.4.16 Characterisation of *endo*-5-Trimethylsilyl Carboxylate-2-norbornene

The monomer was characterised by ^1H NMR, ^{13}C NMR, GCMS and IR. The numbering system shown in figure 3.23 was used for the assignment of the peaks in the NMR spectra.

^1H NMR (500 MHz, CDCl_3): δ (ppm) = 6.19 (dd, 1H, $J = 3.01$ & 5.62 , H_2), 5.91 (dd, 1H, $J = 2.82$ & 5.62 , H_3), 3.18 (m, 1H, H_4), 2.93 (m, 1H, $J = 9.22$ & 3.94 , H_5), 2.88 (m, 1H, H_1), 1.86 (ddd, 1H, $J = 11.63$ & 9.21 & 3.74 , H_7), 1.44-1.34 (m, 2H, $\text{H}_{6\&7'}$), 1.26 (m, 1H, $J = 8.10$, H_6), 0.24 (s, 9H, H_9).

^{13}C NMR (125.7 MHz, CDCl_3): δ (ppm) = 175.63 (C_8), 138.04 (C_2), 132.37 (C_3), 49.95 (C_6), 46.12 (C_4), 44.98 (C_5), 42.91 (C_1), 29.32 (C_7), 0.00 (C_9).

GCMS (EI⁺): RT = 12.36, N-NB-CO₂TMS, 210.0 (C₁₁H₁₈O₂Si, M⁺).

IR (KBr disc, cm⁻¹): 3080 (olefinic C-H stretching), 2980-2867 (saturated C-H stretching), 1736 (asymmetric and symmetric C=O stretching).

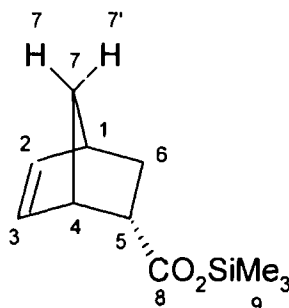


Figure 3.23. Assignment of C and H atoms in N-NB-CO₂TMS.

3.4.4.17 Characterisation of *endo/exo*-5-Methyl Trimethylsilyl Carboxylate-2-norbornene

The monomer was characterised by ¹H NMR, ¹³C NMR, GCMS and IR. The numbering system shown in figure 3.24 was used for the assignment of the peaks in the NMR spectra.

¹H NMR (500 MHz, CDCl₃): δ (ppm) = 6.15 (dd, 0.85H, *J* = 5.69 & 3.01, H_{2,N}), 6.10 (dd, 0.15H, *J* = 5.64 & 3.03, H_{2,X}), 6.03 (dd, 0.15H, *J* = 5.72 & 2.85, H_{3,X}), 5.92 (dd, 0.85H, *J* = 5.73 & 2.90, H_{3,N}), 2.80 (m, 1H), 2.76 (m, 0.85H, H_N), 2.50-1.70 (m, 4.15H), 1.45-1.10 (m, 2H), 0.55 (ddd, 0.85H, *J* = 11.70 & 4.33 & 2.64, H_{7,N}), 0.26 (s, 9H, H₁₀).

¹³C NMR (125.7 MHz, CDCl₃): δ (ppm) = 174.35 (C_{9,N}), 174.13 (C_{9,X}), 137.86 (C_{2,N}), 136.66 (C_{2,X}), 132.43 (C_{3,N}), 49.78 (C_N), 46.52 (C_X), 45.86 (C_N), 45.27 (C_X), 42.77 (C_N), 42.72 (C_X), 42.26 (C_X), 41.24 (C_N), 35.18 (C_N), 35.10 (C_X), 32.73 (C_X), 32.22 (C_N), 0.00 (C₁₀).

GCMS (EI⁺): RT = 13.78, N/X-NB-CH₂CO₂TMS (100%), 224.0 (C₁₂H₂₀O₂Si, M⁺).

IR (KBr disc, cm⁻¹): 3080 (olefinic C-H stretching), 2980-2867 (saturated C-H stretching), 1736 (asymmetric and symmetric C=O stretching).

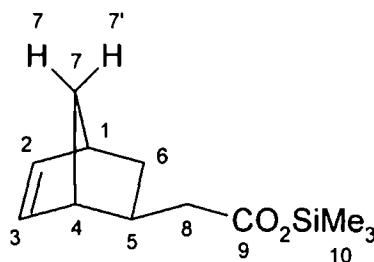


Figure 3.24. Assignment of C and H atoms in N/X-NB-CH₂CO₂TMS.

3.4.4.18 Characterisation of *endo/exo*-5-Ethyl Trimethylsilyl Carboxylate-2-norbornene

The monomer was characterised by ¹H NMR, ¹³C NMR, GCMS and IR. The numbering system shown in figure 3.25 was used for the assignment of the peaks in the NMR spectra.

¹H NMR (500 MHz, CDCl₃): δ (ppm) = 6.12 (dd, 0.81H, *J* = 5.77 & 3.21, H_{2,N}), 6.07 (dd, 0.19H, *J* = 5.74 & 3.03, H_{2,X}), 6.01 (dd, 0.19H, *J* = 5.68 & 2.90, H_{3,X}), 5.92 (dd, 0.81H, *J* = 5.49 & 2.78, H_{3,N}), 2.78 (m, 1.81H), 2.52 (m, 0.19H, H_X), 2.35 (t, 0.38H, H_{9,X}), 2.28 (t, 1.62H, H_{9,N}), 2.04-1.06 (m, 6.19H), 0.50 (ddd, 0.81H, *J* = 11.24 & 4.26 & 2.60, H_{7,N}), 0.27 (s, 9H, H₁₁).

¹³C NMR (125.7 MHz, CDCl₃): δ (ppm) = 174.80 (C_{10,N}), 174.74 (C_{10,X}), 137.49 (C_{2,N}), 136.92 (C_{2,X}), 136.66 (C_{3,X}), 132.35 (C_{3,N}), 49.80 (C_N), 46.33 (C_X), 45.46 (C_N), 45.39 (C_X), 42.74 (C_N), 42.08 (C_X), 38.60 (C_X), 38.50 (C_N), 35.5 (C_X), 35.30 (C_N), 33.06 (C_X), 32.37 (C_N), 31.77 (C_N), 30.09 (C_X), 0.00 (C₁₁).

GCMS (EI⁺): RT = 15.21, N-NBCH₂CH₂CO₂TMS (80%), 238.0 (C₁₃H₂₂O₂Si, M⁺); 15.25, X-NBCH₂CH₂CO₂TMS (20%), 238.0 (C₁₃H₂₂O₂Si, M⁺).

IR (KBr disc, cm⁻¹): 3080 (olefinic C-H stretching), 2980-2867 (saturated C-H stretching), 1736 (asymmetric and symmetric C=O stretching).

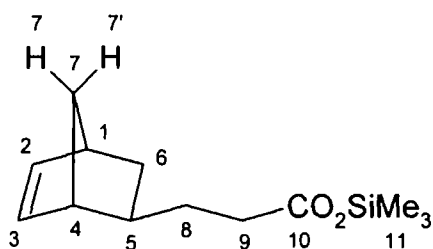


Figure 3.25. Assignment of C and H atoms in N/X-NB-(CH₂)₂CO₂TMS.

3.4.4.19 Characterisation of *endo*-N-(2-norbornene-5-methyl)-1,1,1-trifluoromethanesulfonamide

The monomer was characterised by ¹H NMR, ¹³C NMR, GCMS and IR. The numbering system shown in figure 3.26 was used for the assignment of the peaks in the NMR spectra.

¹H NMR (500 MHz, CDCl₃): δ (ppm) = 6.22 (dd, 1H, *J* = 5.67 & 3.10, H₂), 5.97 (dd, 1H, *J* = 5.67 & 2.88, H₃), 5.29 (m, 1H, NH), 3.07 (m, 1H, H₈), 2.96 (m, 1H, H₈), 2.86 (m, 1H, H₄), 2.91 (m, 1H, H₁), 2.31 (m, 1H, H₅), 1.90 (ddd, 1H, *J* = 11.70 & 9.10 & 3.81, H₇) 1.51 (m, 1H, *J* = 8.36, H₆), 1.30 (m, 1H, *J* = 8.36, H₆), 0.57 (ddd, 1H, *J* = 11.70 & 4.26 & 2.73, H₇).

¹³C NMR (125.7 MHz, CDCl₃): δ (ppm) = 138.72 (C₂), 131.63 (C₃), 119.94 (q, *J* = 321.20, (C₉), 49.81 (C₆), 48.56 (C₈), 44.08 (C₄), 42.66 (C₁), 39.70 (C₅), 30.06 (C₇).

GCMS (EI⁺): RT = 14.71, N-NBCH₂NHSO₂CF₃, 255.0 (C₁₀H₁₄NO₂F₃, M⁺).

IR (KBr disc, cm⁻¹): 3300, 3080 (olefinic C-H stretching), 2980-2867 (saturated C-H stretching).

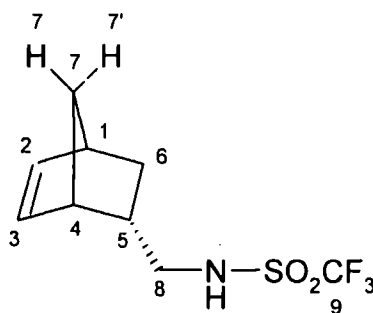


Figure 3.26. Assignment of C and H atoms in N-NBCH₂NHSO₂CF₃.

3.4.4.20 Characterisation of *exo*-N-(2-norbornene-5-methyl)-1,1,1-trifluoromethanesulfonamide

The monomer was characterised by ^1H NMR, ^{13}C NMR, GCMS and IR. The numbering system shown in figure 3.27 was used for the assignment of the peaks in the NMR spectra.

^1H NMR (500 MHz, CDCl_3): δ (ppm) = 6.11 (m, 2H, $\text{H}_{2\&3}$), 5.37 (m, 1H, NH), 3.35 (m, 1H, H_8), 3.26 (m, 1H, H_8), 2.88 (m, 1H, H_1), 2.69 (m, 1H, H_4), 1.41 (m, 1H, H_5), 1.35 (ddd, 1H, $J = 11.74 \& 8.30 \& 2.36$, H_7) 1.29 (m, 1H, $J = 8.86$, H_6), 1.30 (m, 1H, $J = 8.86$, H_6), 0.57 (ddd, 1H, $J = 11.74 \& 3.86 \& 3.74$, H_7).

^{13}C NMR (125.7 MHz, CDCl_3): δ (ppm) = 137.44 (C_2), 136.16 (C_3), 119.95 (q, $J = 321.20$ (C_9), 49.72 (C_8), 45.11 (C_6), 44.10 (C_4), 41.97 (C_1), 39.83 (C_5), 30.90 (C_7).

GCMS (EI^+): RT = 14.62, X-NBCH₂NHSO₂CF₃, 255.0 ($\text{C}_{10}\text{H}_{14}\text{NO}_2\text{F}_3$, M^+).

IR (KBr disc, cm^{-1}): 3300, 3080 (olefinic C-H stretching), 2980-2867 (saturated C-H stretching).

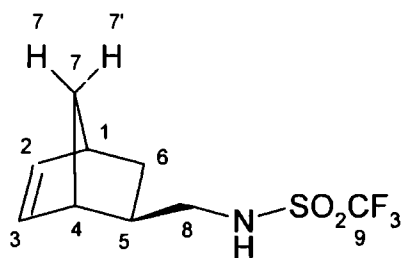


Figure 3.27. Assignment of C and H atoms in X-NBCH₂NHSO₂CF₃.

3.4.4.21 Characterisation of *endo/exo*-N-(2-norbornene-5-ethyl)-1,1,1-trifluoromethanesulfonamide

The monomer was characterised by ^1H NMR, ^{13}C NMR, GCMS and IR. The numbering system shown in figure 3.28 was used for the assignment of the peaks in the NMR spectra.

^1H NMR (500 MHz, CDCl_3): δ (ppm) = 6.17 (dd, 0.85H, $J = 5.70$ & 3.04 , $\text{H}_{2,\text{N}}$), 6.09 (dd, 0.15H, $J = 5.67$ & 3.03 , $\text{H}_{2\&3,\text{X}}$), 6.05 (dd, 0.15H, $J = 5.67$ & 2.92 , $\text{H}_{2\&3,\text{X}}$), 5.93 (dd, 0.85H, $J = 5.70$ & 2.84 , $\text{H}_{3,\text{N}}$), 5.26 (m, 0.15H, NH_X), 5.21 (m, 0.85H, NH_N), 3.34 (m, 0.30H, $\text{H}_{9,\text{X}}$), 3.27 (m, 1.70H, $\text{H}_{9,\text{N}}$), 2.84 (m, 0.15H, $\text{H}_{1\&4,\text{X}}$), 2.80 (m, 0.85H, $\text{H}_{1,\text{N}}$), 2.79 (m, 0.85H, $\text{H}_{4,\text{N}}$), 2.54 (m, 0.15H, $\text{H}_{1\&4,\text{X}}$), 2.05 (m, 1H, H_5), 1.90 (ddd, 0.85H, $J = 11.35$ & 0.08 & 3.91 , $\text{H}_{7,\text{N}}$), 1.69 (m, 0.30H, $\text{H}_{8,\text{X}}$), 1.50 (m, 1H, H_6), 1.40 (m, 1.70H, $\text{H}_{8,\text{N}}$), 1.35 (m, 1H, H_6), 1.34 (m, 0.15H, $\text{H}_{7,\text{X}}$), 1.25 (d, 1H, $J = 8.25$, H), 1.12 (m, 0.15H, $\text{H}_{7',\text{X}}$), 0.57 (ddd, 0.85H, $J = 11.35$ & 4.21 & 2.69 , $\text{H}_{7',\text{N}}$).

^{13}C NMR (125.7 MHz, CDCl_3): δ (ppm) = 138.00 ($\text{C}_{2,\text{N}}$), 136.76 ($\text{C}_{2\&3,\text{X}}$), 136.65 ($\text{C}_{2\&3,\text{X}}$), 131.99 ($\text{C}_{3,\text{N}}$), 119.90 (q, $J = 321.20$, C_{10}), 49.81 (C_6), 46.37 ($\text{C}_{1\&4,\text{X}}$), 45.44 ($\text{C}_{1\&4,\text{N}}$), 44.03 ($\text{C}_{9,\text{X}}$), 43.97 ($\text{C}_{9,\text{N}}$), 42.70 ($\text{C}_{1\&4,\text{N}}$), 42.14 ($\text{C}_{1\&4,\text{X}}$), 37.04 ($\text{C}_{8,\text{X}}$), 35.81 ($\text{C}_{5,\text{X}}$), 35.77 ($\text{C}_{5,\text{N}}$), 35.36 (C_8), 32.90 ($\text{C}_{7,\text{X}}$), 32.16 ($\text{C}_{7,\text{N}}$).

GCMS (EI^+): RT = 16.06, N-NBCH₂CH₂NHSO₂CF₃ (86%), 269.0 ($\text{C}_{10}\text{H}_{14}\text{NO}_2\text{F}_3$, M^+); 16.12, X-NBCH₂CH₂NHSO₂CF₃ (14%), 269.0 ($\text{C}_{10}\text{H}_{14}\text{NO}_2\text{F}_3$, M^+).

IR (KBr disc, cm^{-1}): 3300, 3080 (olefinic C-H stretching), 2980-2867 (saturated C-H stretching).

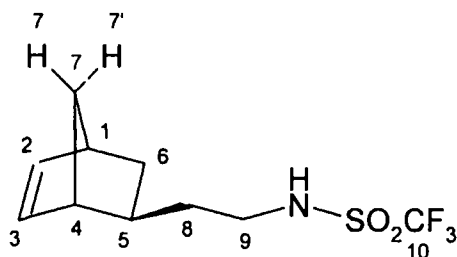


Figure 3.28. Assignment of C and H atoms in N/X-NB(CH₂)₂NHSO₂CF₃.

3.4.4.22 Characterisation of *endo/exo*-N-(2-norbornene-5-propyl)-1,1,1-trifluoromethanesulfonamide

The monomer was characterised by ^1H NMR, ^{13}C NMR, GCMS and IR. The numbering system shown in figure 3.29 was used for the assignment of the peaks in the NMR spectra.

^1H NMR (500 MHz, CDCl_3): δ (ppm) = 6.14 (dd, 0.85H, $J = 5.65$ & 2.98 , $\text{H}_{2,\text{N}}$), 6.09 (dd, 0.15H, $J = 5.65$ & 3.05 , $\text{H}_{2\&3,\text{X}}$), 6.04 (dd, 0.15H, $J = 5.65$ & 2.98 , $\text{H}_{2\&3,\text{X}}$), 5.91 (dd, 0.85H, $J = 5.65$ & 2.86 , $\text{H}_{3,\text{N}}$), 5.24 (m, 0.15H, NH_X), 5.19 (m, 0.85H, NH_N), 3.28 (m, 2H, H_{10}), 2.82 (m, 0.15H, $\text{H}_{1\&4,\text{X}}$), 2.77 (m, 1.70H, $\text{H}_{1\&4,\text{N}}$), 2.53 (m, 0.15H, $\text{H}_{1\&4,\text{X}}$), 1.99 (m, 0.85H, $\text{H}_{5,\text{N}}$), 1.87 (m, 0.85H, $\text{H}_{7,\text{N}}$), 1.60 (m, 2H, H_{10}), 1.40 (m, 1H, H_6), 1.33 (m, 0.15H, $\text{H}_{7,\text{X}}$), 1.32 (m, 0.15H, $\text{H}_{5,\text{X}}$), 1.20 (m, 1H, H_6), 1.17 (m, 2H, H_9), 1.10 (m, 0.15H, $\text{H}_{7,\text{X}}$), 0.50 (ddd, 0.85H, $J = 11.35$ & 4.23 & 2.71 , $\text{H}_{7,\text{N}}$).

^{13}C NMR (125.7 MHz, CDCl_3): δ (ppm) = 137.68 ($\text{C}_{2,\text{N}}$), 136.90 ($\text{C}_{2\&3,\text{X}}$), 136.65 ($\text{C}_{2\&3,\text{X}}$), 132.19 ($\text{C}_{3,\text{N}}$), 119.90 (q, $J = 321.20$, C_{11}), 49.81 ($\text{C}_{6,\text{N}}$), 46.49 ($\text{C}_{1\&4,\text{X}}$), 45.53 ($\text{C}_{1\&4,\text{N}}$), 45.40 ($\text{C}_{6,\text{X}}$), 44.93 ($\text{C}_{8,\text{N}}$), 44.89 ($\text{C}_{8,\text{X}}$), 42.75 ($\text{C}_{1\&4,\text{N}}$), 42.09 ($\text{C}_{1\&4,\text{X}}$), 38.52 ($\text{C}_{5,\text{N}}$), 38.44 ($\text{C}_{5,\text{X}}$), 33.20 ($\text{C}_{10,\text{X}}$), 33.17 ($\text{C}_{7,\text{X}}$), 32.48 ($\text{C}_{7,\text{N}}$), 31.49 ($\text{C}_{10,\text{N}}$), 29.66 ($\text{C}_{9,\text{X}}$), 29.45 ($\text{C}_{9,\text{N}}$).

GCMS (EI^+): RT = 17.30, N-NBCH₂CH₂CH₂NHSO₂CF₃ (80%), 283.0 ($\text{C}_{11}\text{H}_{16}\text{NO}_2\text{F}_3$, M^+); 17.37, X-NBCH₂CH₂CH₂NHSO₂CF₃ (20%), 283.0 ($\text{C}_{11}\text{H}_{16}\text{NO}_2\text{F}_3$, M^+).

IR (KBr disc, cm^{-1}): 3300, 3080 (olefinic C-H stretching), 2980-2867 (saturated C-H stretching).

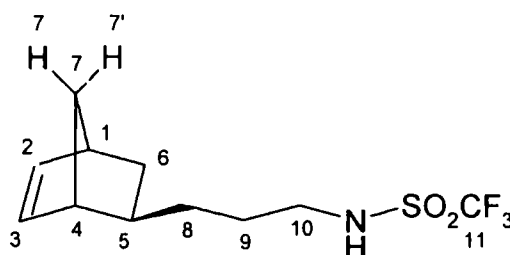


Figure 3.29. Assignment of C and H atoms in N/X-NB(CH₂)₃NHSO₂CF₃.

3.4.4.23 Characterisation of *endo/exo*-5-Trimethoxysilyl-2-norbornene

The monomer was characterised by ^1H NMR, ^{13}C NMR, GCMS and IR. The numbering system shown in figure 3.30 was used for the assignment of the peaks in the NMR spectra.

^1H NMR (500 MHz, CDCl_3): δ (ppm) = 6.11 (dd, 0.64H, $J = 5.56$ & 2.97 , $\text{H}_{2\&3,\text{N}}$), 6.03 (m, 0.72H, $\text{H}_{2\&3,\text{X}}$), 5.91 (dd, 0.64H, $J = 5.57$ & 2.98 , $\text{H}_{2\&3,\text{N}}$), 3.58 (s, 5.74H, $\text{H}_{8,\text{N}}$), 3.51 (s, 3.26H, $\text{H}_{8,\text{X}}$), 3.02 (m, 0.36H, H_X), 2.93 (m, 0.64H, H_N), 2.89 (m, 1H), 1.88 (ddd, 0.36H, $J = 11.10$ & 9.71 & 3.76 , H_X), 1.76 (ddd, 0.64H, $J = 11.36$ & 5.78 & 3.55 , H_N), 1.37 (m, 0.36H, $J = 7.85$, H_X), 1.30-1.04 (m, 3H), 0.50 (ddd, 0.64H, $J = 9.75$ & 5.76 & 1.91 , $\text{H}_{7,\text{N}}$).

^{13}C NMR (125.7 MHz, CDCl_3): δ (ppm) = 137.75 ($\text{C}_{2\&3,\text{N}}$), 135.71 ($\text{C}_{2\&3,\text{X}}$), 134.86 ($\text{C}_{2\&3,\text{X}}$), 133.95 ($\text{C}_{2\&3,\text{N}}$), 51.0 (C_X), 50.97, (C_N), 50.73 (C_X), 47.33 (C_N), 44.20 (C_X), 42.83 (C_N), 42.62 (C_N), 42.28 (C_X), 26.94 (C_X), 26.20 (C_N), 20.28 (C_X), 9.65 (C_N).

GCMS (EI^+): RT = 12.46, N/X-NB-Si(OMe) $_3$, 214.0 ($\text{C}_{10}\text{H}_{18}\text{SiO}_3$, M^+). N:X = 64:36.

IR (KBr disc, cm^{-1}): 3080 (olefinic C-H stretching), 2980-2867 (saturated C-H stretching), 712 (H-C=C).

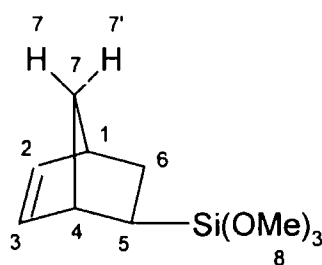


Figure 3.30. Assignment of C and H atoms in N/X-NBSi(OMe) $_3$.

3.4.4.24 Characterisation of *endo/exo*-5-Ethyl Trimethoxysilyl-2-norbornene

The monomer was characterised by ^1H NMR, ^{13}C NMR, GCMS and IR. The numbering system shown in figure 3.31 was used for the assignment of the peaks in the NMR spectra.

^1H NMR (500 MHz, CDCl_3): δ (ppm) = 6.09 (dd, 0.79H, $J = 5.68$ & 2.98 , $\text{H}_{2\&3,\text{N}}$), 6.06 (dd, 0.21H, $J = 5.64$ & 2.89 , $\text{H}_{2\&3,\text{X}}$), 6.00 (dd, 0.21H, $J = 5.64$ & 2.92 , $\text{H}_{2\&3,\text{X}}$), 5.89 (dd, 0.79H, $J = 5.65$ & 2.85 , $\text{H}_{2\&3,\text{N}}$), 3.56 (s, 1.89H, $\text{H}_{10,\text{X}}$), 3.54 (s, 7.11H, $\text{H}_{10,\text{N}}$), 2.76 (m, 1H), 2.72 (m, 0.79H, H_N), 2.52 (m, 0.21H, H_X), 1.93 (m, 0.79H, H_N), 1.81 (ddd, 0.79H, $J = 11.29$ & 9.01 & 3.92 , H_N), 1.51-1.00 (m, 4.21H), 0.75-0.55 (m, 2.42H), 0.47 (ddd, 0.79H, $J = 11.24$ & 4.21 & 2.65 , $\text{H}_{7,\text{N}}$).

^{13}C NMR (125.7 MHz, CDCl_3): δ (ppm) = 137.31 ($\text{C}_{2\&3,\text{N}}$), 137.05 ($\text{C}_{2\&3,\text{X}}$), 136.52 ($\text{C}_{2\&3,\text{X}}$), 132.36 ($\text{C}_{2\&3,\text{N}}$), 50.72 (C_{10}), 50.69 (C_{10}), 49.71 (C_{N}), 46.06 (C_{X}), 45.33 (C_{X}), 45.13 (C_{N}), 42.74 (C_{N}), 42.32 (C_{X}), 42.22 (C_{N}), 42.01 (C_{X}), 33.10 (C_{X}), 32.39 (C_{N}), 29.29 (C_{X}), 27.50 (C_{N}), 8.58 (C_{X}), 8.25 (C_{N}).

GCMS (EI^+): RT = 15.17, N-NB(CH_2) $_2$ Si(OMe) $_3$ (79%), 242.0 ($\text{C}_{12}\text{H}_{22}\text{SiO}_3$, M^+); 15.21, X-NB(CH_2) $_2$ Si(OMe) $_3$ (21%), 283.0 ($\text{C}_{11}\text{H}_{16}\text{NO}_2\text{F}_3$, M^+).

IR (KBr disc, cm^{-1}): 3080 (olefinic C-H stretching), 2980-2867 (saturated C-H stretching), 712 (H-C=C).

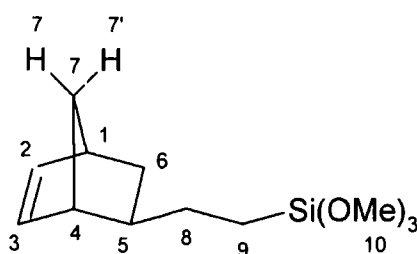


Figure 3.31. Assignment of C and H atoms in N/X-NB(CH_2) $_2$ Si(OMe) $_3$.

3.5 References

- ¹ Funk, J. K.; Andes, C. E.; Sen, A. *Organometallics* **2004**, *23*, 1680 - 1683.
- ² Bell, A.; Amoroso, D.; Protasiewicz, J. D.; Thirupathi, N. US 2005/0187398 A1.
- ³ Flory, P. J. "*Principles of Polymer Chemistry*", *Cornell University Press, Ithaca and London*, **1953**, 178 - 203.
- ³ (a) Dias, S.L.; Nguyen, S.T.; Grubbs, R.H. *JACS* **1997**, *119*, 3887. (b) Haigh, D.M.; Kenwright, A.M.; Khosravi, E. *Macromolecules* **2005**, *38*, 7571-7579. (c) Haigh, D.M.; Kenwright, A.M.; Khosravi, E. *Tetrahedron* **2004**, *60*, 7217-7224.
- ⁴ Funk, J. K.; Andes, C. E.; Sen, A. *Organometallics* **2004**, *23*, 1680 - 1683.

Chapter 4

Investigation of *exo*-Functionalised Norbornenes and Tetracyclododecenes

4.1 Introduction

Following on from the findings in Chapter 3, it is clear that new methods for the preparation of single regioisomers of functionalised norbornene monomers that display high polymerisation activity are necessary. It was also envisaged that in order to create co-polymers with excellent homogeneity, it would be useful for the polymerisation rates of the co-monomers to be normalised. This normalisation of polymerisation rates would only be possible through a reduction or masking of the electronic effect of norbornene functional groups. The convenient synthesis and ease of elaboration of *exo*-5-hydroxy-2-norbornene (X-NB-OH) makes this an excellent base from which to create new high activity monomers.

The alcohol can easily be converted into an acetate functionality, but these typically display high electron withdrawing properties and strong coordinating abilities, which would be expected to severely reduce polymerisation activity. The synthesis of single isomer acetate functionalised tetracyclododecenes from the corresponding functionalised norbornenes was expected to reduce these electronic effects by methylene spacing the functional group away from the vinyl group. These ideas were tested via the synthesis and polymerisation of a family of single regioisomer acetate functionalised norbornenes and tetracyclododecenes.

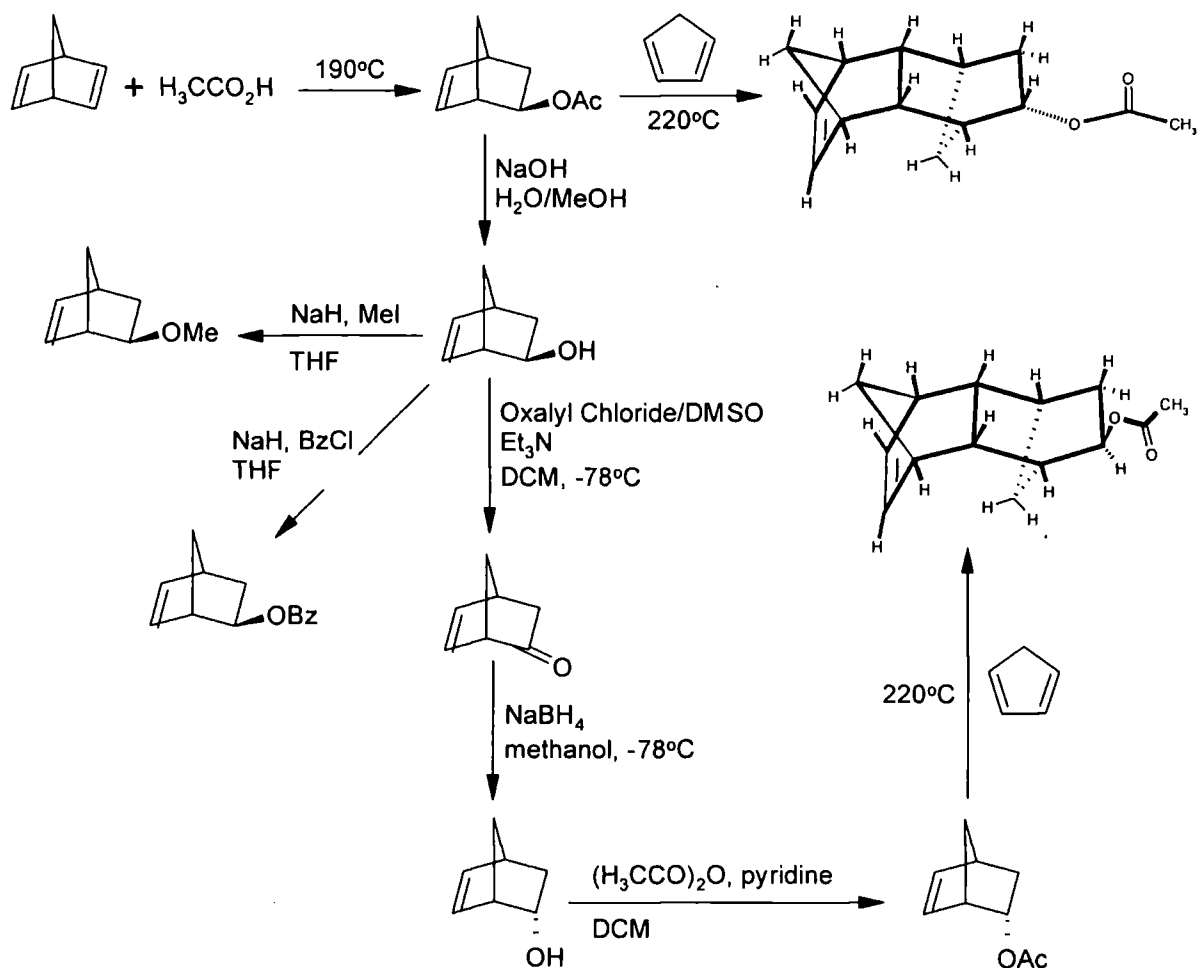
The alcohol can be converted into an ether functionality, which is believed to show high polymerisation activity due to ethers typically displaying only weak electron withdrawing properties and only mild coordinating ability. These ideas were tested via the synthesis and polymerisation of a family of single regioisomer ether functionalised norbornenes.

4.2 Results and Discussion

4.2.1 Synthesis and Characterisation of *exo*-5-Hydroxy-2-norbornene

The procedure used for the synthesis of *exo*-5-acetate-2-norbornene (X-NB-OAc), involves the reaction of acetic acid with an excess of norbornadiene at high temperature, to give the X-monoacetate, scheme 4.1, as a clear, colourless oil.¹ The reaction was shown by ¹³C NMR and GCMS to give a selectivity of > 98 % X-isomer. The selectivity of this reaction is quite amazing considering the absence of a catalyst. The reaction was first carried out on a trial basis using a Carius-tube reaction, with success and then on a much larger scale, using a 2L stainless steel reactor. It took three attempts using the reactor to produce the desired product, due to problems controlling the endotherm and exotherm generated during the course of the reaction. When the reaction loses control and gets too hot, due to the reaction generating an exotherm, the reagents polymerise. This problem was overcome by carefully monitoring the reaction temperature on an internal thermocouple and adjusting the heating accordingly.

The main purification problem encountered with this reaction is the formation of a C₁₂ impurity from the cycloaddition reaction between norbornadiene and cyclopentadiene at the temperatures needed for the high selectivity to be obtained. The impurity could not be removed from the desired product by distillation under reduced pressure, which was surprising considering the impurity's higher boiling point. The GCMS showed the impurity to account for ~ 2 % of the product after distillation. This impurity was not a major problem because it can be removed at a later stage down the synthesis tree, scheme 4.1.



Scheme 4.1

The saponification of the *exo*-5-acetate-2-norbornene (X-NB-OAc) with aqueous sodium hydroxide, followed by the standard work-up, affords the *exo*-5-hydroxy-2-norbornene (X-NB-OH) in high yield (90 %), as soft, white crystals. The isomeric purity of the product is unchanged by the reaction (98 % X). The C₁₂ impurity is also still present in the alcohol but can be removed via recrystallisation from a minimum amount of hexanes. Care has to be taken when drying and storing the X-NB-OH since it readily sublimes. Many attempts were made to grow single crystals for X-ray diffraction analysis via sublimation, but no crystals of high enough quality could be produced.

The cheap cost of the reagents, high selectivity and excellent yields of product generated in this reaction make it a good way to produce an X-functionalised norbornene monomer.

4.2.2 Synthesis and Characterisation of *endo*-5-Hydroxy-2-norbornene

The oxidation of *exo*-5-hydroxy-2-norbornene (X-NB-OH) using CrO₃ and pyridine in dichloromethane proved to be a very dirty, time consuming, low yielding reaction.² Therefore the alternative method utilising oxalyl chloride was used, since this method provided the desired 2-norbornene-5-one (NB=O) in high yield and purity,³ scheme 4.1.

The reduction of NB=O using Lithium tri-*sec*-butylborohydride solution (L-Selectride) proved to be a very unpredictable reaction, with a great range in purity and yield obtained, although it did provide the desired *endo*-5-Hydroxy-2-norbornene (N-NB-OH) with > 99:1 N/X selectivity.² The reduction of NB=O using sodium borohydride (NaBH₄) proved to be a more convenient route,⁴ since it gave the desired N-NB-OH in high yield and purity, with a > 99:1 N/X selectivity, scheme 4.1.

4.2.3 Derivatisation of *endo*- or *exo*-5-Hydroxy-2-norbornene

The reaction of X- or N-NB-OH with acetic anhydride, in the presence of base, produced the corresponding NB-OAc,² scheme 4.1. The products were purified using distillation under reduced pressure, to give clear, colourless oils, in excellent yields (> 85% yield). The GCMS of X-NB-OAc showed the product to have no impurities and consist of X- and N-isomers in a ratio of 98:2, respectively. The GCMS of N-NB-OAc showed the product to have no impurities and consist of X- and N-isomers in a ratio of 1:99, respectively.

The Williamson ether synthesis was used to prepare the *exo*-5-methoxy-2-norbornene (X-NB-OMe) in good yield (55%),⁵ scheme 4.1. The product was purified using distillation under reduced pressure to give a clear, colourless oil. The GCMS and NMR spectroscopic analyses of the purified X-NB-OMe, indicated the product to be a mixture of N- and X-isomers in a ratio of 1:99, respectively. An impurity (< 1%) was detected in the GCMS, which was of identical molecular mass (Mr = 124.1), similar fragmentation pattern, and similar retention time to the X-NB-OMe product. This impurity is likely to be an unknown rearrangement product.

The aromatic ethers X-NB-OCH₂Ph, X-NB-OCH₂C₆H₄Ph and X-NB-OCH₂C₆H₄Br were prepared from the reaction of the corresponding benzyl bromides and chlorides with X-NB-OH,² scheme 4.1, in good yield and purified via silica column chromatography, eluting with hexanes.

4.2.4 Characterisation of *endo*- and *exo*-5-Carboxylic Acid-2-norbornene

Promerus LLC kindly provided the samples of the pure regioisomers of *endo*-5-carboxylic acid-2-norbornene (N-NB-CO₂H) and *exo*-5-carboxylic acid-2-norbornene (X-NBCO₂H) for this work. The growth of single crystals of N-NB-CO₂H and X-NBCO₂H was unsuccessfully attempted using slow recrystallisation or evaporation from solvent systems based on hexanes, ethyl acetate, diethyl ether, dichloromethane, toluene, methanol and tetrahydrofuran.

Single crystals of X-NB-CO₂H and N-NBCO₂H were only successfully produced via their slow sublimation at ambient temperature and an X-ray structural diagram was produced using single-crystal X-ray diffraction, figures 4.1 and 4.2, respectively.

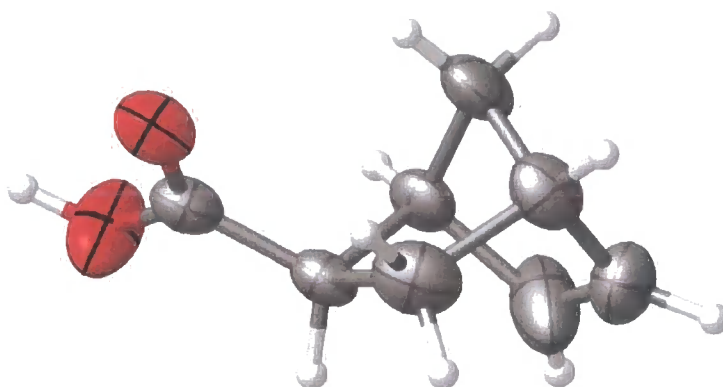


Figure 4.1. X-ray structural diagram of X-NB-CO₂H.

The analysis of N-NB-CO₂H gave full structural refinement, whilst that of X-NBCO₂H gave structural verification but without full refinement.

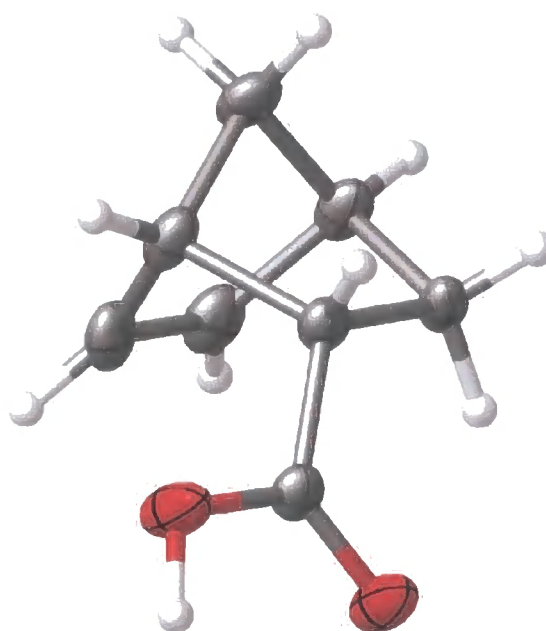
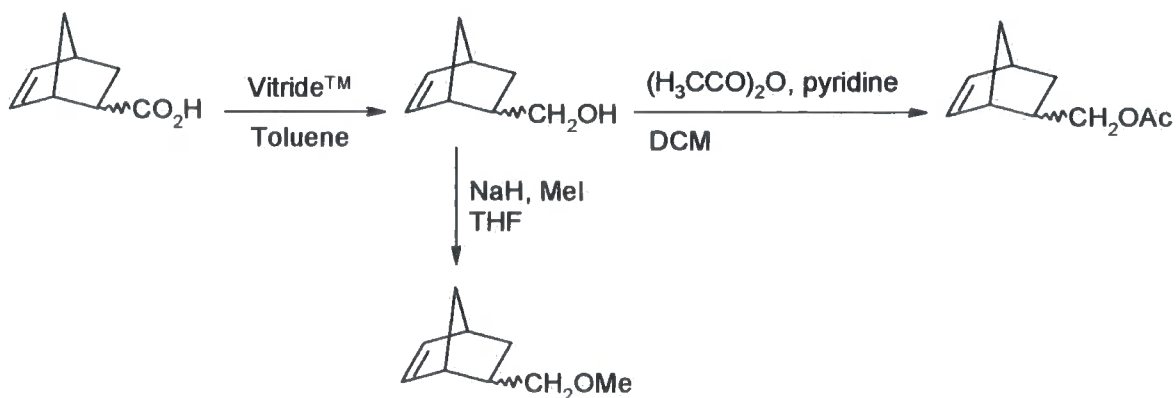


Figure 4.2. X-ray structural diagram of N-NB-CO₂H.

4.2.5 Synthesis and Derivatisation of *endo* and *exo*-5-Methyl Hydroxy-2-norbornene

The *endo* and *exo*-5-methyl hydroxy-2-norbornene (N- and X-NB-CH₂OH) were prepared from the reduction of the corresponding acids (kindly supplied by Promerus LLC) using sodium bis(2-methoxyethoxy)aluminum hydride (Vitride™), which is similar to LiAlH₄, scheme 4.2. The reactions proceeded very cleanly in high yield and further purification beyond standard work-up was not needed before further derivatisation.



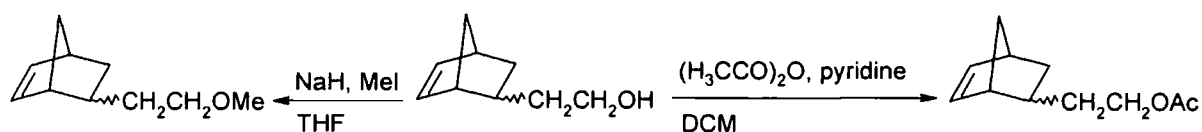
Scheme 4.2

The reaction of X- or N-NB-CH₂OH with acetic anhydride, in the presence of base, produced the corresponding *exo*- and *endo*-5-methyl acetate-2-norbornene (X- or N-NB-CH₂OAc), scheme 4.2. The products were purified using distillation under reduced pressure, to give clear, colourless oils, in excellent yields (> 85% yield). The GCMS of N-NBCH₂OAc showed the product to have no impurities and consist of 100% N-isomer. The GCMS of X-NBCH₂OAc showed the product to have no impurities and consist of 100% X-isomer.

The Williamson ether synthesis was used to prepare the *endo*- and *exo*-5-methyl methoxy-2-norbornene (N- or X-NB-CH₂OMe) in good yield (55%), scheme 4.2. The products were purified using distillation under reduced pressure to give clear, colourless oils. The GCMS and NMR spectroscopic analyses of the purified N- or X-NB-CH₂OMe, indicate the products to be 100% pure and of pure respective isomer.

4.2.6 Derivatisation of *endo/exo*-5-Ethyl Hydroxy-2-norbornene

The N/X- or X-NB(CH₂)₂OFG (FG = OAc, OMe) were prepared from the corresponding alcohols (kindly supplied by Promerus LLC) using standard methods, scheme 4.3. The monomers were purified using distillation under reduced pressure to give the respective products in high purity and yield. The GCMS of *endo/exo*-5-ethyl acetate-2-norbornene (N/X-NB(CH₂)₂OAc) showed the product to have no impurities and consist of N- and X-isomers in a ratio of 80:20, respectively. The GCMS of *endo/exo*-5-ethyl methoxy-2-norbornene (N/X-NB(CH₂)₂OMe) showed the product to have no impurities and consist of N- and X-isomers in a ratio of 80:20, respectively.



Scheme 4.3

4.2.7 Synthesis and Characterisation of *exo*-Tetracyclododecene Acetate

It is well known that Diels-Alder cycloadditions to the norbornene (bicyclo[2.2.1]heptenyl) fragment occur selectively at the *exo*-face.⁶ This is in stark contrast to the known propensity of cyclopentadiene to add to the double bond of bicyclo[2.2.2]-octenyl with profound *endo* selectivity.⁷

The Diels-Alder cycloaddition reaction of a two-fold excess of X-NB-OAc, with cyclopentadiene at 222°C for 8 hours, afforded the new *exo*-tetracyclododecene acetate (X-TD-OAc) product and other higher molecular weight materials, scheme 4.1. The excess X-NB-OAc can be recovered via distillation of the reaction mixture. The X-TD-OAc can be purified via distillation at 130°C under reduced pressure to give a > 50% yield of a white semi-solid. A soft clear crystal of X-TD-OAc was produced using a solution of (X-TD-OAc: hexanes = 95: 5, W/W %, respectively). Crystallisation occurred at -10°C over 4 weeks. X-ray diffraction analysis of the crystal provided a structure with full refinement, figure 4.3.

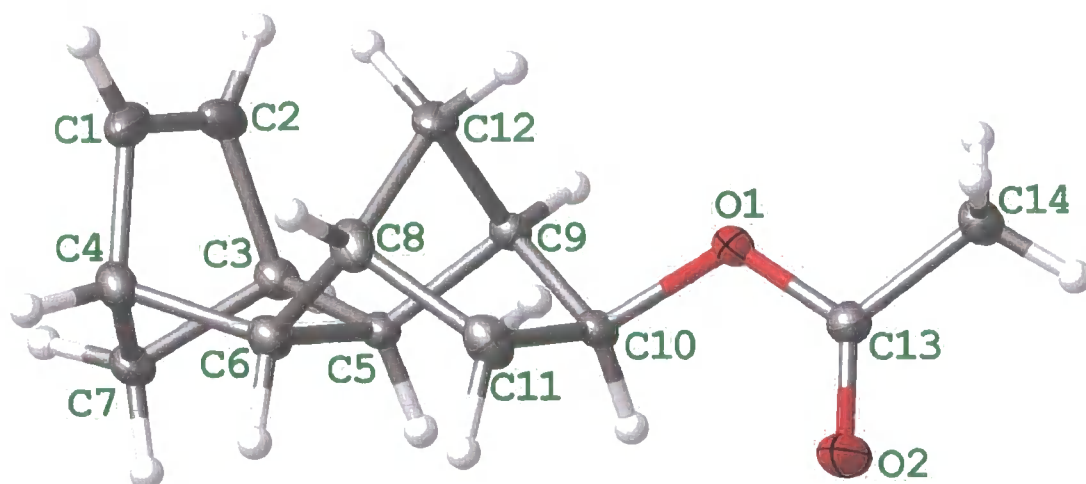


Figure 4.3. X-ray structural diagram of X-TD-OAc.

The structure of the X-TD-OAc was elucidated using the evidence from ¹H, ¹³C, HSQC, HMBC, COSY and NOESY NMR spectroscopy.

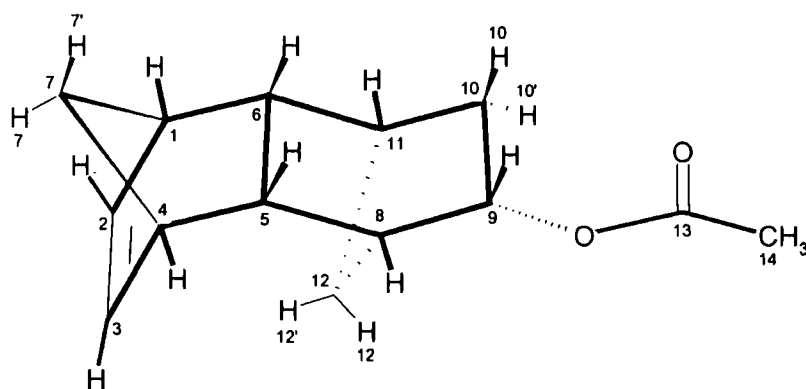


Figure 4.4. Structure and numbering system used for the characterisation of X-TD-OAc by NMR spectroscopy.

The 2D-NMR spectroscopic evidence was particularly useful; since the combination of correlations described below could only be ascribed to the structure of X-TD-OAc, figure 4.4. The NOESY (what the atoms see in space) shows positive correlations between: H_{2&3} and H₇, H_{2&3} and H_{1&4}, H_{2&3} and H_{12'}, H_{7'} and H_{5&6}, H_{5&6} and H₉, H_{5&6} and H₁₀, H₉ and H₁₀, H_{1&4} and H_{11&8}, H₁₂ and H_{10'}.

The HMBC (looking for 3-bond Z couplings) shows positive correlations between: C_{2&3} and H₇, C_{2&3} and H_{5&6}, C_{1&4} and H_{2&3}, C_{5&6} and H₁₂, C_{5&6} and H₇, C_{5&6} and H_{11&8}, C_{11&8} and H_{5&6}, C₁₁ and H₈, C₁₂ and H₁₀, C₁₂ and H₉, C₉ and H_{12'}, C₁₀ and H_{12'}.

The COSY (looking at 4-bond W couplings) shows positive correlations between: H_{2&3} and H_{1&4}, H_{2&3} and H_{5&6}, H_{2&3} and H₇, H_{4&1} and H_{5&6}, H₁₁ and H₈, H₁₀ and H_{12'}, H₉ and H_{12'}. Also H₁₂ does not couple strongly to anything.

4.2.8 Synthesis and Characterisation of *endo*-Tetracyclododecene Acetate

The Diels-Alder cycloaddition reaction of a two-fold excess of N-NB-OAc, with cyclopentadiene at 222°C for 8 hours, afforded the expected *endo*-tetracyclododecene acetate (N-TD-OAc) product and other higher molecular weight materials, scheme 4.1. The excess N-NB-OAc can be recovered via distillation of the reaction mixture. The N-TD-OAc can be purified via distillation at 130°C under reduced pressure to give a > 50% yield of a clear

colourless oil. The structure of the N-TD-OAc was confirmed using the evidence from the GCMS, ^1H , ^{13}C , HSQC, HMBC, COSY and NOESY NMR spectroscopy.

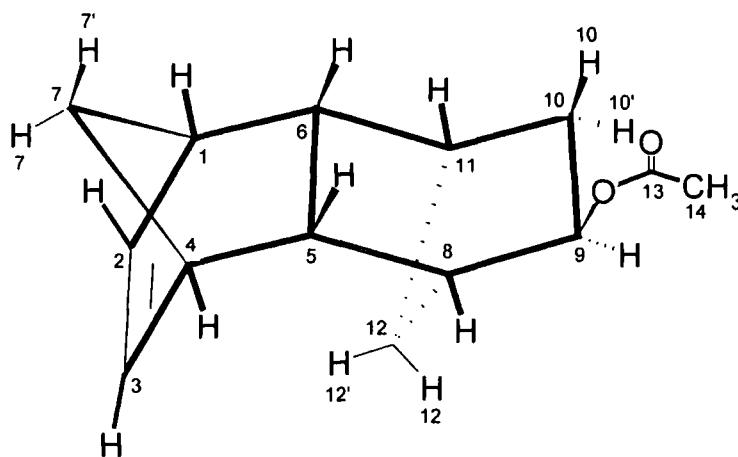


Figure 4.5. Structure and numbering system used for the characterisation of N-TD-OAc by NMR spectroscopy.

The 2D-NMR spectroscopic evidence was particularly useful; since the combination of correlations described below could only be ascribed to the structure of N-TD-OAc, figure 4.5. The NOESY (what the atoms see in space) shows positive correlations between: $\text{H}_{2\&3}$ and $\text{H}_{1\&4}$, $\text{H}_{2\&3}$ and $\text{H}_{12'}$, $\text{H}_{7'}$ and $\text{H}_{5\&6}$, $\text{H}_{5\&6}$ and $\text{H}_{7'}$, H_6 and H_{10} , H_9 and H_{12} , H_9 and $\text{H}_{10'}$, $\text{H}_{1\&4}$ and $\text{H}_{11\&8}$. $\text{H}_{5\&6}$ doesn't correlate to H_9 .

The HMBC (looking for 3-bond Z couplings) shows positive correlations between: $\text{C}_{2\&3}$ and $\text{H}_{5\&6}$, $\text{C}_{2\&3}$ and $\text{H}_{7'}$, $\text{C}_{1\&4}$ and $\text{H}_{2\&3}$, $\text{C}_{5\&6}$ and H_{12} , C_6 and $\text{H}_{10'}$, C_6 and H_{12} , $\text{C}_{5\&6}$ and $\text{H}_{7'}$, $\text{C}_{5\&6}$ and $\text{H}_{11\&8}$, $\text{C}_{11\&8}$ and $\text{H}_{5\&6}$, C_{11} and H_8 , C_{12} and $\text{H}_{5\&6}$, C_5 and H_9 .

The COSY (looking at 4-bond W couplings) shows positive correlations between: $\text{H}_{2\&3}$ and $\text{H}_{1\&4}$, $\text{H}_{4\&1}$ and $\text{H}_{5\&6}$, H_{11} and H_8 , H_{10} and $\text{H}_{12'}$, H_9 and H_{12} , H_9 and $\text{H}_{10'}$.

4.2.9 Polymerisation of *exo*- and *endo*-5-Acetate-2-norbornene

The polymerisation of the X-NB-OAc (X:N, 98:2, respectively) gave a peculiar result, with the polymerisation rate decreasing rapidly, with complete termination of the polymerisation

reaction at approximately 3% monomer consumption, green trend line in figure 4.6. The lack of a **Pd1388** initiator (Pd-H) signal in the ^1H NMR spectrum at the end of the polymerisation reaction, lead to the possibility that the small N-isomer content could be inserting into the Pd-H bond and deactivating the initiator via chelation of the acetate carbonyl, to palladium. This would require the unfavourable insertion through the *endo* face of norbornene to give a 7-membered chelate ring. Although a 7-membered chelate ring would be a rarity, many similar 6-membered chelate rings are described in the literature.⁸ There were no easily visible, new, unexpected signals generated in the ^1H NMR spectra during the polymerisation reaction.

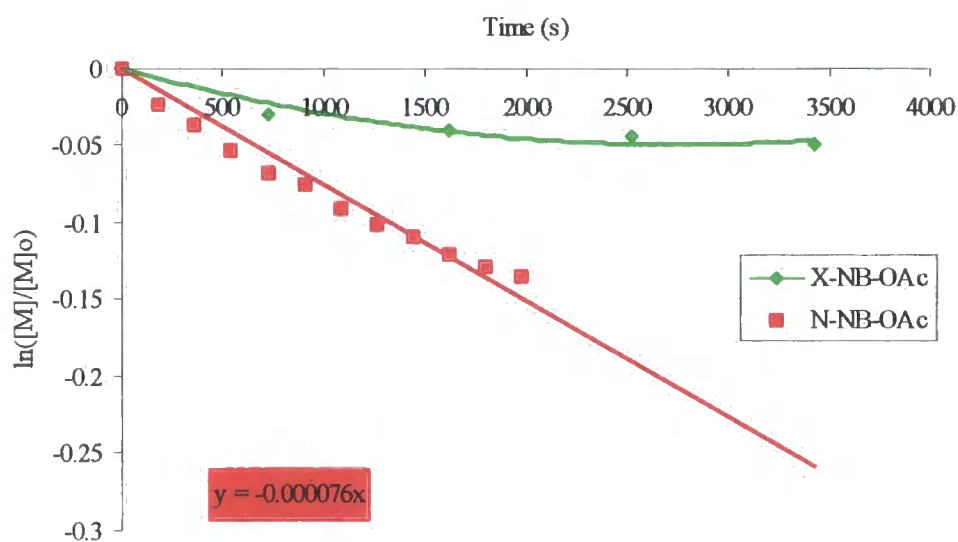


Figure 4.6. Polymerisation of N- and X-NB-OAc at 50°C in TCE- d_2 (50 Monomer: 1 **Pd1388**).

To test this theory, N-NB-OAc was produced as previously described in section 4.2.3 and its polymerisation reaction attempted. Surprisingly the N-NB-OAc polymerised without showing any of the polymerisation termination displayed by its close relative, X-NB-OAc, red trend line in figure 4.6. Therefore, the formation of the stable 7-membered chelate ring must not be occurring.

This evidence leaves the unanswered question of what is happening during the polymerisation of X-NB-OAc that could lead to the premature termination of the polymerisation reaction.

4.2.10 Poly merisation of Acetate Functionalised Norbornenes (NB(CH₂)_nOAc)

The polymerisation rate of the NB(CH₂)_nOAc increases with an increase in methylene spacing as expected for an electron withdrawing group such as –OAc, table 4.1. It is notable that the rate of polymerisation of N/X-NB(CH₂)₂OAc, is the same as the rate for *endo/exo*-5-decyl-2-norbornene under identical polymerisation conditions. This suggests that the simple coordination of the –OAc functional group to the cationic palladium centre is not a major hindrance to polymerisation and that the deactivating electronic effect of the –OAc group is negligible beyond 2 methylene spacings.

Table 4.1. Polymerisation data for 50 NB-(CH₂)_nOAc: 1 Pd1388, at 70°C in benzene-*d*₆.

n	k _p (N) (s ⁻¹)	k _p (X) (s ⁻¹)	k _p (N/X) (s ⁻¹)	[k _p (X)] / [k _p (N)]
0	0.82 × 10 ⁻⁴	Termination	-	-
1	1.66 × 10 ⁻⁴	4.70 × 10 ⁻⁴	-	2.8
2	16.26 × 10 ⁻⁴	32.19 × 10 ⁻⁴	17.88 × 10 ⁻⁴	2.0

These results suggest that the TD-OAc monomers should have good polymerisation activity since the –OAc group will effectively be ethylene spaced and the coordination of the functional group does not seem to reduce polymerisation activity.

4.2.11 Poly merisation of *exo*- and *endo*-Tetracyclododecene Acetate

An examination of the structures of X- and N-TD-OAc suggest that the regio chemistry of the functional group should have a minimal effect upon the polymerisation rates, since it is sufficiently spaced away from the vinylic hydrogens to not cause unfavourable steric interactions as in N-functionalised norbornenes.

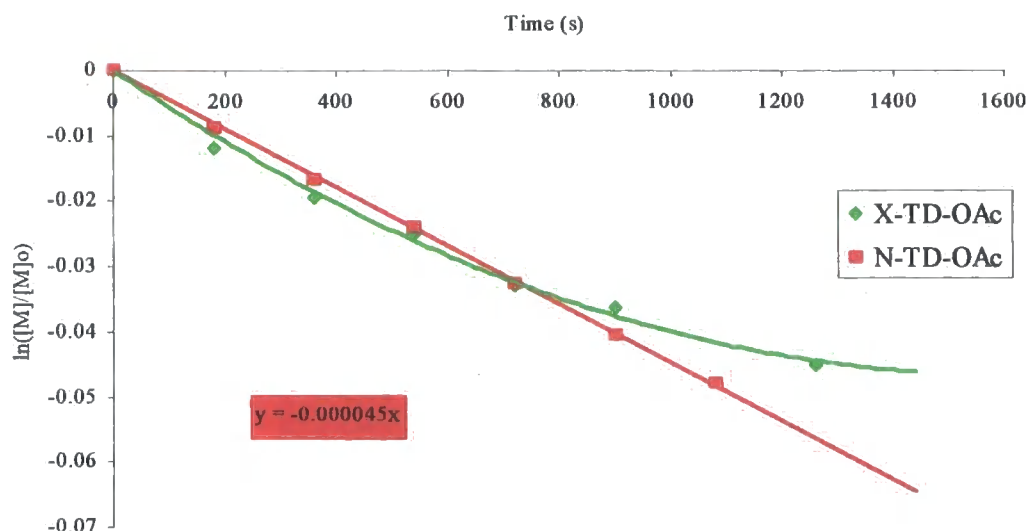


Figure 4.7. Polymerisation of N- and X-TD-OAc at 70°C in benzene- d_6 (50 Monomer : 1 Pd1388).

The deactivating electronic effect of the $-OAc$ functional group upon the double bond, with respect to polymerisation, should be similar in X-NB-OAc and N-TD-OAc. This is not reflected in the respective polymerisation rates, with N-NB-OAc ($k = 8.2 \times 10^{-5} \text{ s}^{-1}$) polymerising slightly faster than X-TD-OAc ($k = 7.6 \times 10^{-5} \text{ s}^{-1}$), at 70°C in benzene- d_6 , figure 4.7. The unexpectedly slow polymerisation rate of both TD-OAc monomers can be attributed to the unfavourable steric interaction between $H_{12'}$ and the vinylic hydrogens, which are being rehybridised from sp^2 to sp^3 , upon coordination and insertion into the palladium-alkyl bond, scheme 4.8. This raises the energy barrier for insertion into the palladium alkyl bond, resulting in a decreased polymerisation rate.

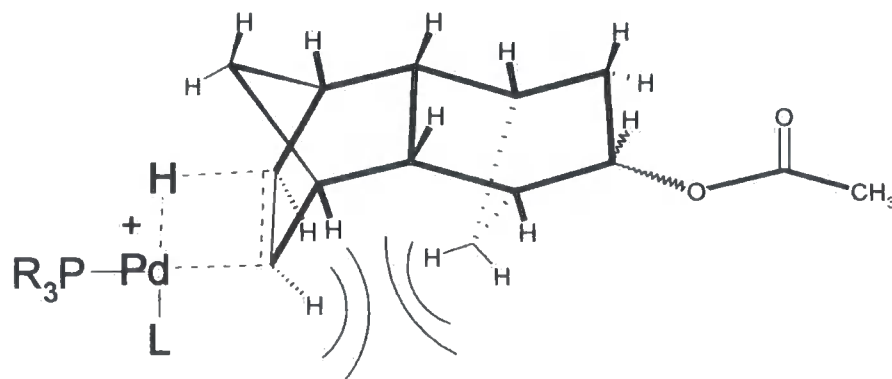


Figure 4.8

The polymerisation of the X-TD-OAc, which is synthesised from X-NB-OAc, displays a decreasing polymerisation rate, which is indicative of a termination step, figure 4.7. There are no easily visible, new signals forming in the ^1H NMR spectra during polymerisation. It seems likely that the polymerisation termination step during the polymerisations of X-NB-OAc and X-TD-OAc are closely related but the exact nature of this termination eludes us.

4.2.12 Poly merisation of Methoxy Functionalised Norbornenes ($\text{NB}(\text{CH}_2)_n\text{OMe}$)

The rate of polymerisation of X-NB-OMe is unsurprisingly fast considering the $-\text{OMe}$ functionality is not strongly electron withdrawing. The polymerisation rate of the N/X- $\text{NB}(\text{CH}_2)_n\text{OMe}$ increases by a different factor, with an increase in methylene spacing, for the N- and X-isomers, table 4.2. The polymerisation rate of N- NBCH_2OMe could be lower than expected due to the formation of a favourable 6-membered chelate ring via coordination of the ether functionality to palladium. The rate of polymerisation of N/X- $\text{NB}(\text{CH}_2)_2\text{OMe}$, is slightly lower than the rate for N/X-NBdecyl under identical polymerisation conditions. This evidence is in agreement that the ether functionality coordinates to cationic palladium, reducing the polymerisation rate.

Table 4.2. Polymerisation data for 50 $\text{NB}(\text{CH}_2)_n\text{OMe}$: 1 **Pd1388**, at 70°C in benzene- d_6 .

n	k_p (N) (s^{-1})	k_p (X) (s^{-1})	k_p (N/X) (s^{-1})	$[\text{k}_p(\text{X})] / [\text{k}_p(\text{N})]$
0	-	6.68×10^{-4}	-	-
1	3.50×10^{-4}	15.35×10^{-4}	-	4.4
2	13.66×10^{-4}	24.99×10^{-4}	19.44×10^{-4}	1.8

The N/X- $\text{NB}(\text{CH}_2)_n\text{OMe}$ family of monomers shows significant solvent effects, with regard to polymerisation rate. In particular this seems to affect the rates of polymerisation of X- and N- isomers with respect to each other. Notice the $[\text{k}_p(\text{X})] / [\text{k}_p(\text{N})]$ factors in the two different solvents, tables 4.2 and 4.3.

Table 4.3. Polymerisation data for 50 NB-(CH₂)_nOMe : 1 Pd1388, at 50°C in TCE-*d*₂.

n	k _p (N) (s ⁻¹)	k _p (X) (s ⁻¹)	k _p (N/X) (s ⁻¹)	[k _p (X)] / [k _p (N)]
0	-	5.22 × 10 ⁻⁴	-	-
1	1.50 × 10 ⁻⁴	17.54 × 10 ⁻⁴	-	11.7
2	6.79 × 10 ⁻⁴	79.70 × 10 ⁻⁴	7.39 × 10 ⁻⁴	11.7

4.3 Conclusions

The convenient synthesis and ease of elaboration of X-NB-OH makes it a good base from which to create new single regioisomer functionalised norbornene monomers that display high polymerisation activity. X-NB-OMe showed very high polymerisation activity. Surprisingly, X-NB-OAc showed lower polymerisation activity than N-NB-OAc. The new single isomer acetate functionalised tetracyclododecenes, X-TD-OAc and N-TD-OAc, show low polymerisation activity due to steric effects that will be general to all functionalised tetracyclododecene monomers. The single regioisomer monomers, X-NB-CH₂OMe and X-NB-CH₂OAc show greater polymerisation activity than the analogous N-NB-CH₂OMe and N-NB-CH₂OAc monomers. The single regioisomer, methylene or multi-methylene spaced, functionalised norbornene monomers employed in this chapter could be used to simplify co-polymerisation reactions and reduce polymerisation attenuating functional group electronic and steric effects.

4.4 Experimental

4.4.1 Materials

The palladium catalyst, $[\text{Pd}(\text{PCy}_3)_2(\text{NCCH}_3)(\text{H})][\text{B}(\text{C}_6\text{F}_5)_4]$ (**Pd1388**) was supplied by Promerus LLC and used without further purification. All liquid monomers were degassed by freeze-thaw-pump cycles before being taken into the glove box. Tetrachloroethane- d_2 and benzene- d_6 were used as supplied in pre-sealed ampules and subsequently kept refrigerated in a glove box. All other solvents (toluene, tetrahydrofuran, chloroform, diethyl ether, dimethyl sulfoxide, hexanes, ethyl acetate, dichloromethane (DCM) and methanol) were used without prior purification. The following reagents were purchased from Sigma Aldrich and used without further purification: hydrochloric acid, norbornadiene, sodium hydroxide, magnesium sulphate, methyl iodide, sodium hydride, ammonium chloride, trimethyl chloro silane, pyridine, dicyclopentadiene, sodium borohydride, Lithium tri-*sec*-butylborohydride solution (L-Selectride), acetic acid, methyl iodide, sodium bis(2-methoxyethoxy)aluminum hydride (Vitride®), copper sulphate, acetic anhydride, dimethylamino pyridine, 2-phenyl benzyl bromide, 4-bromo benzyl bromide and benzyl bromide and silica.

4.4.2 Instrumentation and Measurements

4.4.2.1 Nuclear Magnetic Resonance

^1H NMR spectra were recorded on a Varian Mercury 400 or a Varian Inova 500 using deuteriated solvent lock. Chemical shifts are quoted in ppm, relative to tetramethylsilane (TMS), as the internal reference. ^{31}P NMR spectra were recorded on a Varian/Mercury 400 or a Varian Inova 500 at 121.4 MHz and 202.4 MHz, respectively. ^{13}C NMR spectra were recorded at 125 MHz (2000 scans) using continuous broad band proton decoupling and a 3s recycle delay, and are therefore not quantitative; chemical shifts are quoted in ppm, relative to CDCl_3 (77.550 ppm). The following abbreviations are used in listing NMR spectra: s = singlet, d = doublet, t = triplet, q = quartet, b = broad, m = multiplet.

4.4.2.2 Mass Spectroscopy

Electron Impact (EI) and Electrospray (ES⁺) mass spectra were recorded on a Micromass Autospec spectrometer operating at 70 eV with the ionisation mode as indicated.

4.4.2.3 Infra-red Spectroscopy

Infra-red spectra were recorded on a Perkin Elmer 1600 series FTIR. The spectra obtained were of the pure compound between sodium chloride discs.

4.4.3 General Synthesis

4.4.3.1 General Preparation of NB(CH₂)_nOAc from NB(CH₂)_nOH

Under an inert atmosphere, acetic anhydride (8.19 mL, 86.7 mmol) was added to a flame dried flask containing NB(CH₂)_nOH (54.4 mmol), pyridine (13.76 mL, 170.0 mmol) and dimethylaminopyridine (10 crystals) in DCM (110 mL). The reaction mixture was stirred for 24 hours and checked for completion via TLC. At completion the reaction was quenched with water (90 mL). The aqueous layer was extracted with DCM (4 x 100 mL) and the combined extracts washed with saturated CuSO₄ solution (90 mL), water (90 mL), brine (90 mL), and dried over MgSO₄. The solvent was removed via rotary evaporation to give clear yellow oil.² The residue was purified by distillation under reduced pressure or silica column chromatography to give clear, colourless oil in greater than 80% yield.

4.4.3.2 General Preparation of NB(CH₂)_nOH from NB(CH₂)_nCO₂H

To a 5L three-neck flask were added NB(CH₂)_nCO₂H (1.15 mmol) and anhydrous toluene (1.0 L). The system was kept under a nitrogen blanket, and the flask was equipped with a magnetic stirrer bar, thermometer, addition-funnel and condenser. A pre-mix of Vitride[®] (500 g, 70 wt % in toluene, 1.732 mol) was added to the addition funnel (short exposure to

air is safe if < 2 minutes). With the flask submerged in an ice-water bath, the dilute Vitride[®] was added dropwise over 3 hours while maintaining pot temperature between 5-20 °C. After the addition was complete, the contents were heated to 100 °C for 6 hours (until TLC showed reaction to be complete). The contents were allowed to cool overnight. The solution was slowly added to a beaker containing vigorously stirring 5N HCl (1000 mL). The temperature was maintained < 20 °C with the aid of an ice-bath. After turbidity decreased, the mixture was transferred to a separatory funnel, and the organic phase was diluted with diethyl ether (1.0 L). The aqueous phase was discarded and the organics washed with 1N HCl (3 x 300 mL), 15 wt % aqueous potassium bicarbonate (3 x 300 mL) and water (500 mL). The organics were dried over MgSO₄, filtered, and the solvent removed under reduced pressure to afford NB(CH₂)_nOH in > 95% purity. The products were used in further synthesis reactions without further purification.

4.4.3.3 General Preparation of NB(CH₂)_nOMe from NB(CH₂)_nOH

Under an inert atmosphere, the NB-(CH₂)_nOH (54.6 mmol) was dissolved in dry THF (15 mL) and was added dropwise to a stirred solution of NaH (68.2 mmol) in dry THF (65 mL). After complete addition, the solution was heated at 50°C for 3 hours. After cooling the reaction mixture to room temperature, methyl iodide (19.32 g, 8.47 mL, 136.2 mmol) was added dropwise to the solution; a slight *exotherm* was observed and a cream coloured precipitate was formed. The reaction mixture was stirred for 12 hours. After quenching with NH₄Cl (60 mL) the reaction mixture was extracted into diethyl ether (4 × 50 mL), washed with brine (50 mL) and dried over MgSO₄. The solvent was removed by rotary evaporation to give clear, yellow oil.⁵ The product was purified using distillation under reduced pressure or silica column chromatography to give clear, colourless oil in greater than 60% yield.

4.4.4 Monomer Synthesis and Characterisation

4.4.4.1 Synthesis and Characterisation of *exo*-5-Acetate-2-norbornene

Norbornadiene (414 g, 4.50 mol) and glacial acetic acid (156 g, 2.60 mol) were charged to a 2 L stainless steel pressure vessel. The vessel was cooled in liquid nitrogen, evacuated, sealed and heated to 190°C for 22 hours. The reaction mixture was concentrated on a rotary evaporator to remove excess norbornadiene and acetic acid (the excess norbornadiene can be recovered, there should be little acetic acid remaining). The product X-NB-OAc (350 g, 2.30 mol, 88%), figure 4.9, was obtained by distillation under reduced pressure (49°C, 6.5 mbar).¹ The monomer was characterised by ¹H NMR, ¹³C NMR, GCMS and IR. The numbering system shown in figure 4.9 was used for the assignment of the NMR signals. The GCMS and ¹³C NMR analyses showed the product to have > 98:2, X:N selectivity. An impurity (< 2%) was detected in the GCMS, which had a molecular mass of 158. This impurity is thought to be C₁₂H₁₄, the product of the Diels-Alder reaction between norbornadiene and cyclopentadiene.

¹H NMR (500 MHz, CDCl₃): δ (ppm) = 6.17 (dd, 1H, *J* = 5.87 & 2.86, H₂), 5.91 (dd, 1H, *J* = 5.87 & 3.23, H₃), 4.59 (m, 1H, H₅), 2.82 (s, 1H, H₄), 2.79 (s, 1H, H₁), 1.98 (s, 3H, H₉), 1.64 (ddd, 1H, *J* = 12.59 & 6.91 & 2.73, H₇), 1.59 (m, 1H, *J* = 8.61, H₆), 1.51 (m, 1H, *J* = 8.61, H₆), 1.35 (m, 1H, *J* = 12.59, H₇).

¹³C NMR (125.7 MHz, CDCl₃): δ (ppm) = 171.20 (C₈), 141.14 (C₂), 132.71 (C₃), 75.30 (C₅), 47.35 (C₄), 46.31 (C₆), 40.70 (C₁), 34.67 (C₇), 21.48 (C₉).

GCMS (EI⁺): RT = 8.60, X-NB-OAc, 152.1 (C₉H₁₂O₂, M⁺), 153.1 (MH⁺), 92.1 (MH⁺-C₂H₃O₂), 66.0 (M⁺-C₄H₆O₂). RT = 9.39, N-NB-Ac, 152.1 (C₉H₁₂O₂, M⁺), 153.1 (MH⁺), 92.1 (MH⁺-C₂H₃O₂), 66.0 (M⁺-C₄H₆O₂).

IR (KBr disc, cm⁻¹): 3060 (olefinic C-H stretching), 2980 - 2867 (saturated C-H stretching), 1736 (asymmetric and symmetric C=O stretching).

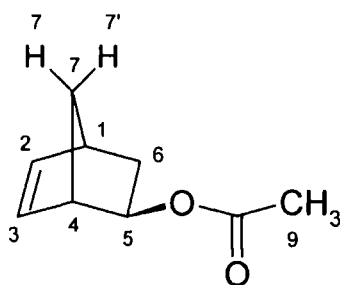


Figure 4.9. Assignment of C and H atoms in X-NB-OAc.

4.4.4.2 Synthesis and Characterisation of *exo*-5-Hydroxy-2-norbornene

A round-bottomed flask was charged with sodium hydroxide pellets (360 g, 9.00 mol), methanol (35 mL) and water (0.5 L). The solution was heated to 80°C under nitrogen with vigorous mechanical stirring and the X-NB-OAc (350 g, 2.30 mol) was added dropwise. After the addition was complete, the mixture was allowed to cool with stirring overnight. The solid was filtered and washed with water. It was dissolved in ether (1 L) and 10% aqueous HCl (175 mL). The ether layer was separated, washed with dilute sodium bicarbonate and brine. The ether solution was dried over MgSO₄, filtered and concentrated at room temperature to give the product (219 g, 2.00 mol, 87%) as white crystals, mp = 85 – 88°C, figure 4.10. The C₁₂H₁₄ impurity was removed by recrystallisation from hexane. The monomer was characterised by ¹H NMR, ¹³C NMR, GCMS and IR. The numbering system shown in figure 4.10 was used for the assignment of the NMR signals. The GCMS and ¹³C NMR analyses showed the product to have > 98:2, X:N selectivity. Attempts to grow high quality crystals of X-NB-OH for single-crystal X-ray diffraction analysis were unsuccessful using both sublimation and slow recrystallisation from various solvents.

¹H NMR (400 MHz, CDCl₃): δ (ppm) = 6.17 (dd, 1H, *J* = 5.76 & 2.89, H₂), 5.95 (dd, 1H, *J* = 5.76 & 3.19, H₃), 3.89 (d, 1H, *J* = 6.74, H₅), 2.81 (s, 1H, H₄), 2.71 (s, 1H, H₁), 2.20 (broad s, 1H, -OH), 1.74 (d, 1H, *J* = 8.51, H₆), 1.64 (ddd, 1H, *J* = 12.14 & 6.78 & 2.66, H₇), 1.56 (m, 1H, H₆), 1.27 (m, 1H, H₇).

¹³C NMR (101 MHz, CDCl₃): δ (ppm) = 140.46 (C₂), 133.58 (C₃), 72.68 (C₅), 50.35 (C₄), 45.74 (C₁), 40.90 (C₆), 37.28 (C₇).

GCMS (EI⁺): RT = 6.27, N-NB-OH, 110.0 (C₇H₁₀O, M⁺), 66.1 (M⁺-C₂H₄O). RT = 6.35, X-NB-OH, 110.0 (C₇H₁₀O, M⁺), 66.0 (M⁺-C₂H₄O).

IR (KBr disc, cm⁻¹): 3100 - 3650 (O-H), 3060 (olefinic C-H stretching), 2980 - 2867 (saturated C-H stretching).

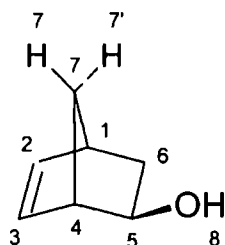


Figure 4.10. Assignment of C and H atoms in X-NB-OH.

4.4.4.3 Synthesis and Characterisation of 2-Norbornene-5-one (method 1)

X-NB-OH (12.0 g, 108.9 mmol) in DCM (300 mL) was added via a cannula to a flame dried flask containing CrO₃ (67.0 g, 670.2 mmol) and pyridine (107.9 mL, 1.342 mol) in DCM (859 mL). The reaction mixture was stirred for 48 hours and filtered through a plug of silica (eluted with DCM). The organics was washed with 5% NaOH, 5% HCl, saturated NaCl, and dried over MgSO₄.² The solvent was removed via rotary evaporation and the crude product purified by silica column chromatography (EtOAc:hexanes = 1:4) to give the product (4.9 g, 45 mmol, 41%) as a white solid, figure 4.11. The monomer was characterised by ¹H NMR, ¹³C NMR, GCMS and IR. The numbering system shown in figure 4.11 was used for the assignment of the NMR signals.

4.4.4.4 Alternative Synthesis and Characterisation of 2-Norbornene-5-one (method 2)

To a three-neck flask equipped with a mechanical stirrer, a nitrogen inlet and an addition funnel was added a solution of oxalyl chloride (2.0 M in DCM, 136 mL, 0.272 mol) in DCM (250 mL). The solution was cooled to -78 °C, and a solution of DMSO (40 mL) in DCM (40 mL) was added dropwise over 30 minutes. A solution of N/X-NB-OH (24 g, 0.218 mol) in DCM (40 mL) was added dropwise. The solution was stirred for 10 minutes and

triethylamine (150 mL) was added over 40 minutes. The mixture was stirred for 10 minutes at -78°C and then allowed to warm to 0°C over 1 hour. Water (250 mL) was added. The organic layer was separated and washed with 0.2N HCl (4 x 200 mL) and brine (2 x 200 mL). The organics were dried over MgSO_4 and most of the solvent removed under reduced pressure.³ The residue was distilled with a 12 in. Vigreux column at reduced pressure ($100\text{--}105^{\circ}\text{C}/15\text{ mmHg}$) to give $\text{NB}=\text{O}$ (17.2g, 75%) as a semi-solid, figure 4.11. The monomer was characterised by ^1H NMR, ^{13}C NMR, GCMS and IR. The numbering system shown in figure 4.11 was used for the assignment of the NMR signals.

^1H NMR (400 MHz, CDCl_3): δ (ppm) = 6.53 (m, 1H, $\text{H}_{2\&3}$), 6.08 (m, 1H, $\text{H}_{2\&3}$), 3.16 (m, 1H, $\text{H}_{1\&4}$), 2.98 (m, 1H, $\text{H}_{1\&4}$), 2.17 (m, 1H, H_6), 1.97 (m, 1H, H_6), 1.95 (m, 1H, H_7), 1.85 (m, 1H, H_7).

^{13}C NMR (75 MHz, CDCl_3): δ (ppm) = 215.77 (C_5), 143.1 ($\text{C}_{2\&3}$), 130.58 ($\text{C}_{2\&3}$), 55.86, 50.92, 40.05, 37.25.

GCMS (EI^+): RT = 6.22, $\text{NB}=\text{O}$, 108.0 ($\text{C}_8\text{H}_8\text{O}$, M^+).

IR (KBr disc, cm^{-1}): 3060 (olefinic C-H stretching), 2980 - 2860 (saturated C-H stretching), 1740 (asymmetric and symmetric C=O stretching).

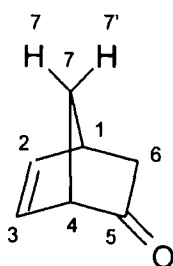


Figure 4.11. Assignment of C and H atoms in $\text{NB}=\text{O}$.

4.4.4.5 Synthesis and Characterisation of *endo*-5-Hydroxy-2-norbornene (method 1)

L-Selectride (1 M in THF, 55 mL, 55 mmol) was added to a flame-dried flask containing N-NB-OH (4.9 g, 45 mmol) in THF (50 mL) at -78°C . The reaction mixture was stirred at -

78°C for 3 hours and -20°C for 1 hour. After quenching with water (20 mL), the aqueous layer was extracted with diethyl ether (5 x 30 mL) and the combined organics washed with water (100 mL), brine (100 mL), and dried over MgSO₄.² The solvent was removed by rotary evaporation and the crude product purified via silica column chromatography (EtOAc:Hexanes = 3:7) to give a pale yellow semi-solid, which although contained the desired product, it was not pure.

4.4.4.6 Alternative Synthesis and Characterisation of *endo*-5-Hydroxy-2-norbornene (Method 2)

NaBH₄ (0.935g, 21.3 mmol) was added dropwise to a solution of NB=O (2.3 g, 21.3mmol) in anhydrous methanol (500 mL) at -78°C. The solution was allowed to warm to ambient temperature overnight followed by the addition of 2N HCl (25 mL) to quench the reaction. The methanol was removed under vacuum and the aqueous residue extracted with diethyl ether (3 x 100 mL). The organics were washed with brine (3 x 50 mL), dried over MgSO₄ and the solvent removed under reduced pressure to afford N-NB-OH (1.45 g, 13.1 mol, 62%) as a pale yellow semi-solid, figure 4.12.⁴ The monomer was used without further purification and was characterised by ¹H NMR, ¹³C NMR, GCMS and IR. The numbering system shown in figure 4.12 was used for the assignment of the NMR signals.

¹H NMR (200 MHz, CDCl₃): δ (ppm) = 6.43 (dd, 1H, *J* = 5.40 & 3.0, H_{2&3}), 6.04 (dd, 1H, *J* = 5.40 & 3.0, H_{2&3}), 4.45 (m, 1H, H), 2.97 (m, 1H, H_{1&4}), 2.80 (m, 1H, H_{1&4}), 2.08 (ddd, 1H, *J* = 12.40 & 4.31 & 3.74, H₇), 1.48 (m, 2H, H_{5&6}), 1.26 (m, 1H, H₆), 0.74 (m, 1H, H₇).

¹³C NMR (50 MHz, CDCl₃): δ (ppm) = 140.18, 130.73, 72.30, 48.13, 47.97, 42.76, 37.60.

GCMS (EI⁺): RT = 6.27, N-NB-OH, 110.0 (C₇H₁₀O, M⁺).

IR (KBr disc, cm⁻¹): 3100 - 3650 (O-H), 3060 (olefinic C-H stretching), 2980 - 2867 (saturated C-H stretching).

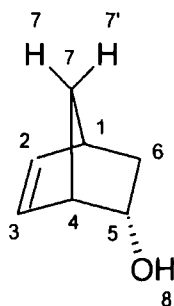


Figure 4.12. Assignment of C and H atoms in N-NB-OH.

4.4.4.7 Synthesis and Characterisation of *endo*-5-Acetate-2-norbornene

The synthesis of this monomer is described in general synthesis, section 4.3.3.1. The crude monomer was purified by distillation under reduced pressure (80°C, 5 mbar) to give the pure product, as a clear, colourless oil, in 90% yield, figure 4.13. The monomer was characterised by ^1H NMR, ^{13}C NMR, GCMS and IR. The numbering system shown in figure 4.13 was used for the assignment of the NMR signals.

^1H NMR (500 MHz, CDCl_3): δ (ppm) = 6.26 (dd, 1H, J = 5.62 & 3.02, H_2), 5.89 (dd, 1H, J = 5.62 & 2.79, H_3), 5.16 (m, 1H, H_5), 3.05 (b, 1H, H_4), 2.76 (b, 1H, H_1), 2.04 (ddd, 1H, J = 12.48, 8.10, 3.63, H_7), 1.89 (s, 3H, H_9), 1.38 (m, 1H, J = 8.80, H_6) 1.24 (bd, 1H, J = 8.80, H_6), 0.84 (m, 1H, J = 12.48, H_7).

^{13}C NMR (125.7 MHz, CDCl_3): δ (ppm) = 171.46 (C_8), 138.66 (C_2), 131.69 (C_3), 75.25 (C_5), 47.78 (C_6), 45.88 (C_4), 42.35 (C_1), 34.71 (C_7), 21.32 (C_9).

GCMS (EI^+): RT = 9.87, N-NB-OAc, 152.0 ($\text{C}_{10}\text{H}_{16}\text{O}$, M^+), 109.0 (M^+ -Ac), 93.1 (M^+ -OAc).

IR (KBr disc, cm^{-1}): 3060 (olefinic C-H stretching), 2980 - 2867 (saturated C-H stretching), 1736 (asymmetric and symmetric C=O stretching).

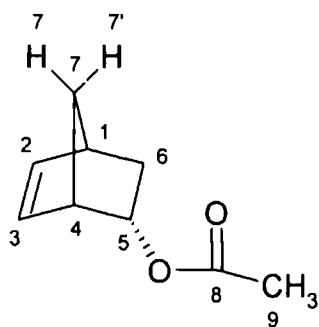


Figure 4.13. Assignment of C and H atoms in N-NB-OAc.

4.4.4.8 Synthesis and Characterisation of *exo*-Tetracyclododecene Acetate

X-NB-OAc (14.0 g, 92.1 mmol) and dicyclopentadiene (3.1 g, 23.5 mmol) were added to a thick-walled carius tube (total volume = 120 mL). The combined liquids were degassed via freeze-vacuum-thaw method (4 times). The tube was sealed whilst frozen, using a hot flame and placed in a protective steel sleeve to thaw. The tube was heated in an oven at 220°C for 8 hours and then allowed to cool. GCMS analysis of the crude reaction mixture revealed that the reaction had proceeded quite cleanly, revealing starting material (X-NB-OAc), the new X-TD-OAc product and other higher molecular weight materials. The excess X-NB-OAc was recovered via distillation of the reaction mixture at 80°C under reduced pressure (~ 9 g recovered). The X-TD-OAc was purified via distillation under reduced pressure (130°C, 25 mbar) to give a white semi-solid (~ 4 g, 20%). A soft clear crystal of X-TD-OAc, figure 4.14, was produced using a solution of (X-TD-OAc : hexanes = 95 : 5, W/W %, respectively). Crystallisation occurred at -10°C over 4 weeks. The crystal was subjected to NMR spectroscopy, GCMS and single crystal X-ray diffraction analysis. The monomer was characterised by ¹H NMR, ¹³C NMR, GCMS and IR. The numbering system shown in figure 4.14 was used for the assignment of the NMR signals.

¹H NMR (500 MHz, CDCl₃): δ (ppm) = 5.94 (m, 2H, H_{2&3}), 4.42 (m, 1H, *J* = 6.91, H₉), 2.86 (s, 1H, H₄), 2.81 (s, 1H, H₁), 2.13 (s, 1H, H₈), 2.08 (m, 1H, H₁₁), 2.05 (m, 1H, *J* = 10.52, H₁₂), 1.96 (s, 3H, H₁₄), 1.92-1.85 (m, 2H, H_{5&6}), 1.59 (ddd, 1H, *J* = 13.15 & 6.92 & 2.83, H₁₀), 1.33-1.28 (m, 2H, H_{10'&7}), 1.17 (m, 1H, *J* = 7.83, H₇), 0.89 (m, 1H, *J* = 10.52, H₁₂).

^{13}C NMR (125.7 MHz, CDCl_3): δ (ppm) = 171.07 (C_{13}), 135.71 & 135.63 ($\text{C}_{2\&3}$), 78.86 (C_9) 53.46 (C_7), 48.32 (C_5), 46.59 & 46.40 ($\text{C}_{1\&4}$), 43.54 (C_8), 43.52 (C_6), 42.42 (C_{10}), 37.18 (C_{11}), 31.04 (C_{12}), 21.58 (C_{14}).

GCMS (EI^+): RT = 17.37, X-TD-OAc, 218.0 ($\text{C}_{14}\text{H}_{18}\text{O}_2$, M^+), 175.5 ($\text{M}^+ - \text{Ac}$), 159.2 ($\text{M}^+ - \text{OAc}$).

IR (KBr disc, cm^{-1}): 3060 (olefinic C-H stretching), 2980 - 2867 (saturated C-H stretching), 1736 (asymmetric and symmetric C=O stretching).

An X-ray structural diagram was produced using single-crystal X-ray diffraction. The analysis gave full structural refinement.

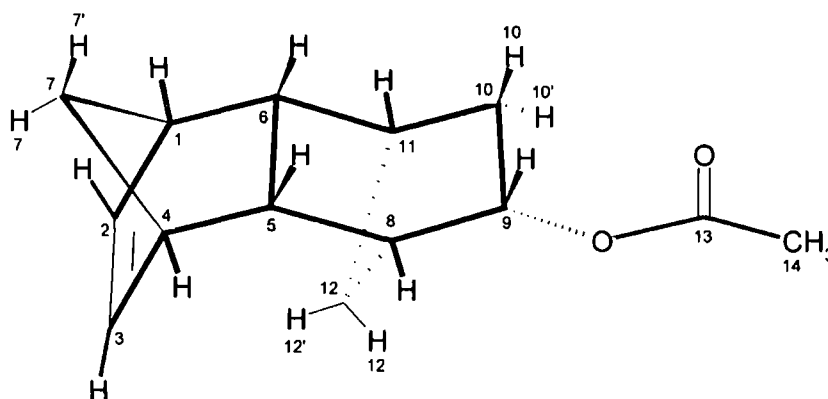


Figure 4.14. Assignment of C and H atoms in X-TD-OAc.

4.4.4.9 Synthesis and Characterisation of *endo*-Tetracyclododecene Acetate

N-NB-OAc (14.0 g, 92.1 mmol) and dicyclopentadiene (3.1 g, 23.5 mmol) were added to a thick-walled carius tube (total volume = 120 mL). The combined liquids were degassed via freeze-vacuum-thaw method (4 times). The tube was sealed whilst frozen, using a hot flame and placed in a protective steel sleeve to thaw. The tube was heated in an oven at 220°C for 8 hours and then allowed to cool. GCMS analysis of the crude reaction mixture revealed that the reaction had proceeded quite cleanly, revealing starting material (N-NB-OAc), the new N-TD-OAc product and other higher molecular weight materials. The excess N-NB-OAc was recovered via distillation of the reaction mixture at 85°C under reduced pressure (~ 6 g

recovered). The N-TD-OAc was purified via distillation under reduced pressure (130°C, 20 mbar) to give a clear colourless liquid (~ 3 g, 15%), figure 4.15. The monomer was characterised by ^1H NMR, ^{13}C NMR, GCMS and IR. The numbering system shown in figure 4.15 was used for the assignment of the NMR signals.

^1H NMR (500 MHz, CDCl_3): δ (ppm) = 6.00 (dd, 1H, $J = 5.59$ & 3.06 , H_2), 5.93 (dd, 1H, $J = 5.59$ & 2.97 , H_3), 4.72 (ddd, 1H, $J = 9.96$ & 4.24 & 3.70 , H_9), 2.88 (bs, 1H, H_4), 2.84 (bs, 1H, H_1), 2.50 (dd, 1H, $J = 8.29$ & 4.18 , H_5), 2.34 (m, 1H, H_8), 2.17 (m, 1H, $J = 10.98$, $\text{H}_{12'}$), 2.08 (dd, 1H, $J = 8.16$ & 4.02 , H_6), 2.04 (s, 3H, H_{14}), 2.03 (m, 1H, H_{11}), 1.97 (m, 1H, $\text{H}_{10'}$), 1.30 (m, 1H, $J = 7.82$, H_7), 1.21 (m, 1H, $J = 7.82$, H_7'), 0.80 (m, 1H, $J = 12.84$, H_{10}), 0.64 (m, 1H, $J = 10.98$, H_{12}).

^{13}C NMR (125.7 MHz, CDCl_3): δ (ppm) = 171.39 (C_{13}), 136.36 (C_2), 135.87 (C_3), 76.11 (C_9), 53.14 (C_7), 48.97 (C_6), 47.21 (C_4), 46.37 (C_1), 42.12 (C_8), 39.78 (C_{10}), 39.17 (C_{11}), 38.78 (C_5), 32.78 (C_{12}), 21.50 (C_{14}).

GCMS (EI^+): RT = 17.01, N-TD-OAc, 218.0 ($\text{C}_{14}\text{H}_{18}\text{O}_2$, M^+), 175.5 ($\text{M}^+ - \text{Ac}$), 159.2 ($\text{M}^+ - \text{OAc}$).

IR (KBr disc, cm^{-1}): 3060 (olefinic C-H stretching), 2980 - 2867 (saturated C-H stretching), 1736 (asymmetric and symmetric C=O stretching).

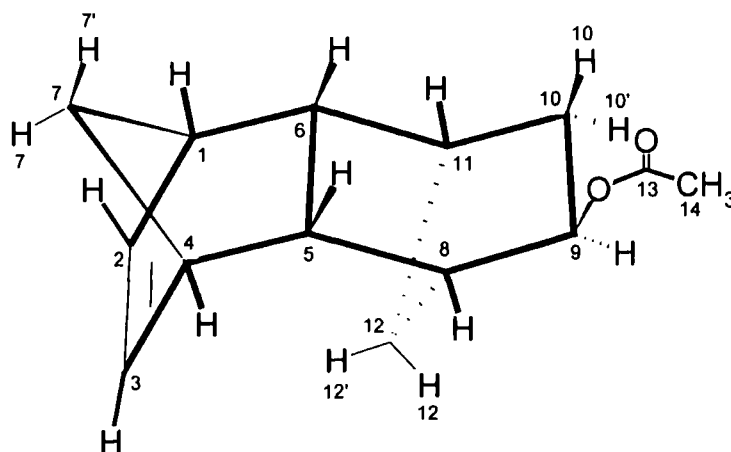


Figure 4.15. Assignment of C and H atoms in N-TD-OAc.

4.4.4.10 Characterisation of *endo*-5-Carboxylic Acid-2-norbornene

The monomer, figure 4.16, was supplied by Promerus LLC and used without further purification. The monomer was characterised by ^1H NMR, ^{13}C NMR and GCMS. The numbering system shown in figure 4.16 was used for the assignment of the NMR signals.

^1H NMR (400 MHz, CDCl_3): δ (ppm) = 6.15 (dd, 1H, $J = 2.89$ & 5.55 , H_2), 6.11 (dd, 1H, $J = 2.95$ & 5.55 , H_3), 3.11 (s, 1H, $\text{H}_{4\&1}$), 2.93 (s, 1H, $\text{H}_{1\&4}$), 2.26 (m, 1H, H_5), 1.95 (m, 1H, H_7), 1.53 (bd, 1H, $J = 8.37$, H_6), 1.38 (m, 1H, H_7), 1.41 (m, 1H, H_6).

^{13}C NMR (100.6 MHz, CDCl_3): δ (ppm) = 183.21 (C_8), 138.35 (C_2), 135.92 (C_3), 46.90 ($\text{C}_{1\&4}$), 46.59 (C_6), 43.37 (C_5), 41.86 ($\text{C}_{1\&4}$), 20.54 (C_7).

GCMS (EI^+): RT = 11.49, N-NB- CO_2H , 138.0 ($\text{C}_8\text{H}_{10}\text{O}_2$, M^+).

Single crystals of N-NB- CO_2H were grown via slow sublimation at ambient temperature and an X-ray structural diagram produced using single-crystal X-ray diffraction. The analysis gave full structural refinement.

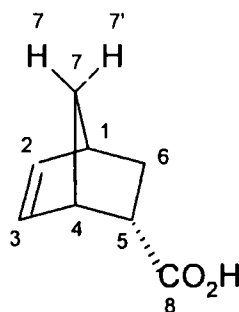


Figure 4.16. Assignment of C and H atoms in N-NB- CO_2H .

4.4.4.11 Characterisation of *exo*-5-Carboxylic Acid-2-norbornene

The monomer, figure 4.17, was supplied by Promerus LLC and used without further purification. The monomer was characterised by ^1H NMR, ^{13}C NMR and GCMS. The numbering system shown in figure 4.17 was used for the assignment of the NMR signals.

^1H NMR (400 MHz, CDCl_3): δ (ppm) = 6.20 (dd, 1H, $J = 5.62$ & 3.03 , $\text{H}_{2\&3}$), 5.99 (dd, 1H, $J = 5.62$ & 2.80 , $\text{H}_{2\&3}$), 3.23 (bs, 1H, $\text{H}_{1\&4}$), 2.99 (dt, 1H, $J = 9.30$ & 3.89 , H_5), 2.91 (bs, 1H, $\text{H}_{1\&4}$), 1.91 (ddd, 1H, $J = 11.89$ & 9.37 & 3.74 , H_7), 1.45 (m, 1H, H_6), 1.39 (m, 1H, H_7), 1.28 (s, 1H, H_6).

^{13}C NMR (100.6 MHz, CDCl_3): δ (ppm) = 181.28 (C_8), 138.11 (C_2), 132.63 (C_3), 49.93 (C_6), 45.89 ($\text{C}_{1\&4}$), 43.44 (C_5), 42.74 ($\text{C}_{1\&4}$), 29.31 (C_7).

GCMS (EI^+): RT = 11.58, X-NB- CO_2H , 138.0 ($\text{C}_8\text{H}_{10}\text{O}_2$, M^+).

Single crystals of X-NB- CO_2H were grown via slow sublimation at ambient temperature and an X-ray structural diagram produced using single-crystal X-ray diffraction. The analysis gave only partial structural refinement.

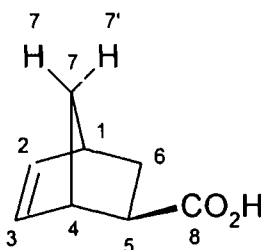


Figure 4.17. Assignment of C and H atoms in X-NB- CO_2H .

4.4.4.12 Synthesis and Characterisation of *exo*-5-Methyl Hydroxy-2-norbornene

The monomer, figure 4.18, was synthesised from X-NB- CO_2H , as described in the general synthesis, section 3.3.3.2. The monomer was characterised by ^1H NMR, ^{13}C NMR, GCMS and IR. The numbering system shown in figure 4.18 was used for the assignment of the NMR signals.

^1H NMR (400 MHz, CDCl_3): δ (ppm) = 6.06 (dd, 1H, $J = 5.64$ & 3.02 , H_2), 6.02 (dd, 1H, $J = 5.64$ & 2.87 , H_3), 3.64 (dd, 1H, $J = 10.58$ & 6.43 , H_8), 3.47 (dd, 1H, $J = 10.58$ & 8.97 , H_8), 2.77 (bs, 1H, $\text{H}_{1\&4}$), 2.71 (bs, 1H, $\text{H}_{1\&4}$), 2.62 (b, 1H, -OH), 1.57 (m, 1H, H_5), 1.31 (m, 2H, H_6), 1.22 (m, 1H, H_7), 1.06 (ddd, 1H, $J = 11.62$, H_7).

^{13}C NMR (100.6 MHz, CDCl_3): δ (ppm) = 136.87 (C_2), 136.57 (C_3), 67.37 (C_8), 45.02, 43.34, 41.83, 41.60, 29.63 (C_7).

GCMS (EI^+): RT = 9.59, X-NB- CH_2OH , 124.0 ($\text{C}_8\text{H}_{12}\text{O}$, M^+).

IR (KBr disc, cm^{-1}): 3100 - 3650 (O-H), 3060 (olefinic C-H stretching), 2980 - 2867 (saturated C-H stretching).

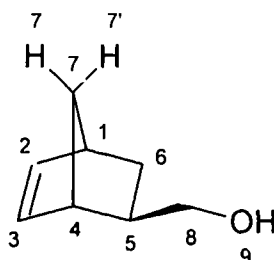


Figure 4.18. Assignment of C and H atoms in X-NB- CH_2OH .

4.4.4.13 Synthesis and Characterisation of *endo*-5-Methyl Hydroxy-2-norbornene

The monomer, figure 4.19, was synthesised from N-NB- CO_2H , as described in the general synthesis, section 3.3.3.2. The monomer was characterised by ^1H NMR, ^{13}C NMR, GCMS and IR. The numbering system shown in figure 4.19 was used for the assignment of the NMR signals.

^1H NMR (400 MHz, CDCl_3): δ (ppm) = 6.08 (m, 1H, $\text{H}_{2\&3}$), 5.91 (m, 1H, $\text{H}_{2\&3}$), 3.31 (m, 1H, H), 3.16 (m, 1H, H), 2.88 (b, 1H, $\text{H}_{1\&4}$), 2.74 (b, 1H, $\text{H}_{1\&4}$), 2.74 (b, 1H, -OH), 2.23 (m, 1H, H_5), 1.75 (m, 1H, H_7), 1.39 (m, 1H, H_8), 1.20 (m, 1H, H_8), 0.45 (m, 1H, H_7).

^{13}C NMR (100.6 MHz, CDCl_3): δ (ppm) = 137.39 (C_2), 132.31 (C_3), 66.25 (C_8), 49.55, 43.66, 44.26, 41.63, 28.89 (C_7).

GCMS (EI^+): RT = 9.53, N-NB- CH_2OMe , 124.0 ($\text{C}_8\text{H}_{12}\text{O}$, M^+).

IR (KBr disc, cm^{-1}): 3100 - 3650 (O-H), 3060 (olefinic C-H stretching), 2980 - 2867 (saturated C-H stretching).

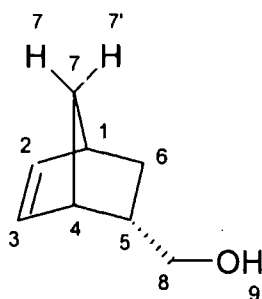


Figure 4.19. Assignment of C and H atoms in X-NB-CH₂OH.

4.4.4.14 Synthesis and Characterisation of *exo*-5-Methyl Methoxy-2-norbornene

The monomer, figure 4.20, was synthesised from X-NBCH₂OH, as described in the general synthesis, section 3.3.3.3. The crude monomer was purified by distillation under reduced pressure (70°C, 80 mbar), to give a clear, colourless oil, in 55% yield. The monomer was characterised by ¹H NMR, ¹³C NMR, GCMS and IR. The numbering system shown in figure 4.20 was used for the assignment of the NMR signals.

¹H NMR (500 MHz, CDCl₃): δ (ppm) = 6.11 (dd, 1H, *J* = 5.62 & 3.03, H₂), 6.07 (dd, 1H, *J* = 5.62 & 2.91, H₃), 3.43 (dd, 1H, *J* = 9.21 & 6.23, H₈), 3.37 (s, 3H, H₉), 3.30 (t, 1H, *J* = 9.21, H₈), 2.82 (b, 1H, H₄), 2.74 (b, 1H, H₁), 1.70 (m, 1H, H₅), 1.31 (m, 2H, H₆), 1.22 (m, 1H, H₇), 1.12 (ddd, 1H, H₇).

¹³C NMR (125.7 MHz, CDCl₃): δ (ppm) = 136.89 (C₂), 136.86 (C₃), 77.88 (C₈), 59.06 (C₉), 45.30 (C₆), 43.93 (C_{1&4}), 41.79 (C_{1&4}), 39.11 (C₅), 29.95 (C₇).

GCMS (EI⁺): RT = 8.58, X-NB-CH₂OMe, 138.0 (C₉H₁₄O, M⁺).

IR (KBr disc, cm⁻¹): 3060 (olefinic C-H stretching), 2980 - 2867 (saturated C-H stretching), 1099 (C-O stretching).

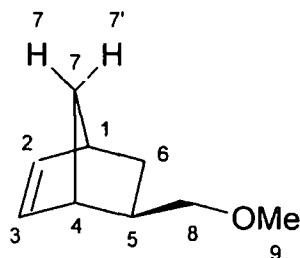


Figure 4.20. Assignment of C and H atoms in X-NB-CH₂OMe.

4.4.4.15 Characterisation of *endo*-5-Methyl Methoxy-2-norbornene

The monomer, figure 4.21, was synthesised from N-NBCH₂OH, as described in the general synthesis, section 3.3.3.3. The crude monomer was purified by distillation under reduced pressure (70°C, 70 mbar), to give a clear, colourless oil, in 55% yield. The monomer was characterised by ¹H NMR, ¹³C NMR, GCMS and IR. The numbering system shown in figure 4.21 was used for the assignment of the NMR signals.

¹H NMR (500 MHz, CDCl₃): δ (ppm) = 6.13 (dd, 1H, *J* = 5.60 & 2.99, H_{2&3}), 5.94 (dd, 1H, *J* = 5.60 & 2.93, H_{2&3}), 3.31 (s, 3H, H₉), 3.09 (dd, 1H, *J* = 9.11 & 6.70, H₈), 3.03 (t, 1H, *J* = 9.11, H₈), 2.90 (b, 1H, H₄), 2.80 (b, 1H, H₁), 2.35 (m, 1H, H₅), 1.83 (ddd, 1H, *J* = 11.60 & 9.20 & 3.85, H₇), 1.43 (dq, 1H, *J* = 8.10 & 2.01, H₆), 1.25 (bd, 1H, *J* = 8.10, H₆), 0.50 (ddd, 1H, *J* = 11.60 & 4.35 & 2.58, H₇).

¹³C NMR (125.7 MHz, CDCl₃): δ (ppm) = 137.37 (C₂), 132.69 (C₃), 76.95 (C₈), 58.99 (C₉), 49.71 (C₆), 44.20 (C₄), 42.44 (C₁), 38.97 (C₅), 29.38 (C₇).

GCMS (EI⁺): RT = 8.66, N-NB-CH₂OMe, 138.0 (C₉H₁₄O, M⁺).

IR (KBr disc, cm⁻¹): 3060 (olefinic C-H stretching), 2980 - 2867 (saturated C-H stretching), 1099 (C-O stretching).

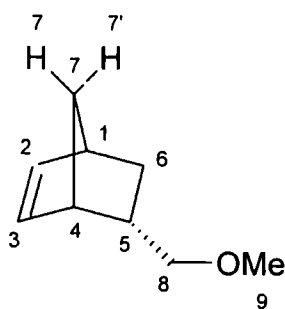


Figure 4.21. Assignment of C and H atoms in N-NB-CH₂OMe.

4.4.4.16 Synthesis and Characterisation of *exo*-5-Methoxy-2-norbornene

Under an inert atmosphere, X-NB-OH (6.00 g, 54.6 mmol) was dissolved in dry THF (15 mL) and was added dropwise to a stirred solution of NaH (1.63 g, 68.2 mmol) in dry THF (65 mL). After complete addition, the solution was heated at 50°C for 3 hours. After cooling the reaction mixture to room temperature, methyl iodide (19.32 g, 8.47 mL, 136.2 mmol) was added dropwise to the solution, a slight exotherm was observed and a cream coloured precipitate was formed. The reaction mixture was stirred for 12 hours. After quenching with NH₄Cl (60 mL) the reaction mixture was extracted into diethyl ether (4 × 50 mL), washed with brine (50 mL) and dried over MgSO₄. The solvent was removed by rotary evaporation to give yellow oil. The residue was purified by distillation under reduced pressure (80 mbar, 62°C) to give the product, a clear and colourless oil (3.7 g, yield = 55%), figure 4.22. The monomer was characterised by ¹H NMR, ¹³C NMR, GCMS and IR. The numbering system shown in figure 4.22 was used for the assignment of the NMR signals. The GCMS and NMR analyses indicated that the product was a mixture of N and X diastereomers in a ratio of 1:99 respectively. An impurity (< 1%) was detected in the GCMS, which was of identical molecular mass (Mr = 124.1), similar fragmenting pattern, and similar retention time to the NB-OMe product. This impurity was likely to be a rearrangement product.

¹H NMR (400 MHz, CDCl₃): δ (ppm) = 6.15 (dd, 1H, *J* = 5.71 & 2.85, H₂), 5.89 (dd, 1H, *J* = 5.71 & 3.25, H₃), 3.35 (d, 1H, *J* = 6.15, H₅), 3.03 (s, 3H, H₈), 2.87 (s, 1H, H₄), 2.76 (s, 1H, H₁), 1.59 (d, 1H, *J* = 8.56, H₇), 1.50 (m, 2H, H₆), 1.29 (dt, 1H, *J* = 12.09 & 2.91, H₇).

^{13}C NMR (101 MHz, CDCl_3): δ (ppm) = 140.84 (C_2), 133.35 (C_3), 82.24 (C_8), 56.99 (C_5), 46.10 (C_4), 46.07 (C_1), 40.55 (C_6), 34.42 (C_7).

GCMS (EI^+): RT = 5.70, X-NB-OMe, 124.0 ($\text{C}_8\text{H}_{12}\text{O}$, M^+), 125.0 (MH^+), 92.0 ($\text{MH}^+ - \text{CH}_3\text{O}$), 58.0 ($\text{MH}^+ - \text{C}_5\text{H}_6$). RT = 5.97, impurity, 124.1 (M^+). RT = 6.38, N-NB-OMe, 124.1 ($\text{C}_8\text{H}_{12}\text{O}$, M^+), 125.1 (MH^+), 92.0 ($\text{MH}^+ - \text{CH}_3\text{O}$), 58.0 ($\text{MH}^+ - \text{C}_5\text{H}_6$), 66 ($\text{M}^+ - \text{C}_3\text{H}_6\text{O}$).

IR (KBr disc, cm^{-1}): 3060 (olefinic C-H stretching), 2980 - 2867 (saturated C-H stretching), 1099 (C-O stretching).

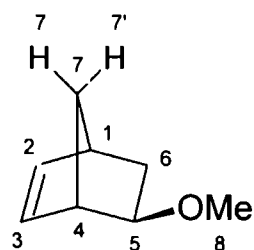


Figure 4.22. Assignment of C and H atoms in X-NB-OMe.

4.4.4.17 Synthesis and Characterisation of *endo*-5-Methyl Acetate-2-norbornene

The synthesis of this monomer, figure 4.23, is described in general synthesis, section 4.3.3.1. The crude monomer was purified by distillation under reduced pressure (95°C , 5 mbar) to give the pure product, as a clear, colourless oil, in 90% yield. The monomer was characterised by ^1H NMR, ^{13}C NMR, GCMS and IR. The numbering system shown in figure 4.23 was used for the assignment of the NMR signals.

^1H NMR (500 MHz, CDCl_3): δ (ppm) = 6.09 (dd, 1H, $J = 5.63$ & 3.03 , H_2), 5.87 (dd, 1H, $J = 5.63$ & 2.82 , H_3), 3.78 (dd, 1H, $J = 10.74$ & 6.65 , H_8), 3.58 (dd, 1H, $J = 10.74$ & 9.66 , H_8), 2.81 (b, 1H, H_4), 2.75 (b, 1H, H_1), 2.31 (m, 1H, H_5), 1.98 (s, 3H, H_{10}), 1.77 (ddd, 1H, $J = 11.74$ & 9.21 & 3.84 , H_7), 1.38 (m, 1H, $J = 8.23$, H_6), 1.18 (m, 1H, $J = 8.23$, H_6), 0.48 (ddd, 1H, $J = 11.73$ & 4.44 & 2.65 , H_7).

^{13}C NMR (125.7 MHz, CDCl_3): δ (ppm) = 171.41 (C_9), 137.85 (C_2), 132.39 (C_3), 68.19 (C_8), 49.62 (C_6), 44.09 (C_4), 42.44 (C_1), 37.99 (C_5), 29.23 (C_7), 21.27 (C_{10}).

GCMS (EI⁺): RT = 11.69, N-NB-CH₂OAc, 107.2 (M⁺-OAc), 65.9 (M⁺-C₅H₈O₂).

IR (KBr disc, cm⁻¹): 3060 (olefinic C-H stretching), 2980 - 2867 (saturated C-H stretching), 1736 (asymmetric and symmetric C=O stretching).

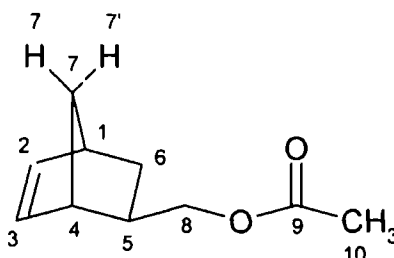


Figure 4.23. Assignment of C and H atoms in N-NB-CH₂OAc.

4.4.4.18 Synthesis and Characterisation of *exo*-5-Methyl Acetate-2-norbornene

The synthesis of this monomer, figure 4.24, is described in general synthesis, section 4.3.3.1. The crude monomer was purified by distillation under reduced pressure (90°C, 5 mbar) to give the pure product, as a clear, colourless oil, in 90% yield. The monomer was characterised by ¹H NMR, ¹³C NMR, GCMS and IR. The numbering system shown in figure 4.24 was used for the assignment of the NMR signals.

¹H NMR (500 MHz, CDCl₃): δ (ppm) = 6.07 (m, 2H, H_{2&3}), 4.12 (dd, 1H, *J* = 10.92 & 6.43, H₈), 3.93 (dd, 1H, *J* = 10.92 & 9.47, H₈), 2.82 (b, 1H, H₄), 2.68 (b, 1H, H₁), 2.05 (s, 3H, H₁₀), 1.70 (m, 1H, H₅), 1.36-1.22 (m, 3H, H_{6&7}), 1.13 (ddd, 1H, H₇).

¹³C NMR (125.7 MHz, CDCl₃): δ (ppm) = 171.34 (C₉), 137.09 (C₂), 136.39 (C₃), 68.77 (C₈), 45.10 (C₆), 43.82 (C₁), 41.75 (C₄), 38.10 (C₅), 29.76 (C₇), 21.21 (C₁₀).

GCMS (EI⁺): RT = 11.63, X-NB-CH₂OAc, 166.0 (C₁₀H₁₄O₂, M⁺), 124.1, 107.1 (M⁺-OAc).

IR (KBr disc, cm⁻¹): 3060 (olefinic C-H stretching), 2980 - 2867 (saturated C-H stretching), 1736 (asymmetric and symmetric C=O stretching).

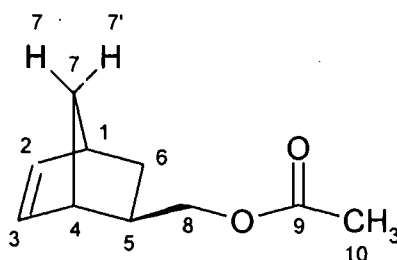


Figure 4.24. Assignment of C and H atoms in X-NB-CH₂OAc.

4.4.4.19 Synthesis and Characterisation of *endo/exo*-5-Ethyl Methoxy-2-norbornene

The monomer, figure 4.25, was synthesised from N/X-NBCH₂CH₂OH, as described in general synthesis, section 4.3.3.3. The crude monomer was purified by distillation under reduced pressure (70°C, 50 mbar) to give the pure product, as a clear, colourless oil, in 50% yield. The monomer was characterised by ¹H NMR, ¹³C NMR, GCMS and IR. The numbering system shown in figure 4.25 was used for the assignment of the NMR signals.

¹H NMR (500 MHz, CDCl₃): δ (ppm) = 6.13 (dd, 0.75H, *J* = 5.60 & 2.98, H₂), 6.09 (dd, 0.25H, *J* = 5.62 & 3.06, H_{2,X}), 6.01 (dd, 0.25H, *J* = 5.62 & 2.98, H_{3,X}), 5.93 (dd, 0.75H, *J* = 5.60 & 2.82, H_{3,N}), 3.50-3.35 (m, 2H, H₉), 3.34 (s, 0.75H, H_{10,X}), 3.33 (s, 2.25H, H_{10,N}), 2.81 (b, 0.25H, H_{4,X}), 2.77 (b, 1.50H, H_{1&4,N}), 2.54 (b, 0.25H, H_{1,X}), 2.09 (m, 0.75H, H_{5,N}), 1.88 (m, 0.75H, H_{7,N}), 1.70-1.10 (m, 2.50H, H_{6,X&8&H5,X}), 1.40 (m, 0.75H, H_{6,N}), 1.32 (m, 0.25H, H_{7,X}), 1.23 (m, 0.75H, H_{6,N}), 1.13 (m, 0.25H, H_{7,X}), 0.53 (m, 0.75H, H_{7,N}).

¹³C NMR (125.7 MHz, CDCl₃): δ (ppm) = 137.37 (C_{2,N}), 136.97 (C_{2,X}), 136.49 (C_{3,X}), 132.58 (C_{3,N}), 72.51 (C_{9,X}), 72.38 (C_{9,N}), 58.85 (C_{10,X}), 58.81 (C_{10,N}), 49.80 (C_{6,N}), 46.66 (C_{1,X}), 45.75 (C_{1&4,N}), 45.46 (C_{6,X}), 42.74 (C_{1&4,N}), 42.16 (C_{4,X}), 36.59 (C_{5,X}), 35.52 (C_{8,X}), 35.47 (C_{5,N}), 34.82 (C_{8,N}), 33.24 (C_{7,X}), 32.43 (C_{7,N}).

GCMS (EI⁺): RT = 10.29, N-NB-CH₂CH₂OMe, 152.0 (C₁₀H₁₆O, M⁺), 119.9 (MH⁺ -OMe). RT = 10.35, X-NB-CH₂CH₂OMe, 152.0 (C₁₀H₁₆O, M⁺), 119.9 (MH⁺ -OMe).

IR (KBr disc, cm⁻¹): 3060 (olefinic C-H stretching), 2980 - 2867 (saturated C-H stretching), 1099 (C-O stretching).

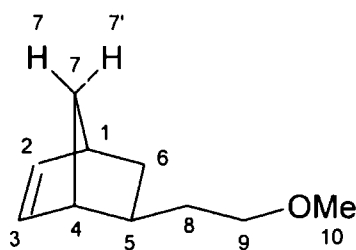


Figure 4.25. Assignment of C and H atoms in N/X-NB-(CH₂)₂OMe.

4.4.4.20 Synthesis and Characterisation of *endo/exo*-5-Ethyl Acetate-2-norbornene

The monomer, figure 4.26, was synthesised from N/X-NB(CH₂)₂OAc, as described in general synthesis, section 4.3.3.1. The crude monomer was purified by distillation under reduced pressure (80°C, 4 mbar) to give the pure product, as a clear, colourless oil, in 90% yield. The monomer was characterised by ¹H NMR, ¹³C NMR, GCMS and IR. The numbering system shown in figure 4.26 was used for the assignment of the NMR signals.

Characterisation of N-NB(CH₂)₂OAc.

¹H NMR (500 MHz, CDCl₃): δ (ppm) = 6.14 (dd, 1H, *J* = 5.65 & 2.99, H₂), 5.93 (dd, 1H, *J* = 5.65 & 2.83, H₃), 4.05 (bs, 2H, H₉), 2.78 (m, 2H, H_{1&4}), 2.06 (m, 1H, H₅), 2.05 (s, 3H, H₁₁), 1.87 (ddd, 1H, *J* = 3.78 & 9.06 & 11.34, H₇), 1.46 (m, 1H, H₈), 1.41 (m, 1H, H₆), 1.39 (m, 1H, H₈), 1.23 (bd, 1H, *J* = 8.14, H₆), 0.54 (ddd, 1H, *J* = 2.71 & 4.24 & 11.34, H₇).

¹³C NMR (125.7 MHz, CDCl₃): δ (ppm) = 171.47 (C₁₁), 137.57 (C₂), 132.40 (C₃), 64.28 (C₉), 49.79 (C₆), 45.69 (C_{1&4}), 42.69 (C_{1&4}), 35.56 (C₅), 33.71 (C₈), 32.36 (C₇), 21.31 (C₁₁).

GCMS (EI⁺): RT = 13.18, N-NB-(CH₂)₂OMe, 180.0 (C₁₁H₁₆O₂, M⁺).

IR (KBr disc, cm⁻¹): 3060 (olefinic C-H stretching), 2980 - 2867 (saturated C-H stretching), 1736 (asymmetric and symmetric C=O stretching).

Characterisation of X-NB(CH₂)₂OAc.

¹H NMR (500 MHz, CDCl₃): δ (ppm) = 6.08 (dd, 1H, *J* = 5.66 & 3.17, H₂), 6.03 (dd, 1H, *J* = 5.66 & 2.90, H₃), 4.12 (m, 2H, H₉), 3.83 (bs, 1H, H₄), 2.55 (bs, 1H, H₁), 2.05 (s, 3H, H₁₁),

1.75 (m, 1H, H₈), 1.69 (m, 1H, H₈), 1.41 (m, 1H, H₅), 1.33 (m, 2H, H₆), 1.30 (m, 1H, H₇), 1.14 (m, 1H, J = 11.42, H₇).

¹³C NMR (125.7 MHz, CDCl₃): δ (ppm) = 171.46 (C₁₁), 136.82 (C₂), 136.61 (C₃), 64.24 (C₉), 46.55 (C₄), 45.45 (C₆), 42.16 (C₁), 35.50 (C₅), 35.42 (C₈), 33.08 (C₇), 21.29 (C₁₁).

GCMS (EI⁺): RT = 13.18, X-NB-(CH₂)₂OMe, 180.0 (C₁₁H₁₆O₂, M⁺).

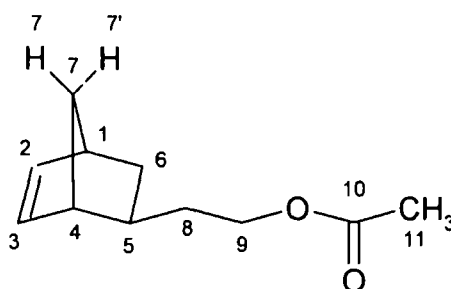


Figure 4.26. Assignment of C and H atoms in N/X-NB-(CH₂)₂OAc.

4.4.4.21 Synthesis and Characterisation of *exo*-5-Benzyloxy-2-norbornene

X-NB-OH (4.20 g, 38.2 mmol) in THF (20 mL) was added via cannula to a flame dried flask containing NaH (1.34 g, 55.8 mmol) in THF (20 mL), under nitrogen, at 0°C. The reaction mixture was stirred at 50°C for 3 hrs and then allowed to cool. Benzyl bromide (13.2 mL, 111.0 mmol) was added to the reaction mixture via cannula and the mixture stirred for 24 hrs. The reaction was quenched with an aqueous solution of NH₄Cl (50 mL), and the organics extracted with diethyl ether (4 × 100 mL). The organics were washed with brine (500 mL) and dried under MgSO₄.² The solvent was removed on a rotary evaporator and the crude oil product distilled under reduced pressure (110°C, 70 mbar), to give clear colourless oil (7.2 g, 36.0 mmol, 94 % yield). The monomer was characterised by ¹H NMR, ¹³C NMR and GCMS. The numbering system shown in figure 4.27 was used for the assignment of the NMR signals.

¹H NMR (400.0 MHz, CDCl₃): δ (ppm) = 6.37 (m, 5H, H_{Ph}), 6.23 (dd, 1H, J = 5.71 & 2.86, H_{2&3}), 5.96 (dd, 1H, J = 5.71 & 3.29, H_{2&3}), 4.57 (m, 2H, H₈), 3.64 (m, 1H), 2.99 (bs, 1H, H_{1&4}), 2.86 (bs, 1H, H_{1&4}), 1.81 (m, 1H, H₆), 1.60 (m, 2H), 1.49 (m, 1H, H₇).

^{13}C NMR (125.7 MHz, CDCl_3): δ (ppm) = 140.99, 139.20, 133.46, 128.62, 127.85, 127.68, 80.32, 71.44, 46.76, 46.34, 40.71, 34.78.

GCMS (EI^+): RT = 13.42, X-NB- OCH_2Ph , 199.9 ($\text{C}_{14}\text{H}_{16}\text{O}$, M^+).

IR (KBr disc, cm^{-1}): 3060 (olefinic C-H stretching), 2980 - 2867 (saturated C-H stretching), 1099 (C-O stretching).

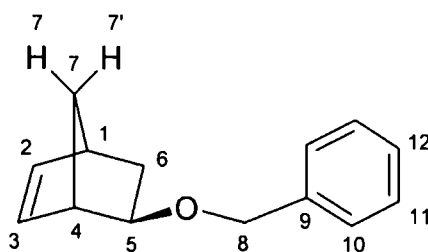


Figure 4.27. Assignment of C and H atoms in X-NB- OCH_2Ph .

4.4.4.22 Synthesis and Characterisation of *exo*-5-(11-Phenyl Benzyloxy)-2-norbornene

X-NB-OH (4.20 g, 38.2 mmol) in THF (20 mL) was added via cannula to a flame dried flask containing NaH (1.34 g, 55.8 mmol) in THF (20 mL), under nitrogen, at 0°C . The reaction mixture was stirred at 50°C for 3 hrs and then allowed to cool. 2-phenylbenzyl bromide (25.0 g, 101.0 mmol) was added to the reaction mixture via cannula and the mixture stirred for 48 hrs. The reaction was quenched with an aqueous solution of NH_4Cl (50 mL), and the organics extracted with diethyl ether (4×100 mL). The organics were washed with brine (500 mL) and dried under MgSO_4 .² The solvent was removed on a rotary evaporator and the crude oil product purified via silica column chromatography using hexanes as solvent ($R_f = 0.2$), to give cloudy colourless oil (9.52 g, 34.5 mmol, 90 % yield). The monomer was characterised by ^1H NMR and GCMS. The numbering system shown in figure 4.28 was used for the assignment of the NMR signals.

^1H NMR (400.0 MHz, CDCl_3): δ (ppm) = 7.60-7.20 (m, 9H, H_{Ph}), 6.10 (m, 1H, $\text{H}_{2\&3}$), 5.80 (dd, 1H, $\text{H}_{2\&3}$), 4.37 (m, 2H, H_8), 3.42 (m, 1H), 2.78 (m, 2H, $\text{H}_{1\&4}$), 1.70-1.20 (m, 3H), 0.80 (m, 1H, H_7).

GCMS (EI⁺): RT =21.02, X-NB-OCH₂C₆H₄Ph, 276.1 (C₁₄H₁₆O, M⁺).

IR (KBr disc, cm⁻¹): 3060 (olefinic C-H stretching), 2980 - 2867 (saturated C-H stretching), 1099 (C-O stretching).

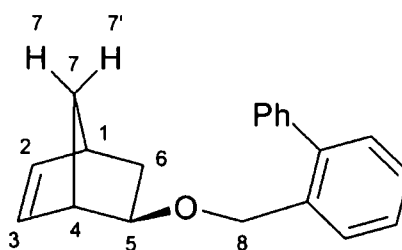


Figure 4.28. Assignment of C and H atoms in X-NB-OCH₂C₆H₄Ph.

4.4.4.23 Synthesis and Characterisation of *exo*-5-(12-Bromo Benzyloxy)-2-norbornene

X-NB-OH (4.20 g, 38.2 mmol) in THF (20 mL) was added via cannula to a flame dried flask containing NaH (1.34 g, 55.8 mmol) in THF (20 mL), under nitrogen, at 0°C. The reaction mixture was stirred at 50°C for 3 hrs and then allowed to cool. 4-bromobenzyl bromide (25.0 g, 100.0 mmol) was added to the reaction mixture via cannula and the mixture stirred for 48 hrs. The reaction was quenched with an aqueous solution of NH₄Cl (50 mL), and the organics extracted with diethyl ether (4 × 100 mL). The organics were washed with brine (500 mL) and dried under MgSO₄.² The solvent was removed on a rotary evaporator and the crude oil product purified via silica column chromatography using hexanes as solvent (R_f = 0.1), to give cloudy colourless oil (9.50 g, 34.0 mmol, 89 % yield). The monomer was characterised by ¹H NMR and GCMS. The numbering system shown in figure 4.29, was used for the assignment of the NMR signals.

¹H NMR (400.0 MHz, CDCl₃): δ (ppm) = 7.46 (m, 2H, *J* = 8.41, H_{Ph}), 6.23 (m, 2H, *J* = 8.41, H_{Ph}), 6.19 (dd, 1H, *J* = 5.67 & 2.90, H_{2&3}), 5.92 (dd, 1H, *J* = 5.76 & 3.28, H_{2&3}), 4.48 (m, 2H, H₈), 3.58 (m, 1H), 2.93 (bs, 1H, H_{1&4}), 2.82 (bs, 1H, H_{1&4}), 1.72 (m, 1H), 1.57 (m, 2H), 1.40 (m, 1H).

GCMS (EI⁺): RT =18.25, X-NB-OCH₂C₆H₄Br, 180.0 (C₁₄H₁₅OBr, M⁺).

IR (KBr disc, cm^{-1}): 3060 (olefinic C-H stretching), 2980 - 2867 (saturated C-H stretching), 1099 (C-O stretching).

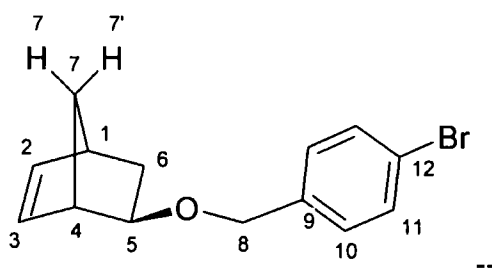


Figure 4.29. Assignment of C and H atoms in X-NB-OBzBr.

4.4.5 NMR Scale Addition Polymerisation Reactions

All addition polymerisation reactions were prepared in a Braun glove box under an inert atmosphere. Typically, the relevant palladium complex (3.60×10^{-6} mole, 1 equivalent) was dissolved in deuterated solvents. The relevant monomer (1.80×10^{-4} mole, 50 equivalents) was then dissolved in the initiator solution. The solution was transferred to an NMR tube fitted with a Young's tap, allowing the vessel to be closed under a nitrogen atmosphere. The reactions were monitored using arrayed ^1H spectroscopy. In all cases, the integrated intensities of the monomer vinyl signals (polymerisation) and initiator Pd-H signal (initiation) were measured against the previous NMR integrations.

4.4.6 Polymerisation of Functionalised Norbornenes Using Pd1388

The NMR scale polymerisation reactions were run as described in the general section 4.3.5. The experimental conditions and polymerisation rates are shown in table 4.4.

Table 4.4. Polymerisations of 50 Monomer: 1 **Pd1388** (5.0 mg, 3.60×10^{-6} mol).

Monomer	Temp (°C)	Solvent	k_p (N/X) (s ⁻¹)	k_p (N) (s ⁻¹)	k_p (X) (s ⁻¹)
X-NB-OAc (27.4 mg, 1.80×10^{-4} mol)	70	Benzene- <i>d</i> ₆	-	-	Termination
N-NB-OAc (27.4 mg, 1.80×10^{-4} mol)	70	Benzene- <i>d</i> ₆	-	0.82×10^{-4}	-
X-NB-OMe (22.3 mg, 1.80×10^{-4} mol)	70	Benzene- <i>d</i> ₆	-	-	6.68×10^{-4}
X-NB-CH ₂ OMe (24.8 mg, 1.80×10^{-4} mol)	70	Benzene- <i>d</i> ₆	-	-	15.35×10^{-4}
N-NB-CH ₂ OMe (24.8 mg, 1.80×10^{-4} mol)	70	Benzene- <i>d</i> ₆	-	3.50×10^{-4}	-
X-NBCH ₂ OAc (29.9 mg, 1.80×10^{-4} mol)	70	Benzene- <i>d</i> ₆	-	-	4.70×10^{-4}
N-NBCH ₂ OAc (29.9 mg, 1.80×10^{-4} mol)	70	Benzene- <i>d</i> ₆	-	1.66×10^{-4}	-
N/X-NB(CH ₂) ₂ OMe (27.4 mg, 1.80×10^{-4} mol)	70	Benzene- <i>d</i> ₆	19.44×10^{-4}	13.66×10^{-4}	24.99×10^{-4}
N/X-NB(CH ₂) ₂ OAc (32.4 mg, 1.80×10^{-4} mol)	70	Benzene- <i>d</i> ₆	17.88×10^{-4}	16.26×10^{-4}	32.19×10^{-4}
X-TD-OAc (39.3 mg, 1.80×10^{-4} mol)	70	Benzene- <i>d</i> ₆	-	-	Termination
N-TD-OAc (39.3 mg, 1.80×10^{-4} mol)	70	Benzene- <i>d</i> ₆	-	-	4.5×10^{-5}
X-NB-OAc (27.4 mg, 1.80×10^{-4} mol)	50	TCE- <i>d</i> ₂	-	-	Termination
N-NB-OAc (27.4 mg, 1.80×10^{-4} mol)	50	TCE- <i>d</i> ₂	-	7.6×10^{-5}	-
X-NB-OMe (22.3 mg, 1.80×10^{-4} mol)	50	TCE- <i>d</i> ₂	-	-	5.22×10^{-4}
X-NB-CH ₂ OMe (24.8 mg, 1.80×10^{-4} mol)	50	TCE- <i>d</i> ₂	-	-	17.54×10^{-4}

Monomer	Temp (°C)	Solvent	$k_p(N/X)$ (s ⁻¹)	$k_p(N)$ (s ⁻¹)	$k_p(X)$ (s ⁻¹)
N-NB-CH ₂ OMe (24.8 mg, 1.80×10^{-4} mol)	50	TCE- <i>d</i> ₂	-	1.50×10^{-4}	-
X-NBCH ₂ OAc (29.9 mg, 1.80×10^{-4} mol)	50	TCE- <i>d</i> ₂	-	-	3.11×10^{-4}
N-NBCH ₂ OAc (29.9 mg, 1.80×10^{-4} mol)	50	TCE- <i>d</i> ₂	-	4.7×10^{-5}	-
N/X-NB(CH ₂) ₂ OMe (27.4 mg, 1.80×10^{-4} mol)	50	TCE- <i>d</i> ₂	7.39×10^{-4}	6.79×10^{-4}	7.97×10^{-3}
X-NB-OCH ₂ Ph (36.0 mg, 1.80×10^{-4} mol)	50	Benzene- <i>d</i> ₆	-	-	4.8×10^{-5}
X-NB-OCH ₂ C ₆ H ₄ Ph (49.7 mg, 1.80×10^{-4} mol)	50	Benzene- <i>d</i> ₆	-	-	3.6×10^{-5}
X-NB-OCH ₂ C ₆ H ₄ Br (50.2 mg, 1.80×10^{-4} mol)	50	Benzene- <i>d</i> ₆	-	-	20×10^{-5}

4.5 References

- ¹ Feiring, A. E.; Crawford, M. K.; Farnham, W. B.; French, R. H.; Leffew, K. W.; Petrov, V. A.; Schadt, F. L.; Wheland, R. C.; Zumstag, F. C. *J. Fluorine Chem.* **2003**, *122*, 11 - 16.
- ² Mayo, P.; Orlova, G.; Goddard, J. D.; Tam, W. *J. Org. Chem.* **2001**, *66*, 5182 - 5191.
- ³ Wang, G. T.; Wang, S.; Chen, Y.; Gentles, R.; Sowin, T. *J. Org. Chem.* **2001**, *66* (6), 2052 - 2056.
- ⁴ Oppolzer, W.; Chapuls, C.; Dupuld, D.; Guo, M. *Helvetica Chimica Acta* **1985**, *68*, 2104.
- ⁵ Lynn, D. M.; Kanaoka, S.; Grubbs, R. H. *J. Am. Chem. Soc.* **1996**, *118*, 784.
- ⁶ Williams, R. V.; Sung, C. L. A. *J. Chem. Soc., Chem. Commun.* **1987**, 590.
- ⁷ Williams, R. V.; Todime, M. M. R.; Enemark, P. *J. Org. Chem.* **1993**, *58*, 6740 - 6744.

Chapter 5

Investigation of Family of Monomers Based on *endo*-5-Methyl-*exo*-5-carboxylic Acid-2-norbornene

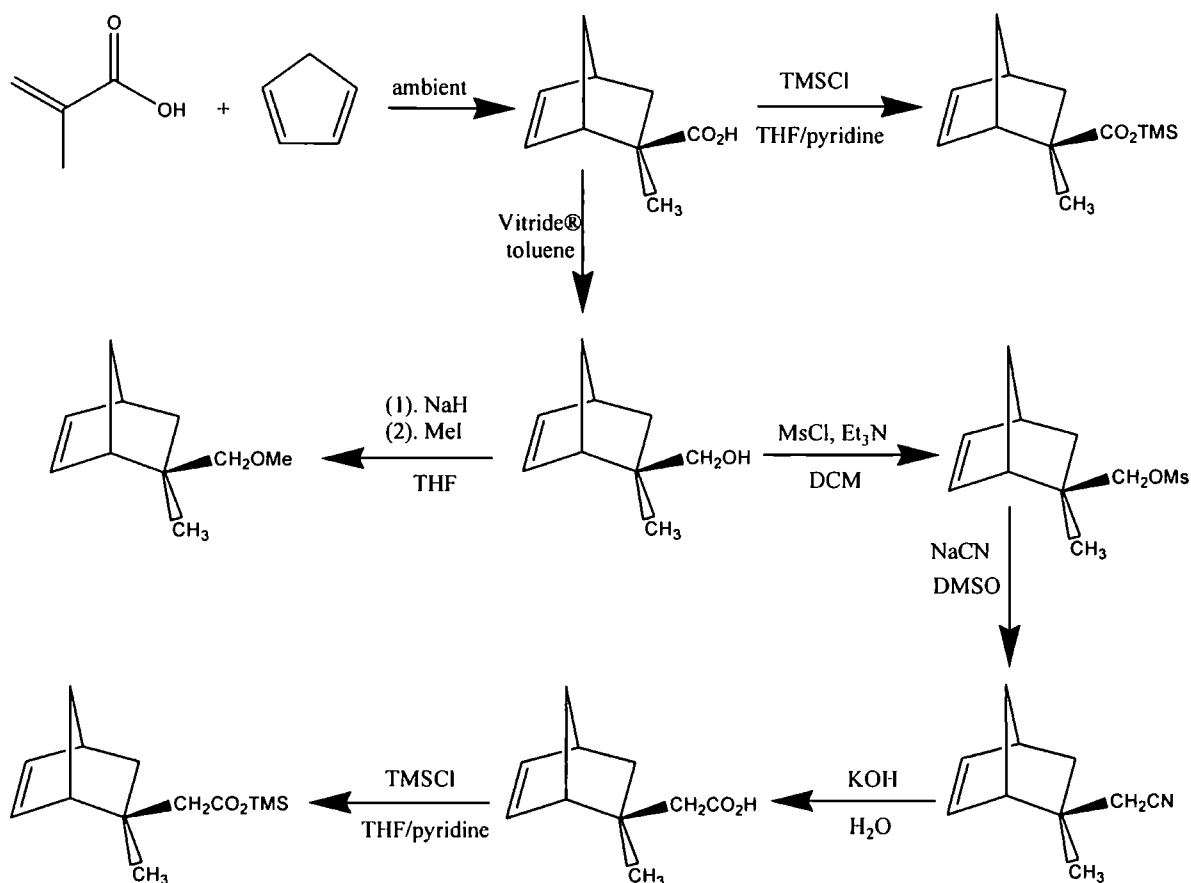
5.1 Introduction

Following on from the findings in Chapter 3, it is clear that new methods for the preparation of single regioisomers of functionalised norbornenes that display high polymerisation activity are necessary. It was also envisaged that in order to create co-polymers with excellent homogeneity it would be useful for the polymerisation rates of the co-monomers to be normalised. This normalisation of polymerisation rates would only be possible through a reduction or masking of the electronic effect of norbornene functional groups. The convenient synthesis and ease of elaboration of NB(N-Me)(X-CO₂H) makes this an excellent base from which to create new high activity monomers.

5.2 Results and Discussion

5.2.1 Synthesis Tree

The synthesis tree below proposed for the synthesis of the N-Me family of norbornene derivatives will be discussed in the following sections.



Scheme 5.1

5.2.2 Synthesis and Characterisation of *endo*-5-Methyl-*exo*-5-carboxylic Acid-2-norbornene

The Diels-Alder cycloaddition reaction of cyclopentadiene and methacrylic acid is well known to produce a mixture of X- and N-isomers, with the ratio dependent on the reaction

conditions.^{1, 2} A pure sample of NB(N-Me)(X-CO₂H) can be obtained in a large-scale preparation when equimolar amounts of methacrylic acid and freshly cracked cyclopentadiene are stirred for 5 days. The desired X-CO₂H isomer precipitates directly from the reaction mixture, needing filtration and washing with cold pentane to give the pure product, NB(N-Me)(X-CO₂H), in 33% yield, scheme 5.1.³ The products regiochemistry was confirmed using ¹H, ¹³C, HSQC, HMBC and NOESY NMR spectroscopy. Single crystals of NB(N-Me)(X-CO₂H) were grown via slow recrystallisation from ethyl acetate at ambient temperature and an X-ray structural diagram with full structural refinement produced using single-crystal X-ray diffraction, figure 5.1.

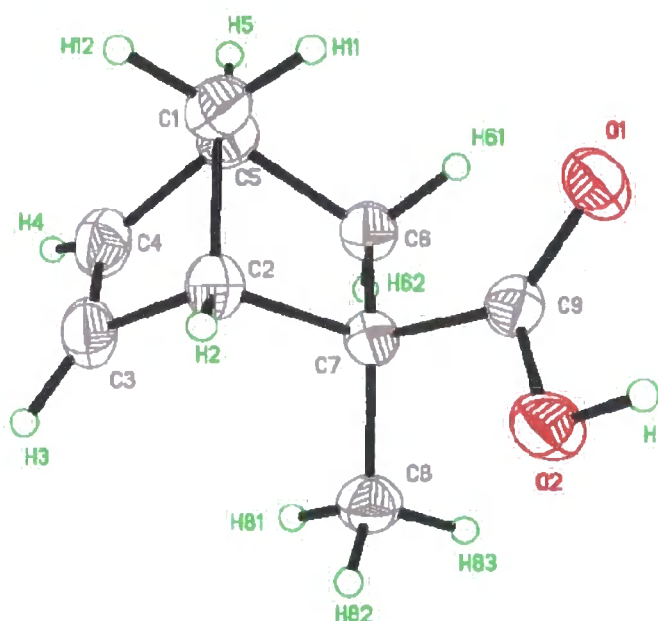


Figure 5.1. X-ray structural diagram of NB(N-Me)(X-CO₂H).

5.2.3 Synthesis of the Trimethylsilyl Carboxylate Functionalised Norbornenes (NB(N-Me)(X-(CH₂)_nCO₂TMS))

The NB(CH₂)_nCO₂TMS monomers are readily formed from the base catalysed reaction of an excess of TMS-Cl, with the corresponding acid functionalised norbornene, scheme 5.1. The pure products were obtained via a very efficient yet careful distillation under reduced pressure. Moisture had to be kept away from the reagents during production and purification to prevent de-protection of the acid functionality.

5.2.4 Synthesis of *endo*-5-Methyl-*exo*-5-methyl Hydroxy-2-norbornene

The NB(N-Me)(X-CH₂OH) was prepared from the reduction of the acid using the standard Vitride[®] reducing agent, scheme 5.1. The reaction proceeded very cleanly in high yield and further purification beyond standard work-up was not needed before further derivatisation.

5.2.5 Synthesis of *endo*-5-Methyl-*exo*-5-methyl Methoxy-2-norbornene

The Williamson ether synthesis was used to prepare the NB(N-Me)(X-CH₂OMe) in good yield (55%), scheme 5.1. The products were purified using distillation under reduced pressure to give a clear, colourless oil.

5.2.6 Synthesis of *endo*-5-Methyl-*exo*-5-methyl Carboxylic Acid-2-norbornene

Standard chain extension procedures were employed for the synthesis of NB(N-Me)(X-CH₂CO₂H), scheme 5.1.

The NB(N-Me)(X-CH₂OH) was converted into *endo*-5-methyl-*exo*-5-methoxy-mesylate-2-norbornene (NB(N-Me)(X-CH₂OMs)) using methane sulfonyl chloride in high yield and purity (> 90%). This mesylate product was sufficiently pure to be used in the next reaction step without further purification. The mesylate product was shown to have a lower thermal stability than the similar mesylate substituted norbornene, *endo/exo*-5-methoxy-mesylate-2-norbornene (N/X-NBCH₂OMs), decomposing in a highly exothermic manner at approximately 154°C (figure 5.2), compared with 194°C (figure 5.3).

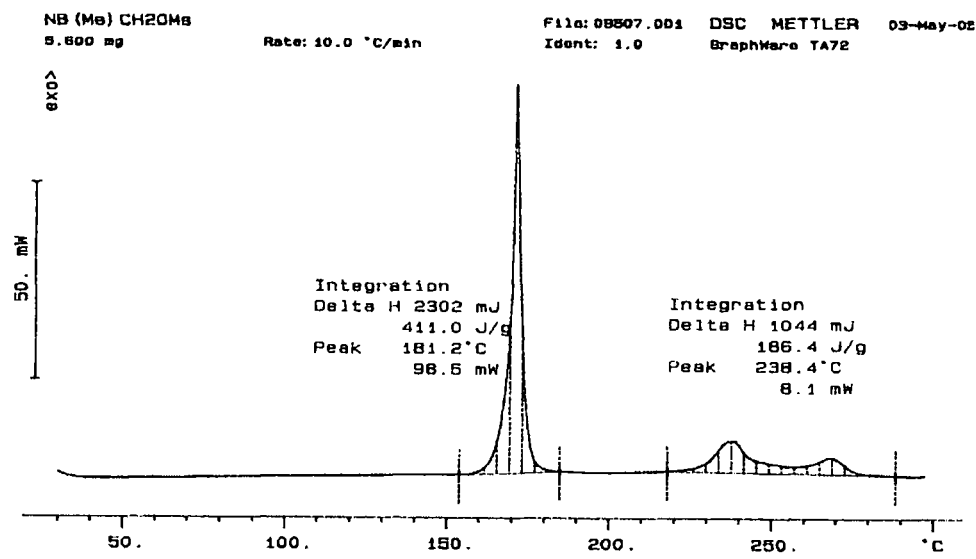


Figure 5.2. DSC trace for NB(N-Me)(X-CH₂OMs).

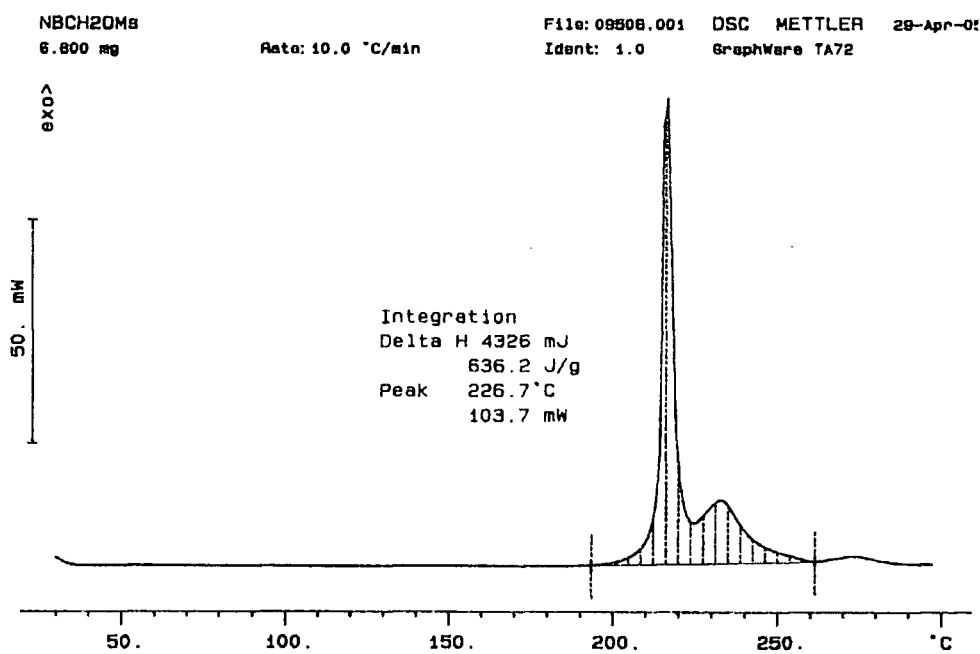


Figure 5.3. DSC trace for N/X-NBCH₂OMs

The *endo*-5-methyl-*exo*-5-cyanomethyl-2-norbornene (NB(N-Me)(X-CH₂CN)) was prepared via the reaction of the mesylate compound with sodium cyanide at 80°C in DMSO. Care must be taken to keep all reaction mixtures and wastes basic at all times since cyanide salts can produce highly toxic hydrogen cyanide in acidic conditions. The substitution of the –OMs group with –CN proved to be very slow when compared with similar reactions, with only 70% conversion after 72 hours. The addition of extra sodium cyanide and additional

heating failed to drive the reaction to completion, so work-up and purification was attempted at this stage. This stabilisation of the mesylate product with respect to substitution must be related to the electronic or steric effect of the N-Me norbornene substituent. The work-up of this reaction is particularly laborious since the DMSO makes separation of aqueous and organic layers very slow. The crude black nitrile product was purified via silica column chromatography, eluting with ethyl acetate and hexanes, to give a yellow oil, in 47% yield.

The NB(N-Me)(X-CH₂CN) was oxidised using aqueous potassium hydroxide and was recovered using standard techniques, to give the *endo*-5-methyl-*exo*-5-methyl carboxylic acid-2-norbornene (NB(N-Me)(X-CH₂CO₂H)) as a white solid, in good yield.

5.2.7 Attempted Synthesis of *endo*-5-Methyl-*exo*-5-methylmagnesium Bromide-2-norbornene

The *endo*-5-methyl-*exo*-5-bromomethyl-2-norbornene (NB(N-Me)(X-CH₂Br)) was produced from the corresponding X-CH₂OMs using LiBr in 2-pentanone, in good yield. The monomer was purified using silica column chromatography, eluting with cyclohexane.

The synthesis of the -MgBr, Grignard reagent was attempted using magnesium shavings in THF and diethyl ether, without success. This is possibly linked to the steric or electronic effect of the N-Me group or the radical rearrangement of the polycyclic ring under the reaction conditions employed.

5.2.8 Polymerisation of Monomers

In order to discuss the polymerisation characteristics of this interesting family of monomers it is necessary to compare their activity to analogous monomers with the same functionality but without the N-Me group. It is expected that the N-Me group within this family of monomers will affect the polymerisation activity through both steric and electronic effects, meaning that its influence may be variable depending on the nature of the X-substituents, steric size and electronic nature.

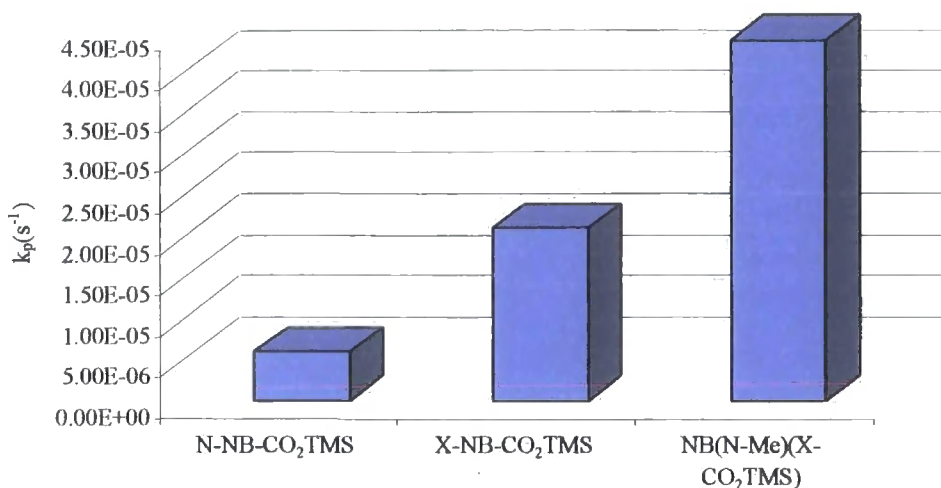


Figure 5.4. Polymerisation data for 50 monomer : 1 **Pd1388**, at 70°C in benzene-*d*₆.

The most surprising results were displayed by the NB(N-Me)(X-(CH₂)_nCO₂TMS) family of monomers, with the N-Me functionality seemingly increasing the polymerisation activity of the -CO₂TMS monomers, when compared with their analogous N- and X- functionalised monomers, figures 5.4 and 5.5.

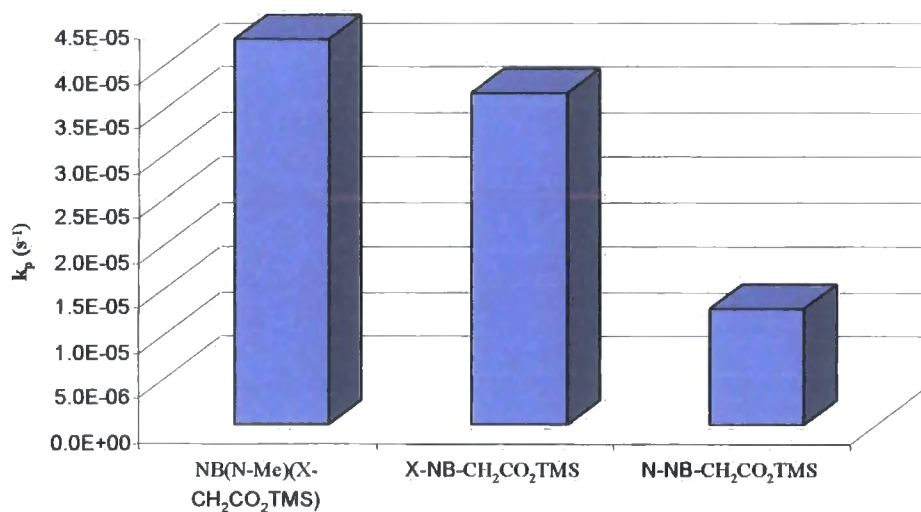


Figure 5.5. Polymerisation data for 50 monomer : 1 **Pd1388**, at 70°C in benzene-*d*₆.

From figures 5.4 and 5.5, it seems that the effect making the N-Me functionalised monomers more active than their analogous N-H monomers, is decreasing as the -CO₂TMS functionality is spaced away from the norbornene framework. It is not possible to separately

assign these rate differences to electronic or steric effects. The effect shown opposes the expected decrease in activity for monomers containing an N-functional group discussed in previous chapters.

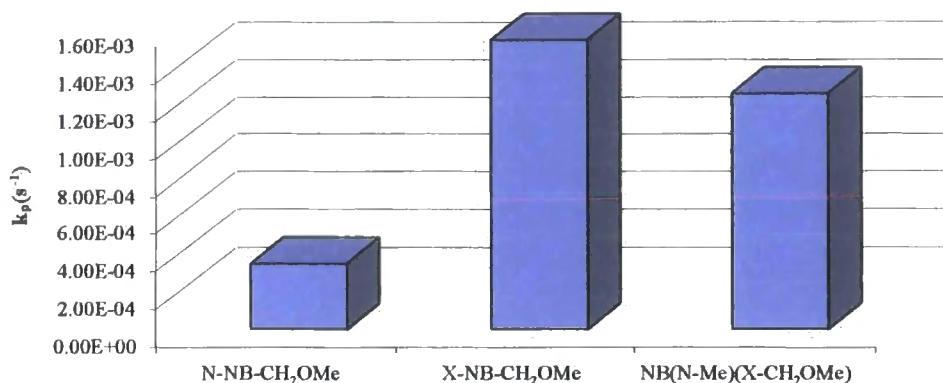


Figure 5.6. Polymerisation data for 50 monomer : 1 **Pd1388**, at 70°C in benzene-*d*₆.

The NB(N-Me)(X-CH₂OMe) and NB(N-Me)(X-CH₂HFA) monomers, figure 5.6 and 5.7 respectively, both show a level of activity that is only slightly lower than their analogous X-NBCH₂FG counterparts, which again is surprising considering the expected deactivating steric effect of the N-Me group.

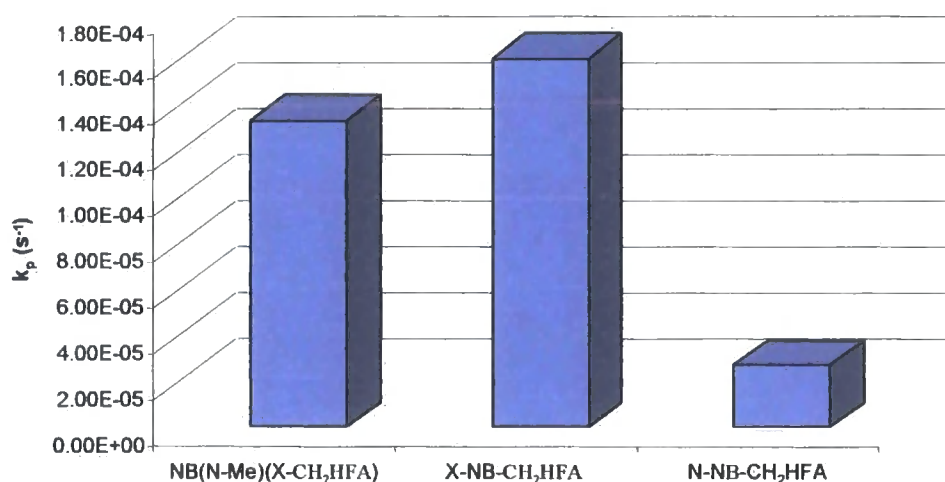


Figure 5.7. Polymerisation data for 50 monomer : 1 **Pd1388**, at 70°C in benzene-*d*₆.

5.3 Conclusions

Although the aim of normalising the polymerisation rates of all functionalised monomers cannot be achieved by using this particular family of monomers, the polymerisation results displayed do indicate that they have the potential to address the need for easily synthesised, highly active, single isomer functionalised-norbornene monomers. The N-Me group within this family of monomers appears to affect the polymerisation activity through both steric and electronic effects, meaning that its influence is variable depending on the nature of the X-substituents, steric size and electronic nature.

5.4 Experimental

5.4.1 Materials

The palladium catalyst, $[\text{Pd}(\text{PCy}_3)_2(\text{NCCH}_3)(\text{H})][\text{B}(\text{C}_6\text{F}_5)_4]$ (**Pd1388**) and norbornene monomer, NB(N-Me)(X-CH₂HFA) were supplied by Promerus LLC and used without further purification. All liquid monomers were degassed by freeze-thaw-pump cycles before being taken into the glove box. Tetrachloroethane-*d*₂ and benzene-*d*₆ were used as supplied in pre-sealed ampoules and subsequently kept refrigerated in a glove box. All other solvents (toluene, tetrahydrofuran, chloroform, diethyl ether, dimethyl sulfoxide, hexanes, ethyl acetate, dichloromethane and 2-pentanone) were used without prior purification. The following reagents were purchased from Sigma Aldrich and used without further purification: lithium bromide, sodium cyanide, hydrochloric acid, potassium hydroxide, sodium hydroxide, magnesium sulphate, methyl iodide, sodium hydride, ammonium chloride, trimethyl chloro silane, potassium bicarbonate, methacrylic acid, triethylamine, methane sulfonyl chloride, sodium bis(2-methoxyethoxy)aluminum hydride (Vitride®) and silica.

5.4.2 Instrumentation and Measurements

5.4.2.1 Nuclear Magnetic Resonance

¹H NMR spectra were recorded on a Varian Mercury 400 or a Varian Inova 500 using deuteriated solvent lock. Chemical shifts are quoted in ppm, relative to tetramethylsilane (TMS), as the internal reference. ³¹P NMR spectra were recorded on a Varian/Mercury 400 or a Varian Inova 500 at 121.4 MHz and 202.4 MHz, respectively. ¹³C NMR spectra were recorded at 125 MHz (2000 scans) using continuous broad band proton decoupling and a 3s recycle delay, and are therefore not quantitative; chemical shifts are quoted in ppm, relative to CDCl₃ (77.550 ppm). The following abbreviations are used in listing NMR spectra: s = singlet, d = doublet, t = triplet, q = quartet, b = broad, m = multiplet.

5.4.2.2 Mass Spectroscopy

Electron Impact (EI) and Electrospray (ES⁺) mass spectra were recorded on a Micromass Autospec spectrometer operating at 70 eV with the ionisation mode as indicated.

5.4.2.3 Infra-red Spectroscopy

Infra-red spectra were recorded on a Perkin Elmer 1600 series FTIR. The spectra obtained were of the pure compound between sodium chloride discs.

5.4.3 Monomer Synthesis and Characterisation

5.4.3.1 Synthesis and Characterisation of *endo*-5-Methyl-*exo*-5-carboxylic Acid-2-norbornene

To a single-neck 5L round bottom flask containing a magnetic stirrer was added freshly cracked cyclopentadiene (939 g, 14.2 mol) and methacrylic acid (1203 g, 14.2 mol). The contents were stirred for 24 hours and then left to stand for 60 hours, over which a white powder precipitated from solution. The flask was cooled at 10°C for several hours to encourage the precipitation of the norbornene product. The solid was collected by vacuum filtration and rinsed with cold pentane (2 L, -10°C) to remove unreacted methacrylic acid, dicyclopentadiene and NB(X-Me)(N-CO₂H). The white powder (700 g) was recrystallised in hexanes (~ 50 w %) to give transparent crystals of NB(N-Me)(X-CO₂H) (621 g, 29 %) upon cooling over 24 hours. Single crystals were grown via slow recrystallisation from ethyl acetate at ambient temperature and an X-ray structural diagram produced using single-crystal X-ray diffraction. The analysis gave full structural refinement. The monomer was characterised by ¹H NMR, ¹³C NMR and GCMS. The numbering system shown in figure 5.8, was used for the assignment of the NMR signals.

¹H NMR (500 MHz, CDCl₃): δ (ppm) = 6.25 (dd, 1H, *J* = 5.59 & 2.96, H_{2&3}), 6.12 (dd, 1H, *J* = 5.59 & 3.17, H_{2&3}), 3.07 (s, 1H, H_{4&1}), 2.86 (s, 1H, H_{1&4}), 2.45 (dd, 1H, *J* = 12.02 & 3.96, H₇), 1.48 (m, 2H, H₆), 1.18 (m, 3H, H₈), 0.89 (m, 1H, *J* = 12.02, H₇).

¹³C NMR (125.6 MHz, CDCl₃): δ (ppm) = 186.03, 139.03, 133.82, 50.71, 49.77, 49.32, 43.13, 37.64 and 24.49.

GCMS (EI⁺): RT = 11.82, NB(N-Me)(X-CO₂H), 152.0 (C₉H₁₂O₂, M⁺).

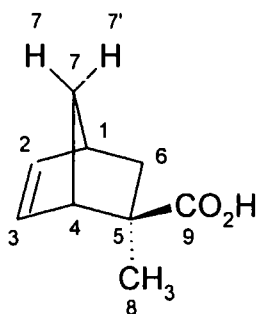


Figure 5.8. Assignment of C and H atoms in NB(N-Me)(X-CO₂H).

5.4.3.2 Synthesis and Characterisation of *endo*-5-Methyl-*exo*-5-trimethylsilyl Carboxylate-2-norbornene

To a solution of NB(N-Me)(X-CO₂H) (15.0 g, 67 mmol) and TMS-Cl (10.9 g, 100 mmol) in anhydrous THF (100 mL) was slowly added pyridine (8.48 g, 107 mmol). After the addition, the solution was stirred at ambient temperature for 12 hours. The white salt was removed via filtration and the remaining solution concentrated under vacuum. Pure product was obtained by distillation under reduced pressure (temperature = 40°C).

Note: Since TMSCl and the final product are very sensitive to moisture; all reagents should be of anhydrous grade and kept under nitrogen blanket.

The monomer was characterised by ¹H NMR, ¹³C NMR and GCMS. The numbering system shown in figure 5.9 was used for the assignment of the NMR signals.

¹H NMR (500 MHz, CDCl₃): δ (ppm) = 6.22 (dd, 1H, *J* = 5.64 & 2.30, H₂), 6.08 (dd, 1H, *J* = 5.64 & 3.41, H₃), 2.99 (bs, 1H, H₄), 2.82 (bs, 1H, H₁), 2.41 (dd, 1H, *J* = 12.02 & 3.99, H₇), 1.44 (bd, 1H, *J* = 8.66, H₆), 1.32 (bd, 1H, *J* = 8.66, H₆), 1.10 (s, 3H, H₈), 0.83 (dd, 1H, *J* = 12.01 & 2.63, H₇), 0.29 (s, 9H, H₁₀).

¹³C NMR (125.7 MHz, CDCl₃): δ (ppm) = 179.81 (C₉), 138.91 (C₂), 133.95 (C₃), 50.71 (C₄), 49.23 (C₆), 43.13 (C₁), 37.69 (C₇), 24.34 (C₈), 0.03 (C₁₀).

GCMS (EI⁺): RT = 12.44, NB(N-Me)(X-CO₂TMS), 224.0 (C₁₂H₂₀O₂Si, M⁺).

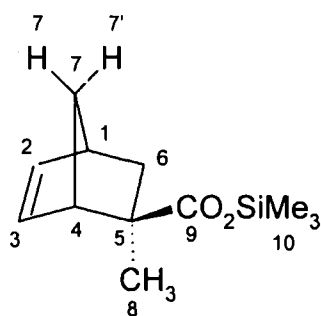


Figure 5.9. Assignment of C and H atoms in NB(N-Me)(X-CO₂TMS).

5.4.3.3 Synthesis and Characterisation of *endo*-5-Methyl-*exo*-5-methyl Hydroxy-2-norbornene

To a 5L three-neck flask were added NB(N-Me)(X-CO₂H) (174.8 g, 1.15 mmol) and anhydrous toluene (1000 mL). The system was kept under a nitrogen blanket, and the flask was equipped with a magnetic stirrer bar, thermometer, addition-funnel and condenser. A pre-mix of Vitride[®] (500 g, 70 wt % in toluene, 1.73 mol) was added to the addition funnel (short exposure to air is safe if < 2 minutes). With the flask submerged in an ice-water bath, the dilute Vitride[®] was added dropwise over 3 hours while maintaining pot temperature between 5-20 °C. After the addition was complete, the contents were heated to 100 °C for 6 hours (until TLC showed reaction to be complete). The contents were allowed to cool overnight. The solution was slowly added to a beaker containing vigorously stirring 5N HCl (1000 mL). The temperature was maintained < 20 °C with the aid of an ice-bath. After turbidity decreased, the mixture was transferred to a separatory funnel, and the organic phase was diluted with diethyl ether (1,0 L). The aqueous phase was discarded and the organics washed with 1N HCl (3 x 300 mL), 15 wt % aqueous potassium bicarbonate (3 x 300 mL) and water (500 mL). The organics were dried over MgSO₄, filtered, and the solvent removed under reduced pressure to afford NB(N-Me)(X-CH₂OH) (152 g, 96%, in > 95% purity).

The monomer was characterised by ¹H NMR, ¹³C NMR and GCMS. The numbering system shown in figure 5.10 was used for the assignment of the NMR signals.

¹H NMR (300 MHz, CDCl₃): δ (ppm) = 6.12 (m, 2H, H_{2&3}), 3.56 (m, 2H, H₉), 2.76 (bs, 1H, H_{1&4}), 2.55 (bs, 1H, H_{1&4}), 2.14 (m, 1H, -OH), 1.55 (d, 1H, *J* = 8.62, H₆), 1.44 (m, 1H, *J* =

11.72 & 3.71, H₇), 1.35 (d, 1H, *J* = 8.62, H₆), 0.91 (s, 3H, H₈), 0.77 (m, 1H, *J* = 11.72 & 2.68, H₇).

¹³C NMR (75 MHz, CDCl₃): δ (ppm) = 136.75, 135.68, 72.26, 47.85, 47.61, 43.70, 37.34, 22.87.

GCMS (EI⁺): RT = 10.21, NB(N-Me)(X-CH₂OH), 138.0 (C₉H₁₄O, M⁺).

IR (KBr disc, cm⁻¹): 3100 - 3650 (O-H), 3060 (olefinic C-H stretching), 2980 - 2867 (saturated C-H stretching).

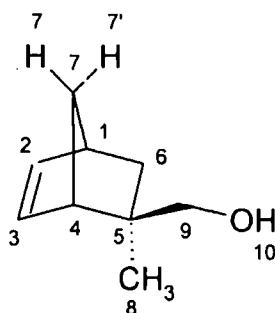


Figure 5.10. Assignment of C and H atoms in NB(N-Me)(X-CH₂OH).

5.4.3.4 Synthesis and Characterisation of *endo*-5-Methyl-*exo*-5-methyl Methoxy-2-norbornene

Under an inert atmosphere, the NB(N-Me)(X-CH₂OH) (7.53 g, 54.6 mmol) was dissolved in dry THF (15 mL) and was added dropwise to a stirred solution of NaH (68.2 mmol) in dry THF (65 mL). After complete addition, the solution was heated at 50°C for 3 hours. After cooling the reaction mixture to room temperature, methyl iodide (19.32 g, 8.47 mL, 136.2 mmol) was added dropwise to the solution; a slight exotherm was observed and a cream coloured precipitate was formed. The reaction mixture was stirred for 12 hours. After quenching with NH₄Cl (60 mL) the reaction mixture was extracted into diethyl ether (4 × 50 mL), washed with brine (50 mL) and dried over MgSO₄. The solvent was removed by rotary evaporation to give clear, yellow oil. The product was purified using distillation under reduced pressure (70°C, 60 mbar) to give clear, colourless oil in (5.0 g, 32.8 mmol, 60%).

The monomer was characterised by ^1H NMR, ^{13}C NMR and GCMS. The numbering system shown in figure 5.11 was used for the assignment of the NMR signals.

^1H NMR (500 MHz, CDCl_3): δ (ppm) = 6.10 (m, 2H, $\text{H}_{2\&3}$), 3.36 (s, 3H, H_{10}), 3.31 (dd, 2H, J = 8.85 & 6.7, H_9), 2.76 (bs, 1H, $\text{H}_{1\&4}$), 2.56 (bs, 1H, $\text{H}_{1\&4}$), 1.58 (bd, 1H, J = 8.44, H_6), 1.48 (dd, 1H, J = 11.71 & 3.78, H_7), 1.35 (bd, 1H, J = 8.44, H_6), 0.91 (s, 3H, H_8), 0.79 (m, 1H, J = 11.71, H_7).

^{13}C NMR (125.7 MHz, CDCl_3): δ (ppm) = 136.89 (C_2), 135.72 (C_3), 83.03 (C_9), 59.55 (C_{10}), 48.59 (C_1), 47.96 (C_6), 43.34 (C_4), 42.77 (C_5), 37.85 (C_7) and 23.81 (C_8).

GCMS (EI^+): RT = 9.29, NB(N-Me)(X- CH_2OMe), 152.0 ($\text{C}_{10}\text{H}_{16}\text{O}$, M^+).

IR (KBr disc, cm^{-1}): 3060 (olefinic C-H stretching), 2980 - 2867 (saturated C-H stretching), 1099 (C-O stretching).

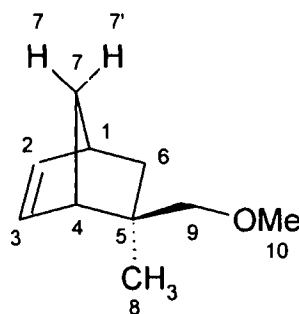


Figure 5.11. Assignment of C and H atoms in NB(N-Me)(X- CH_2OMe).

5.4.3.5 Synthesis and Characterisation of *endo*-5-Methyl-*exo*-5-methoxy-mesylate-2-norbornene

NB(N-Me)(X- CH_2OH) (74.8 g, 540 mmol) was dissolved in 250 ml dichloromethane. Methanesulfonyl chloride (65.6 g, 0.54 mol) was added and the mixture then cooled to -12.5°C with a methanol-ice bath. Triethylamine (65.6 g, 650 mmol) was added slowly dropwise, keeping the reaction temperature below -1.0°C . Copious white solids precipitate. The addition was complete after 30 minutes. The reaction warmed to 13.7°C over 40

minutes. GC analysis showed all starting material had been consumed. The mixture was treated with 200 ml water and the phases separated. The organic phase was washed with 200 ml 1N HCl and then with brine until the washing gave pH~6. The organic portion was dried over anhydrous magnesium sulphate, filtered, and rotary evaporated to give 100 g (90% yield) orange liquid. NMR was satisfactory to use product further. The monomer was characterised by ^1H NMR. The numbering system shown in figure 5.12 was used for the assignment of the NMR signals.

^1H NMR (400 MHz, CDCl_3): δ (ppm) = 6.11 (m, 1H, $\text{H}_{2\&3}$), 6.10 (m, 1H, $\text{H}_{2\&3}$), 4.10 (s, 2H, H_9), 2.96 (s, 3H, H_{10}), 2.78 (s, 1H, $\text{H}_{1\&4}$), 2.57 (s, 1H, $\text{H}_{1\&4}$), 1.48 (m, 2H), 1.39 (m, 1H), 0.91 (s, 3H, H_8), 0.80 (m, 1H, H_7).

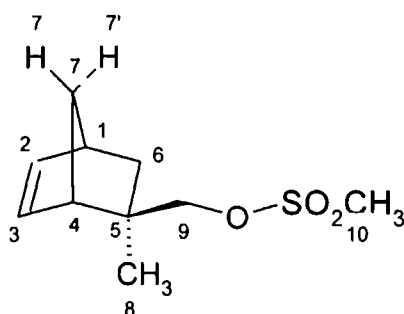


Figure 5.12. Assignment of C and H atoms in $\text{NB}(\text{N-Me})(\text{X-CH}_2\text{OMs})$.

5.4.3.6 Synthesis and Characterisation of *endo*-5-Methyl-*exo*-5-bromomethyl-2-norbornene

$\text{NB}(\text{N-Me})(\text{X-CH}_2\text{OMs})$ (10.3 g, 46.3 mmol), anhydrous lithium bromide (6.2 g, 69.4 mmol), and 100 ml 2-pentanone were mixed together at room temperature to give a yellow solution. The mixture was refluxed for two hours and then allowed to stir at room temperature overnight. Water was added to dissolve the salts. Ethyl acetate was added and mixed. The phases were separated and the aqueous phase extracted with 2 x 100 ml ethyl acetate. The organic portions were dried over anhydrous sodium sulfate, filtered, and rotary evaporated to give a brown oil and solid. The crude product was shown to contain a ratio of $\text{NB}(\text{N-Me})(\text{X-CH}_2\text{OMs})$: $\text{NB}(\text{N-Me})(\text{X-CH}_2\text{Br}) = 1 : 3$ respectively by ^1H NMR. The crude product was purified via column chromatography on silica gel (35g) and cyclohexane (250

mL) to give clear, colourless oil. R_f (cyclohexane) = 0.80. Yield = 65%. The monomer was characterised by ¹H NMR, ¹³C NMR, GCMS and IR. The numbering system shown in figure 4.13 was used for the assignment of the NMR signals.

¹H NMR (400 MHz, CDCl₃): δ (ppm) = 6.15 (dd, 1H, *J* = 5.60 & 2.80, H₃), 6.11 (dd, 1H, *J* = 5.60 & 3.20, H₂), 3.56 (s, 1H, H₈), 2.82 (s, 1H, H₄), 2.65 (s, 1H, H₁), 1.65 (dd, 1H, *J* = 11.98 & 3.75, H₇), 1.54 (d, 1H, *J* = 8.91, H₆), 1.42 (d, 1H, *J* = 8.91, H₆), 1.01 (s, 1H, H₉), 0.97 (dd, 1H, *J* = 12.98 & 2.72, H_{7'}).

¹³C NMR (101 MHz, CDCl₃): δ (ppm) = 137.09 (C₂), 135.78 (C₃), 50.24 (C₄), 48.29 (C₈), 47.96 (C₆), 43.68 (C₁), 40.16 (C₇), 27.15 (C₅), 24.86 (C₉).

GCMS (EI⁺): RT = 110.0 (C₇H₁₀O, M⁺), 66.0 (M⁺-C₂H₄O).

IR (KBr disc, cm⁻¹): 3100 - 3650 (O-H), 3060 (olefinic C-H stretching), 2980 - 2867 (saturated C-H stretching).

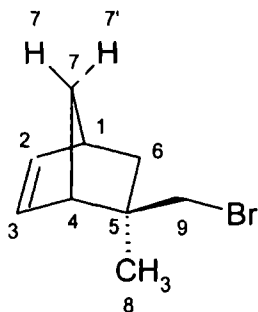


Figure 5.13. Assignment of C and H atoms in NB(N-Me)(X-CH₂Br).

5.4.3.7 Synthesis and Characterisation of *endo*-5-Methyl-*exo*-5-cyanomethyl-2-norbornene

NB(N-Me)(X-CH₂OMs) (64.5 g, 85% purity, 320 mmol) was dissolved in DMSO (500 mL). Sodium cyanide (31.0 g, 500 mmol) was added to the stirred solution and the reaction mixture heated at 80°C for 24 hours. Upon quenching and working-up a small aliquot it was apparent that the reaction was incomplete (50% conversion of starting material). The reaction mixture was heated for a further 48 hours with conversion being monitored via GC.

After ~ 90 hours of heating the conversion appeared to stop at 70% even upon the addition of more sodium cyanide (10.3 g, 170 mmol). The decision was made to work-up the reaction at this stage. The reaction mixture was added to water (1000 mL) and MTBE (1000 mL). The organic layer was separated and washed with water (7 x 500 mL). These separations are very difficult in the first few instances, with separation time being > 24 hours. The aqueous cyanide waste and all equipment were carefully decontaminated using an excess of bleach. The organic layer was dried over MgSO₄ and the solvent removed under reduced pressure to yield black oil (32 g). The crude product was purified in three lots using silica column chromatography and solvent system of 1 EtOAc: 5 hexanes. This gave a pale yellow oil (22.0 g, 150 mmol, yield = 47%). The monomer was characterised by ¹H NMR, ¹³C NMR and GCMS. The numbering system shown in figure 5.14 was used for the assignment of the NMR signals.

¹H NMR (400 MHz, CDCl₃): δ (ppm) = 6.13 (m, 1H, H_{2&3}), 6.10 (m, 1H, H_{2&3}), 2.83 (bs, 1H, H_{4&1}), 2.55 (bs, 1H, H_{1&4}), 2.45 (d, 2H, *J* = 14.11, H₉), 1.57 (ddd, 1H, *J* = 11.97 & 3.63 & 2.32, H₇), 1.49 (m, 2H, H₆), 1.05 (m, 3H, H₈), 0.99 (m, 1H, *J* = 11.97, H₇).

¹³C NMR (100.6 MHz, CDCl₃): δ (ppm) = 136.93 (C₂), 135.00 (C₃), 119.17 (C₁₀), 51.00 (C_{1&4}), 47.98 (C₆), 43.64 (C_{1&4}), 40.46 (C₅), 39.93 (C₇), 31.30 (C₉), 25.36 (C₈)

GCMS (EI⁺): RT = 11.97, NB(N-Me)(X-CH₂CN), 147.0 (C₁₀H₁₃N, M⁺).

IR (KBr disc, cm⁻¹): 3060 (olefinic C-H stretching), 2980 - 2867 (saturated C-H stretching).

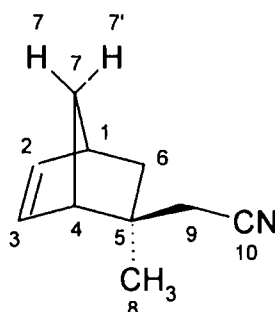


Figure 5.14. Assignment of C and H atoms in NB(N-Me)(X-CH₂CN).

5.4.3.8 Synthesis and Characterisation of *endo*-5-Methyl-*exo*-5-methyl Carboxylic Acid-2-norbornene

The NB(N-Me)(X-CH₂CN) (4.5 g, 27.9 mmol) was added to aqueous potassium hydroxide (14 g in 140 mL) and stirred with heating at 100°C for 48 hours. The resulting solution was cooled and diluted with water (150 mL). This solution was extracted with diethyl ether (2 x 150 mL), acidified to pH 3, extracted again with chloroform (5 x 50 mL). The combined chloroform extracts were washed with water (2 x 50 mL), dried over MgSO₄, filtered, and the solvent removed under reduced pressure. The colourless liquid was purified via extraction from organic solvent using aqueous NaOH and then re-acidification and extraction with organic solvent to yield a white solid (2.7 g, 18 mmol, 65%). The monomer was characterised by ¹H NMR, ¹³C NMR and GCMS. The numbering system shown in figure 5.15 was used for the assignment of the NMR signals.

¹H NMR (400 MHz, CDCl₃): δ (ppm) = 11.25 (s, 1H, -OH), 6.12 (dd, 1H, *J* = 5.62 & 2.89, H₂), 6.07 (dd, 1H, *J* = 5.62 & 2.89, H₃), 2.80 (bs, 1H, H_{4&1}), 2.61 (bs, 1H, H_{1&4}), 2.50 (d, 2H, *J* = 14.26, H₉), 1.75 (dd, 1H, *J* = 11.88 & 3.80, H₇), 1.57 (bd, 1H, *J* = 8.79, H₆), 1.44 (bd, 1H, *J* = 8.79, H₆), 1.00 (s, 3H, H₈), 0.94 (dd, 1H, *J* = 11.88 & 2.52, H₇).

¹³C NMR (100.6 MHz, CDCl₃): δ (ppm) = 179.90 (C₉), 136.87 (C₂), 135.21 (C₃), 51.55 (C_{4&1}), 48.13 (C₆), 47.50 (C₉), 43.77 (C_{1&4}), 40.37 (C₈), 40.15 (C₇), 25.22(C₅).

GCMS (EI⁺): RT = 13.63, NB(N-Me)(X-CH₂CO₂H), 166.0 (C₁₀H₁₄O₂, M⁺).

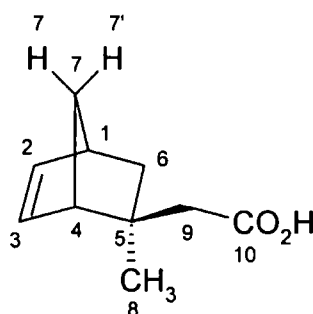


Figure 5.15. Assignment of C and H atoms in NB(N-Me)(X-CH₂CO₂H).

5.4.3.9 Synthesis and Characterisation of *endo*-5-Methyl-*exo*-5-methyl Trimethylsilyl Carboxylate-2-norbornene

To a solution of NB(N-Me)(X-CH₂CO₂H) (2.7 g, 18 mmol) and TMS-Cl (2.9 g, 27 mmol) in anhydrous THF (27 mL) was slowly added pyridine (2.2 g, 29mmol). After the addition, the solution was stirred at ambient temperature for 12 hours. The white salt was removed via filtration and the remaining solution concentrated under vacuum. Pure product was obtained by distillation under reduced pressure (temperature = 40°C).

Note: Since TMSCl and the final product are very sensitive to moisture; all reagents should be of anhydrous grade and kept under nitrogen blanket.

The monomer was characterised by ¹H NMR, ¹³C NMR and GCMS. The numbering system shown in figure 5.16 was used for the assignment of the NMR signals.

¹H NMR (400 MHz, CDCl₃): δ (ppm) = 6.06 (m, 2H, H_{2&3}), 2.75 (m, 1H, H_{4&1}), 2.53 (m, 1H, H_{1&4}), 2.43 (d, 2H, *J* = 14.29, H₉), 1.72 (ddd, 1H, *J* = 11.95 & 3.72 & 1.80, H₇), 1.54 (m, 1H, *J* = 8.72, H₆), 1.38 (m, 1H, *J* = 8.72, H₆), 0.94 (s, 3H, H₈), 0.88 (m, 1H, H₇), 0.26 (s, 9H, H₁₁).

¹³C NMR (100.6 MHz, CDCl₃): δ (ppm) = 173.63 (C₁₀), 136.70 (C₂), 135.23 (C₃), 51.60 (C_{4&1}), 49.01 (C₉), 48.10 (C₆), 43.72 (C_{1&4}), 40.32 (C₅), 40.95 (C₇), 25.12 (C₈), 0.00 (C₁₁).

GCMS (EI⁺): RT = 14.35, NB(N-Me)(X-CH₂CO₂TMS), 238.0 (C₁₃H₂₂O₂Si, M⁺).

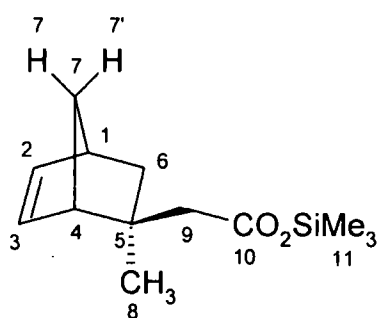


Figure 5.16. Assignment of C and H atoms in NB(N-Me)(X-CH₂CO₂TMS).

5.4.4 NMR Scale Addition Polymerisation Reactions

All addition polymerisation reactions were prepared in a Braun glove box under an inert atmosphere. Typically, the relevant palladium complex (3.60×10^{-6} mole, 1 equivalent) was dissolved in deuterated solvent. The relevant monomer (1.80×10^{-4} mole, 50 equivalents) was then dissolved in the initiator solution. The solution was transferred to an NMR tube fitted with a Young's tap, allowing the vessel to be closed under a nitrogen atmosphere. The reactions were monitored using arrayed ^1H spectroscopy. In all cases, the integrated intensities of the monomer vinyl signals (polymerisation) and initiator Pd-H signal (initiation) were measured against the previous NMR integrations.

5.4.5 Polymerisation of Functionalised Norbornenes using Pd1388

The NMR scale polymerisation reactions were run as described in the general section 5.4.4. The experimental detail and polymerisation results are shown in table 5.1.

Table 5.1. Polymerisations of 50 Monomer: 1 Pd1388 (5.0 mg, 3.60×10^{-6} mol).

Monomer	Temp (°C)	Solvent	k_p (N/X) (s ⁻¹)
NB(N-Me)(X-CO ₂ H) (27.4 mg, 1.80×10^{-4} mol)	50	Benzene- <i>d</i> ₆	1×10^{-6}
NB(N-Me)(X-CO ₂ H) (27.4 mg, 1.80×10^{-4} mol)	70	Benzene- <i>d</i> ₆	5×10^{-6}
NB(N-Me)(X-CO ₂ TMS) (40.3 mg, 1.80×10^{-4} mol)	50	Benzene- <i>d</i> ₆	3×10^{-6}
NB(N-Me)(X-CO ₂ TMS) (40.3 mg, 1.80×10^{-4} mol)	70	Benzene- <i>d</i> ₆	4.4×10^{-5}
NB(N-Me)(X-CH ₂ OMe) (27.4 mg, 1.80×10^{-4} mol)	70	Benzene- <i>d</i> ₆	12.52×10^{-4}
NB(N-Me)(X-CH ₂ CO ₂ TMS) (45.5 mg, 1.80×10^{-4} mol)	70	Benzene- <i>d</i> ₆	4.3×10^{-5}
NB(N-Me)(X-CH ₂ HFA) (52.5 mg, 1.80×10^{-4} mol)	70	Benzene- <i>d</i> ₆	13.4×10^{-5}

5.5 References

¹ Meek, J. S.; Trapp, W. B. *J. Am. Chem. Soc.* **1957**, *79*, 3909.

² Moriarty, R. M.; Chien, C. C.; Adams, T. B. *J. Org. Chem.* **1979**, *44*, 2206.

³ Katritzky, A. R.; Hong, Q.; Yang, Z.; Cundy, D. J.; Brown-Wensley, K. *Organic Preparations and procedures international* **1995**, 27 (5), 574 - 575.

Chapter 6

6 Origins of the Functional Group Homologation Effect: Molecular Modelling and NMR Spectroscopic Investigations

6.1 Introduction

The electronic effect of the functional group on norbornene is a key contributor to the monomers polymerisation activity. In this chapter attempts will be made to determine the key changes in a functionalised norbornenes structure, upon the methylene spacing of its functional group, with a view to using these findings as a tool to quickly and easily predict the polymerisation activity of new monomers.

The sp^2 carbons within norbornenes structure are expected to be the most important with respect to polymerisation activity, since they are a key component of both aspects of a coordination-insertion addition polymerisation mechanism. In order to understand how the electronic structure of a functionalised norbornene monomer affects polymerisation activity we have to consider which of its molecular orbitals and that of the cationic palladium catalyst interact during a typical coordination-insertion polymerisation mechanism.

Our investigations will be centred on the carboxylic acid ($-CO_2H$), acetate ($-OAc$), methoxy ($-OMe$) and trifluoromethanesulfonamide ($-TFS$) functionalised families of norbornene monomers. ^{13}C NMR spectroscopic shifts within the monomer structures and molecular modelling studies using the carboxylic acid functionalised monomers will be used to rationalise the effects of introducing methylene spacers (homologation) between norbornene and its functional group. The molecular modelling studies will pay particular attention to changes in the bond lengths, bond angles and Mulliken atomic charges.

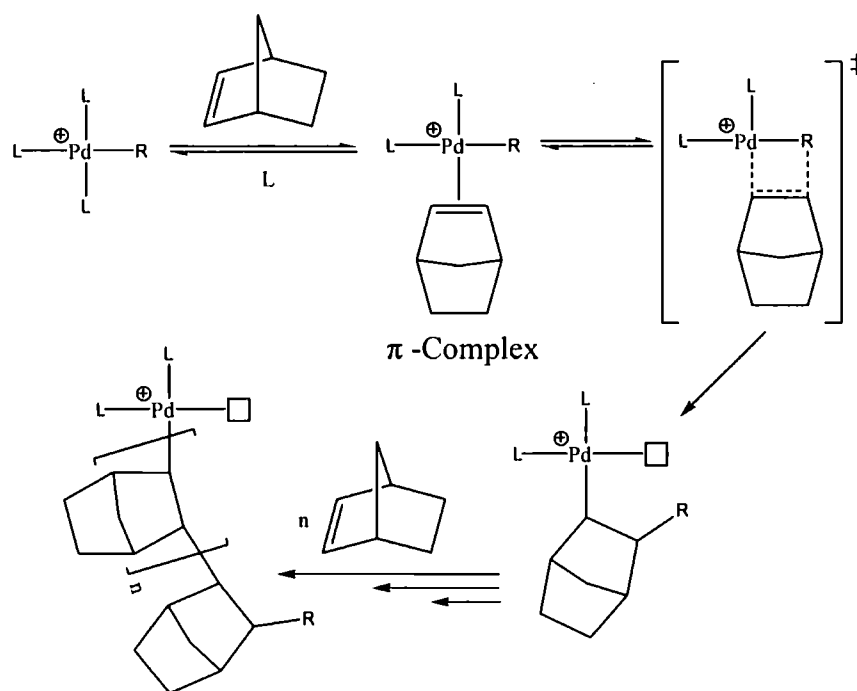
Molecular modelling studies (density functional theory) have been used by Kyoung Hoon Kim et al.,¹ to study palladium-based catalysts commonly used for the polymerisation of *endo/exo*-5-methyl-2-norbornene-carboxylate ($N/X-NBCO_2Me$). Three isomers of the

catalyst complex, *exo* face coordination of the *exo* monomer, *exo* face coordination of the *endo* monomer, and *endo* face coordination of the *endo* monomer, were analysed. It was shown through the relative energies of the catalyst complexes, molecular geometries, and binding energies, that the *endo-endo* isomer was the most stable and catalytically inactive due to an intramolecular interaction between Pd and carbonyl oxygen of the ester group. Additionally, the phosphine ligand, PCy₃, is shown to be effective in preventing the oxygen atom from coordination to the Pd. This result suggests that the catalyst deactivating effects discussed would be minimised in the polymerisation systems used in this work, since the catalyst used in this work is [Pd(PCy₃)₂(NCCH₃)(H)][B(C₆F₅)₄] (**Pd1388**).

6.2 Results and Discussion

6.2.1 Polymerisation Mechanism

Norbornene and its related monomers are widely accepted to polymerise through a coordination-insertion mechanism, using a cationic palladium catalyst. The insertion step proceeds via a four-centred transition state, scheme 6.1.



Scheme 6.1. Coordination-insertion addition polymerisation mechanism.

In order to understand how the electronic structure of a functionalised norbornene monomer affects polymerisation activity we have to consider which of its molecular orbitals and that of the cationic palladium catalyst interact during a typical coordination-insertion polymerisation mechanism. During the coordination stage of the polymerisation mechanism the bonding can be considered to arise from two independent components as illustrated in figure 6.1.²

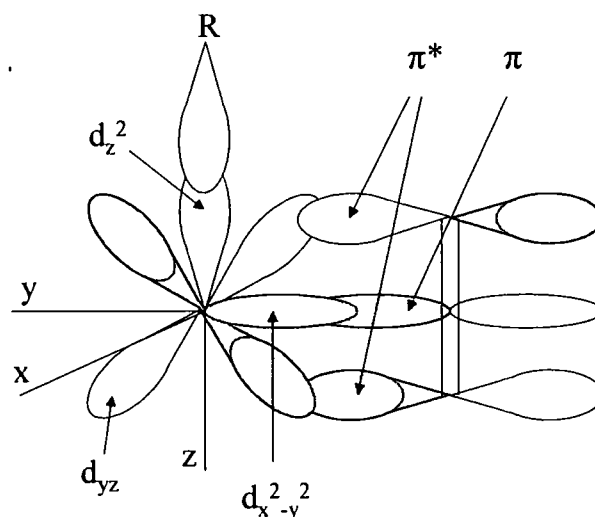


Figure 6.1. Overlap of relevant orbitals in the ground-state olefin-metal π -complex formed via the coordination of a norbornene monomer to the cationic palladium centre. Where R = growing polymer chain and the norbornene is represented by a simple C=C.

In the first part, σ -type overlap occurs between the filled π -orbital of the olefin and the suitably directed $d_{x^2-y^2}$ vacant hybrid metal orbital, figure 6.1. This is reinforced by the second component, that derives from the overlap of a filled metal d_{yz} orbital with the vacant π^* antibonding orbital of the olefin; these orbitals have π -symmetry with respect to the bonding axis and allow Pd \rightarrow C=C π back bonding to assist the σ C=C \rightarrow Pd bond, figure 6.1.² The flexible interplay of these two components may allow our experimental observations to be rationalised.

The donation of π -bonding electrons into the metal σ -orbital and the introduction of electrons into the π^* antibonding orbital of the olefin both weaken the π -bonding in the olefin, resulting in a distortion from planarity and lengthening of the olefin C=C. The two components are synergistically related; as one component increases, it tends to promote an

increase in the other. This means the metal-alkene bond is essentially electroneutral, with donation and back-acceptance approximately balanced.

At the transition state for insertion the alkyl group migrates through overlap with the cationic palladium d_z^2 and d_{yz} orbitals and the olefin π^* antibonding orbitals,² figure 6.2.

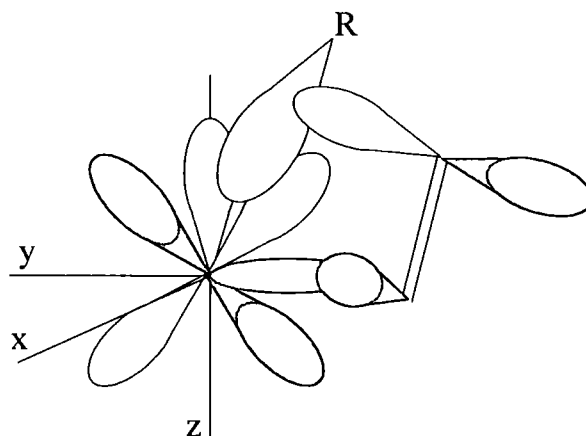


Figure 6.2. Overlap of relevant orbitals in the transition state for the insertion of a norbornene monomer into the cationic palladium-alkyl bond. Where R = growing polymer chain and the norbornene is represented simply by C=C.

The substituents, R and R', of a polymerising olefin, $R-C=C-R'$, have a significant effect upon the balance between donation and back-acceptance as already described. It is expected that an increase in the electron withdrawing nature of the substituents R and R', will result in stronger π -back-bonding interactions. Stronger π -back-bonding interactions will result in a stabilisation of the ground-state olefin-metal π -complex and therefore cause an increase in the energy barrier (ΔG^\ddagger) for the insertion of the olefin into the palladium-alkyl bond, figure 6.3.

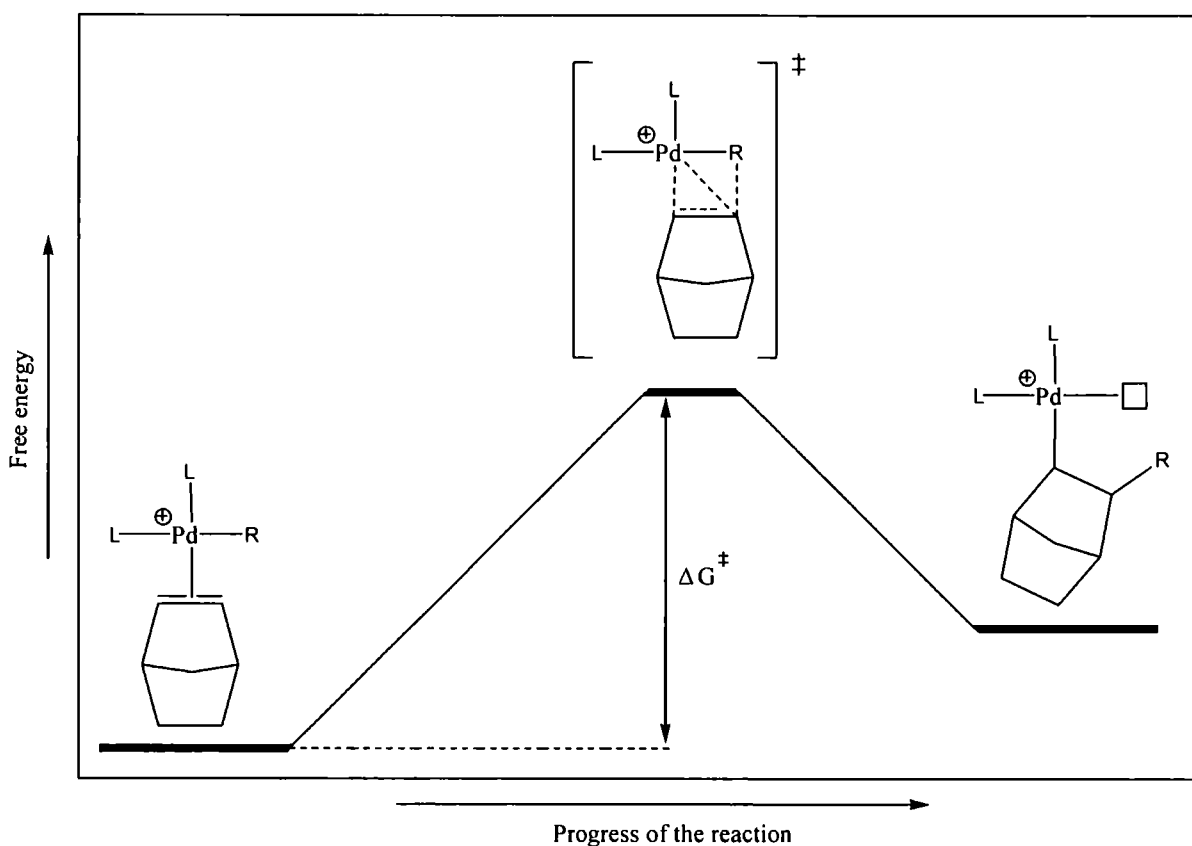


Figure 6.3. Reaction coordinate diagram for the insertion of norbornene into a cationic palladium-alkyl bond. Where L = neutral ligand, R = alkyl, □ = vacant site.

It is thought that the insertion of the norbornene monomer into the cationic palladium-alkyl bond is the rate determining step for polymerisation and consequently the higher the energy barrier for insertion (ΔG^\ddagger), the slower the polymerisation reaction will occur.

If the electronic nature of the functional group in norbornene has a similar effect upon the monomer C=C as described above, an electron withdrawing substituent will cause the monomer to polymerise at a slower rate. The methylene spacing of electron withdrawing functional groups in norbornene such as -OAc, -CO₂TMS, -TFS and -OMe, would be expected to increase the electron density within the C=C, and subsequently account for the observed increase in polymerisation activity described in previous chapters.

The following sections will attempt to show how the methylene spacing of the electron withdrawing functional group in norbornene affects the structure of the monomers bicyclic structure, paying particular attention to the C=C, with a view to using these findings as a tool to quickly and easily predict the polymerisation activity of new monomers.

6.2.2 Assessing Differences, Effects and Error

Statistical analysis has been used to highlight potential relationships between the polymerisation activity (k_p) of the carboxylic acid functionalised family of norbornene monomers and a number of input variables; ^{13}C NMR resonances, atomic distances, bond angles and Mulliken atomic charges. Dr. Ann G-Jensen (Staff Statistician, Lubrizol Analytical Services) assisted the statistical analysis. Statistical conclusions based on the data are given in the results and discussion section. A direct correlation between an input variable and the polymerisation activity signifies that as the input value increases, so too does the polymerisation activity. The opposite applies to an inverse correlation. The variation in k_p and in each of the input variables (^{13}C NMR, bond angles, atomic distances and Mulliken atomic charges) is relatively small. Thus, it is important to ask the question of whether the differences observed from $n = 0$ to 1 to 2 are real differences in the polymerisation activity of the monomer or not. The ^{13}C NMR resonance's, atomic distances, bond angles and Mulliken atomic charges are numbers generated from sources which can be regarded as carrying no error, since if the same method is used to measure the variables again, identical output numbers would be generated.

A preliminary estimate of uncertainty in the polymerisation rate results is obtained from 2 polymerisation reactions for the X/N-NB-CO₂TMS monomer. Replicated runs provide information about the expected variation in polymerisation rate results produced under identical conditions. This information may be used as a baseline for comparing polymerisation rate results produced under different conditions (different monomers). The results from the replicated runs are in table 6.1.

Table 6.1. Propagation rate results from replicated runs.

Run	$k_p \text{ N (s}^{-1}\text{)}$	$k_p \text{ X (s}^{-1}\text{)}$
1	1.265×10^{-5}	3.657×10^{-5}
2	1.283×10^{-5}	3.652×10^{-5}
Average	1.274×10^{-5}	3.6545×10^{-5}
Std. Dev.	1.27279×10^{-7}	3.53553×10^{-8}
Range	1.8000×10^{-7}	5.0000×10^{-8}

To conclude that different monomers yield significantly different k_p results, the observed difference between monomers should be at least 2.55×10^{-6} for the N-regioisomer and 7.07×10^{-7} for the X-regioisomer. These values are 20 times the standard deviation in replicated run results for the N and X-regioisomers, respectively. Typically, we would not require such a large difference, however, these criteria reflect the lack of information available for making decisions.

Table 6.2. Polymerisation rates/ k_p (s^{-1}) for NB(CH₂)_nFG at 70°C in benzene-*d*₆ (50 monomer : 1 Pd1388).

Monomer Family	n			
	0	1	2	3
X-NB(CH ₂) _n CO ₂ TMS	1.8×10^{-5}	3.7×10^{-5}	57.3×10^{-5}	-
N-NB(CH ₂) _n CO ₂ TMS	0.6×10^{-5}	1.3×10^{-5}	18.3×10^{-5}	-
X-NB(CH ₂) _n OAc	-	47.0×10^{-5}	321.9×10^{-5}	-
N-NB(CH ₂) _n OAc	8.2×10^{-5}	16.6×10^{-5}	162.6×10^{-5}	-
X-NB(CH ₂) _n TFS	-	3.5×10^{-5}	20.2×10^{-5}	41.2×10^{-5}
N-NB(CH ₂) _n TFS	-	1.1×10^{-5}	7.5×10^{-5}	13.9×10^{-5}

The variation in k_p for the replicated runs is very small relative to the observed variation in k_p results for the functionalised norbornene monomers, from $n = 0$ to $n = 1$ to $n = 2$, table 6.2. This suggests that the changes in k_p shown in table 6.2 are real and not simply chance variation.

6.2.3 ¹³C NMR Spectroscopic Investigations

It is envisaged that the electronic environment of the carbon atoms within a functionalised norbornenes structure must be changing significantly upon the methylene spacing of the monomers functional group, to account for the observed changes in the monomers polymerisation activity. This change in electronic environment should be displayed in the ¹³C NMR spectrum for the relative monomers, since a shift in NMR resonance is related to the electronic environment of the atom concerned.

In a simple approximation, the ^{13}C NMR resonance for a particular carbon atom would be expected to shift down-field (increase in ppm) if electron density is withdrawn from it, due to it being de-shielded with respect to the magnetic field applied by the spectrometer.

An inspection of the ^{13}C NMR resonance shifts within the carboxylic acid, acetate, methoxy and trifluoromethanesulfonamide functionalised families of norbornene monomers reveals a number of general trends, but it is clear that the N and X-regioisomers of the respective monomers behave very differently and consequently need to be discussed separately.

6.2.3.1 ^{13}C NMR Spectroscopic Investigations of the *exo*-Regioisomers

The observed shifts in the polymerisation rates for the X-carboxylic acid functionalised norbornene monomers upon methylene spacing of the functional group may be related to a shift in the ^{13}C NMR resonance at C6, and possibly at C7, table 6.3; see numbering scheme in figure 6.4. The ^{13}C NMR resonance shifts for C1, C2, C3, C4 and C5, show no clear relationships with the polymerisation activity that could be statistically verified, table 6.3.

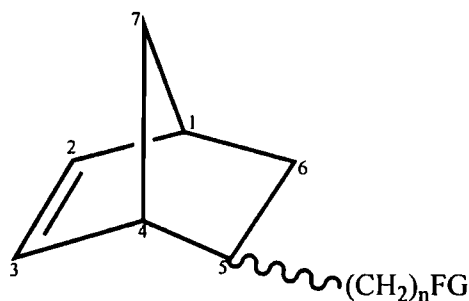


Figure 6.4. Assignment of carbon atoms in $\text{NB}(\text{CH}_2)_n\text{FG}$, where FG = functional group.

The ^{13}C NMR resonance for C6 shows an inverse correlation with the polymerisation activity of the monomer upon methylene spacing of the carboxylic acid functional group, table 6.3. This indicates that as the polymerisation activity increases, the C6 resonance shifts up-field, due to increased shielding from the electron withdrawing groups.

Table 6.3. ^{13}C NMR for $\text{X-NB}(\text{CH}_2)_n\text{CO}_2\text{H}$ and relationship to polymerisation activity (k_p).

Carbon No.	n			Relationship of ^{13}C signal to k_p X
	0	1	2	
1	41.90	42.26	42.08	Unclear
2	138.21	136.66	136.92	Unclear
3	136.05	136.66	136.66	Unclear
4	46.83	45.27	45.39	Unclear
5	44.99	35.10	35.50	Unclear
6	46.56	46.52	46.33	Inverse
7	30.62	32.73	33.06	Direct

In opposition to the results for C6, the ^{13}C NMR resonance for C7 shows a direct correlation with the polymerisation activity of the monomer, table 6.3. This indicates that as the polymerisation activity increases, the C7 resonance shifts down-field, due to decreased shielding from the electron withdrawing groups.

The ^{13}C NMR resonances for the vinyl, C2 and C3, do not follow a linear trend, when correlated against polymerisation activity of the monomer, table 6.3. This is surprising given the importance of these atoms during a polymerisation reaction. The C2 resonance shifts up-field, when the first methylene spacer is introduced, but is relatively unaffected by further methylene spacing, table 6.3. This indicates an increased shielding to the electron withdrawing groups. While the C3 resonance unexpectedly shifts down-field, when the first methylene spacer is introduced, but is unaffected by further methylene spacing, table 6.3. This indicates a decreased shielding to the electron withdrawing groups.

Table 6.4. ^{13}C NMR for $\text{X-NB}(\text{CH}_2)_n\text{OMe}$ and relationship to polymerisation activity (k_p).

Carbon No.	n			Relationship of ^{13}C signal to k_p X
	0	1	2	
1	46.07	41.79	46.66	Unclear
2	140.08	136.89	136.97	Unclear
3	133.31	136.86	136.49	Unclear
4	46.1	43.93	42.18	Inverse
5	56.99	39.11	36.59	Inverse
6	40.55	45.3	45.46	Direct
7	34.42	29.95	33.24	Unclear

The ^{13}C NMR resonances for the vinyl, C2 and C3, of the -OMe (table 6.4), -OAc (table 6.5) and -TFS (table 6.6) families of X-functionalised norbornene monomers tend to follow the general trends described for the carboxylic acid monomer family.

Table 6.5. ^{13}C NMR for X-NB(CH₂)_nOAc and relationship to polymerisation activity (k_p).

Carbon No.	n			Relationship of ^{13}C signal to k_p X
	0	1	2	
1	40.7	43.86	46.55	Direct
2	141.14	137.09	136.82	Inverse
3	132.71	136.39	136.61	Direct
4	47.35	41.75	42.16	Unclear
5	75.3	38.1	35.5	Inverse
6	46.31	45.1	45.45	Unclear
7	34.67	29.76	33.08	Unclear

Table 6.6. ^{13}C NMR for X-NB(CH₂)_nTFS and relationship to polymerisation activity (k_p).

Carbon No.	n			Relationship of ^{13}C signal to k_p X
	1	2	3	
1	41.97	42.14	42.09	Unclear
2	137.44	136.76	136.9	Unclear
3	136.16	136.64	136.65	Unclear
4	44.1	46.37	46.49	Direct
5	39.83	35.81	38.44	Unclear
6	45.11	49.81	45.4	Unclear
7	30.9	32.9	33.17	Direct

The apparent decrease or reversal in polarisation of the C2=C3 may have an effect on the monomers' polymerisation activity. William Tam's publications divulge that there is generally more electron density at C3 than C2 within X-substituted norbornenes, when the norbornene substituent is electron withdrawing.³ This polarisation of the C=C would clearly affect the regiochemistry of the polymerisation insertion step, since we are essentially adding a highly polarised Pd⁺-H moiety across the C=C. With the Pd⁺ expected to favour the side of the C=C with the highest electron density. It is not apparent if or why a decrease in the polarisation of the C2=C3 would cause an increase in polymerisation activity, although it has to be noted that norbornene has very high polymerisation activity but has no C=C polarisation, due to its symmetry.

The relationships between k_p (X) and the ^{13}C NMR resonances for other carbon sites within the monomers are inconsistent across the four families of monomers, shown in tables 6.3, 6.4, 6.5 and 6.6, which makes logical conclusions impossible.

These results cast doubts over our ability to use ^{13}C NMR spectroscopy as a tool to predict the polymerisation activity of new X-functionalised monomers without running polymerisation kinetic experiments.

6.2.3.2 ^{13}C NMR Spectroscopic Investigations of the *endo*-Regioisomers

The observed shift in the polymerisation activity for the N-carboxylic acid functionalised norbornene monomers upon methylene spacing of the functional group may be related to a shift in the ^{13}C NMR resonance at C1, C2 and C4, table 6.7; see numbering scheme in figure 6.4. The ^{13}C NMR resonance shifts for C3, C5, C6 and C7, show no clear relationships with the polymerisation activity that could be statistically verified.

Table 6.7. ^{13}C NMR for N-NB(CH₂)_nCO₂H and relationship to polymerisation activity (k_p).

Carbon No.	n			Relationship of ^{13}C signal to k_p N
	0	1	2	
1	42.91	42.77	42.74	Inverse
2	138.04	137.86	137.49	Inverse
3	132.37	132.43	132.35	Unclear
4	46.12	45.86	45.46	Inverse
5	44.98	35.18	35.30	Unclear
6	49.95	49.78	49.80	Unclear
7	29.32	32.22	31.77	Unclear

The shift from high to low polymerisation activity appears to be related to a shift from low to high ^{13}C NMR resonance at C1, C2 and C4, table 6.7. To ascertain if these results have any general meaning, they have been compared against the same carbon atoms in other electron-withdrawing group, N-functionalised norbornene monomers. The relationships between polymerisation activity and ^{13}C NMR resonances for the same carbon atoms, across different

families of monomers are inconsistent; see tables 6.8 and 6.9. This is similar to the relationships described for the X-regioisomers, in section 6.2.3.1,

Table 6.8. ^{13}C NMR for N-NB(CH₂)_nOAc and relationship to polymerisation activity (k_p).

Carbon No.	n			Relationship of ^{13}C signal to k_p N
	0	1	2	
1	42.44	42.35	42.69	Unclear
2	137.85	138.66	136.82	Unclear
3	132.39	131.69	132.4	Unclear
4	44.09	45.88	45.69	Unclear
5	37.99	35.25	35.56	Unclear
6	49.62	47.78	49.79	Unclear
7	29.23	34.71	32.36	Unclear

Table 6.9. ^{13}C NMR for N-NB(CH₂)_nTFS and relationship to polymerisation activity (k_p).

Carbon No.	n			Relationship of ^{13}C signal to k_p N
	1	2	3	
1	42.66	42.7	42.75	Direct
2	138.72	138	137.68	Inverse
3	131.63	131.99	132.19	Direct
4	44.08	45.44	45.53	Direct
5	39.7	35.77	38.52	Unclear
6	49.81	49.81	49.81	No Variation
7	30.06	32.16	32.48	Direct

These results cast doubts over our ability to use ^{13}C NMR spectroscopy as a tool to predict the polymerisation activity of new N-functionalised monomers without running polymerisation kinetic experiments.

6.2.4 Molecular Modelling Studies of Carboxylic Acid Functionalised Norbornenes

In order to gain further understanding of the functional group methylene spacing effect on the polymerisation rate of functionalised norbornene monomers, we investigated the molecular structures of a family of carboxylic acid functionalised norbornenes.

All theoretical calculations were performed on isolated molecules, using Kohn-Sham DFT with the B97-2 hybrid exchange-correlation energy functional.⁴ We have confirmed that qualitatively similar results are obtained with the widely used B3LYP DFT functionals. All calculations were performed using the cc-pVTZ basis set.⁵ Molecular structures were optimised and analytic harmonic vibrational frequencies were calculated in order to confirm that the located stationary points are minima on the potential energy surface.⁶ All calculations were performed using the Gaussian 03 program.⁷ The bond angles, bond lengths and Mulliken atomic charges for the molecules were extracted from the molecular models using the Jmol modeling package. The data obtained from Jmol was plotted against the polymerisation activity data obtained in previous chapters, and, relationships between the data sets highlighted.

An inspection of the relationships between polymerisation activity and bond lengths, bond angles and Mulliken atomic charges showed that the N and X-regioisomers of the monomers behave very differently and consequently need to be discussed separately.

6.2.4.1 Molecular Modelling of *exo*-Carboxylic Acid Functionalised Norbornenes

It is clear that the sp^2 C2 and C3 atoms play the most significant role in a coordination-insertion polymerisation mechanism, as discussed in detail in section 6.2.1. It is surprising then, that the C2=C3 bond length does not change during the methylene spacing of the highly electron withdrawing carboxylic acid group, table 6.10. This detail was also replicated for the N-functionalised monomers, discussed in the following section.

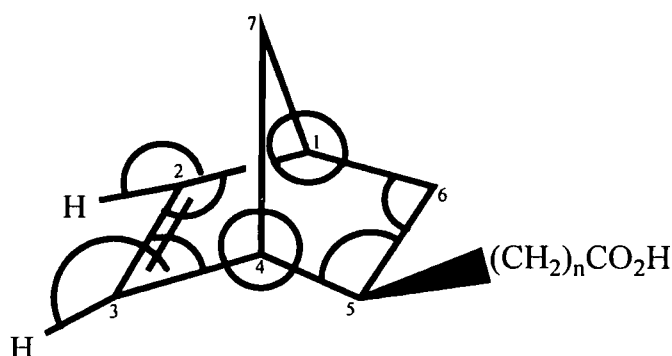


Figure 6.5. Atom numbering scheme for X-NB(CH₂)_nCO₂H

The effects of methylene spacing upon the norbornene structure are clearly much more subtle than initially hypothesised; this is in agreement with the complicated ^{13}C NMR data already discussed. To aid the elucidation of trends during the methylene spacing of the carboxylic acid functional group, the atomic distance and bond angle data for X-NB-Et are included in the tables. This monomer can effectively be considered as having the number of methylene spacers, n , between norbornene and the electron withdrawing carboxylic acid group, where the functional group behaves electronically like a simple alkyl functionality.

Table 6.10. Atomic distances (Å) for X-NB(CH₂)_nCO₂H, X-NB-Et and relationships to k_p

Carbon No.	n			X-NB-Et	Relationship of atomic distances to k_p X
	0	1	2		
C1-C2	1.512	1.514	1.514	1.514	Unclear
C2-C3	1.333	1.333	1.333	1.333	No Variation
C3-C4	1.512	1.513	1.513	1.513	Unclear
C4-C5	1.580	1.564	1.565	1.565	Unclear
C5-C6	1.550	1.554	1.554	1.554	Unclear
C1-C6	1.557	1.555	1.556	1.555	Unclear
C4-C7	1.535	1.537	1.536	1.537	Unclear
C1-C7	1.535	1.536	1.535	1.535	No Variation
C2-C6	2.461	2.458	2.460	2.459	Unclear
C3-C5	2.442	2.449	2.453	2.455	Direct
C1-C4	2.239	2.239	2.238	2.238	Inverse
C7-C2	2.340	2.339	2.339	2.339	Unclear
C7-C3	2.341	2.338	2.338	2.238	Unclear

There are a small number of bond and atomic distance changes throughout the norbornene structure upon the methylene spacing of the carboxylic acid functionality, although none show any significant relationship with the polymerisation activity, table 6.10. The C4-C5 bond decreases in length by 0.015 Å and the C5-C6 bond increases in length by 0.004 Å, upon the first methylene spacer being introduced into the X-monomers structure, although no significant change occurs for either bond upon the addition of the second methylene spacer, table 6.10. This suggests that the changing bond lengths are a result of the steric changes around C5 when the carboxylic acid group is no longer directly bound to C5. It is difficult to

rationalise if this would cause the polymerisation activity of the monomer to change.

The atomic distance between C3 and C5 is shown to have a direct relationship with the polymerisation activity; atomic distance increases as polymerisation activity increases. The atomic distance between C3 and C5 increases during the first (0.007 Å) and second (0.004 Å) methylene spacing, furthermore the X-NB-Et monomer shows an additional (0.002 Å) increase, table 6.10. This particular changing of structure is also displayed by a bond angle change, table 6.11. The C3-C4-C5 bond angle is shown to have a direct relationship with the polymerisation activity; bond angle increases as polymerisation activity increases. The bond angle between C3-C4-C5 increases upon the first (1.2°) and second (0.1°) methylene spacer being introduced into the monomer, furthermore the X-NB-Et monomer shows an additional (0.2°) increase. High polymerisation activity results also tend to be associated with high bond angle results for C5-C6-C1.

The C4-C5-C6 bond angle is shown to have an inverse relationship with the polymerisation activity; bond angle decreases as polymerisation activity increases. The bond angle between C4-C5-C6 decreases upon the first (0.1°) and second (0.2°) methylene spacer being introduced into the monomer. High polymerisation activity results also tend to be associated with low bond angle results for angle C7-C1-C6.

Table 6.11. Angles (degrees) for X-NB(CH₂)_nCO₂H, X-NB-Et and relationships to k_p X

Carbon No.	n			X-NB-Et	Relationship of angles to k _p X
	0	1	2		
3,4,7	100.4	100.1	100.1	100.0	Unclear
7,4,5	101.4	101.5	101.5	101.5	Unclear
2,1,7	100.3	100.1	100.2	100.2	Unclear
7,1,6	100.3	100.3	100.1	100.2	Inverse
2,1,6	106.6	106.4	106.6	106.5	Unclear
1,7,4	93.7	93.5	93.5	93.5	Unclear
1,2,3	107.5	107.4	107.4	107.4	Unclear
2,3,4	107.4	107.4	107.4	107.4	No Variation
4,5,6	102.1	102.0	101.8	101.8	Inverse
5,6,1	103.2	103.4	103.5	103.5	Direct
3,4,5	104.3	105.5	105.6	105.8	Direct
H-C2 to C2-C1	186.6	186.7	186.5	-	Unclear
H-C3 to C3-C4	186.9	187.1	186.8	-	Unclear

It is interesting to note that the bond angles C1-C2-C3 and C2-C3-C4 do not change during the introduction of methylene spacers, table 6.11. This finding adds weight to the idea that the C2=C3 is structurally unaffected by the methylene spacing of the carboxylic acid group. The bond angles for C2-C1-C7 and C2-C1-C6 do not change significantly during the methylene spacing.

The *endo* deformability effect, considers that the *exo* face of norbornene is more reactive than the *endo* face because the olefin part of isolated norbornene is already non-planar with its hydrogen atoms bent to the *endo* face. Further bending to reach the transition state for the *exo*-insertion reaction requires less energy than for the *endo*-insertion reaction, where bending all the way back to the *exo* side is required.⁸ The olefin carbon atoms are pyramidal, with the hydrogen atoms bent toward the *endo* face. We define the pyramidalisation or bending angle as the dihedral angle between H-C2 and C2-C1 (and also between H-C3 and C3-C4) with respect to the C2-C3 axis, figure 6.5. It was thought that this *endo* deformability maybe responsible for the observed polymerisation rate changes during functional group methylene spacing. The results in table 6.11 show there to be no clear

correlation between polymerisation activity and the *endo*-deformity, making this hypothesis unlikely.

The main structural changes within the X-norbornene monomers, measured using the atomic distances, bond lengths and bond angles described, all involve the C3, C4, C5 and perhaps C6, atoms. It appears from the data that all the other structural changes are simply a reaction to the changes occurring at these key atom locations. These key changes could possibly be localised even further, to the C5 and C4 atoms. This is not surprising given that these carbon atoms are the shortest link between the C=C and the electron withdrawing substituent, meaning they are the most heavily affected atom locations when the functional group is methylene spaced away from the norbornene structure.

The Mulliken atomic charges show a number of interesting trends during the methylene spacing of the carboxylic acid functional group, table 6.12. There is an increase in negative charge (electron density) associated with C2 and C3 as the methylene spacing increases and the polymerisation activity increases. This is suggesting that as the C2=C3 bond becomes more electron rich; it causes the monomers' polymerisation activity to increase. This idea is in full agreement with the coordination-insertion polymerisation mechanism discussed in detail in section 6.2.1. It is also notable that there is always more negative charge associated with C3 than C2, which is in full agreement with William Tam's publications.³

Table 6.12. Mulliken atomic charges (e) for X-NB(CH₂)_nCO₂H and relationship to k_p

Carbon No.	n			Relationship of input to k _p X
	0	1	2	
1	-0.103751	-0.100856	-0.100323	Direct
2	-0.149236	-0.151925	-0.156038	Inverse
3	-0.17608	-0.176618	-0.177934	Inverse
4	-0.065775	-0.058572	-0.054955	Direct
5	-0.159246	-0.131615	-0.149293	Unclear
6	-0.087638	-0.069471	-0.088276	Unclear
7	-0.098513	-0.102857	-0.100993	Unclear

There is also a significant relationship between the electron density at C1 and C4 and polymerisation activity, with less electron density resulting in an increased polymerisation activity. The electron density associated with the C5, C6 and C7 atoms, appears to oscillate with each additional methylene spacer, but this trend can only be verified upon further results using additional spacers.

6.2.4.2 Molecular Modelling of *endo*-Carboxylic Acid Functionalised Norbornenes

The C2=C3 bond length does not change during the methylene spacing of the highly electron withdrawing carboxylic acid group, table 6.13. This detail is also replicated for the X-functionalised monomers.

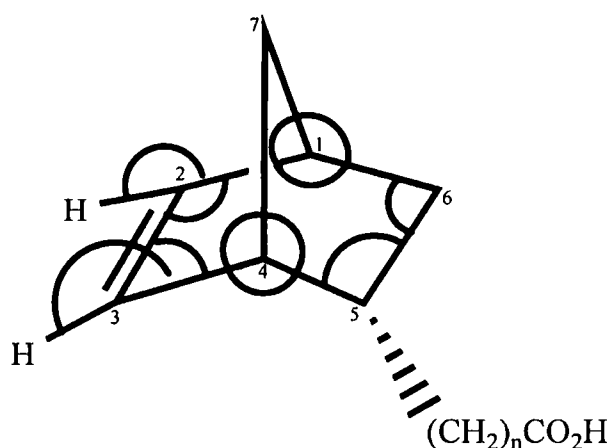


Figure 6.6. Atom numbering scheme for N-NB(CH₂)_nCO₂H

The effects of methylene spacing upon the structure of N-functionalised norbornenes are shown to be different in a number of ways from effects described in section 6.2.4.1, for their X-analogues.

Table 6.13. Atomic distances (Å) for N-NB(CH₂)_nCO₂H and relationship to k_p

Carbon No.	n			Relationship of input to k _p N
	0	1	2	
C1-C2	1.511	1.513	1.512	Unclear
C2-C3	1.332	1.333	1.333	Unclear
C3-C4	1.513	1.513	1.513	No Variation
C4-C5	1.561	1.564	1.566	Direct
C5-C6	1.561	1.554	1.554	Unclear
C1-C6	1.558	1.556	1.556	Unclear
C4-C7	1.539	1.536	1.536	Unclear
C1-C7	1.536	1.537	1.536	Unclear
C2-C6	2.450	2.450	2.449	Inverse
C3-C5	2.505	2.483	2.483	Unclear
C1-C4	2.242	2.243	2.241	Inverse
C7-C2	2.335	2.338	2.338	Unclear
C7-C3	2.339	2.338	2.340	Direct

There are a number of bond and atomic distance changes in the N-functionalised norbornene structure upon the methylene spacing of the carboxylic acid functional group, table 6.13. The C4-C5 and C7-C3 bond lengths show a direct relationship with the polymerisation activity; bond length increases as polymerisation activity increases. The C4-C5 bond length increases during the first (0.003 Å) and second (0.002 Å) methylene spacing. This is the opposite structural change shown by the C4-C5 bond in the X-regioisomer discussed in section 6.2.4.1. The C1-C4 and C2-C6 bond lengths show a inverse relationship with the polymerisation activity; bond length increases as polymerisation activity increases.

When the first methylene spacer is introduced into the N-monomers structure: C5-C6 bond length increases by 0.003 Å; C1-C6 bond length decreases by 0.002 Å and the C4-C7 bond length decreases by 0.003 Å. Although no change in bond length occurs for the C5-C6, C1-C6, C4-C7 bonds, upon the addition of the second methylene spacer. The bond length changes described for the C5-C6 and C1-C6 bonds are similar to those observed for the corresponding X-regioisomers discussed in the section 6.2.4.1. This suggests that the changing bond lengths are a result of the sterics changing around C5 when the carboxylic

acid group is no longer directly bound to C5. It is difficult to rationalise if this would cause the polymerisation activity of the monomer to change.

This particular changing of structure is also displayed by a bond angle change, table 6.14. The C3-C4-C5 bond angle is shown to have an inverse relationship with the polymerisation activity; bond angle decreases as polymerisation activity increases. The bond angle between C3-C4-C5 increases upon the first (1.5°) and second (0.1°) methylene spacer being introduced into the monomer. This is the opposite structural change shown by the C3-C4-C5 bond angle in the X-regioisomer discussed in section 6.2.4.1.

The C4-C5-C6 and C2-C3-C4 bond angles are also shown to have inverse relationships with the polymerisation activity; bond angle decreases as polymerisation activity increases. The bond angle between C4-C5-C6 decreases upon the first (0.3°) and second (0.2°) methylene spacer being introduced into the monomer, which is similar to the structural change shown by the X-regioisomer discussed in section 6.2.4.1. The bond angle between C2-C3-C4 decreases upon the first (0.1°) and second (0.1°) methylene spacer being introduced into the monomer, which is different to the results for the X-regioisomers, where no change was observed. A high polymerisation activity result is associated with a low bond angle result when $n = 2$, for angle C7-C1-C6.

Table 6.14. Angles (degree) for N-NB(CH₂)_nCO₂H and relationship to k_p

Angles	n			Relationship of input to k _p N
	0	1	2	
3,4,7	100.1	100.1	100.2	Direct
7,4,5	98.4	99.6	99.8	Direct
2,1,7	100.1	100.1	100.1	No Variation
7,1,6	101.2	100.5	100.5	Unclear
2,1,6	105.9	105.9	105.9	No Variation
1,7,4	93.6	93.7	93.7	Unclear
1,2,3	107.4	107.5	107.5	Unclear
2,3,4	107.6	107.5	107.4	Inverse
4,5,6	102.6	102.3	102.1	Inverse
5,6,1	102.4	103.2	103.3	Direct
3,4,5	109.1	107.6	107.5	Inverse
H-C2 to C2-C1	187.3	186.3	186.7	Unclear
H-C3 to C3-C4	186.1	185.5	186.1	Unclear

The C7-C4-C5 and C5-C6-C1 bond angles are shown to have direct relationships with the polymerisation activity; bond angle increases as polymerisation activity increases. The bond angle for C7-C4-C5 increases upon the first (1.2°) and second (0.2°) methylene spacer being introduced into the monomer. The bond angle for C5-C6-C1 increases upon the first (0.8°) and second (0.1°) methylene spacer being introduced into the monomer.

The bond angles for C1-C2-C3, C2-C1-C7 and C2-C1-C6 are the same for n = 0, 1, and 2; this is similar to the results for the X-regioisomers.

The results in table 6.14 show there to be no clear correlation between polymerisation activity and the *endo*-deformity, which is in agreement with the results for the X-functionalised norbornenes.

There are a large number of significant structural changes within the N-functionalised norbornene monomers, measured using the atomic distances, bond lengths and bond angles described; all involve the C3, C4, C5, C6 and C7 atoms. Although many of the structural

changes differ from those occurring in the analogous X-regioisomers, these key structural changes could again possibly be localised to the C3, C4 and C5 atoms.

The Mulliken atomic charges do not show many clear relationships with the polymerisation activity during the methylene spacing of the carboxylic acid functional group, table 6.15. There is a decrease in electron density associated with C2 and an increase in electron density at C3 as the methylene spacing increases and the polymerisation activity increases. This result is different from the X-regioisomer described in the previous section, where electron density increased for both C2 and C3.

Table 6.15. Mulliken atomic charges (e) for N-NB(CH₂)_nCO₂H and relationship to k_p

Carbon No.	n			Relationship of input to k _p N
	0	1	2	
1	-0.100155	-0.099774	-0.100229	Unclear
2	-0.159932	-0.150621	-0.14744	Inverse
3	-0.147846	-0.194163	-0.179728	Unclear
4	-0.075224	-0.068864	-0.090541	Direct
5	-0.150289	-0.131455	-0.138584	Unclear
6	-0.071122	-0.079279	-0.082478	Direct
7	-0.10154	-0.094705	-0.092451	Inverse

There is also a significant relationship between polymerisation activity and the electron density at C6, C7 and C4. The C6 and C4 negative electron densities are shown to have direct relationships with the polymerisation activity; electron density increases as polymerisation activity increases. The C7 negative electron densities are shown to have inverse relationships with the polymerisation activity; electron density decreases as polymerisation activity increases. The electron density associated with the C1, C3, C4 and C5 atoms, appears to oscillate with each additional methylene spacers, but this trend can only be verified upon further results using additional spacers.

6.3 Conclusions

^{13}C NMR spectroscopy shifts are used to attempt to rationalise the effects of introducing methylene spacers between norbornene and its functional group. The key bicyclic carbons within the monomer structures displayed no regular or consistent trends in ^{13}C NMR signal shifts, upon the methylene spacing of the $-\text{CO}_2\text{TMS}$, $-\text{OMe}$, $-\text{NHSO}_2\text{CF}_3$ and $-\text{OAc}$ functionalities. This suggests that a norbornene monomers polymerisation activity cannot be predicted solely on the basis on its ^{13}C NMR signals.

Theoretical calculations are performed on isolated molecules of *endo*- and *exo*-NB- $(\text{CH}_2)_n\text{CO}_2\text{H}$, where $n = 0, 1$ and 2 , using the Gaussian 03 program, to rationalise the effects of introducing methylene spacers between norbornene and its functional group. The relationships between polymerisation activity and bond lengths, bond angles and Mulliken atomic charges are examined. Although the relationships shown for the *exo*-regioisomers differ from those occurring in the analogous *endo*-regioisomers, the main structural changes for both regioisomers involve the C3, C4, C5 and perhaps C6, atoms, which is not surprising given that these carbon atoms are nearest the electron withdrawing substituent. The results obtained suggest that although the structure of the norbornene monomers are changing slightly during the methylene spacing of the electron withdrawing functional groups, the changes observed cannot be used to justify the monomers changes in polymerisation activity. This suggests that a norbornene monomers polymerisation activity cannot be predicted solely on the analysis of its theoretical molecular structure.

The future work should look more deeply into the theoretical calculations, including the cationic palladium catalyst in the calculations. The calculations need to particularly focus on the ground and transition states for the coordination and insertion of the norbornene monomers into the palladium alkyl bond. These ideas are justified in more detail in the polymerisation mechanism section 6.2.1.

6.4 References

-
- ¹ Kim, K. H.; Han, Y. -K.; Lee, S. U.; Chun, S. -H.; Ok, J. H. *J. Mol Model* **2003**, *9*, 304 – 307.
- ² Greenwood, N. N.; Earnshaw, A. *Chemistry of the Elements – Second Edition*.
- ³ Mayo, P.; Orlova, G.; Goddard, J. D.; Tam, W. *J. Org. Chem.* **2001**, *66*, 5182 - 5191.
- ⁴ Bradley, T. W.; Wilson, P. J.; Tozer, D. J. *J. Chem. Phys.* **2001**, *115*, 9233 - 9242.
- ⁵ Dunning, T. H. *J. Chem Phys.* **1971**, *55*, 716 - 723.
- ⁶ Dunning, T. H. *J. Chem. Phys.* **1989**, *90*, 1007.
- ⁷ Gaussian 03, Revision C.02, Frisch, M. J.; Trucks, G. W.; Schlegel, H. B.; Scuseria, G. E.; Robb, M. A.; Cheeseman, J. R.; Montgomery, J. A.; Vreven, Jr., T.; Kudin, K. N.; Burant, J. C.; Millam, J. M.; Iyengar, S. S.; Tomasi, J.; Barone, V.; Mennucci, B.; Cossi, M.; Scalmani, G.; Rega, N.; Petersson, G. A.; Nakatsuji, H.; Hada, M.; Ehara, M.; Toyota, K.; Fukuda, R.; Hasegawa, J.; Ishida, M.; Nakajima, T.; Honda, Y.; Kitao, O.; Nakai, H.; Klene, M.; Li, X.; Knox, J. E.; Hratchian, H. P.; Cross, J. B.; Bakken, V.; Adamo, C.; Jaramillo, J.; Gomperts, R.; Stratmann, R. E.; Yazyev, O.; Austin, A. J.; Cammi, R.; Pomelli, C.; Ochterski, J. W.; Ayala, P. Y.; Morokuma, K.; Voth, G. A.; Salvador, P.; Dannenberg, J. J.; Zakrzewski, V. G.; Dapprich, S.; Daniels, A. D.; Strain, M. C.; Farkas, O.; Malick, D. K.; Rabuck, A. D.; Raghavachari, K.; Foresman, J. B.; Ortiz, J. V.; Cui, Q.; Baboul, A. G.; Clifford, S.; Cioslowski, J.; Stefanov, B. B.; Liu, G.; Liashenko, A.; Piskorz, P.; Komaromi, I.; Martin, R. L.; Fox, D. J.; Keith, T.; Al-Laham, M. A.; Peng, C. Y.; Nanayakkara, C. Y.; Challacombe, M.; Gill, P. M. W.; Johnson, B.; Chen, W.; Wong, M. W.; Gonzalez, C.; and Pople, J. A. *Gaussian, Inc., Wallingford CT, 2004*.
- ⁸ Koga, N.; Ozawa, T.; Morokuma, K. *J. Phys. Org. Chem*, **1990**, *3*, 519 - 533.

Appendix

Data for the crystal structure of X-TD-OAc

Table I. Crystal data and structure refinement for X-TD-OAc.

Empirical formula	C ₁₄ H ₁₈ O ₂	
Formula weight	218.28	
Temperature	120(2) K	
Wavelength	0.71073 Å	
Crystal system	Triclinic	
Space group	$P\bar{1}$ (no. 2)	
Unit cell dimensions	$a = 6.1273(7)$ Å	$\alpha = 104.72(1)^\circ$
	$b = 8.6586(11)$ Å	$\beta = 91.12(1)^\circ$
	$c = 11.1099(14)$ Å	$\gamma = 93.72(1)^\circ$
Volume	568.5(1) Å ³	
Z	2	
Density (calculated)	1.275 g/cm ³	
Absorption coefficient	0.083 mm ⁻¹	
F(000)	236	
Crystal size	0.3 × 0.2 × 0.1 mm ³	
θ range for data collection	2.7 to 29.0°	
Index ranges	$-8 \leq h \leq 8, -11 \leq k \leq 11, -15 \leq l \leq 15$	
Reflections collected	6553	
Independent reflections	2994 [R(int) = 0.0229]	
Reflections with $I > 2\sigma(I)$	2437	
Completeness to $\theta = 28.99^\circ$	99.2 %	
Absorption correction	None	
Refinement method	Full-matrix least-squares on F ²	
Data / restraints / parameters	2994 / 0 / 217	
Largest final shift/e. s.d. ratio	0.000	
Goodness-of-fit on F ²	1.038	
Final R indices [$I > 2\sigma(I)$]	R1 = 0.0426, wR2 = 0.1092	
R indices (all data)	R1 = 0.0517, wR2 = 0.1143	
Largest diff. peak and hole	0.391 and -0.209 e.Å ⁻³	

Table II. Atomic coordinates ($\times 10^5$) and equivalent isotropic displacement parameters ($\text{\AA}^2 \times 10^4$) for X-TD-OAc. $U(\text{eq})$ is defined as one third of the trace of the orthogonalized U_{ij} tensor.

	x	y	z	$U(\text{eq})$
O(1)	60718(12)	24640(9)	20189(7)	185(2)
O(2)	69830(15)	15900(10)	222(8)	289(2)
C(1)	9350(20)	75921(14)	44975(12)	250(3)
C(2)	30300(20)	79228(13)	48617(11)	231(3)
C(3)	42663(18)	82171(13)	37620(10)	181(2)
C(4)	7159(18)	76461(13)	31497(11)	214(2)
C(5)	43125(16)	66140(12)	27218(10)	154(2)
C(6)	18506(17)	62266(13)	22843(11)	185(2)
C(7)	24918(19)	90083(13)	31686(11)	202(2)
C(8)	14376(18)	44778(13)	23548(12)	218(2)
C(9)	49733(17)	50639(12)	30264(10)	156(2)
C(10)	51343(18)	38572(13)	17620(10)	171(2)
C(11)	27122(19)	34659(14)	12826(11)	233(3)
C(12)	28663(18)	43484(13)	34759(11)	203(2)
C(13)	69736(16)	14400(12)	10722(10)	177(2)
C(14)	79270(20)	1167(15)	15045(12)	229(3)

Table III. Bond lengths [Å] and angles [°] for X-TD-OAc.

O(1)-C(13)	1.3453(12)	C(7)-H(71)	0.972(14)
O(1)-C(10)	1.4578(12)	C(7)-H(72)	1.011(14)
O(2)-C(13)	1.2062(13)	C(8)-C(12)	1.5398(17)
C(1)-C(2)	1.3294(18)	C(8)-C(11)	1.5464(16)
C(1)-C(4)	1.5135(17)	C(8)-H(8)	0.970(14)
C(1)-H(1)	0.936(15)	C(9)-C(10)	1.5322(15)
C(2)-C(3)	1.5168(16)	C(9)-C(12)	1.5423(15)
C(2)-H(2)	0.964(15)	C(9)-H(9)	0.974(13)
C(3)-C(7)	1.5441(16)	C(10)-C(11)	1.5534(15)
C(3)-C(5)	1.5665(15)	C(10)-H(10)	0.993(13)
C(3)-H(3)	0.971(13)	C(11)-H(111)	0.946(14)
C(4)-C(7)	1.5478(16)	C(11)-H(112)	1.032(15)
C(4)-C(6)	1.5668(15)	C(12)-H(121)	1.001(13)
C(4)-H(4)	1.001(13)	C(12)-H(122)	0.989(13)
C(5)-C(9)	1.5414(14)	C(13)-C(14)	1.4967(15)
C(5)-C(6)	1.5644(14)	C(14)-H(141)	0.966(14)
C(5)-H(5)	0.989(13)	C(14)-H(142)	0.959(16)
C(6)-C(8)	1.5409(16)	C(14)-H(143)	0.990(18)
C(6)-H(6)	1.000(14)		
C(13)-O(1)-C(10)	117.77(8)	C(7)-C(4)-C(6)	98.65(8)
C(2)-C(1)-C(4)	108.05(10)	C(1)-C(4)-H(4)	115.4(8)
C(2)-C(1)-H(1)	126.6(9)	C(7)-C(4)-H(4)	118.0(8)
C(4)-C(1)-H(1)	125.0(9)	C(6)-C(4)-H(4)	113.2(8)
C(1)-C(2)-C(3)	107.40(10)	C(9)-C(5)-C(6)	103.69(8)
C(1)-C(2)-H(2)	126.2(8)	C(9)-C(5)-C(3)	121.36(9)
C(3)-C(2)-H(2)	126.1(8)	C(6)-C(5)-C(3)	102.87(8)
C(2)-C(3)-C(7)	99.34(9)	C(9)-C(5)-H(5)	109.0(8)
C(2)-C(3)-C(5)	109.91(9)	C(6)-C(5)-H(5)	111.8(7)
C(7)-C(3)-C(5)	98.91(8)	C(3)-C(5)-H(5)	107.8(8)
C(2)-C(3)-H(3)	115.4(8)	C(8)-C(6)-C(5)	102.40(8)
C(7)-C(3)-H(3)	117.3(8)	C(8)-C(6)-C(4)	122.77(9)
C(5)-C(3)-H(3)	113.9(8)	C(5)-C(6)-C(4)	102.48(8)
C(1)-C(4)-C(7)	98.97(9)	C(8)-C(6)-H(6)	109.7(8)
C(1)-C(4)-C(6)	110.68(9)	C(5)-C(6)-H(6)	112.0(8)

C(4)-C(6)-H(6)	107.2(8)	H(121)-C(12)-H(122)	108.8(11)
C(3)-C(7)-C(4)	93.50(8)	O(2)-C(13)-O(1)	123.48(10)
C(3)-C(7)-H(71)	114.5(8)	O(2)-C(13)-C(14)	125.66(10)
C(4)-C(7)-H(71)	112.1(9)	O(1)-C(13)-C(14)	110.86(9)
C(3)-C(7)-H(72)	113.4(7)	C(13)-C(14)-H(141)	111.2(8)
C(4)-C(7)-H(72)	111.8(7)	C(13)-C(14)-H(142)	110.1(10)
H(71)-C(7)-H(72)	110.6(11)	H(141)-C(14)-H(142)	112.4(13)
C(12)-C(8)-C(6)	105.05(9)	C(13)-C(14)-H(143)	110.1(10)
C(12)-C(8)-C(11)	99.71(9)	H(141)-C(14)-H(143)	106.6(13)
C(6)-C(8)-C(11)	105.83(10)	H(142)-C(14)-H(143)	106.2(13)
C(12)-C(8)-H(8)	117.5(8)		
C(6)-C(8)-H(8)	115.3(8)		
C(11)-C(8)-H(8)	111.8(8)		
C(10)-C(9)-C(5)	105.32(8)		
C(10)-C(9)-C(12)	99.50(8)		
C(5)-C(9)-C(12)	104.86(8)		
C(10)-C(9)-H(9)	113.9(8)		
C(5)-C(9)-H(9)	114.8(8)		
C(12)-C(9)-H(9)	116.8(8)		
O(1)-C(10)-C(9)	106.20(8)		
O(1)-C(10)-C(11)	111.33(9)		
C(9)-C(10)-C(11)	103.49(8)		
O(1)-C(10)-H(10)	106.7(8)		
C(9)-C(10)-H(10)	115.0(8)		
C(11)-C(10)-H(10)	114.0(8)		
C(8)-C(11)-C(10)	103.05(9)		
C(8)-C(11)-H(111)	110.6(8)		
C(10)-C(11)-H(111)	109.6(8)		
C(8)-C(11)-H(112)	114.9(8)		
C(10)-C(11)-H(112)	111.3(8)		
H(111)-C(11)-H(112)	107.3(11)		
C(8)-C(12)-C(9)	94.34(8)		
C(8)-C(12)-H(121)	111.8(8)		
C(9)-C(12)-H(121)	112.4(7)		
C(8)-C(12)-H(122)	114.2(8)		
C(9)-C(12)-H(122)	114.8(8)		

Table IV. Anisotropic displacement parameters ($\text{\AA}^2 \times 10^4$) for X-TD-OAc. The anisotropic displacement factor exponent takes the form: $-2\pi^2 [h^2 a^{*2} U_{11} + \dots + 2 h k a^* b^* U_{12}]$

	U_{11}	U_{22}	U_{33}	U_{23}	U_{13}	U_{12}
O(1)	229(4)	161(4)	171(4)	42(3)	36(3)	59(3)
O(2)	422(5)	280(5)	181(4)	63(3)	63(4)	122(4)
C(1)	306(6)	185(5)	274(6)	65(5)	145(5)	68(5)
C(2)	371(7)	168(5)	154(5)	24(4)	47(5)	85(5)
C(3)	193(5)	150(5)	189(5)	24(4)	3(4)	11(4)
C(4)	174(5)	187(5)	282(6)	54(5)	16(4)	40(4)
C(5)	155(5)	152(5)	156(5)	41(4)	22(4)	12(4)
C(6)	169(5)	184(5)	193(5)	32(4)	-14(4)	20(4)
C(7)	237(5)	166(5)	215(6)	64(4)	38(4)	43(4)
C(8)	139(5)	181(5)	315(6)	32(5)	4(4)	-10(4)
C(9)	158(5)	163(5)	144(5)	32(4)	0(4)	15(4)
C(10)	202(5)	152(5)	166(5)	45(4)	20(4)	42(4)
C(11)	234(6)	189(6)	243(6)	-2(5)	-59(5)	20(4)
C(12)	235(6)	162(5)	228(6)	74(4)	72(4)	23(4)
C(13)	168(5)	177(5)	171(5)	17(4)	15(4)	8(4)
C(14)	263(6)	209(6)	221(6)	51(5)	27(5)	73(5)

Table V. Hydrogen coordinates ($\times 10^3$) and isotropic displacement parameters ($\text{\AA}^2 \times 10^3$) for X-TD-OAc.

	x	y	z	U(iso)
H(1)	-19(2)	726(2)	495(1)	37(4)
H(2)	367(2)	786(2)	565(1)	34(4)
H(3)	569(2)	881(2)	397(1)	23(3)
H(4)	-80(2)	776(2)	285(1)	24(3)
H(5)	523(2)	683(2)	205(1)	21(3)
H(6)	160(2)	629(2)	141(1)	24(3)
H(71)	280(2)	911(2)	234(1)	32(4)
H(72)	210(2)	1007(2)	372(1)	23(3)
H(8)	-9(2)	409(2)	232(1)	29(4)
H(9)	628(2)	519(2)	357(1)	21(3)
H(10)	611(2)	423(2)	117(1)	23(3)
H(111)	233(2)	236(2)	117(1)	26(4)
H(112)	247(2)	371(2)	43(1)	32(4)
H(121)	298(2)	321(2)	350(1)	23(3)
H(122)	238(2)	496(2)	429(1)	22(3)
H(141)	915(2)	-29(2)	101(1)	32(4)
H(142)	832(3)	47(2)	238(2)	46(5)
H(143)	682(3)	-80(2)	141(2)	49(5)

Data for the crystal structure of N-NB-CO₂H

Table VI. Crystal data and structure refinement for (N-NB-CO₂H).

Empirical formula	C ₈ H ₁₀ O ₂	
Formula weight	138.16	
Temperature	120(2) K	
Wavelength	0.71073 Å	
Crystal system	Triclinic	
Space group	P $\bar{1}$ (no. 2)	
Unit cell dimensions	$a = 6.1306(6)$ Å	$\alpha = 92.39(1)^\circ$
	$b = 10.172(1)$ Å	$\beta = 96.72(1)^\circ$
	$c = 17.585(2)$ Å	$\gamma = 100.08(1)^\circ$
Volume	1070.1(2) Å ³	
Z	6	
Density (calculated)	1.286 g/cm ³	
Absorption coefficient	0.092 mm ⁻¹	
F(000)	444	
Crystal size	0.4 × 0.3 × 0.2 mm ³	
θ range for data collection	2.28 to 29.00°	
Index ranges	$-8 \leq h \leq 8, -13 \leq k \leq 13, -23 \leq l \leq 23$	
Reflections collected	12071	
Independent reflections	5650 [R(int) = 0.0413]	
Reflections with $I > 2\sigma(I)$	4580	
Completeness to $\theta = 29.00^\circ$	99.3 %	
Absorption correction	None	
Refinement method	Full-matrix least-squares on F ²	
Data / restraints / parameters	5650 / 0 / 391	
Largest final shift/e.s.d. ratio	0.003	
Goodness-of-fit on F ²	1.064	
Final R indices [$I > 2\sigma(I)$]	R1 = 0.0523, wR2 = 0.1473	
R indices (all data)	R1 = 0.0616, wR2 = 0.1537	
Largest diff. peak and hole	0.589 and -0.251 e.Å ⁻³	

Table VII. Atomic coordinates ($\times 10^5$) and equivalent isotropic displacement parameters ($\text{Å}^2 \times 10^4$) for (N-NB-CO₂H). U(eq) is defined as one third of the trace of the orthogonalized U_{ij} tensor.

	x	y	z	U(eq)
O(1)	31060(20)	69812(10)	23917(6)	367(3)
O(2)	28354(18)	90554(10)	20793(6)	314(2)
O(3)	59116(19)	92439(10)	11258(6)	319(2)
O(4)	62116(17)	71726(9)	14457(5)	289(2)
O(5)	50230(20)	33162(10)	46000(6)	370(3)
O(6)	50952(19)	52963(10)	41039(6)	332(2)
C(1)	22940(20)	99118(14)	41899(8)	290(3)
C(2)	31900(20)	88332(15)	40922(8)	308(3)
C(3)	13290(20)	76724(14)	37982(7)	254(3)
C(4)	4620(20)	79726(13)	29594(7)	243(3)
C(5)	-5390(20)	92478(15)	30799(8)	292(3)
C(6)	-2150(20)	95069(14)	39654(8)	271(3)
C(7)	-5670(30)	80688(14)	42133(9)	312(3)
C(8)	22400(20)	80786(13)	24351(7)	234(3)
C(11)	66060(30)	61532(16)	-5764(8)	360(4)
C(12)	56780(20)	72337(17)	-5041(8)	334(3)
C(13)	75430(20)	84210(14)	-2926(8)	260(3)
C(14)	85420(20)	82416(12)	5495(7)	224(3)
C(15)	96200(20)	69914(14)	4634(8)	281(3)
C(16)	91180(20)	66028(13)	-4122(8)	276(3)
C(17)	93490(20)	79924(14)	-7360(8)	281(3)
C(18)	67950(20)	81495(12)	10862(7)	216(3)
C(21)	95800(20)	40561(15)	29472(9)	298(3)
C(22)	90980(20)	32665(15)	35145(8)	281(3)
C(23)	68280(20)	24091(13)	32672(8)	257(3)
C(24)	50940(20)	33707(13)	32622(7)	223(3)
C(25)	56730(20)	42841(14)	26078(7)	242(3)
C(26)	76500(20)	37356(14)	23114(8)	265(3)
C(27)	68930(30)	22209(14)	23977(8)	288(3)
C(28)	51090(20)	40999(12)	40232(7)	217(3)

Table VIII. Bond lengths [Å] and angles [°] for (N-NB-CO₂H).

O(1)-C(8)	1.3203(15)	C(13)-C(17)	1.5384(18)
O(1)-H(01)	0.89(2)	C(13)-C(14)	1.5654(18)
O(2)-C(8)	1.2208(16)	C(13)-H(13)	0.988(17)
O(3)-C(18)	1.3232(15)	C(14)-C(18)	1.5016(18)
O(3)-H(02)	0.88(2)	C(14)-C(15)	1.5424(17)
O(4)-C(18)	1.2229(15)	C(14)-H(14)	0.954(17)
O(5)-C(28)	1.3162(15)	C(15)-C(16)	1.5549(19)
O(5)-H(05)	0.92(3)	C(15)-H(15A)	0.998(18)
O(6)-C(28)	1.2209(15)	C(15)-H(15B)	0.970(17)
C(1)-C(2)	1.324(2)	C(16)-C(17)	1.5357(19)
C(1)-C(6)	1.521(2)	C(16)-H(16)	0.967(18)
C(1)-H(1)	1.006(19)	C(17)-H(17A)	0.966(19)
C(2)-C(3)	1.517(2)	C(17)-H(17B)	0.961(18)
C(2)-H(2)	1.05(2)	C(21)-C(22)	1.334(2)
C(3)-C(7)	1.5446(19)	C(21)-C(26)	1.510(2)
C(3)-C(4)	1.5693(18)	C(21)-H(21)	0.979(18)
C(3)-H(3)	0.940(18)	C(22)-C(23)	1.513(2)
C(4)-C(8)	1.5009(18)	C(22)-H(22)	0.942(19)
C(4)-C(5)	1.5460(18)	C(23)-C(27)	1.5390(19)
C(4)-H(4)	0.958(19)	C(23)-C(24)	1.5649(17)
C(5)-C(6)	1.5520(19)	C(23)-H(23)	0.951(17)
C(5)-H(5A)	0.975(18)	C(24)-C(28)	1.5010(17)
C(5)-H(5B)	0.996(18)	C(24)-C(25)	1.5436(18)
C(6)-C(7)	1.530(2)	C(24)-H(24)	0.984(17)
C(6)-H(6)	0.964(19)	C(25)-C(26)	1.5534(18)
C(7)-H(7A)	1.02(2)	C(25)-H(25A)	0.997(17)
C(7)-H(7B)	1.044(18)	C(25)-H(25B)	0.957(16)
C(11)-C(12)	1.331(2)	C(26)-C(27)	1.5485(19)
C(11)-C(16)	1.518(2)	C(26)-H(26)	0.953(17)
C(11)-H(11)	0.960(19)	C(27)-H(27A)	0.980(18)
C(12)-C(13)	1.511(2)	C(27)-H(27B)	0.956(19)
C(12)-H(12)	1.00(2)		
C(8)-O(1)-H(01)	112.2(14)	C(18)-O(3)-H(02)	111.9(14)

C(28)-O(5)-H(05)	106.7(14)	H(7A)-C(7)-H(7B)	111.3(15)
C(2)-C(1)-C(6)	107.56(12)	O(2)-C(8)-O(1)	122.77(12)
C(2)-C(1)-H(1)	128.8(10)	O(2)-C(8)-C(4)	124.79(11)
C(6)-C(1)-H(1)	123.5(10)	O(1)-C(8)-C(4)	112.43(11)
C(1)-C(2)-C(3)	108.29(12)	C(12)-C(11)-C(16)	107.49(13)
C(1)-C(2)-H(2)	126.0(11)	C(12)-C(11)-H(11)	128.4(11)
C(3)-C(2)-H(2)	125.4(11)	C(16)-C(11)-H(11)	124.0(11)
C(2)-C(3)-C(7)	99.45(11)	C(11)-C(12)-C(13)	107.61(13)
C(2)-C(3)-C(4)	106.21(11)	C(11)-C(12)-H(12)	130.0(11)
C(7)-C(3)-C(4)	98.91(11)	C(13)-C(12)-H(12)	122.1(11)
C(2)-C(3)-H(3)	116.4(11)	C(12)-C(13)-C(17)	100.04(11)
C(7)-C(3)-H(3)	118.8(11)	C(12)-C(13)-C(14)	105.72(10)
C(4)-C(3)-H(3)	114.5(11)	C(17)-C(13)-C(14)	100.29(10)
C(8)-C(4)-C(5)	115.66(11)	C(12)-C(13)-H(13)	117.1(10)
C(8)-C(4)-C(3)	112.83(11)	C(17)-C(13)-H(13)	117.6(10)
C(5)-C(4)-C(3)	103.05(10)	C(14)-C(13)-H(13)	113.9(10)
C(8)-C(4)-H(4)	107.5(11)	C(18)-C(14)-C(15)	115.63(11)
C(5)-C(4)-H(4)	109.6(11)	C(18)-C(14)-C(13)	111.61(10)
C(3)-C(4)-H(4)	108.0(11)	C(15)-C(14)-C(13)	103.01(10)
C(4)-C(5)-C(6)	103.33(11)	C(18)-C(14)-H(14)	109.4(10)
C(4)-C(5)-H(5A)	110.8(10)	C(15)-C(14)-H(14)	107.5(10)
C(6)-C(5)-H(5A)	110.4(10)	C(13)-C(14)-H(14)	109.5(10)
C(4)-C(5)-H(5B)	112.5(10)	C(14)-C(15)-C(16)	103.00(10)
C(6)-C(5)-H(5B)	112.2(10)	C(14)-C(15)-H(15A)	111.9(11)
H(5A)-C(5)-H(5B)	107.6(14)	C(16)-C(15)-H(15A)	113.0(11)
C(1)-C(6)-C(7)	100.03(11)	C(14)-C(15)-H(15B)	110.7(10)
C(1)-C(6)-C(5)	105.31(11)	C(16)-C(15)-H(15B)	108.2(10)
C(7)-C(6)-C(5)	100.45(11)	H(15A)-C(15)-H(15B)	109.8(14)
C(1)-C(6)-H(6)	119.7(11)	C(11)-C(16)-C(17)	99.86(12)
C(7)-C(6)-H(6)	114.0(11)	C(11)-C(16)-C(15)	105.88(11)
C(5)-C(6)-H(6)	114.7(11)	C(17)-C(16)-C(15)	100.78(11)
C(6)-C(7)-C(3)	94.56(10)	C(11)-C(16)-H(16)	116.0(10)
C(6)-C(7)-H(7A)	111.2(10)	C(17)-C(16)-H(16)	117.3(10)
C(3)-C(7)-H(7A)	114.2(11)	C(15)-C(16)-H(16)	114.8(10)
C(6)-C(7)-H(7B)	111.1(10)	C(16)-C(17)-C(13)	93.80(10)
C(3)-C(7)-H(7B)	113.5(10)	C(16)-C(17)-H(17A)	115.0(11)

C(13)-C(17)-H(17A)	112.7(11)	C(25)-C(24)-H(24)	112.1(9)
C(16)-C(17)-H(17B)	112.9(10)	C(23)-C(24)-H(24)	106.8(10)
C(13)-C(17)-H(17B)	111.2(10)	C(24)-C(25)-C(26)	102.70(10)
H(17A)-C(17)-H(17B)	110.4(15)	C(24)-C(25)-H(25A)	110.6(10)
O(4)-C(18)-O(3)	122.80(12)	C(26)-C(25)-H(25A)	113.4(10)
O(4)-C(18)-C(14)	124.52(11)	C(24)-C(25)-H(25B)	111.6(9)
O(3)-C(18)-C(14)	112.68(11)	C(26)-C(25)-H(25B)	112.1(9)
C(22)-C(21)-C(26)	107.67(12)	H(25A)-C(25)-H(25B)	106.5(13)
C(22)-C(21)-H(21)	127.2(10)	C(21)-C(26)-C(27)	100.52(11)
C(26)-C(21)-H(21)	124.7(10)	C(21)-C(26)-C(25)	106.40(11)
C(21)-C(22)-C(23)	107.48(12)	C(27)-C(26)-C(25)	100.05(10)
C(21)-C(22)-H(22)	126.7(11)	C(21)-C(26)-H(26)	119.4(10)
C(23)-C(22)-H(22)	125.0(11)	C(27)-C(26)-H(26)	115.5(10)
C(22)-C(23)-C(27)	100.64(11)	C(25)-C(26)-H(26)	112.5(10)
C(22)-C(23)-C(24)	106.39(11)	C(23)-C(27)-C(26)	93.39(10)
C(27)-C(23)-C(24)	99.24(10)	C(23)-C(27)-H(27A)	114.2(10)
C(22)-C(23)-H(23)	115.5(10)	C(26)-C(27)-H(27A)	114.9(10)
C(27)-C(23)-H(23)	118.7(10)	C(23)-C(27)-H(27B)	114.6(11)
C(24)-C(23)-H(23)	114.2(10)	C(26)-C(27)-H(27B)	111.7(11)
C(28)-C(24)-C(25)	114.63(11)	H(27A)-C(27)-H(27B)	107.7(15)
C(28)-C(24)-C(23)	113.91(10)	O(6)-C(28)-O(5)	122.38(12)
C(25)-C(24)-C(23)	103.36(10)	O(6)-C(28)-C(24)	123.84(11)
C(28)-C(24)-H(24)	105.9(10)	O(5)-C(28)-C(24)	113.70(11)

Table IX. Anisotropic displacement parameters ($\text{\AA}^2 \times 10^4$) for (N-NB-CO₂H). The anisotropic displacement factor exponent takes the form: $-2\pi^2[h^2 a^* U_{11} + \dots + 2 h k a^* b^* U_{12}]$

	U ₁₁	U ₂₂	U ₃₃	U ₂₃	U ₁₃	U ₁₂
O(1)	488(6)	320(6)	407(6)	145(5)	259(5)	221(5)
O(2)	427(6)	296(5)	289(5)	70(4)	162(4)	164(4)
O(3)	449(6)	258(5)	333(5)	75(4)	197(5)	178(4)
O(4)	402(5)	251(5)	268(5)	61(4)	138(4)	136(4)
O(5)	684(8)	233(5)	212(5)	25(4)	112(5)	97(5)
O(6)	532(7)	247(5)	243(5)	23(4)	111(4)	99(4)
C(1)	300(7)	296(7)	250(6)	-24(5)	55(5)	-11(5)
C(2)	269(7)	413(8)	237(6)	7(6)	11(5)	64(6)
C(3)	308(7)	260(6)	209(6)	42(5)	68(5)	67(5)
C(4)	245(6)	269(6)	210(6)	-20(5)	28(5)	45(5)
C(5)	275(7)	352(7)	269(7)	-4(5)	42(5)	118(6)
C(6)	279(6)	280(6)	277(7)	-1(5)	84(5)	86(5)
C(7)	335(7)	312(7)	299(7)	3(6)	139(6)	28(6)
C(8)	280(6)	259(6)	175(5)	-1(5)	22(5)	93(5)
C(11)	422(8)	376(8)	241(7)	-67(6)	140(6)	-84(7)
C(12)	265(7)	543(9)	177(6)	-6(6)	41(5)	25(6)
C(13)	295(7)	296(7)	233(6)	75(5)	108(5)	116(5)
C(14)	227(6)	207(6)	239(6)	-12(5)	34(5)	44(5)
C(15)	307(7)	292(7)	280(7)	27(5)	56(5)	140(5)
C(16)	358(7)	229(6)	276(6)	8(5)	160(5)	67(5)
C(17)	303(7)	276(7)	305(7)	63(5)	156(6)	80(5)
C(18)	273(6)	208(6)	172(5)	-24(4)	10(4)	72(5)
C(21)	228(6)	318(7)	371(7)	37(6)	99(5)	71(5)
C(22)	209(6)	367(7)	296(7)	56(6)	38(5)	120(5)
C(23)	272(6)	246(6)	291(7)	60(5)	101(5)	100(5)
C(24)	197(6)	262(6)	219(6)	-1(5)	41(4)	60(5)
C(25)	273(6)	297(7)	185(6)	17(5)	40(5)	120(5)
C(26)	309(7)	288(7)	234(6)	44(5)	113(5)	92(5)
C(27)	329(7)	270(6)	293(7)	-24(5)	112(6)	92(5)
C(28)	187(5)	250(6)	223(6)	15(5)	54(4)	48(4)

Table X. Hydrogen coordinates ($\times 10^4$) and isotropic displacement parameters ($\text{\AA}^2 \times 10^3$) for (N-NB-CO₂H).

	x	y	z	U(iso)
H(01)	4180(40)	7050(20)	2087(13)	59(6)
H(02)	4890(40)	9180(20)	1442(13)	54(6)
H(05)	4920(40)	3850(20)	5029(15)	71(7)
H(1)	3060(30)	10859(19)	4342(11)	40(5)
H(2)	4900(30)	8800(20)	4151(11)	46(5)
H(3)	1660(30)	6810(18)	3848(10)	35(4)
H(4)	-700(30)	7246(19)	2756(11)	39(5)
H(5A)	-2120(30)	9089(17)	2882(10)	32(4)
H(5B)	210(30)	10019(17)	2819(10)	35(4)
H(6)	-1210(30)	10042(17)	4159(10)	37(4)
H(7A)	-2130(30)	7559(19)	4003(11)	42(5)
H(7B)	-280(30)	8049(17)	4809(11)	38(5)
H(11)	5880(30)	5237(19)	-681(10)	41(5)
H(12)	4070(30)	7312(18)	-520(11)	44(5)
H(13)	7180(30)	9317(17)	-373(9)	30(4)
H(14)	9710(30)	8979(17)	719(10)	31(4)
H(15A)	8990(30)	6264(18)	782(10)	40(5)
H(15B)	11230(30)	7218(16)	597(9)	27(4)
H(16)	10010(30)	5995(17)	-600(10)	32(4)
H(17A)	8980(30)	7989(18)	-1286(11)	41(5)
H(17B)	10780(30)	8543(17)	-575(10)	31(4)
H(21)	10850(30)	4789(18)	2954(10)	37(4)
H(22)	9880(30)	3328(17)	4012(11)	40(5)
H(23)	6480(30)	1638(17)	3548(10)	33(4)
H(24)	3600(30)	2808(17)	3147(9)	32(4)
H(25A)	6070(30)	5240(17)	2806(10)	31(4)
H(25B)	4430(30)	4226(15)	2217(9)	26(4)
H(26)	7870(30)	3982(17)	1805(10)	34(4)
H(27A)	5450(30)	1824(17)	2104(10)	35(4)
H(27B)	7970(30)	1714(18)	2258(11)	40(5)

Table XI. Hydrogen bonds for (N-NB-CO₂H) [Å and °].

D-H...A	d(D-H)	d(H...A)	d(D...A)	<(DHA)
O(1)-H(01)...O(4)	0.89(2)	1.77(2)	2.6587(14)	177(2)
O(3)-H(02)...O(2)	0.88(2)	1.77(2)	2.6542(14)	180(2)
O(5)-H(05)...O(6)#1	0.92(3)	1.73(3)	2.6453(14)	173(2)

Symmetry transformations used to generate equivalent atoms: #1 -x+1,-y+1,-z+1

Data for the statistical analysis in chapter 6

Figure I

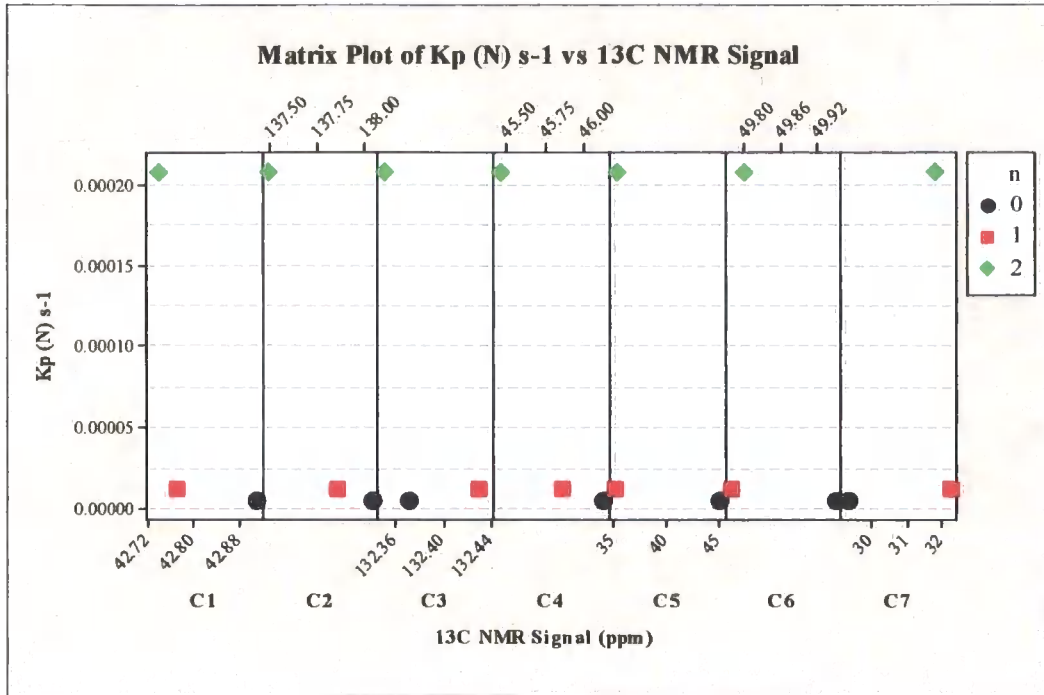


Figure II

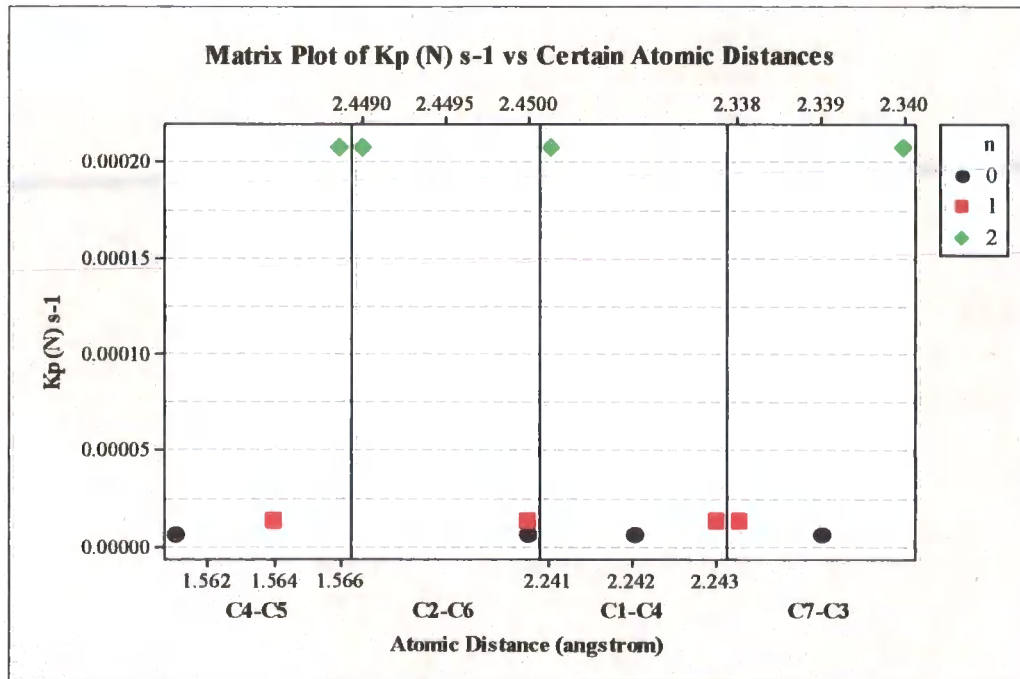


Figure III

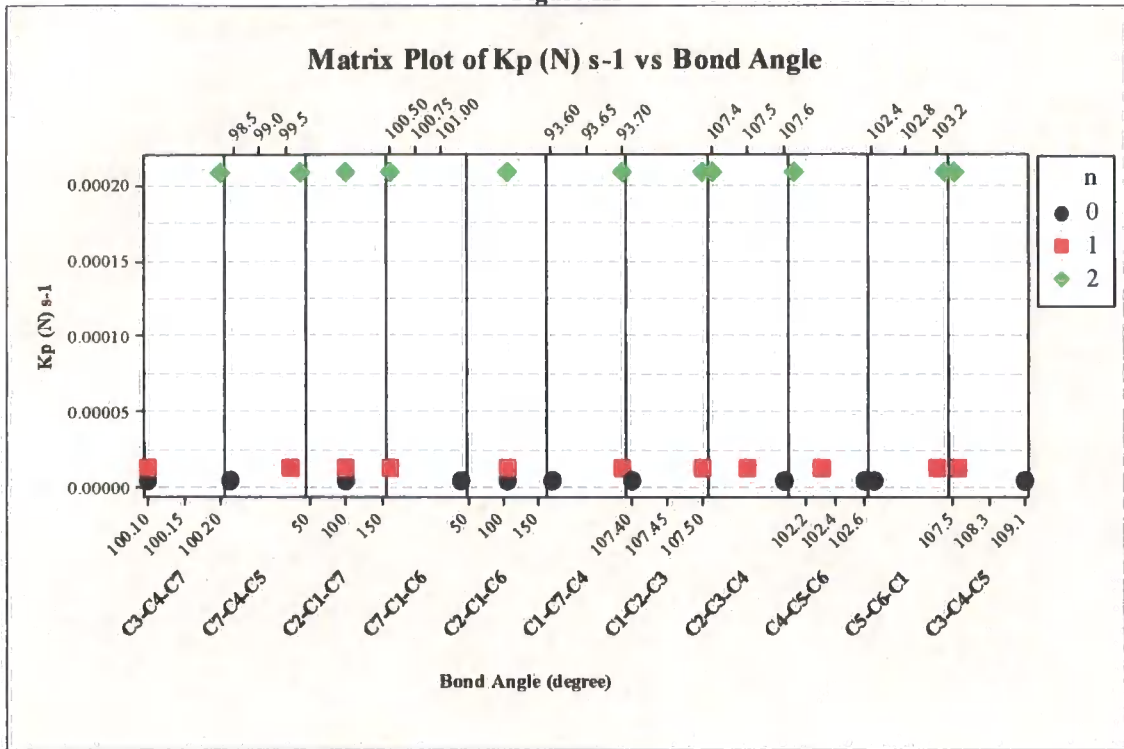


Figure IV

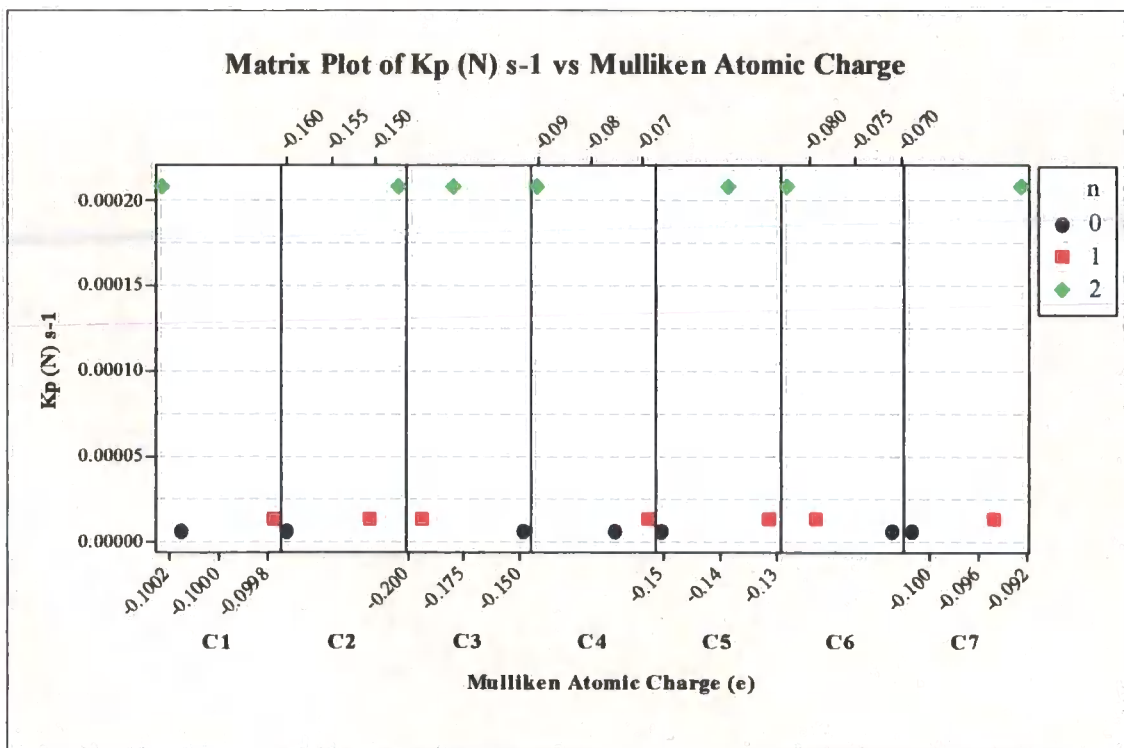


Figure V

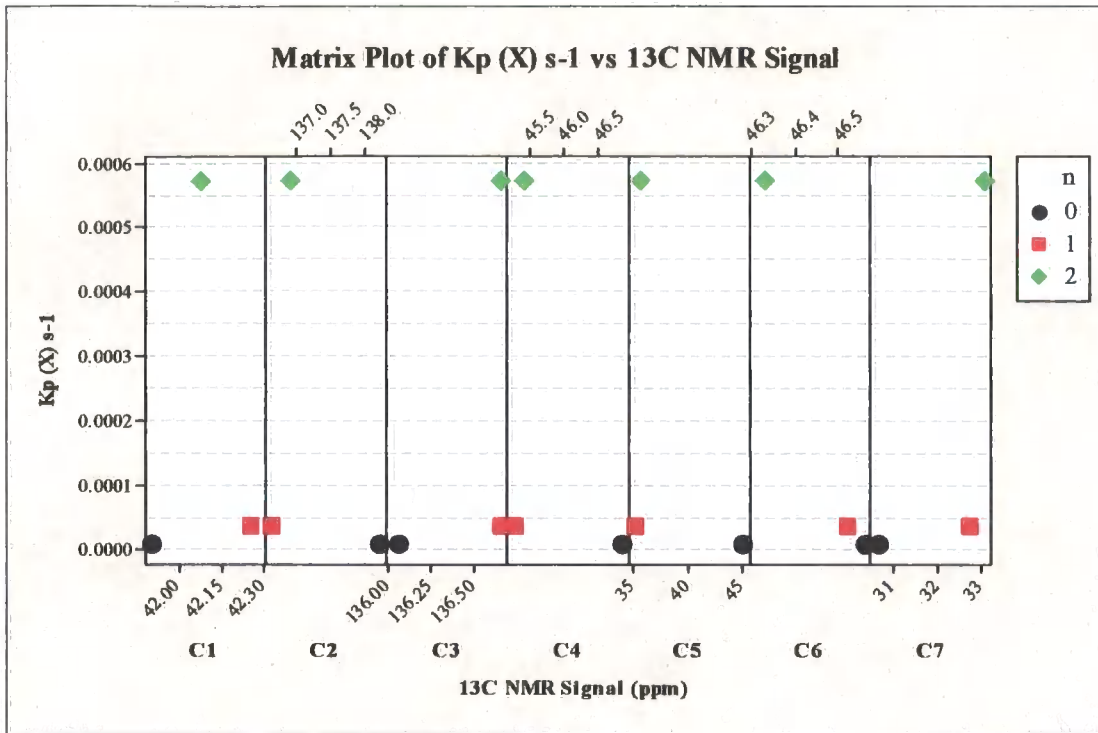


Figure VI

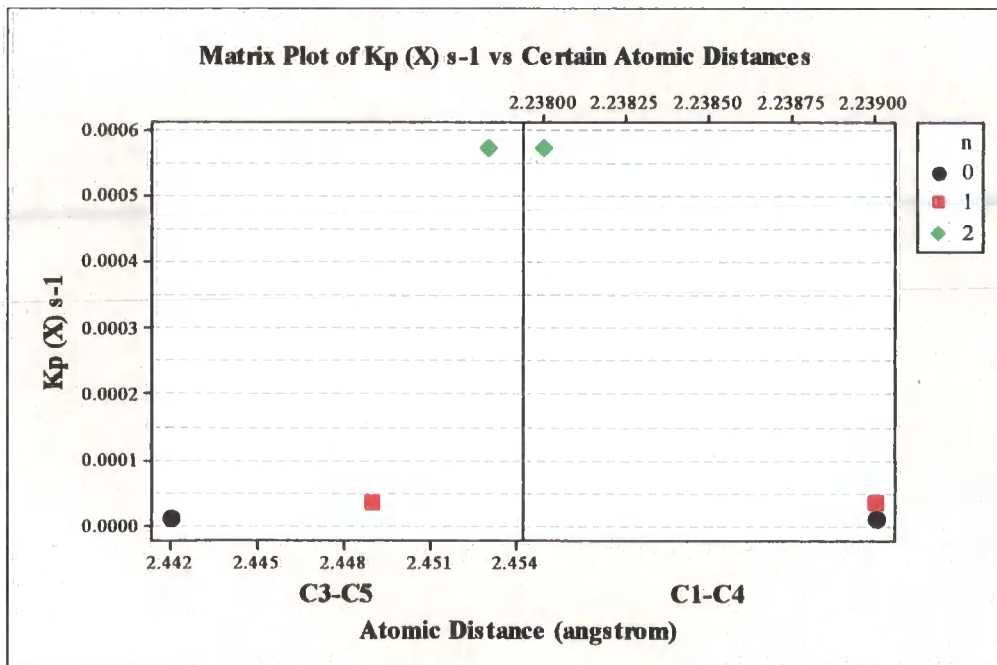


Figure VII

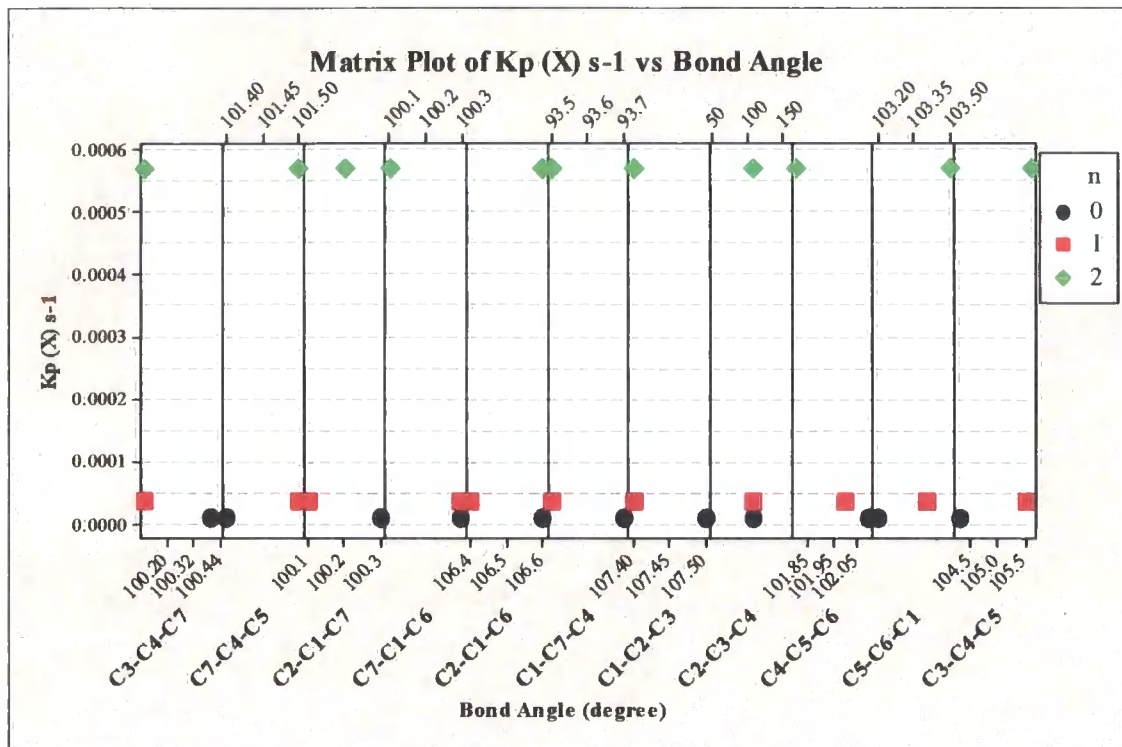


Figure VIII

